Depositional modes and post-depositional mineral formation in a Pleistocene sediment record from Lake Towuti, Indonesia

Inauguraldissertation
der Philosophisch-naturwissenschaftlichen Fakultät
der Universität Bern

vorgelegt von

Marina Alexandra Morlock

von Karlsruhe (Deutschland)

Leiter der Arbeit:

PD Dr. Hendrik Vogel

Co-Leiter der Arbeit:

Prof. Dr. Flavio S. Anselmetti

Institut für Geologie &
Oeschger-Zentrum für Klimaforschung
Universität Bern

Depositional modes and post-depositional mineral formation in a Pleistocene sediment record from Lake Towuti, Indonesia

Inauguraldissertation
der Philosophisch-naturwissenschaftlichen Fakultät
der Universität Bern

vorgelegt von

Marina Alexandra Morlock

von Karlsruhe (Deutschland)

Leiter der Arbeit:

PD Dr. Hendrik Vogel

Co-Leiter der Arbeit:

Prof. Dr. Flavio S. Anselmetti

Institut für Geologie &
Oeschger-Zentrum für Klimaforschung
Universität Bern

Von der Philosophisch-naturwissenschaftlichen Fakultät angenommen.

Bern, 18. Dezember 2018

Der Dekan:
Prof. Dr. Zoltan Balogh

Content

Abbreviations

BIF	Banded Iron Formation
DEM	Digital Elevation Model
EM	End-member
ENSO	El Niño - Southern Oscillation
FTIRS	Fourier-Transform-Infrared-Spectroscopy
ICDP	International Continental Scientific Drilling Program
ICP-MS	Inductively Coupled Plasma Mass Spectrometry
ICP-AES	Inductively Coupled Plasma Atomic Emission Spectrometry
IODP	Integrated Ocean Discovery Program
IPWP	Indo-Pacific Warm Pool
kyr BP	kilo years Before Present (1000 years before 1950)
LGM	Last Glacial Maximum
mblf	metres below lake floor
mcd	metres composite depth
µCT	High-resolution X-ray computed micro-tomography
TDP	Towuti Drilling Project
XRF	X-ray Fluorescence
XRD	X-ray Diffraction

SUMMARY

This thesis is part of an international collaboration of scientists, who drilled Indonesian Lake Towuti in 2015. In a combined scientific effort, the Towuti Drilling Project recovered around 1,000 m of sediment cores, including cores of the entire 165 m thick sediment infill at the main coring location, Site 1. The main objectives of the project were to study climate history in the heart of the Indo-Pacific Warm Pool, one of three major centres of atmospheric convection, to get insights into iron recycling and microbial processes in modern and ancient sediment, analogous to Archean ocean sediments, and to explore biologic evolution in a lake where numerous species are endemic.

The work presented here focuses on geochemical, mineralogical, and geotechnical aspects of the lake sediment record and the modern catchment, contributing to all of the above-mentioned areas of research. Adopting a source-to-sink approach, the modern lake system is initially characterised by identifying the main sedimentation sources and depositional processes in tropical Lake Towuti. Samples of bedrock, soils, and lake surface sediments reveal differential fault activity in the catchment and alternating wet and dry climate phases as the main drivers of modern and recent (last 60,000 years) sedimentation.

Building upon these results, the 100-m long continuous lacustrine sequence as well as the underlying, more heterogeneous ~65 m of sediment are studied in detail. Mineralogy and grain-size patterns record long-term basin evolution and changes in transport processes related to lake-level fluctuations. In the early extensional phase, repeated cycles of silting and peat formation, with standing water bodies, swamps and rivers in close proximity, offered diverse habitats to aquatic organisms. The formation of a permanent lake likely corresponds to the initial lake colonisation by riverine species, before subsidence and rapid lake surface expansion formed the lake we find today.

In greater detail, high-resolution X-ray computed micro-tomography (µCT) imaging visualises authigenic siderite ($FeCO_3$) and millerite (NiS) in unprocessed sediments from Lake Towuti. This technique allows the study of post-sedimentary overprinting of the sediments and helps to identify processes related to the formation of the authigenic minerals. Particularly intriguing is the high within-sample heterogeneity of probable mechanisms of mineral formation, which suggests that geochemical and isotopic proxy interpretation of iron carbonates in ferruginous sediments could be errorneous. The analysis adds a new perspective to the highly controversial approach of reconstructing Precambrian seawater composition from iron carbonate isotopes.

Lastly, a high-resolution geochemical data set is produced from X-ray fluorescence (XRF) core scanning, to establish an objective stratigraphy of the 100-m long lacustrine record. End-member modelling as a statistical tool to unmix large data sets robustly separates sedimentation processes identified in earlier chapters of this thesis. It facilitates the generation of an objective, quantitative, and consistent characterisation of depositional processes and post-depositional alterations in the complex setting of Lake Towuti.

Overall this thesis ties the regional history of Lake Towuti to aspects of environmental, climatic, tectonic, microbial, and biodiversity research, highlighting the multifaceted outcome of international scientific collaboration in tropical Southeast Asia, an area which already played a key role in establishing the theory of evolution more than 150 years ago.

ACKNOWLEDGEMENTS

This thesis is the result of four years of intense, enjoyable, laborious, demanding, and rewarding work. There are many facets of life as a PhD-student: travelling the world (literally), fighting bugs on the drill rig, eating rice at least twice a day for 2.5 months, enthusiastically cutting mud in a lab six floors underground, patting the XRF scanner multiple times a day, endlessly troubleshooting R scripts and excel spreadsheets… but above all it has been a stimulating learning process and valuable time of my life.

Also, I particularly want to emphasize the importance and value of the active contribution of our Indonesian colleagues, without whom this project would not have been possible.

Therefore, I'd like to say THANK YOU

To Hendrik, my main supervisor, who took me four years ago from a 60-cm sediment core from Gerzensee, a small puddle 25 km from Bern, to explore Lake Towuti, 2000x bigger, with its long and complex history. Thanks a lot for your guidance, discussions, support, criticism, and encouragement during the last four years!

To Flavio, head of the qPal-group, for discussions and supervision in all practical aspects of Quaternary research, and particularly for retreats and group meetings.

To Andy Cohen for evaluating my thesis and coming the long way from Arizona to my thesis defence.

To Jim Russell, one of the main PIs of the Towuti Drilling Project, for going through all the organisational troubles of such a large project, for advice and discussions about Lake Towuti, his challenging, yet helpful comments on my manuscripts, and for taking it easy on the spicy dishes at project dinners.

To our Indonesian colleagues, particularly Tia, Tika, and Silvi, for their tremendous efforts and indispensable help during and after the drilling operations, which made the visits to Indonesia so much easier (or actually at all possible) for us foreigners. Thanks for driving us around, for translations and explanations of Indonesian food, life and beyond.

To the TDP team, some 30 scientists from across the world, for making this project possible, for fun times during the drilling, sampling at LacCore and the project meetings. Thanks particularly to Daniel, Luis, Ascelina and Martin for the close cooperation, interesting discussions and data sharing.

To my colleagues in Office 003, Marius, Lukas, Eva, and Michi, for making the everyday work fun and enjoyable, over a coffee and some cookies, in the reclining chair or hard-working at our desks. Thanks especially to Marius for his help with Illustrator and any other issues that came up in everyday life, and to Michi for his endless knowledge in GIS.

To the entire qPal-group, particularly Stefano, Julia and Valentin, for discussions about work and beyond, for enduring Mensa food (almost) every day and for coming along on the journey through my PhD.

To the Oeschger Centre for supporting my studies, both master and PhD, and for organising events such as the Young Researchers Meeting, PhD Apéros and the OCCR summer school, which bring young scientists from different disciplines together and which are a great way to get back to the bigger picture when you're too caught up in your own data.

To Nicole, Andrea and John, for a great time in Toulouse and Bern, always involving good food.

To Oliver for teaching me the fundamentals of scientific work during my master thesis: to be precise in your wording and careful in what you interpret.

To Ece, Alena, Mättu, Tobi, and Patrik for discussions, sharing fun and troubles in a PhD-student's life, (climate) beers, lunches, dinners, hiking, swimming, biking, jazz, jass, and tukatoo.

To my parents for always supporting me, wherever I went, whatever I did.

To Moritz - takk skal du ha, vi har det so bra.

“[…] Such apparently unimportant facts as the presence of certain types of plants or animals in one island rather than in another, are now shown to be dependent on the long series of past geological changes -- on those marvellous astronomical revolutions which cause a periodic variation of terrestrial climates […]. And although these various causes are far too complex in their combined action to enable us to follow them out in the case of any one species, yet their broad results are clearly recognisable; and we are thus encouraged to study more completely every detail and every anomaly in the distribution of living things, in the firm conviction that by so doing we shall obtain a fuller and clearer insight into the course of nature […]”

Alfred Russel Wallace

English naturalist and explorer

(Island Life, 1880, 3rd ed. 1911, p. 544)

Chapter 1

Introduction

1. Introduction

1.1 Motivation and aims

Lake sediments are powerful archives of climatic and environmental change (Smol et al., 2001; Cohen, 2003). Lake sediments can record changes in lake-internal mechanisms, for example seasonal water column mixing (Zolitschka et al., 2015), catchment processes, e.g. flood-induced runoff and erosion (Gilli et al., 2013), and global climate, e.g. glacial-interglacial cycles (Johnson et al., 2016; Melles et al., 2012; Williams et al., 1997). Temporal resolution of sediment records can vary from sub-annual to decadal depending on sedimentation rates and water column oxygenation. Settings with low sedimentation rates or subsidence rates balancing or exceeding sedimentation rates often cover several hundred thousand to millions of years (Johnson et al., 2016; Melles et al., 2012; Williams et al., 1997). This diversity makes lakes very fascinating, but also complex palaeoenvironmental archives, where each lake has to be deciphered individually. In the last century, lake sediments have been established as reliable archives for climatic and environmental change (Smol et al., 2001; Cohen, 2003). While precise dating can be a challenge, lake sediments usually provide continuous terrestrial records of a well-defined area. In contrast, the source area for marine sediments is commonly less well-known, spreads over a larger area, and temporal resolution is lower compared to lacustrine sediment archives.

The humid tropics are a highly dynamic environment where many processes, e.g. weathering, are more intense compared to the mid and high latitudes (Pope, 2013). Around 80 % of the terrestrial biodiversity is found in the tropics, which cover around 40 % of the Earth's surface (~36 % of the landmass; State of the Tropics Report, 2014). Yet, particularly in humid tropical regions, access is often difficult due to the dense vegetation cover. Lake sediments can help to understand environmental change at scales much larger than the lake itself and provide a regional scale assessment of changes in climate and environmental variables over longer time scales.

By 2050, a projected 50 % of the world's population will live in the tropics. Under projected climate change and socioeconomic development, large parts of Southeast Asia will be vulnerable and exposed to the effects of climate change in multiple economic sectors by 2050 (Byers et al., 2018; Figure 1.1). A thorough understanding of local climate change impacts is essential for risk evaluation and the implementation of adaptation and mitigation strategies. Equally important is nature conservation: In the last 30 years, nearly ⅓ of the tropics suffered from degradation, mainly through increased anthropogenic influence, through activities such as deforestation (State of the Tropics Report, 2014). With increasing anthropogenic activities and human-induced climate change, it is pressing to gain a better understanding of climate and environmental change in the tropics, their global forcings and local or regional responses. A lake sediment record, which records historic variability of climate change, weathering, and vegetation dynamics, puts the observed and projected changes into context.

In Switzerland, a dense network of palaeoclimatological records exists. In contrast, in Indonesia, only a few terrestrial palaeoclimate records exist, mostly from speleothems (e.g. Ayliffe et al., 2013; Griffiths et al., 2010a; Griffiths et al., 2010b; Partin et al., 2007) and even fewer from lake sediments (e.g. Dam et al., 2001; van der Kaars & Dam, 1995). Our understanding of past climate is based on these few data points, usually hundreds of kilometres apart. This may be sufficient (yet not satisfactory) to

understand large-scale processes such as the general monsoonal patterns, but is far from satisfactory for providing a complete picture of regional and local impacts of climate change.

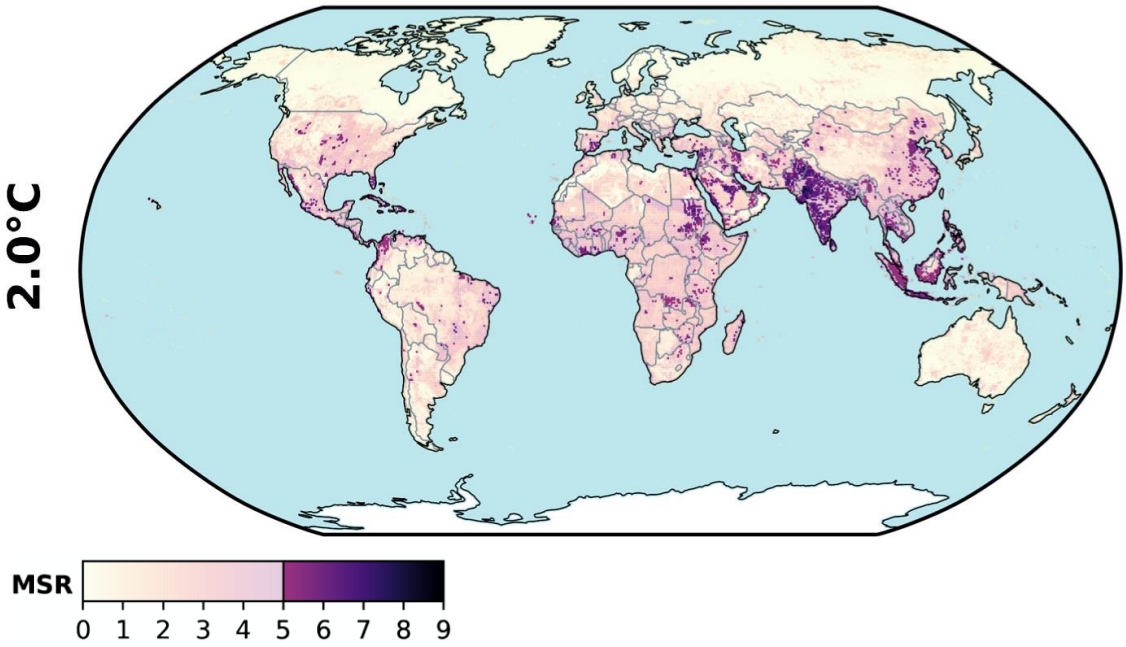

Figure 1.1 Map displaying the multi-sector risk (MSR) for a projected 2°C average warming relative to preindustrial conditions and socioeconomic development scenario SSP2 for the year 2050. Colour coding indicates the number of economic sectors, where the level of tolerable risk is exceeded. MSR > 5 is regarded as severe. Figure from Byers et al. (2018), see article for details

Therefore, this thesis aims to add another dot on the map of climate and environmental reconstructions in tropical Southeast Asia. The work is part of the Towuti Drilling Project (TDP) and contains the results of sediment core analyses from Lake Towuti, located on Sulawesi Island, Indonesia. The sediments were recovered during an international drilling campaign, co-sponsoredby the International Continental Scientific Drilling Program (ICDP), in 2015. Analyses include the geochemical and mineralogical study of catchment bedrock and soils, lake surface sediments, and sediment cores of TDP Site 1, the main drill site of the project. Specifically, the following questions are addressed:

1. Which sources and processes influence modern sedimentation in Lake Towuti, and which of the identified mechanisms can be related to climatic changes in the past?
2. How did the landscape and hydrology at Lake Towuti change through its existence, and which major changes occurred to the lake system?
3. What can be learnt from Lake Towuti as an analogue system to palaeoenvironments of the Archean on Earth and for interpreting sediments on Mars?
4. How can we extract signals from a lake system with multiple influencing parameters? And further, what can we learn about the environmental history of the Indo-Pacific region from the study of these individual signals?

1.2 Drilling long-lived lakes

Drilling long-lived lakes is challenging and usually requires joint logistical and funding efforts. The ICDP has played an important role in supporting and co-financing such projects. Founded in 1996, the program provides support, services and tools to realise multinational drilling projects on land. Its marine counterpart, the Integrated Ocean Discovery Program (IODP) has existed under various names since the foundation of the Deep Sea Drilling Project (DSDP) in 1966. Both programs have contributed enormously to combining scientific efforts and standardising analytical approaches in research on (unconsolidated) sediments. Today, ICDP has 22 member countries, and more than 40 drilling projects have been completed in the ICDP framework (Figure 1.2), with just under 10,000 scientists involved in ICDP projects (ICDP online, 2017). Several long-lived lakes have become target sites for international scientific drilling expeditions in the last decades, e.g. Lake Baikal and Lake Ohrid. Such lakes, defined as lakes that have existed for more than 100,000 years, are of particular interest to palaeolimnological research, because they potentially contain long records of climate and environmental change. Only a few dozen long-lived lakes exist globally.

In the last two decades, several ICDP projects in lakes across the globe have addressed climate and environmental change during (parts of) the Quaternary as one of their main targets (Figure 1.2). Most prominently, these include African lakes (e.g. the East African rift lakes in Kenya and Ethiopia, completed in 2014), lakes from South and Central America (e.g. Petén Itzá, Guatemala, in 2006 and Lake Junin, Peru, in 2015), Eastern Europe (Lake Ohrid, Macedonia, in 2013), and Asia (e.g. Lake El'gygytgyn in 2008/2009 and Lake Van, Turkey, in 2010). However, no lakes from the Southeast Asian tropics have been previously drilled within the ICDP.

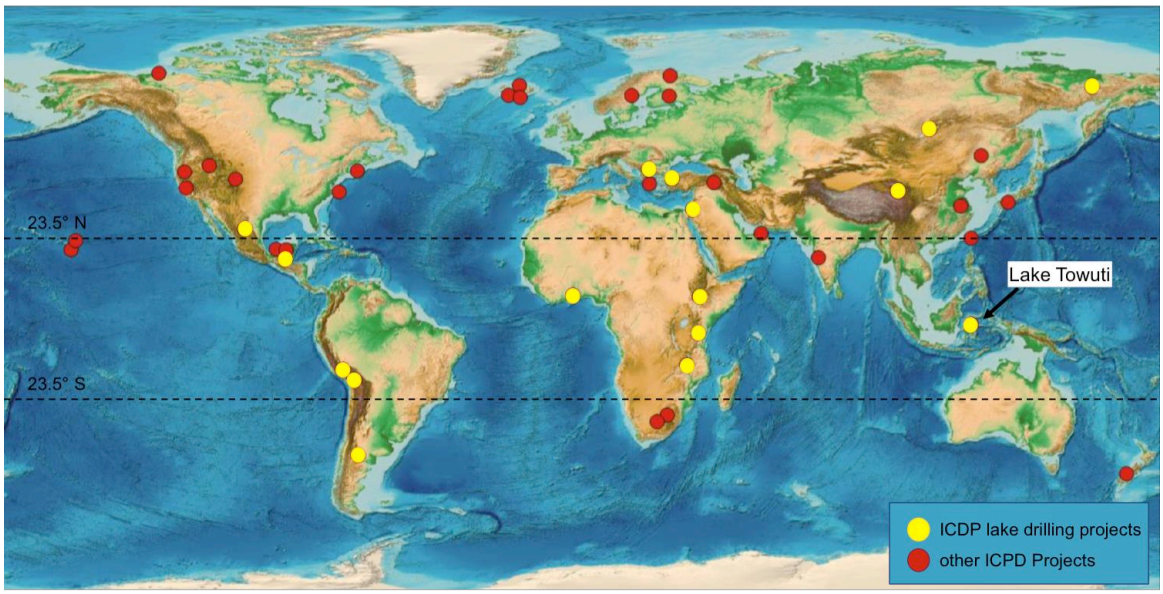

Figure 1.2 ICDP project locations, modified from ICDP (2016)

Four Southeast Asian lakes or lake systems have been suggested to be long-lived: Lake Inlé in Myanmar, Lake Lanao in the Philippines, and Lake Poso and the Malili Lakes in Indonesia (Martens, 1997). Of these, the Indonesian lakes are by far better studied than Lakes Inlé and Lanao. Following pre-site surveys and shorter sediment

coring in 2010 and the years thereafter, an international team of scientists, including three scientists from Switzerland (Hendrik Vogel, Luis Ordoñez and myself), recovered cores of the entire sediment infill from Lake Towuti in 2015. The lake is part of the Malili Lake System on Sulawesi Island, Indonesia.

1.2.1 The Towuti Drilling Project

During the 2.5 month coring expedition in 2015, the Towuti Drilling Project recovered ~1000 m of sediment cores from 3 sites (10 holes) in the deep northern lake basin (Figure 1.3). Primary target Site 1 reached bedrock at 162 m below lake floor (m b.l.f.), recovering ~97 m of lake sediments (Unit 1) overlying ~65 m of coarser-grained deposits (Unit 2; Russell et al., 2016). The sequence includes 18 tephra deposits and 19 normally graded event deposits, which together correspond to roughly 4 m of the record. At present, analyses to establish a reliable age-depth model for the cores are still in progress. The initial publication of the Towuti Drilling Project, summarising drilling activities, data acquired on site, and preliminary results of the borehole lithologies, can be found in Appendix I.1 of this thesis. Impressions from fieldwork are shown in Figure 1.4.

The three main objectives of the Towuti Drilling Project were focused on regional climate history, subsurface biosphere, and long-term evolution of the lake basin, linked to speciation and biologic evolution in the lake. These main scientific topics are themes of Chapters 2-5 of this thesis and are described in more detail below.

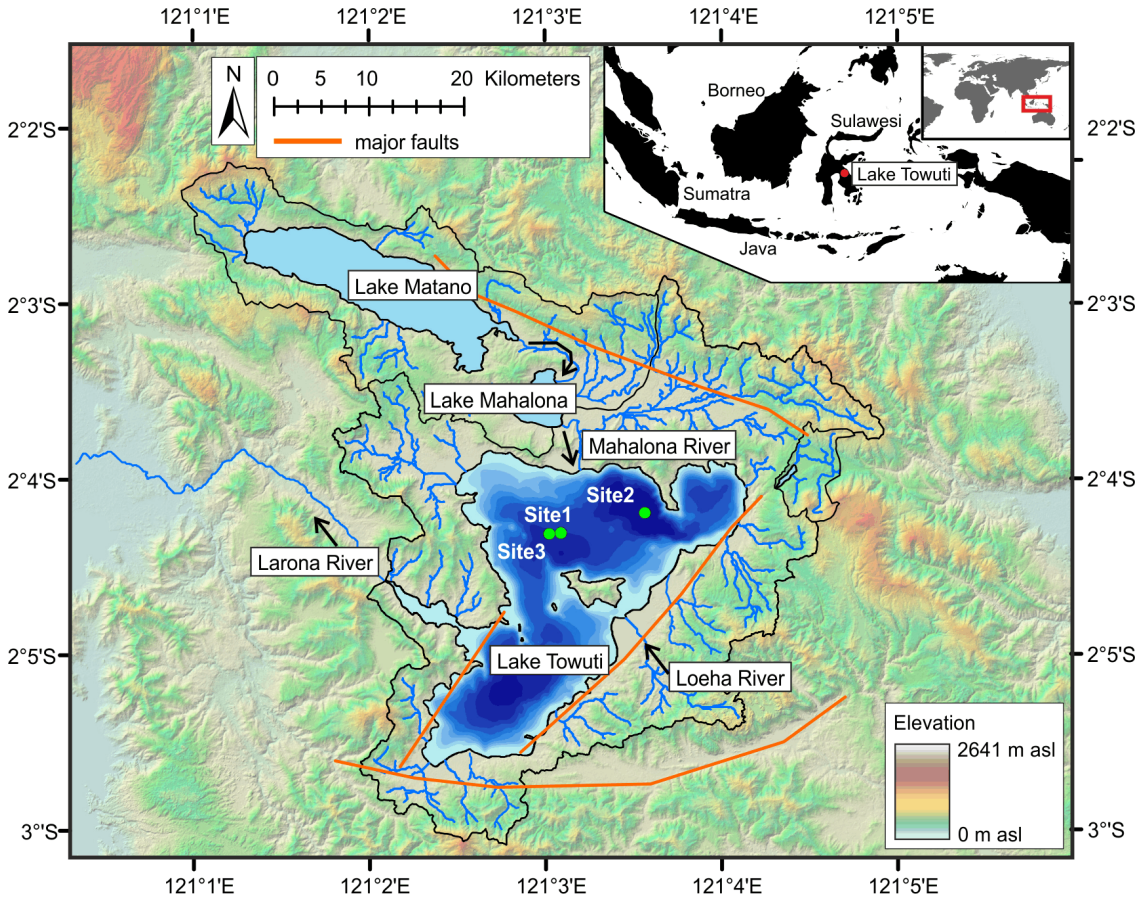

Figure 1.3 Map of the Malili Lake System, with Lake Towuti and TDP coring sites

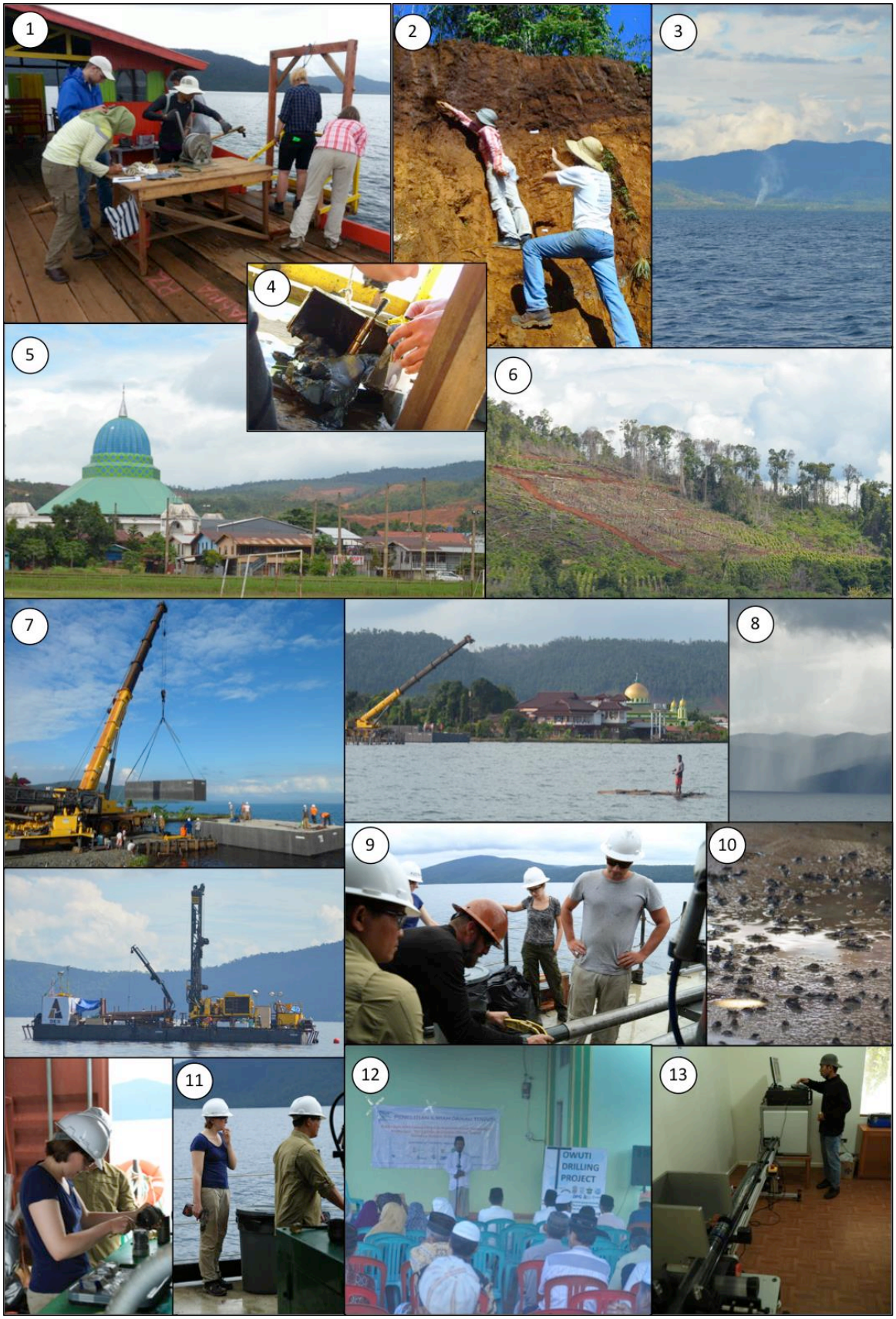

Figure 1.4 (1) Surface sediment sampling on Lake Towuti - 85 samples, recovered with a hand-operated winch. (2) Taking soil samples in tropical heat. (3) Forest clearance fires on the shores of Lake Towuti. (4) A grab sampler full of dark green mud. (5) The mosque

of Sorowako, our research base on the shores of Lake Matano. Mining activities for nickel-rich laterite deposits in the background. (6) Pepper plantation on the shores of Lake Towuti. Around 25 % of the catchment are now deforested, mainly due to anthropogenic activities. (7) Drilling barge assemblage in Timampu, Lake Towuti. The 220-t crane was a big sight in the small town. (8) Daily heavy downpour on Lake Matano. (9) Core recovery on the barge. (10) Bug infestation remains after night shift. (11) Waiting for the next core to come on deck, prepared to reduce core expansion. (12) Public outreach to local municipalities. (13) MSCL-scanning in the field lab

1.3 The Malili Lake System

The Malili Lake System is located in the centre of Sulawesi Island and consists of the three connected lakes Matano, Mahalona, and Towuti and two small satellite lakes, Lontoa and Mesapi. Of the Malili Lakes, Lake Matano is the deepest (590 m max. water depth) and supposedly oldest (Brooks, 1950), followed by Lake Towuti (200 m max. water depth) and shallow Lake Mahalona (62 m max. water depth). The lakes together drain a catchment area of ~2,300 km^2. The lake system is hydrologically open, with one outflow draining into the Bay of Bone through the Larona River, which today is artificially dammed for hydropower production. A strong El Niño event in 1997/98 led to a lake-level drop of 3 m in Lake Towuti, resulting in a transition to closed-basin status of the lake (Tauhid & Arifian, 2000).

The Malili lakes are mostly surrounded by dense, closed-canopy rainforest. Since the 1970s, active mining operations have been conducted to exploit the nickel-rich lateritic soils around the lakes. Mining activities are concentrated to the west of the lake system, mainly in the catchment of Lake Matano. Today, pepper farming is an increasing economic sector, for which pristine rain forest is cut and burnt on the flanks of Lake Towuti. This deforestation is most intense to the NW and NE of the lake. Based on satellite images, approximately 25 % of Towuti's catchment is currently deforested. Timber production is mostly undertaken with selective felling of commercially valuable species and without extensive use of automated, industrial style machinery.

1.3.1 Climate

The Malili Lakes receive an annual precipitation of ~2500 mm, which is controlled by the twice-annual passage of the Intertropical Convergence Zone (ITCZ) and is strongly influenced by the Australian-Indonesian Summer Monsoon (Konecky et al., 2016). Peak rainfall occurs in months MAM, while months ASO are relatively dry. On longer time scales, southeast Asian climate is tightly coupled to northern hemisphere glaciations (Mohtadi et al., 2011; Russell et al., 2014; Turney et al., 2004) as well as orbitally-forced changes in insolation (Carolin et al., 2013; Clement et al., 2004), and subsequent changes in the monsoon systems (Konecky et al., 2016; Mohtadi et al., 2011; Wang et al., 2008). Exposure of the Sunda Shelf during sea level falls of more than 40 m relative to today may further impact regional climate and atmospheric circulation patterns. The climate of the last glacial maximum (LGM) was characterised by drier conditions in most parts of tropical and subtropical Asia (De Deckker et al., 2002; Partin et al., 2007; Reeves et al., 2013; Russell et al., 2014). However, very few palaeoclimate records exist from the region and climate reconstructions in tropical terrestrial archives are often discontinuous (e.g. Meckler et al., 2012) or only cover

selective periods of the last glacial-interglacial cycle (e.g. Ayliffe et al., 2013), highlighting the needs for long and continuous records in order to document the regional response to global climate change and forcing.

1.3.2 Tectonics

On Sulawesi Island, three major strike-slip fault systems, the Palu-Koro, Matano, and Lawanopo faults, accommodate the collision between Australia and Sundaland (Asia), which leads to a clockwise rotation and northward movement of eastern Sulawesi relative to Sundaland (Hall, 1996). The prominent Matano Fault, a highly segmented sinistral fault system, runs north of the Malili Lakes and has created accommodation space for lake sedimentation in the last several hundred thousand years. Frequent earthquakes occur in the area (168 between 2010 and 2016), including several above magnitude five. A shallow focus MW 6.1 earthquake occurred in 2011 on the shore of Lake Matano, causing damage to buildings and a potential surface rupture length of 39 km (Watkinson & Hall, 2016). Detailed tectonic studies of the area are still lacking, but geomorphologic and fault kinematics analyses suggest rapid slip rates along the Matano fault and activity throughout the Quaternary (Bellier et al., 2006). Investigating changes in hydrology and sediment sourcing through the history of Lake Towuti may help to better constrain fault activity and Quaternary slip rates in the region.

1.3.3 Biodiversity

Sulawesi is part of the zoogeographic region of Wallacea, which consists of islands located between the continental shelves of Asia and Australia. The area has been recognised as one of 25 global biodiversity hotspots (Myers et al., 2000). While most of Java, Sumatra, and Borneo were connected to the Asian continent during glacial sea level lowstands (>40 m lower than present), Sulawesi and the surrounding islands remained isolated during these times. This supported the development of a largely endemic fauna, with 71 % of the mammals endemic to the island (Groves, 1976). The fauna on Sulawesi is distinctly different from the large islands to the west, but shares some general similarities with the Australian flora (Van Welzen et al., 2011). The region is named after the British naturalist and explorer Alfred R. Wallace, who spent many years exploring and describing the region's flora and fauna in great detail (e.g. Wallace, 1869). By discovering that similarity and distribution of species on different islands depend on water depth between the respective islands, his descriptions and concepts strongly supported Darwin's evolutionary theory, which was developed around the same time. In addition, his observations led to the definition of the Wallace line, which broadly separates fauna of Australian and Asian origin.

Already in the 19th century, the Malili Lake System was recognised as a unique system and biodiversity hotspot (Sarasin & Sarasin, 1898). Since then, extensive research has been carried out to study species distribution, endemism and adaptive radiation in the lakes (Bramburger et al., 2008; Glaubrecht & von Rintelen, 2008; Haffner et al., 2001; Herder et al., 2006; Sabo et al., 2008; Vaillant et al., 2011; von Rintelen et al., 2010; von Rintelen et al., 2004). While many other long-lived lakes, e.g. the African Great Lakes, Lake Baikal and the Caspian lakes, share high endemism and biodiversity, the Malili Lake System is comparatively young, making it a prime site to study radiation mechanisms (Vaillant et al., 2011). One of the main enigmas arising from studies of the Malili Lake System is that all three lakes have high numbers of endemic species, despite

being interconnected by rivers. This suggests that habitat specialisation is one of the main drivers for adaptive radiation in the Malili Lakes (von Rintelen & Cai, 2009). Further, genetic analyses of different species groups suggest multiple colonisation events of the lakes (von Rintelen et al., 2012). The study of Lake Towuti sediments, which cover the entire sedimentation history of the lake, can help to address these proposed mechanisms and arising questions. Previous studies on Lake Towuti sediment cores have shown that the lake was continuously connected to upstream lakes Mahalona and Matano the last 60,000 years (Costa et al., 2015; Vogel et al., 2015; Morlock et al., 2018 - Chapter 2 of this thesis).

1.3.4 Geochemistry

One of the reasons for the exceptional fauna in the Malili Lakes is their unique geochemistry (Vaillant et al., 2011). Located in the East Sulawesi Ophiolite, the majority of the Malili lakes catchment consists of mafic and ultramafic rocks, which are overlain by deeply weathered laterite soils (Kadarusman et al., 2004). The two deep lakes, Matano and Towuti, are weakly thermally stratified and have a persistent pycnocline at around 100 m water depth, below which oxygen is depleted (Costa et al., 2015; Crowe et al., 2008). Dissolved iron concentrations in the hypolimnion are exceptionally high (up to 140 mmol/L in Lake Matano; Crowe et al., 2008). In the epilimnion, chromium concentrations reach values of up to 180 nmol/L (Lake Matano; Crowe et al., 2008), potentially toxic to species in the long-term (Vaillant et al., 2011). At the same time, dissolved phosphorus (50.2 mmol/L) and nitrogen (55 mmol/L, both in Lake Matano) concentrations are very low, which is accompanied by a low phytoplankton density (0.013mg/L; Sabo et al., 2008). Less data exists from Lake Towuti, but similar values are anticipated. Despite current anoxia in the hypolimnion, Lake Towuti has been suggested to mix occasionally on decadal time scales (Hasberg et al., 2018 - Appendix I, Chapter I.2 of this thesis).

The geochemistry of the Malili lakes is rare in aquatic systems on Earth today, but shares some key characteristics with Precambrian oceans and conditions on Mars. Ocean conditions during the Archean (4 to 2.5 billion years ago) are reconstructed to have been ferruginous and oxygen-poor (Canfield et al., 2008), similar to Lake Towuti today. Banded iron formations (BIFs), which are deposits associated to these early oceans (Posth et al., 2011), are characterised by alternating siderite- and silicate-rich iron beds, which today have undergone varying degrees of diagenetic overprinting. Analogously, the ferruginous sediments of Lake Towuti contain siderite (Tamuntuan et al., 2015), which forms under anoxic conditions in the water column or in the sediment. The sediments of Lake Towuti, which have not experienced such complex diagenetic histories as BIFs, can therefore help to identify processes of authigenic mineral formation and early phases of secondary mineral alteration, under conditions analogous to Archean oceans.

With respect to geochemistry and mineralogy, e.g. the abundance of mafic and Fe-bearing minerals, Lake Towuti sediments have also been suggested as an analogue to sediments found on Mars. In Gale Crater, the US Mars Curiosity rover is currently exploring a >200 m thick sequence of mudstones containing a range of iron-rich minerals, which may be associated with redox-stratified lake sediments (Grotzinger et al., 2015; Hurowitz & McLennan, 2007). To that end, understanding environmental changes in Lake Towuti and their expression in mineralogy may help to interpret

variations found in Martian rocks. In particular, mineral identification by remote non-destructive methods such as infrared spectroscopy can contribute to a reliable identification and interpretation of minerals on Mars, where established methods such as X-ray diffraction (XRD) are more difficult to apply on a larger spatial scale.

1.4 Outline of the thesis

In many ways Lake Towuti is a unique system: a long-lived lake, surrounded by thick soils developed on ultramafic bedrock, exposed to a humid tropical climate and subject to active tectonic disturbance. This interplay of different processes (tectonic, climatic, diagenetic) also challenges a comprehensive scientific evaluation of the record. Yet, the previous paragraphs show that many things can be learnt from exploring changes in this lake system through time. In the following chapters, this thesis provides a detailed characterisation of this complex system through its existence, transfers an understanding of processes occurring in Lake Towuti to comparable systems, and explores new methods to tackle the challenge of multiple forcings within one sediment record.

Chapter 2 describes the interplay between climatic and tectonic factors in the modern system of Lake Towuti and applies these insights to two sediment cores covering the last 30,000 and 60,000 years, respectively. By connecting modern lake surface samples from across the lake to sedimentation changes across glacial-interglacial climates, this chapter describes erosion and transport processes in a highly dynamic tropical lake system and sets the stage for the long sediment record recovered by the Towuti Drilling Project.

Chapter 3 looks into long-term changes in lake basin sedimentation and hydrology, starting from initial lateritic soil formation to the establishment of the permanent water body found today. This allows us to study changes in aquatic habitats, sediment transport processes and catchment hydrology across several hundred thousand years.

Chapter 4 focuses on the visualization of siderite in unprocessed and unconsolidated sediments from Lake Towuti, to study siderite formation processes and their implication for iron carbonate chemistry and isotopic composition, e.g. in Archean oceans.

Chapter 5 addresses the challenge of separating the complex interplay of different processes at Lake Towuti. To extract several signals from a single data set, end-member modelling is applied to a high-resolution geochemical record from the Lake Towuti sediments. This statistical approach to separate complex data sets allows for the identification of six sediment sources related to climatic and tectonic processes, diagenesis, and lake productivity.

Appendix I contains papers and manuscripts that I contributed to as a co-author.

Appendix I.1 gives an initial description of drilling activities, data acquired on site, and preliminary results of the lithologies for the three TDP drill sites.

Appendix I.2 uses the same set of surface sediment samples as Chapter 2, but focuses on lake-internal processes that influence modern sedimentation. By evaluating mineralogy and grain size patterns across the lake, this chapter identifies the main

sources of fluvial input and analyses the distribution of tephra particles, diatoms, and organic matter in the lake.

Appendix I.3 uses a subset of surface sediment samples to study iron geochemistry and mineralogy of Lake Towuti to understand changes in catchment and lake sedimentation and explores the comparison to and implications for Martian sediments.

Appendix II contains a detailed description of the X-ray fluorescence (XRF) core-scanning measurement correction used in Chapter 5.

Appendix III gives an overview over all measured samples that provide the basis for this thesis.

1.5 References

Ayliffe LK, Gagan MK, Zhao JX, Drysdale RN, Hellstrom JC, Hantoro WS, Griffiths ML, Scott-Gagan H, St Pierre E, Cowley JA, Suwargadi BW. (2013). Rapid interhemispheric climate links via the Australasian monsoon during the last deglaciation. Nat Commun, 4, 2908. doi: 10.1038/ncomms3908

Bellier O, Sébrier M, Seward D, Beaudouin T, Villeneuve M, Putranto, E. (2006). Fission track and fault kinematics analyses for new insight into the Late Cenozoic tectonic regime changes in West-Central Sulawesi (Indonesia). Tectonophysics, 413(3-4), 201-220. doi: 10.1016/j.tecto.2005.10.036

Bramburger AJ, Hamilton PB, Hehanussa PE, Haffner GD. (2008). Processes regulating the community composition and relative abundance of taxa in the diatom communities of the Malili Lakes, Sulawesi Island, Indonesia. Hydrobiologia, 615(1), 215-224. doi: 10.1007/s10750-008-9562-2

Brooks JL. (1950). Speciation in Ancient Lakes (Concluded). The Quarterly Review of Biology, 25(2), 131-176. doi: 10.1086/397539

Byers E, Gidden M, Leclère D, Balkovic J, Burek P, Ebi K, Greve P, Grey D, Havlik P, Hillers A, Johnson N, Kahil T, Krey V, Langan S, Nakicenovic N, Novak R, Obersteiner M, Pachauri S, Palazzo A, Parkinson S, Rao ND, Rogelj J, Satoh Y, Wada Y, Willaarts B, Riahi K. (2018). Global exposure and vulnerability to multi-sector development and climate change hotspots. Environmental Research Letters, 13(5), 055012. doi: 10.1088/1748-9326/aabf45

Carolin SA, Cobb KM, Adkins JF, Clark B, Conroy JL, Lejau S, Malang J, Tuen AA. (2013). Varied Response of Western Pacific Hydrology to Climate Forcings over the Last Glacial Period. Science, 340(6140), 1564-1566. doi: 10.1126/science.1233797

Clement AC, Hall A, Broccoli AJ. (2004). The importance of precessional signals in the tropical climate. Climate Dynamics, 22(4), 327-341. doi: 10.1007/s00382-003-0375-8

Cohen AS. (2003). Paleolimnology. The History and Evolution of Lake Systems. New York: Oxford University Press.

Costa KM, Russell JM, Vogel H, Bijaksana S. (2015). Hydrological connectivity and mixing of Lake Towuti, Indonesia in response to paleoclimatic changes over the last 60,000years. Palaeogeography, Palaeoclimatology, Palaeoecology, 417, 467-475. doi: 10.1016/j.palaeo.2014.10.009

Crowe SA, O'Neill AH, Katsev S, Hehanussa PE, Haffner GD, Sundby B, Mucci A, Fowle, DA. (2008). The biogeochemistry of tropical lakes: A case study from Lake Matano, Indonesia. Limnology Oceanography, 53(1), 319-331.

Dam RAC, Fluin J, Suparan P, van der Kaars S. (2001). Palaeoenvironmental developments in the Lake Tondano area (N. Sulawesi, Indonesia) since 33,000 yr BP. Palaeogeography, Palaeoclimatology, Palaeoecology, 171, 147-183.

De Deckker P, Tapper NJ, van der Kaars S. (2002). The status of the Indo-Pacific Warm Pool and adjacent land at the Last Glacial Maximum. Global and Planetary Change, 35, 25-35.

Gilli A, Anselmetti FS, Glur L, Wirth SB. (2013). Lake Sediments as Archives of Recurrence Rates and Intensities of Past Flood Events. In: Schneuwly-Bollschweiler M, Stoffel M, Rudolf-Miklau F (Eds.) Dating Torrential Processes on Fans and Cones (Vol. 47). Dordrecht, Netherlands: Springer.

Glaubrecht M, von Rintelen T. (2008). The species flocks of lacustrine gastropods: Tylomelania on Sulawesi as models in speciation and adaptive radiation. Hydrobiologia, 615(1), 181-199. doi: 10.1007/s10750-008-9568-9

Griffiths ML, Drysdale RN, Gagan MK, Frisia S, Zhao J-x, Ayliffe LK, Hantoro WS, Hellstrom JC, Fischer MJ, Feng Y-X. (2010a). Evidence for Holocene changes in Australian–Indonesian monsoon rainfall from stalagmite trace element and stable isotope ratios. Earth and Planetary Science Letters, 292(1-2), 27-38. doi: 10.1016/j.epsl.2010.01.002

Griffiths ML, Drysdale RN, Vonhof HB, Gagan MK, Zhao J-x Ayliffe LK, Hantoro WS, Hellstrom JC, Cartwright I, Frisia S, Suwargadi BW. (2010b). Younger Dryas–Holocene temperature and rainfall history of southern Indonesia from δ18O in speleothem calcite and fluid inclusions. Earth and Planetary Science Letters, 295(1-2), 30-36. doi: 10.1016/j.epsl.2010.03.018

Grotzinger JP, Gupta S, Malin MC, Rubin DM, Schieber J, Siebach K, Sumner DY, Stack KM, Vasavada AR, Arvidson RE, Calef III F, Edgar L, Fischer WF, Grant JA, Griffes J, Kah LC, Lamb MP, Lewis KW, Mangold N, Minitti ME, Palucis M, Rice M, Williams RM, Yingst RA, Blake D, Blaney D, Conrad P, Crisp J, Dietrich WE, Dromart G, Edgett KS, Ewing RC, Gellert R, Hurowitz JA, Kocurek G, Mahaffy P, McBride MJ, McLennan SM, Mischna M, Ming D, Milliken R, Newsom H, Oehler D, Parker TJ, Vaniman D, Wiens RC, Wilson SA. (2015). Deposition, exhumation, and paleoclimate of an ancient lake deposit, Gale crater, Mars. Science, 350(6257), aac7575. doi: 10.1126/science.aac7575

Groves CP. (1976). The origin of the mammalian fauna of Sulawesi (Celebes). Zeitschrift für Säugetierkunde, 41, 201-216.

Haffner GD, Hehanussa PE, Hartoto D. (2001). The biology and physical processes of large lakes of Indonesia: Lakes Matano and Towuti. In: Munawar M, Hecky RE (Eds.) The Great Lakes of the World (GLOW): Food-web, health and integrity (pp. 183-192). Leiden, The Netherlands: Backhuys Publishers.

Hall R. (1996). Reconstructing Cenozoic SE Asia. In: Hall R, Blundell DJ (Eds.) Tectonic Evolution of SE Asia (Vol. 106, pp. 153-184). London, UK: Geological Society London Special Publication.

Hasberg AKM, Melles M, Wennrich V, Just J, Held P, Morlock MA, Vogel H, Russell JM, Bijaksana S, Opitz S. (2018). Modern sedimentation processes in Lake Towuti, Indonesia, revealed by the composition of surface sediments. Sedimentology.

Herder F, Nolte AW, Pfaender J, Schwarzer J, Hadiaty RK, Schliewen UK. (2006). Adaptive radiation and hybridization in Wallace's Dreamponds: evidence from sailfin silversides in the Malili Lakes of Sulawesi. Proc Biol Sci, 273(1598), 2209-2217. doi: 10.1098/rspb.2006.3558

Hurowitz JA, McLennan SM. (2007). A ~3.5 Ga record of water-limited, acidic weathering conditions on Mars. Earth and Planetary Science Letters, 260(3-4), 432-443. doi: 10.1016/j.epsl.2007.05.043

ICDP online (2017). International Continental Scientific Drilling Program. Retrieved 09/13, 2018, from www.icdp-online.org/

ICDP (2016). Roadmap for Operational Support in the International Continental Scientific Drilling Program Supporting Continental Scientific Drilling: Perspectives from within and without. Potsdam, Germany: International Continental Scientific Program, GFZ - German Research Centre for Geosciences.

Johnson TC, Werne JP, Brown ET, Abbott A, Berke M, Steinman BA, Halbur J, Contreras S, Grosshuesch S, Deino A, Scholz CA, Lyons RP, Schouten S, Damste JS. (2016). A

progressively wetter climate in southern East Africa over the past 1.3 million years. Nature, 537(7619), 220-224. doi: 10.1038/nature19065

Kadarusman A, Miyashita S, Maruyama S, Parkinson CD, Ishikawa A. (2004). Petrology, geochemistry and paleogeographic reconstruction of the East Sulawesi Ophiolite, Indonesia. Tectonophysics, 392(1-4), 55-83. doi: 10.1016/j.tecto.2004.04.008

Konecky B, Russell JM, Bijaksana S. (2016). Glacial aridity in central Indonesia coeval with intensified monsoon circulation. Earth and Planetary Science Letters, 437, 15-24. doi: 10.1016/j.epsl.2015.12.037

Martens K. (1997). Speciation in ancient lakes. TREE, 12.

Meckler AN, Clarkson MO, Cobb KM, Sodemann H, Adkins JF. (2012). Interglacial Hydroclimate in the Tropical West Pacific Through the Late Pleistocene. Science, 336, 1301-1304. doi: 10.1126/science.1218340

Melles M, Brigham-Grette J, Minyuk PS, Nowaczyk NR, Wennrich V, DeConto RM, Anderson PM, Andreev AA, Coletti A, Cook TL, Haltia-Hovi E, Kukkonen M, Lozhkin AV, Rosén P, Tarasov P, Vogel H, Wagner B. (2012). 2.8 Million Years of Arctic Climate Change from Lake El'gygytgyn, NE Russia. Science, 337(6092), 315-320. doi: 10.1126/science.1222135

Mohtadi M, Oppo DW, Steinke S, Stuut J-BW, De Pol-Holz R, Hebbeln D, Lückge A. (2011). Glacial to Holocene swings of the Australian-Indonesian monsoon. Nature Geoscience, 4. doi: 10.1038/ngeo1209

Myers N, Mittermeier RA, Mittermeier CG, Gda Fonseca GAB, Kent J. (2000). Biodiversity hotspots for conservation priorities. Nature, 403, 853-858.

Partin JW, Cobb KM, Adkins JF, Clark B, Fernandez DP. (2007). Millennial-scale trends in west Pacific warm pool hydrology since the Last Glacial Maximum. Nature, 449(7161), 452-455. doi: 10.1038/nature06164

Pope GA. (2013). Weathering in the Tropics, and Related Extratropical Processes. In J F Shroder (Ed.), Treatise on Geomorphology (Vol. 4, pp. 179-196). San Diego: Academic Press.

Reeves JM, Bostock HC, Ayliffe LK, Barrows TT, De Deckker P, Devriendt LS, Dunbar GB, Drysdale RN, Fitzsimmons KE, Gagan MK, Griffiths ML, Haberle SG, Jansen JD, Krause C, Lewis S, McGregor HV, Mooney SD, Moss P, Nanson GC, Purcell A, van der Kaars S. (2013). Palaeoenvironmental change in tropical Australasia over the last 30,000 years – a synthesis by the OZ-INTIMATE group. Quaternary Science Reviews, 74, 97-114. doi: 10.1016/j.quascirev.2012.11.027

Russell JM, Bijaksana S, Vogel H, Melles M, Kallmeyer J, Ariztegui D, Crowe S, Fajar S, Hafidz A, Haffner D, Hasberg A, Ivory S, Kelly C, King J, Kirana K, Morlock M, Noren A, O'Grady R, Ordonez L, Stevenson J, von Rintelen T, Vuillemin A, Watkinson I, Wattrus N, Wicaksono S, Wonik T, Bauer K, Deino A, Friese A, Henny C, Imran, Marwoto R, Ngkoimani LO, Nomosatryo S, Safiuddin LO, Simister R, Tamuntuan G. (2016). The Towuti Drilling Project: paleoenvironments, biological evolution, and geomicrobiology of a tropical Pacific lake. Scientific Drilling, 21, 29-40. doi: 10.5194/sd-21-29-2016

Russell JM, Vogel H, Konecky B, Bijaksana S, Huang Y, Melles M, Wattrus N, Costa KM, King JW. (2014). Glacial forcing of central Indonesian hydroclimate since 60,000 y BP. PNAS, 111(14), 5100-5105. doi: 10.1073/pnas.1402373111

Sabo E, Roy D, Hamilton PB, Hehanussa PE, McNeely R, Haffner GD. (2008). The plankton community of Lake Matano: factors regulating plankton composition and relative abundance in an ancient, tropical lake of Indonesia. Hydrobiologia, 615(1), 225-235. doi: 10.1007/s10750-008-9560-4

Sarasin P, & Sarasin F. (1898). Die Süßwassermollusken von Celebes. . Wiesbaden, Germany: Kreidel.

Smol JP, Birks HJ, Last WM. (2001). Tracking Environmental Change Using Lake Sediments. Netherlands: Springer.

State of the Tropics Report (2014). State of the Tropics 2014 Report. In: Harding S, McComiskie R, Wolff M, Trewin D, Hunter S (Eds.). Cairns, Australia: James Cook University.

Tamuntuan G, Bijaksana S, King J, Russell JM, Fauzi U, Maryunani K, Aufa N, Safiuddin LO. (2015). Variation of magnetic properties in sediments from Lake Towuti, Indonesia, and its paleoclimatic significance. Palaeogeography, Palaeoclimatology, Palaeoecology, 420, 163-172. doi: 10.1016/j.palaeo.2014.12.008

Tauhid YI, & Arifian J. (2000). Long-term observations on the hydrological condition of Lake Towuti. Jurnal Sains Teknologi Modifikasi Cuaca, 1, 93-100.

Turney CSM, Kershaw AP, Clemens SC, Branch N, Moss PT, Fifield LK. (2004). Millennial and orbital variations of El Nino/Southern Oscillation and high-latitude climate in the last glacial period. Nature, 428, 306-310.

Vaillant JJ, Haffner GD, Cristescu ME. (2011). The ancient lakes of Indonesia: towards integrated research on speciation. Integr Comp Biol, 51(4), 634-643. doi: 10.1093/icb/icr101

van der Kaars WA, Dam MAC. (1995). A 135,000-year record of vegetational and climatic change from the Bandung area, West-Java, Indonesia. Palaeogeography, Palaeoclimatology, Palaeoecology, 117, 55-72.

Van Welzen PC, Parnell JAN, Slik JWF. (2011). Wallace's Line and plant distributions: two or three phytogeographical areas and where to group Java? Biological Journal of the Linnean Society, 103, 531-545.

Vogel H, Russell JM, Cahyarini SY, Bijaksana S, Wattrus N, Rethemeyer J, Melles M. (2015). Depositional modes and lake-level variability at Lake Towuti, Indonesia, during the past ~29 kyr BP. Journal of Paleolimnology, 54(4), 359-377. doi: 10.1007/s10933-015-9857-z

von Rintelen K, Cai Y. (2009). Radiation of endemic speices flocks in ancient lakes: systematic revision of the freshwater shrimp Caridina H. Milne Edwards, 1837 (Crustacea: Decapoda: Atyidae) from the ancient lakes of Sulawesi, Indonesia, with the description of eight new species. The Raffles Bulletin of Zoology, 57(2), 343-452.

von Rintelen K, Glaubrecht M, Schubart CD, Wessel A, Von Rintelen T. (2010). Adaptive radiation and ecological diversification of Sulawesi's ancient lake shrimps. Evolution, 64(11), 3287-3299. doi: 10.1111/j.1558-5646.2010.01043.x

von Rintelen, T von Rintelen K, Glaubrecht M, Schubart CD, Herder F. (2012). Aquatic biodiversity hotspots in Wallacea: the species flocks in the ancient lakes of Sulawesi, Indonesia. In: Gower DJ, Johnson K, Richardson J, Rosen B, Rüber L, Williams S (Eds.) Biotic Evolution and Environmental Change in Southeast Asia (pp. 291-315). Cambridge: Cambridge University Press.

von Rintelen T, Wilson AB, Meyer A, Glaubrecht M. (2004). Escalation and trophic specialization drive adaptive radiation of freshwater gastropods in ancient lakes on Sulawesi, Indonesia. Proc Biol Sci, 271(1557), 2541-2549. doi: 10.1098/rspb.2004.2842

Wallace AR. (1869). The Malay Archipelago: re-printed by Penguin Classic.

Wang Y, Cheng H, Edwards RL, Kong X, Shao X, Chen S, Wu J, Jiang X, Wang X, An Z. (2008). Millennial- and orbital-scale changes in the East Asian monsoon over the past 224,000 years. Nature, 451(7182), 1090-1093. doi: 10.1038/nature06692

Watkinson IM, Hall R. (2016). Fault systems of the eastern Indonesian triple junction: evaluation of Quaternary activity and implications for seismic hazards. In: Cummins PR, Meilano I (Eds.) Geohazards in Indonesia: Earth Science for Disaster Risk Reduction. (Vol. 441, pp. 71-120). London, UK: Geological Society, London, Special Publications.

Williams DF, Peck J, Karabanov EB, Prokopenko AA, Kravchinsky V, King JW, Kuzmin MI. (1997). Lake Baikal Record of Continental Climate Response to Orbital Insolation During the Past 5 Million Years. Science, 278, 1114-1117. doi: 10.1126/science.278.5340.1114

Zolitschka B, Francus P, Ojala AEK, Schimmelmann A. (2015). Varves in lake sediments - a review. Quaternary Science Reviews, 117, 1-41. doi: 10.1016/j.quascirev.2015.03.019

CHAPTER 2

Climatic and tectonic controls on source-to-sink processes in the tropical, ultramafic catchment of Lake Towuti, Indonesia

Marina A. Morlock, Hendrik Vogel, Valentin Nigg, Luis Ordoñez, Ascelina K. M. Hasberg, Martin Melles, James M. Russell, Satria Bijaksana & the TDP Science Team

published in the Journal of Paleolimnology

CHAPTER 3

Long-term tectonic basin evolution and associated changes in catchment dynamics and depositional environments in tropical Lake Towuti, Indonesia

Marina A. Morlock, Hendrik Vogel, Daniel Ariztegui, Martin Melles, James M. Russell, Satria Bijaksana & the TDP science team

manuscript in preparation

CHAPTER 4

Temporal and spatial variability of siderite formation in ferruginous sediments

Marina A. Morlock, Hendrik Vogel, Jebril Hadi, Anneleen Foubert, Daniel Ariztegui, Martin Melles, James M. Russell, Satria Bijaksana & the TDP science team

under review in Geology

CHAPTER 5

Sedimentation processes in tropical Lake Towuti: Palaeoenvironmental insights from end-member modelling of high-resolution XRF core-scanning data

Marina A. Morlock, Hendrik Vogel, James M. Russell, Martin Melles & Satria Bijaksana

manuscript in preparation

Chapter 2

Climatic and tectonic controls on source-to-sink processes in the tropical, ultramafic catchment of Lake Towuti, Indonesia

Marina A. Morlock, Hendrik Vogel, Valentin Nigg, Luis Ordoñez, Ascelina K. M. Hasberg, Martin Melles, James M. Russell, Satria Bijaksana & the TDP Science Team

published in the Journal of Paleolimnology, 2018

2. Climatic and tectonic controls on source-to-sink processes in the tropical, ultramafic catchment of Lake Towuti, Indonesia

Marina A. Morlock[1,*], Hendrik Vogel[1], Valentin Nigg[1], Luis Ordoñez[2], Ascelina K. M. Hasberg[3], Martin Melles[3], James M. Russell[4], Satria Bijaksana[5] & the TDP Science Team

[1]*Institute of Geological Sciences and Oeschger Centre for Climate Change Research, University of Bern, 3012 Bern, Switzerland*
[2]*Department of Earth Sciences, University of Geneva, 1205 Geneva, Switzerland*
[3]*Institute of Mineralogy and Geology, University of Cologne, 50674 Cologne, Germany*
[4]*Department of Earth, Environmental, and Planetary Sciences, Brown University, Providence RI 02912, USA*
[5]*Faculty of Mining and Petroleum Engineering, Institut Teknologi Bandung, Bandung 40132, Indonesia*

**corresponding author: marina.morlock@geo.unibe.ch*

Journal of Paleolimnology, 2018 (online first), doi: 10.1007/s10933-018-0059-3

2.1 Abstract

Humid tropical landscapes are subject to intense weathering and erosion, which strongly influence sediment mobilisation and deposition. In this setting, we aimed to understand how geomorphology and hydroclimate altered the style and intensity of erosion and sediment composition in a tropical lake and its tectonically active catchment. Lake Towuti (2.75°S, 121.5°E) is one of the oldest and deepest lakes in Indonesia, with uninterrupted lacustrine sedimentation over several glacial-interglacial cycles. Here we present results from a novel set of Lake Towuti surface sediment, bedrock and soil samples from the catchment, and two existing sediment cores that extend to 30,000 and 60,000 years before present. We studied the catchment morphology, soil properties, geochemistry, and clay and bulk mineralogy. Results from several river long profiles show clear signs of tectonic activity, which enhances river incision, favours mass movement processes, and together with remobilisation of fluvial deposits, strongly influences modern sedimentation in the lake. Material from the Mahalona River, the lake's largest inflow, dominates modern sediment composition in Towuti's northern basin. The river transports Al-poor and Mg-rich sediments (mainly serpentines) to the lake, indicating river incision into the Mg-rich serpentinised peridotite bedrock. Relatively small, but important additional contributions of material, come from direct laterite-derived input and the Loeha River, which both provide Al-rich and Mg-poor sediment to the lake. Over time, the Al/Mg and kaolinite-to-serpentine ratios varied strongly, primarily in response to lake-level fluctuations driven by hydroclimatic changes. In the past 60,000 years, both the Al/Mg and kaolinite-to-serpentine ratios showed variations sensitive to changes in climate boundary conditions across glacial-interglacial cycles, while tectonic activity had less influence on changes in sediment composition on these short time-scales.

Keywords Laterite, Erosion, Hydroclimate, Lake Towuti, Lake level, Tropical palaeoclimate

2.2 Introduction

In the humid tropics, intense weathering results in a thick soil cover that is very susceptible to erosion by mass-wasting and high rainfall events. Soils provide an important resource for economic development in many (tropical) countries, both for agricultural use and mineral exploitation (U.S. Geological Survey 2017). Specifically, laterites are autochthonous weathering products characterised by high concentrations of immobile elements such as Fe and Al in the upper soil horizons (Widdowson 2007). There are several studies of laterite properties in tropical Africa (Ogunsanwo 1988; Omotoso et al. 2012; Adunoye 2014), but there is little known about how laterite properties influence erosion and sedimentary processes. Similarly, although a number of studies described the laterization of ultramafic bedrock (Golightly and Arancibia 1979; Colin et al. 1990; Brand et al. 1998; Sagapoa et al. 2011; Marsh et al. 2013), these studies often focused on ore exploration. The interaction between climate, soil properties, catchment geomorphology, and sedimentary processes has rarely been explored in laterite landscapes, and in the humid tropics in general.

Equatorial Lake Towuti (2.75°S, 121.5°E, 560 km^2, ~200 m maximum water depth; Figure 2.1) is one of the oldest lakes in Indonesia (Von Rintelen et al. 2012). The catchment geology consists of dunites, lherzolites, and harzburgites of the East Sulawesi Ophiolite complex (Kadarusman et al. 2004), upon which thick laterites have developed. Particles and solutes delivered to the lake are exceptionally rich in iron, but very poor in sulphur and macronutrients, setting the stage for unusual biogeochemical cycles, ultraoligotrophy, and a highly adapted, mostly endemic lake fauna and flora (Haffner et al. 2001; Crowe et al. 2008; Von Rintelen et al. 2012). Most of the lake is surrounded by dense, closed-canopy rainforest; however, based on satellite images, ~25 % of the lake catchment is now deforested as a consequence of anthropogenic activities. Previous studies of Lake Towuti suggest that during the past 60,000 years, hydrologic changes driven by changing global climate boundary conditions had large impacts on lake sedimentation (Russell et al. 2014; Vogel et al. 2015). Lake-level lowstands were accompanied by delta progradation into the deeper basins, which favours lateral transport processes relative to pelagic sedimentation (Vogel et al. 2015). This change in depositional modes leads to coarser-grained sediments in the deeper basins and associated changes in mineralogy (Weber et al. 2015; Goudge et al. 2017). In 2015 the International Continental Scientific Drilling Program (ICDP) Towuti Drilling Project (TDP) recovered cores through the entire sediment infill of Lake Towuti, which record uninterrupted lacustrine sedimentation over several glacial-interglacial cycles (Russell et al. 2016).

We carried out novel analyses of bedrock and soil samples from Lake Towuti's catchment, along with geomorphological analyses, to characterise and understand modern source-to-sink processes around this tropical lake system. We analysed the inorganic geochemistry, clay and bulk mineralogy, and sedimentological characteristics of bedrock, soils, and lake surface sediment and core samples to disentangle the effects of climatic and tectonic processes and their influence on erosion and sedimentation. We applied this understanding to interpret mineralogical and geochemical variations in two sediment cores that extend 30 and 60 kilo years before present (kyr BP). This study links

modern sedimentation processes to existing and new palaeoclimate reconstructions from Lake Towuti to better understand modern tropical lake systems and how such systems change under different climate boundary conditions. Such a study is timely, given the unprecedented rates of anthropogenically induced change that tropical regions are currently undergoing.

2.2.1 Hydrologic setting

Lake Towuti is part of the Malili Lake System, a chain of five tectonic lakes located on the island of Sulawesi, Indonesia (Figure 2.1). The lake receives annual precipitation of ~2700 mm, with peak rainfall (~330 mm/month) in austral autumn (MAM), and comparatively dry (~140 mm/month) austral spring months (ASO; Konecky et al. 2016). Lake Towuti is a hydrologically open lake with one outflow, the Larona River (Figure 2.1C). The lake is split into two connected major basins to the north and south (Figure 2.1C and Figure 2.2), which are separated by bedrock highs above and below the current water surface (Vogel et al. 2015; Russell et al. 2016). To the north, the lake is connected to upstream Lakes Matano and Mahalona via the Mahalona River (Figure 2.1D), which dominates water and sediment input to Towuti's northern basin (Costa et al. 2015). The large catchment of the Mahalona River includes the Lampenisu River catchment, which is characterised by Quaternary alluvium and partly serpentinised peridotites. Together, the two rivers comprise 25 % (293 km^2) of the catchment area of Lake Towuti, excluding the catchments of Lakes Matano and Mahalona. Despite severe drying during the last glacial maximum (Russell et al. 2014) and associated lake-level lowstands, the lake remained hydrologically connected to upstream lakes via the Mahalona River throughout the last 60,000 years (Costa et al. 2015). Lake Towuti's southern basin has four prominent inflows. The Loeha River drains a catchment hosting metasedimentary rock to the east of the lake, the only source of felsic minerals in the catchment of Lake Towuti (Figure 2.1B and D, Costa et al. 2015). Three rivers at the southern tip of the lake jointly drain 10 % of the lake's catchment and are underlain by ultramafic rocks. Lake Towuti's western and northeastern shores are dominated by steep slopes and densely vegetated catchments with no major permanent river drainage (Figure 2.1D).

2.3 Materials and methods

2.3.1 Geotechnical and geomorphological analysis

River and catchment morphology were analysed using a digital elevation model (DEM) of the Lake Towuti region. The DEM is based on data from NASA's Shuttle Radar Topography Mission at 1 arc-second (30 m) spatial resolution (available at: http://earthexplorer.usgs.gov, last accessed: February 09 2017). Rivers and catchment boundaries were identified using the hydrology toolset in ArcGIS 10.1 (Esri, USA). Catchment sizes, river lengths, trunk channel relief, and long profiles were calculated based on this DEM data set.

In total, 18 bedrock samples (from 12 locations) and 6 laterite profiles (21 samples) were collected in May-July 2015 (Figure 2.1C). Samples cover varying degrees of serpentinisation of the peridotite bedrock and represent all the vertical zones of the laterites. Because of accessibility, all samples were taken northwest of the lake (Figure 2.1C). Representative laterite samples, formed on serpentinised and non-serpentinised

peridotites, were dried at 110°C overnight and their plasticity index (I_p), grain-size distributions, soil cohesion (c), and friction angle (angle of internal friction φ) were determined at the geotechnical laboratory of the Bern University of Applied Sciences in Burgdorf, Switzerland. Grain-size data were acquired following Swiss norms SN 670 816a and SN 670 902-1. Samples were treated with 15 ml $Na(PO_3)_6$ for 24 h before settling, wet, and dry sieving. The resulting grain-size distribution curves were categorized following the Unified Soil Classification System and corresponding geotechnical parameters were selected according to Swiss Norm SN 670 010. The parameters φ and c were determined in repeated direct shearing tests, for which varying loads (20, 40, and 80 kN) were applied to the samples for 20 h before samples were sheared at a rate of 1 mm per minute under undrained conditions (German Industrial Norm DIN 18137-1 and DIN 18137-3). To calculate the plasticity index, plastic and liquid limits of samples were determined following Swiss Norm SN 670 345b, which follows Casagrande (1932).

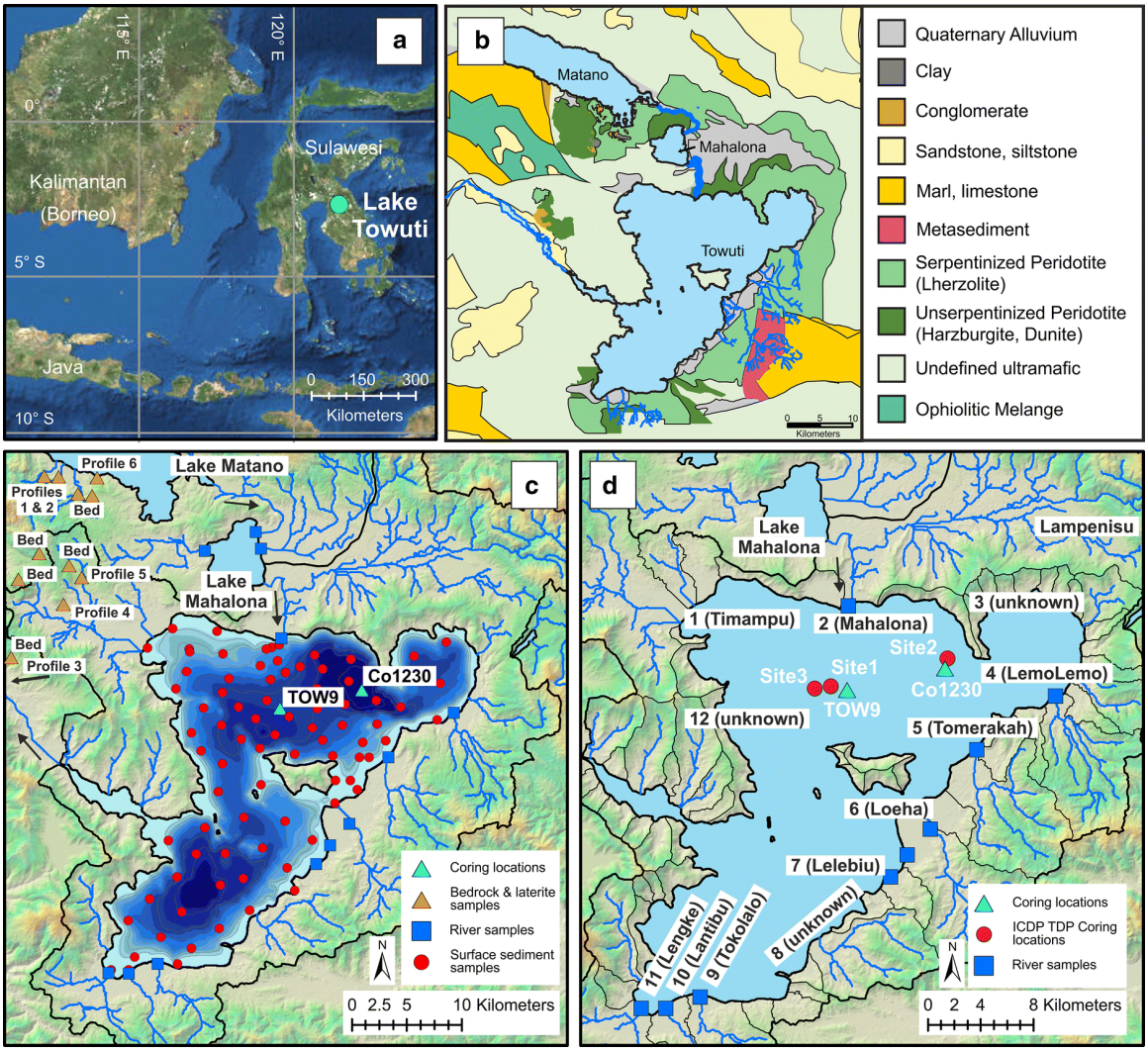

Figure 2.1 a) Location of Lake Towuti on the island of Sulawesi, Indonesia. b) Geologic map of the Malili lake system with Lake Towuti and upstream Lakes Mahalona and Matano, modified after Costa et al. (2015). c) Map of the sampling locations around Lake Towuti; data for river bedload (squares) from Costa et al. (2015). d) Map of Lake Towuti, with river names and sampling locations. Red circles indicate the three coring sites of the ICDP Towuti Drilling Project

2.3.2 Surface sediment collection and sediment coring

In 2015, 84 surface sediment samples from across the entire lake were recovered from water depths between 2.8 and 195.5 m with a grab sampler. Samples integrate the uppermost 3-5 cm of recovered sediment, representing 200-250 yr of sediment accumulation in the deep basins (Russell et al. 2014; Vogel et al. 2015). Core Co1230 (19.8 m long, base ^{14}C-dated to 27 kyr BP) was recovered from a distal position to the Mahalona River Delta in the northern basin at ~203 m water depth in 2010 (Vogel et al. 2015). Core IDLE-TOW10-9B-1K (hereafter TOW9) was recovered from 154 m water depth. This 11.5-m core was dated to ~45 kyr BP by ^{14}C dating at 8.95 m depth, and the sedimentation rate over this interval was extrapolated to an age of 60 kyr BP for the core base (Russell et al. 2014).

2.3.3 Geochemistry and grain size

The geochemical composition of bedrock, laterite, lake surface sediment samples, and sediment samples from core Co1230 was determined by inductively coupled plasma mass spectrometry (ICP-MS) after full acid digestion (HF, HCl, HNO_3, $HClO_4$) of the samples at the Activation Laboratories Ltd. in Ontario, Canada. Because detection limits were reached for many elements in bedrock and laterite samples, these samples were also measured with wavelength dispersive X-ray fluorescence (WD-XRF), and results are reported for concentrations of K, Mg, Cr, and Ni. For WD-XRF analysis, samples were ground in an oscillating tungsten-carbide mill, dried in an oven at 100°C for 12 h, and heated to 1050°C for two hours. Of the burnt rock powder 1.2121 g were mixed with 6.0000 g of lithium-tetraborate ($Li_2B_4O_7$), placed in a Pt-Au crucible and melted in a Bead Machine (Perl X'3) at 1250°C. Major element concentrations were analysed on a Philips PW2400 WD-XRF spectrometer at the University of Lausanne, Switzerland. The lower detection limit is 0.01 weight-% (wt-%) for all elements. The geochemical composition of the bedload of eight rivers is available from Costa et al. (2015), and Goudge et al. (2017) provide grain-size specific chemical and mineralogical data on bedload and suspended load for the Mahalona River. Geochemistry of sediment core TOW9 is available from Russell et al. (2014).

Based on the ICP-MS measurements, we calculated the Chemical Index of Alteration (CIA) of Nesbitt and Young (1982) as a measure of the degree of chemical weathering of different samples. The index is based on the relative accumulation of the less mobile Al_2O_3 relative to more easily soluble Na_2O, K_2O, and $CaO_{silicate}$ in a weathered substrate, e.g. bedrock, soil or sediment. Because calcareous rocks are largely absent in the catchment of Lake Towuti and petrographic observations do not indicate the presence of detrital $CaCO_3$, we assumed all CaO in the system is derived from silicate rocks ($CaO_{silicate}$). Grain-size measurements of sediment core Co1230 are available from Vogel et al. (2015), who analysed the samples on a laser diffractometer (Malvern Mastersizer 2000S). The grain-size distribution of lake surface sediments was measured at the University of Cologne, Germany, with a Beckman Coulter LS13320 laser diffractometer. Samples were treated with 15 ml H_2O_2 (30 %), 10 ml HCl (10 %) and NaOH (1 M) prior to analysis.

2.3.4 Bulk and clay mineralogy

One representative laterite profile over both serpentinised and unserpentinised peridotite bedrock, respectively, was analysed for bulk mineralogy by x-ray diffraction (XRD) on a PANalytical Cubix^3 goniometer with a Cu-tube and a monochromator (45 kV, 40 mA, 5-60° 2θ). The bulk mineralogy of a lake surface sediment transect from the Mahalona River mouth to coring site TOW9 was determined by XRD on a PANalytical X'Pert Pro with a Cu X-ray tube (40 kV, 40 mA, 5-60° 2θ). Prior to analysis, freeze-dried samples were mixed and homogenized with 10 wt-% LiF to provide a standard for peak integration and quantification. Additionally, thin sections of bedrock and saprolite zone samples were examined with a polarizing light microscope.

Clay mineralogical analyses were performed on all sediment samples. The <2-µm size fraction (clay size) was separated from the sample by Atterberg separation (Robinson 1922; ~0.5 g of sample, 4.5-h settling time, 6-cm settling height, 21°C). For XRD analyses on oriented clay mounts, the clay fraction was added to three glass plates and dried overnight. One glass plate was measured immediately on a Phillips PW1830 Goniometer (40 kV, 30 mA, 2-40° 2θ), another plate was kept in an ethylene-glycol-saturated atmosphere for at least 48 h prior to measurement, and one plate was heated at 550°C for 1.5 h before measurement (Supplementary Material [SM] Figure S2.1A). By comparing the three treatment spectra, we identified characteristic peaks for smectites (5.2° 2θ), illite (8.8° 2θ), serpentines (12.24° 2θ), and kaolinite (12.5° 2θ) in the ethylene-glycol-saturated spectrum (SM Figure S2.1A). Kaolinite and serpentine peaks were separated using peak separation software (MacDiff, R. Petschick, Frankfurt, Germany, 2001), the output being peak height in absolute counts. Only selected XRD measurements were done for the highly cemented laterite samples. To further evaluate the interpretation and separation of kaolinite from serpentine minerals by XRD analysis, clay separates of core Co1230 and all bulk samples were also measured by mid-infrared (MIR) Fourier-Transform-Infrared-Spectroscopy (FTIRS). For this, 0.011 ±0.0001 g of freeze-dried material was mixed with 0.5 ±0.0005 g of spectroscopic grade KBr and homogenised for at least three minutes. FTIRS analyses were performed at the University of Bern, Switzerland, using a Bruker Vertex 70 equipped with an HTS-XT accessory unit, a liquid nitrogen cooled MCT (Mercury-Cadmium-Telluride) detector, and a KBr beam splitter, in the wavenumber range 3750-520 cm^{-1} at a resolution of 4 cm^{-1}. All measurements were performed in diffuse reflectance mode. Several mineral-characteristic absorbance peaks appear as prominent features in the Towuti samples. Diagnostic peaks for kaolinite were centred at 692, 913, 3620 cm^{-1}, caused by translational, librational, and stretching vibrations of OH groups, respectively, in kaolinite group minerals (Chester and Elderfield 1973; Farmer 1974; Madejová 2003; Chukanov 2014). Identified absorbance peaks diagnostic for serpentine group minerals were centred at 640, 958, and 3685 cm^{-1}, caused by bending, libration, and stretching vibrations of OH, respectively (Farmer 1974; Madejová 2003; Chukanov 2014). Peak integrals of diagnostic peaks are highly correlated for the individual mineral groups, emphasizing that absorbance in the analysed regions is diagnostic for the respective mineral group, without significant bias from other phases absorbing in the same region (Chester and Elderfield 1973). For further analysis, peak areas with highest correlation to clay XRD and geochemical composition were chosen. These were peaks at wavenumbers 900.8-924.6 cm^{-1} for kaolinite and 3674.9-3694.2 cm^{-1} for serpentine.

2.3.5 Statistics and data analysis

All statistical analyses were performed in R (R Development Core Team 2008). For Pearson correlation tests, normality of the variables was tested with the Shapiro-Wilks test. If the data were not normally distributed, Spearman's rank correlation was used to test for correlations. Statistical parameters are given as mean and one standard deviation. All maps were created in ArcGIS 10.1 (Esri, USA). Unless otherwise stated, interpolation of the surface sediment measurements is based on Kriging (Gaussian process regression) with a fixed radius of 5 km and a minimum of 5 data points used for calculations. Raster size is 50 x 50 m. A geometrical classification was chosen for data visualisation.

2.4 Results

2.4.1 Catchment morphology

The three connected lakes of the Malili Lake System (excluding its two satellite lakes) drain a hydrologic catchment area of 2430 km^2. Upstream lakes and their surroundings account for a catchment area of 1286 km^2. We assume that Lakes Matano and Mahalona function as sediment traps, providing water, but little sediment, leaving an area of 1144 km^2 to supply the majority of sediment to Lake Towuti (SM Table S2.1). Rivers drain 86 % of Towuti's catchment (excluding upstream lake catchments), whereas 14 % of the area may be drained by surface runoff and/or ephemeral streams, or is left undrained. The catchments around Lake Towuti have mean slope angles between 13.1° and 16.8° (Figure 2.2, SM Table S2.1). The trunk channel relief (as defined by Whipple et al. 1999) varies between 150 and 680 m over distances from 5 to 43 km. Excluding the catchments that feed into upstream Lakes Matano and Mahalona, the Mahalona River drains the largest catchment (293 km^2 catchment size, 43 km length, 14.5° average catchment slope), the majority of which consists of the Lampenisu River, followed by the Timampu River (141 km^2 catchment size, 18 km length, 13.1° average catchment slope) and the Loeha River (84 km^2 catchment size, 21 km length, 15.5° average catchment slope). Several knickpoints are present in the river courses to the east of Lake Towuti (Figure 2.2). Most prominent, the Loeha River drops by 400 m over a distance of 2.5 km (average river slope 9.1°). Along the Lampenisu River profile, the Matano Fault, a highly segmented, sinistral strike-slip fault with an extensional component (Watkinson and Hall 2016), creates an elevation offset of about 50 m over a distance of 400 m (average river slope 7.1°), which is also clearly visible in an abrupt change of slope angle in the northern part of the Lampenisu River catchment (Figure 2.2). Rivers to the south and northwest have well-developed river profiles. The three major rivers, the Mahalona (north), Loeha (east), Timampu (northwest), and the southernmost rivers, have wide alluvial plains in their lower course. Observations during fieldwork in 2015 indicated that the rivers on these alluvial plains presently cut into fluvial gravel deposits and have wide stream channels with exposed gravel bars along both sides of the active channel.

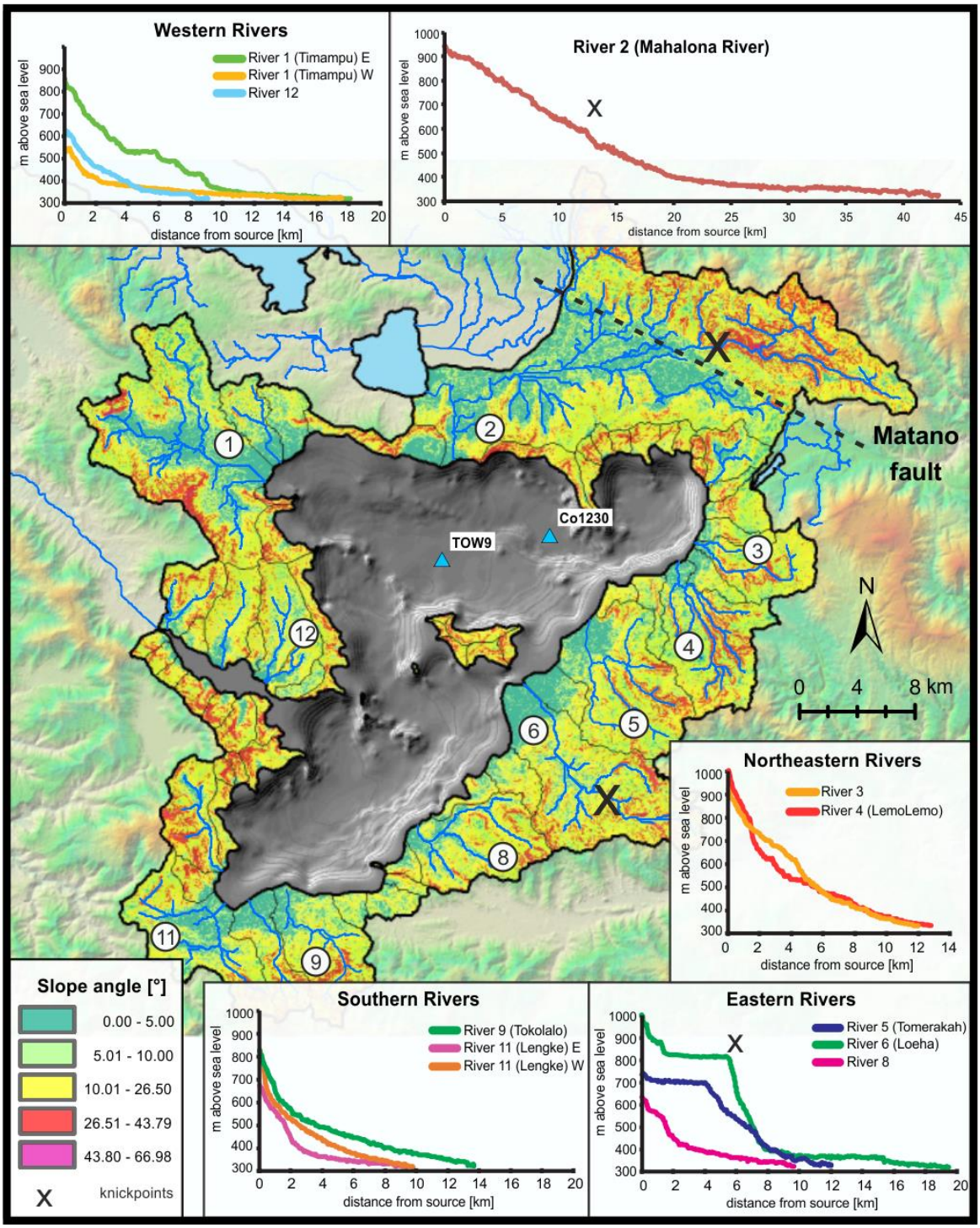

Figure 2.2 Slope angles [°] in the Lake Towuti catchment. Colour classification is partly based on the critical angle of internal friction as determined in direct shearing tests on the sampled laterite material (26.5° and 43.79° for upper and lower laterite horizons, respectively). Slope data are based on the DEM. Insets: Long profiles of all major rivers flowing into Lake Towuti. Profiles are based on DEM analysis and were computed by the ArcGIS 10.1 hydrology toolset

2.4.2 Laterites

The six laterite profiles investigated (Figure 2.3 and SM Figure S2.2) varied in thickness between 2 and 6 m and show a clear colour zonation with the uppermost horizon characterised by dark red material (approximately 0.2-1 m thick, 6 samples). Going deeper, this grades into a lighter red colour (0-1 m thick, 5 samples), followed by a yellow intermediate zone (1-2 m thick, 7 samples), then a green-grey-coloured saprolite zone (0.5-3 m thick, 5 samples) just above the unweathered parent rock. The colour zonation is very clearly reflected in elemental gradients, which are similar in soil profiles over varying degrees of bedrock serpentinisation (Figure 2.3, SM Figure S2.2 and Table S2.2). In the laterites, Al, Fe, Ti, K, Cr, Zr, Zn, and Mn are enriched relative to the saprolite and bedrock, peaking in the red rather than the uppermost dark red zone (Figure 2.3 and SM Figure S2.2). In contrast, Mg and Ca have the highest concentrations in the saprolite and bedrock, and decrease markedly upwards in the laterite (Figure 2.3 and SM Figure S2.2). Nickel concentrations peak in the saprolite zone with an average concentration of 1.5 ±1.1 %. Laterite profiles 1, 3, and 4 are located on slopes and coarse pebbles were visible in the dark red matrix of the uppermost zone, but the pebbles were not included in the samples used for analysis. Average concentrations of Al ranged from 4.3 ±1.2 % in the uppermost dark red horizon to 0.9 ±0.9 % in the bedrock. Likewise, Fe (dark red zone: 32.8 ±15.8 %; bedrock: 5.8 ±0.3 %) and Ti (dark red zone: 0.1 ±0.06 %; bedrock: 0.03 ±0.05 %) were concentrated in the laterite relative to unweathered bedrock. Mg concentrations increased from 6.8 ±6.5 % in the uppermost horizon to 39.3 ±6.3 % in the bedrock. The CIA shows strongly increasing values from bedrock (mean 33.6 ±15.3) to the overlying laterite (mean 94.0 ±9.1).

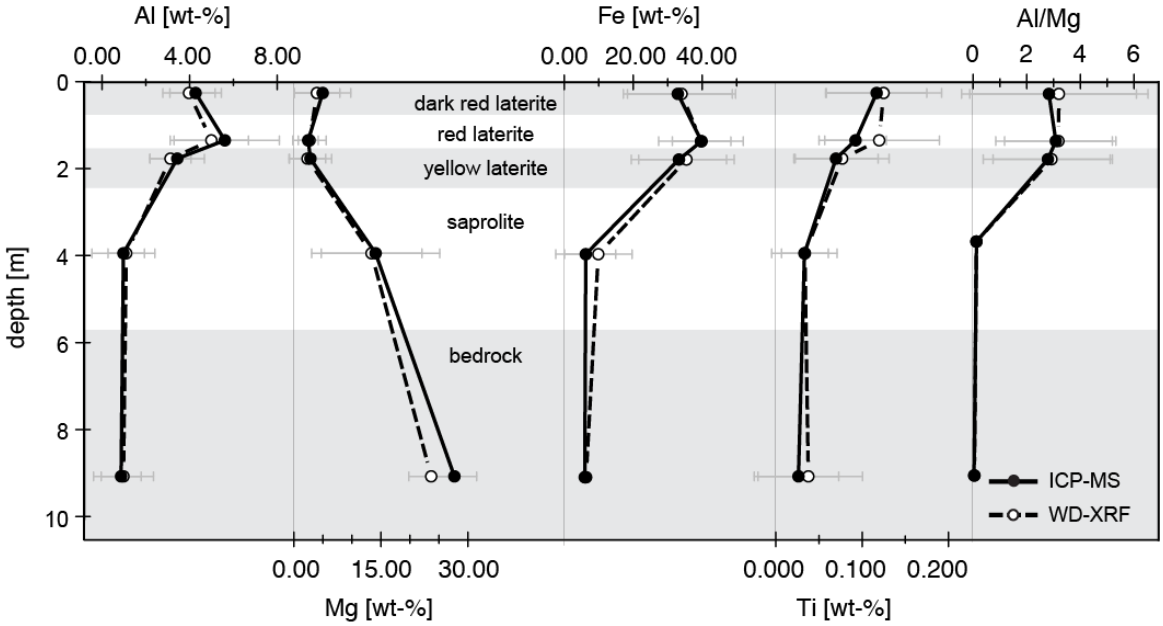

Figure 2.3 Average element concentrations of six laterite profiles (for data from individual profiles, see SM Figure S2.5). Depth is the average depth of each of the five zones. Error bars correspond to ± one standard deviation

Bulk XRD and thin section analyses show that unserpentinised rocks consist of olivine (>60 %), clino- and orthopyroxenes (diopside and enstatite, 10-25 %), and small amounts (<5 %) of accessory minerals such as magnetite, illmenite, amphiboles, and

goethite. Parts of the bedrock have undergone secondary serpentinisation close to the surface (SM Figure S2.3A). The main mineral phases in serpentinised samples are chrysotile and antigorite, with small amounts of magnetite and chlorite. In places, initially serpentinised peridotites have undergone a second alteration to form very fine-grained olivine and amphiboles (tremolite). In the weathering crust of the bedrock samples, serpentine and magnetite rinds are observed around disintegrating olivine grains (SM Figure S2.3C). Small amounts of (clino)pyroxenes and amphiboles remain present in the saprolite and lower laterite zone. Veins in the saprolite and laterite are filled with very fine-grained secondary quartz crystals (SM Figure S2.3B). In the laterite horizons, goethite is the dominant mineral phase (SM Figure S2.4), and smectites are present in the yellow laterite horizon (SM Figure S2.4). FTIR spectroscopy further indicates the presence of kaolinite in the upper laterite horizons, whereas serpentines are more common in the lower laterite and saprolite zone (SM Figure S2.2C).

Geotechnical parameters of the laterites are summarised in SM Figure S2.5. Grain-size distribution curves are classified as silt with sand (ML) for sample Lat 8 a+b (profile 4, red and yellow laterite zone), elastic silt (MH) for sample Lat 9 b+c (profile 5, red and yellow laterite zone), silty sand (SM) for sample Lat 10 b+c and Sap 3 (profile 6, red laterite zone, and profile 2, saprolite zone, respectively), and elastic silt with sand (MH) for sample Lat 10 d+e (profile 6, yellow laterite zone). Coarse fractions (>0.063 mm) of all five samples are dominated by magnetite grains, with occasional quartz and metal oxide concretions. The internal angles of friction (φ) for samples Lat 10 b+c (red laterite horizon) and 10 d+c (yellow laterite horizon) are 43.8° and 26.5°, respectively, with material density of 2.3 and 1.5 g cm^{-3}, respectively. The φ-angles based on classification of grain size distribution curves are 34° in the saprolite zone, 25-28° in the lower (lower red and yellow zone combined), and 33.6° in the upper laterite (dark red and upper red zone combined) horizons. Plasticity indices (I_P) are around 5 % in the upper laterite horizon and saprolite zone, and 20-35 % in the lower laterite horizon. Water content is 9.8 % in the saprolite zone, between 44.3 and 104.2 % in the yellow laterite horizons, and 17.9 % in the red laterite horizon.

2.4.3 Lake surface sediments

Lake surface sediments close to the Mahalona River inflow are characterised by high Mg concentrations, whereas Al, Ni, and Fe concentrations are low (Figure 2.4 and SM Figure S2.6). This pattern decreases with increasing distance from the river mouth. Similarly, sediments at the southern tip of the lake are depleted in Al and Ti, and enriched in Mg (Figure 2.4). In general, coarser-grained samples show a closer resemblance to bedrock samples, whereas the elemental composition of fine-grained samples is more similar to the composition of the laterites (Figure 2.4 and SM Figure S2.6). The lake surface sediments have a mean CIA of 79.3 ±8.6. Values are lowest close to the inlets of the Mahalona and Loeha Rivers (CIA < 70), and peak in the northeast and south of the lake (CIA >85; SM Figure S2.6B). Delta sediments of the Loeha River are characterised by low concentrations of Ni, Cr, Co, and Fe and high concentrations of K, Ti, Al, Sb, and Sr (Figure 2.4, SM Figure S2.6, and Hasberg et al. 2018). Except for isolated patches close to shore, e.g. close to the Mahalona River inflow, Al, Ni, and Ti concentrations are mostly homogenous across the lake (Figure 2.4 and SM Figure S2.6). Ca and Mg concentrations are generally higher in the northern (Ca: 0.72 %; Mg: 7.13 %) compared to the southern (Ca: 0.45 %; Mg: 5.33 %) lake basin.

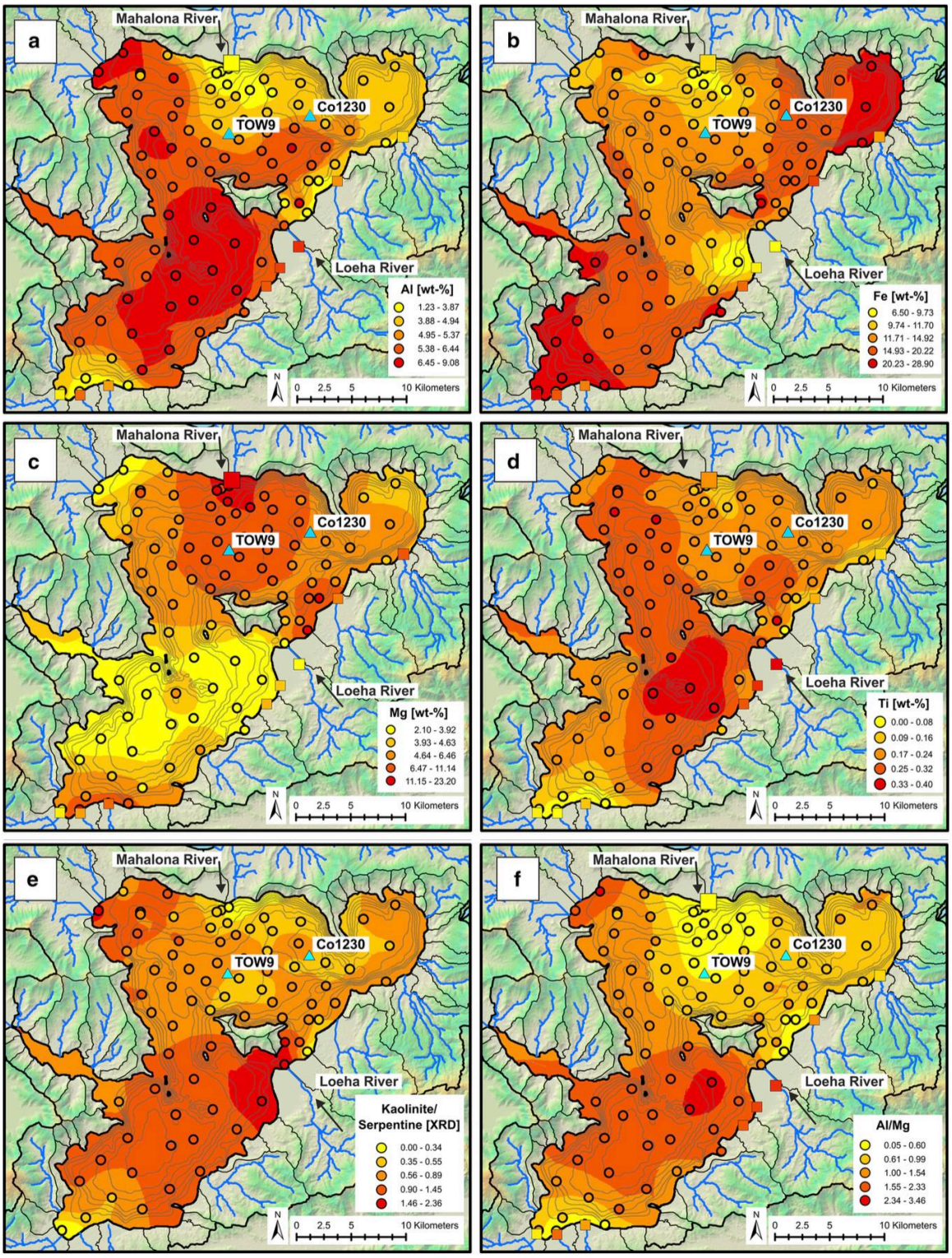

Figure 2.4 a-d) Element concentrations of Al, Fe, Mg, and Ti determined by ICP-MS e) kaolinite-to-serpentine ratio determined by clay XRD and f) Al/Mg ratio determined by ICP-MS on 84 surface sediment samples, indicated by colour-coded circles. Background colouring is based on kriging interpolation of the surface sediment measurements. Grey lines represent the lake bathymetry with a 20-m line spacing (maximum water depth is ~200 m), data for river bedload (squares) from Costa et al. (2015), symbol size is scaled to catchment size (no data available for clay minerals)

The kaolinite-to-serpentine ratio is high in sediments off the Loeha River inflow and in areas without significant riverine runoff, whereas values are lower close to the Mahalona River and at the inflow of the southernmost rivers (Figure 2.4E and SM Figure S2.6G). Clay mineralogical analysis shows general agreement between XRD results of the clay fraction (peak height) and bulk MIR-FTIRS measurements (peak area) for kaolinite and serpentine (Pearson correlation r=0.50, and Spearman's rank correlation r=0.69, respectively, p<0.01, n=79, SM Figure S2.1), and also between clay XRD results and Al and Mg concentrations in the bulk sediment (Pearson correlation r=0.56, and Spearman's rank correlation r=0.64, respectively, p<0.01, n=79, SM Figure S2.1). Bulk XRD analyses show a decrease in serpentines and amphiboles and an increase in quartz content (SM Figure S2.7) with distance from the Mahalona River, indicating that key elements are related to main mineral composition. The smectite-to-illite ratio is generally lower in the southern lake basin, especially around the Loeha River, whereas smectite is enriched relative to illite in the northern basin (SM Figure S2.6H).

2.4.4 Sediment cores

Coring location Co1230 is more heavily influenced by hyperpycnal flows and turbidite deposition from the Mahalona Delta compared to coring location TOW9 (Vogel et al. 2015). The fine-grained pelagic sediments of the two cores, however, show very similar trends in their geochemical composition. The Al/Mg ratio is low in the middle to late Holocene (6-4 kyr BP), between 27 and 15 kyr BP, and prior to 58 kyr BP (TOW9 only, Figure 2.5A). High Al/Mg values occur at 2 and 13-11 kyr BP, between 41-32 kyr BP, and at 55 kyr BP. Ti concentrations show a similar pattern, which is overlain by an overall decreasing trend from 55 to 15 kyr BP (Figure 2.5B, Russell et al. 2014).

Kaolinite and serpentine measured by clay-size MIR-FTIRS (band depth) and clay XRD (peak height) in Co1230 are strongly correlated (Pearson correlation r=0.77, and r=0.73, respectively, p<0.01, n=14, SM Figure S2.1), as are clay XRD kaolinite and serpentine with concentrations of bulk Al and Mg (Pearson correlation r=0.71, and r=0.87, respectively, p<0.01, n=15, SM Figure S2.1). Core TOW9 shows coherent trends in clay XRD kaolinite and serpentine and concentrations of Al and Mg over the past 60 kyr (Figure 2.5A and C), but clay XRD and geochemical concentrations were not determined on the same sediment horizons, precluding analysis of correlation. The kaolinite-to-serpentine ratio is generally higher between 55 and 27 kyr BP compared to 27-0 kyr BP and prior to 58 kyr BP. For the past ~40 kyr, a similar pattern appears for kaolinite and serpentine, determined by near-infrared spectroscopy on other sediment cores from Towuti's northern basin (Goudge et al. 2017).

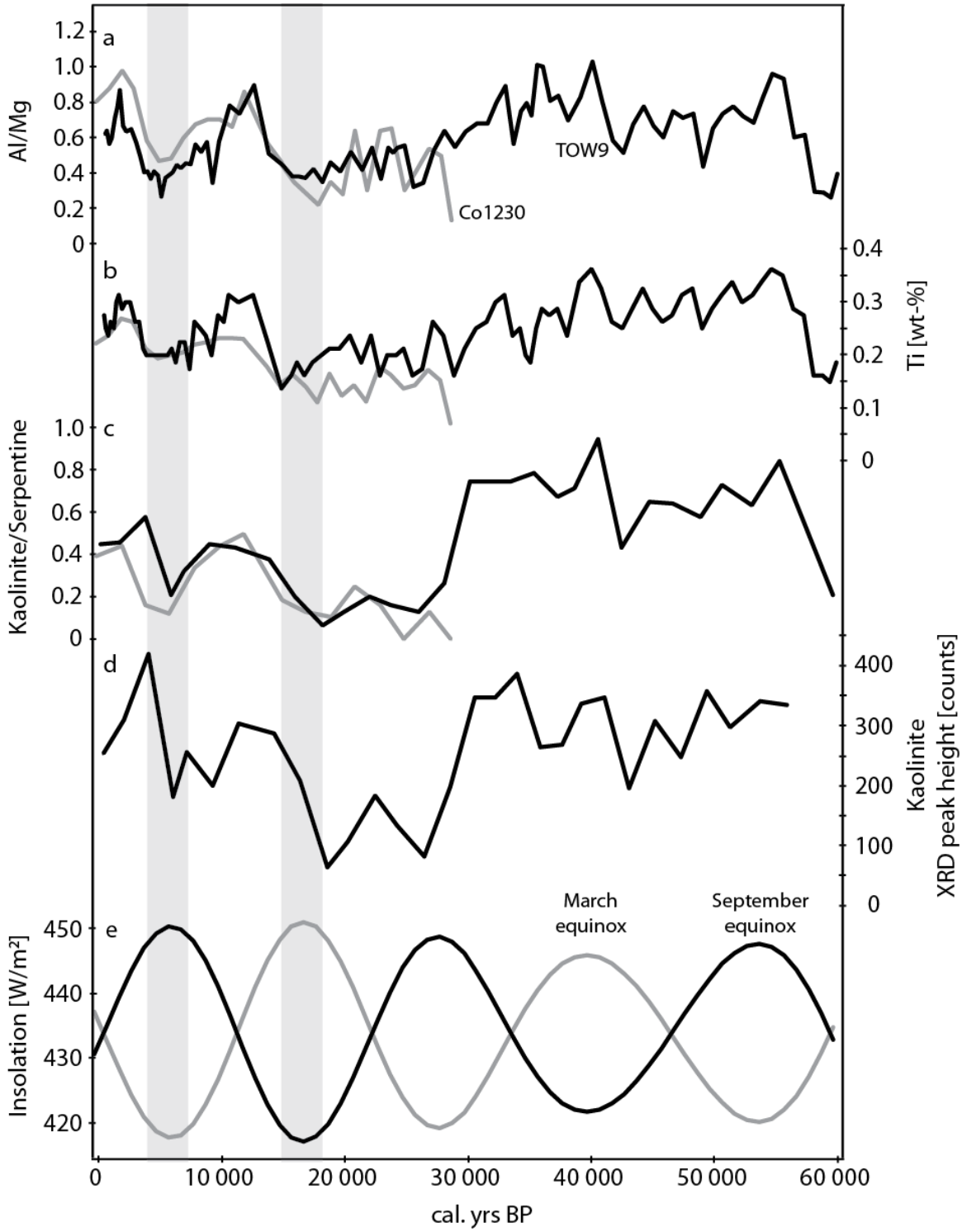

Figure 2.5 a) Al/Mg ratio, b) Ti concentrations, c) kaolinite-to-serpentine ratio, and d) kaolinite content determined by clay XRD, of the two sediment cores, Co1230 and TOW9. The cores are located close to the two main sites of the ICDP Towuti Drilling Project (Figure 2.1D). e) Mean daily insolation for March and September equinoxes at 2°S

2.5 Discussion

2.5.1 Weathering and erosion processes in Lake Towuti's catchment

The laterite profiles around Lake Towuti closely follow a geochemical and mineralogical zonation characteristic of well-developed tropical laterites (Colin et al. 1990; Brand et al. 1998; Marsh et al. 2013). We did not observe major differences in laterite zonation and elemental composition between the laterites across varying degrees of bedrock serpentinisation (SM Figure S2.2). Bedrock and laterite mineralogy indicate that olivine weathers readily whereas pyroxene remains present in the saprolite zone and lower laterite horizons. Veins in the saprolite and laterite consist mainly of secondary quartz (SM Figure S2.3) and may thus serve as a quartz source to the lake sediments in the ultramafic part of the lake catchment. Very high goethite concentrations in the upper laterite horizon and steep element concentration gradients through the laterite horizons indicate that most other components have been transformed or leached from the profiles (Golightly and Arancibia 1979; SM Figure S2.4).

Peak elemental concentrations in the red rather than the uppermost dark red zone of laterite profiles from slope positions, e.g. in Fe and Al (Figure 2.3 and SM Figure S2.2A), suggest surficial reworking by slope processes. Coarse pebbles in the uppermost zone of some profiles support the idea of potential input of less weathered material from upslope positions. Features of slope processes, including slope creep and mass wasting, were clearly visible during fieldwork. Slopes with a steepness above the empirically determined critical angle of friction (25-43°, i.e. areas that exceed the Mohr-Coulomb failure criterion) are found throughout the catchments and suggest that slope processes such as landslides are a prevalent feature in catchments around Lake Towuti and possibly similarly structured tropical catchments. Geotechnical analyses of the laterites around Towuti (SM Figure S2.5) suggest that upper laterite horizons have a larger grain size, lower water uptake capacity (IP of ~5 %), and are stable at higher slope angles (φ-angle 43.8°) compared to clay-rich lower laterite horizons with water content of up to 100 % (I_P of 18-20 %) and a low (26.5°) critical angle of internal friction. Our analysis suggests that lower laterite horizons fail more readily compared to upper soil layers and thus function as a slip plane, mobilising the entire soil package when slope failures occur.

Seismicity-induced slope failure has been recognised as an important process in the erosion of tropical landscapes (Thomas 1996), and in Lake Towuti's active tectonic setting, strong earthquakes occur regularly (Jones et al. 2014). Recently, a shallow-focus MW 6.1 earthquake occurred in 2011 at the shore of Lake Matano, with a potential surface rupture length of 39 km (Watkinson and Hall 2016). Detailed tectonic studies of the area are still lacking, but geomorphologic evidence and fault kinematics analyses suggest rapid slip rates along the Matano fault and activity throughout the Quaternary (Bellier et al. 2006). Our analysis therefore suggests seismically triggered slope failures are important to erosion and sediment supply in tectonically active landscapes. In such environments, fault activity and seismic events enhance the mobilisation of the entire soil package, despite dense vegetation cover, and facilitate erosion of fine-grained soil material below the compacted upper laterite crust. In addition, slope processes also contribute directly to sedimentation in near-shore areas. Especially in the W and NE of the lake, steep slopes are located close to the lakeshore, such that mass movement material can directly reach the lake without intermediate fluvial transport and sorting of

the material. During fieldwork in 2015, several mass movement deposits, which directly reach the lake shore, were observed. There is, however, no indication that such material directly reaches the coring sites in the deep northern lake basin.

Tectonics and lithologic changes also strongly affect the river catchments around Lake Towuti (Figure 2.2 and Figure 2.3). Steep hillslopes (>26°) along the Mahalona River and its tributaries north of the Matano Fault trace, in contrast to slope angles of mostly less than 5° located south of the fault (Figure 2.2), suggest a strong influence of tectonics on sediment mobilisation and composition. Tectonic uplift and earthquake-triggering of slope failures in this catchment provide a constant flux of sediment to the river system, and ultimately, to the lake. Gravel deposits that accumulated in former riverbeds of the alluvial plain, observed during fieldwork, point to a sizeable contribution of remobilized sediments in the overall load that enters the lake. To the east of Lake Towuti, bedrock abrasion at the river knickpoint of the Loeha River, in combination with tectonic disturbance along a fault running parallel to the eastern lake shore (Watkinson and Hall 2016), likely explains the strong geochemical difference of the Loeha compared to the other rivers (SM Figure S2.8). As such, relatively small river catchments that are strongly influenced by tectonic disturbance can exert a strong influence on the geochemical composition of sediments deposited in the lake. Profiles of the smaller rivers to the northwest and south show no signs of recent tectonic activity, which results in a relatively low erosive capacity compared to the Mahalona and Loeha Rivers and thus a smaller influence on sediment composition at the sink.

2.5.2 The influence of erosional processes on lake sedimentation

The lake surface sediment geochemistry provides detailed information on the spatial variations in erosional processes and sediment composition in Lake Towuti. In areas of the lake where catchments are small and steep and valley incision is minimal, e.g. in the NE and SW, the elemental composition of the surface sediment closely resembles the laterite horizons. In these areas, slopes above the critical angle of friction are located close to the lake and mass movement processes may provide an important contribution to sedimentation. This is supported by high CIA values indicating weathered material across the western and northeastern parts of the lake compared to poorly weathered material delivered by the Mahalona and Loeha Rivers (SM Figure S2.6B). Clay mineralogy analysis also shows a high kaolinite-to-serpentine ratio across the southern lake basin and close to the western lakeshore, where river inflow is small (Figure 2.4E). In these areas, laterite material may also be mobilised and transferred into the lake by shore erosion.

Geochemistry and mineralogy of the lake sediments (Figure 2.4) close to major rivers, e.g. the Mahalona, show that these rivers cut deeply through the laterite soils, transporting fresh or poorly weathered material that is derived from the bedrock and saprolite zone (SM Figure S2.8; Goudge et al. 2017). This signal is also amplified by hydrodynamic sorting in the river deltas (SM Figure S2.6; data described in detail by Hasberg et al. 2018). In addition to providing a more complete picture of the spatial extent of fluvial influence in the northern basin compared to previous studies, our results also confirm the finding by Costa et al. (2015), Vogel et al. (2015), and Goudge et al. (2017) that the Mahalona River exerts a dominant control on the present-day sediment composition of Towuti's northern basin. Our data further indicate that the mobilisation of

fluvial deposits from the alluvial plains of the major rivers likely plays a role in lake sedimentation close to the river mouths.

2.5.3 Al/Mg as a proxy for lake level changes

The spatial patterns of chemically inert elements in the lake (e.g. Al, Mg, K, and Ti) show that today's sediment composition in the deep northern lake basin is a mixture of bedrock-derived sediments from the Mahalona River, sediments from the Loeha River, and laterite-derived input (SM Figure S2.8). In the catchment, Al, K, and Ti are enriched in the laterite horizons, whereas Mg is a characteristic element in the bedrock. Because K and Ti concentrations are relatively low (<1 % in the lake sediments; Figure 2.4), the ratio of Al and Mg was chosen to represent the relative contribution of bedrock and laterite erosion in Towuti's catchment. The Al/Mg patterns (Figure 2.4F) correspond to gradients in mineralogy, namely in the abundance of kaolinite and serpentine in laterite and bedrock (as expressed in the kaolinite-to-serpentine ratio). Sediments sourced from the Loeha River are characterised by higher K concentrations relative to the rivers draining ultramafic catchments (SM Figure S2.8). The chemical composition of lake sediments and the sediment cores suggests that the Loeha River has a small (<10 %) but detectable influence on sediment composition at the coring site (SM Figure S2.8). The Loeha River currently drains into the southern basin, but Costa et al. (2015) suggested that sediment from the Loeha reaches the location of core TOW9. The Al/Mg ratio at the locations of TOW9 (0.56) and Co1230 (0.87) also indicates sources other than the Mahalona River (Al/Mg of 0.15 and 0.21 in bedload and suspended load, respectively; Goudge et al. 2017), e.g. input from laterite soils (Al/Mg between 0.83 and 2.14, Figure 2.3) and the Loeha River (Al/Mg=2.62; Costa et al. 2015). Fine-grained Mahalona River sediments (Al/Mg of 0.32 and 0.37 in bedload and suspended load <32 µm, respectively; Goudge et al. 2017) and smaller rivers entering the northern basin (Al/Mg between 0.22 and 0.28; Costa et al. 2015; SM Figure S2.8; no data available for the Timampu River) cannot account for such high values. Therefore, the Al/Mg ratio and the relation between Al-Mg-K provide information about the importance of the Mahalona relative to the Loeha River and laterite-derived sediments (SM Figure S2.8).

Although bedrock geology, tectonic processes, and erosion in the catchment regulate the general composition of sediments in the lake, this composition is modified by changes in regional hydroclimate and lake level fluctuations. Decreased lake levels lead to a lower hydrologic base level and increased hydrologic gradients, which cause deeper incision. This favours bedrock erosion relative to surficial laterite erosion, and thus a lower Al/Mg ratio of the Mahalona River during lake level low stands. Remobilisation of bedrock-derived material in the alluvial river plains during lake-level low stands favours the deposition of Mg-rich material in the deeper lake basins. Furthermore, following the interpretation of Vogel et al. (2015), a lower lake level decreases the distance between the shoreline and coring sites, causing a stronger influence of riverine suspended load and an increase in grain size at the coring locations. Because large grain sizes are enriched in Mg relative to Al (Goudge et al. 2017), this effect lowers Al/Mg during dry periods. In addition, runoff is reduced, which decreases discharge volume and long-distance sediment transport capacity of the rivers. This likely reduces the influence of the Loeha River relative to the Mahalona River, which is located much closer to the coring site. Hence, we expect a lower Al/Mg ratio in the northern lake basin during drier climate conditions. In contrast, during lake-level high stands, lower

hydrologic gradients favour a higher proportional erosion of laterite soils compared to bedrock incision, and a change from erosion to accumulation in the alluvial plains around the lake. The distance between shoreline and coring sites increases, which decreases grain size, whereas higher river discharge may increase long-distance transport capacity of the rivers, increasing the influence of the Loeha River at the coring site. These factors all increase the Al/Mg in the lake sediments during wet phases. Therefore, a high Al/Mg ratio indicates wet phases in the regional climate.

Disentangling the relative influences of tectonics and climate on lake sediment composition over time can be challenging. If fault activity in the whole lake catchment changes, sedimentation rates in the lake should change accordingly. This is not apparent in our sediment records, which span the past 60,000 years. If fault activity was enhanced along the Matano Fault, both river incision and soil erosion from steepening slopes in the river catchment should increase. If both effects were equally strong over millennial time scales, tectonic activity along the Matano Fault would not change the Al/Mg ratio in the lake significantly. In contrast, if the Loeha catchment is more strongly influenced by tectonics, K deposition at the coring sites should increase relative to Mg. This is more difficult to disentangle in the record, but an increase in kaolinite from the laterites, coinciding with an increase in K from the Loeha and a decrease in Mg from the Mahalona, would generally point towards climate (i.e. higher lake levels) rather than tectonics as the driving factor for the observed changes.

2.5.4 Lake Towuti's palaeoclimate record

In the past 60 kyr, Al/Mg, K, and kaolinite show similar trends in the record (Figure 2.5), suggesting a dominant influence of climate processes on pelagic sedimentation in the northern basin. Changes in the past 30 kyr are seen at both coring sites, TOW9 and Co1230 (excluding event layers; Figure 2.5A and B), emphasizing the homogeneity of pelagic sedimentation in the northern basin. In the past 60 kyr, the Al/Mg ratio shows lowest values in the mid-Holocene (6-4 kyr BP), in MIS2, and around 58 kyr BP (Figure 2.5A). The latter two intervals correspond to glacial periods with substantial extents of northern hemisphere ice sheets. Based on data from the modern lake, our proxy record suggests that lake level was lower and climate conditions were drier during these periods compared to today. Accordingly, high Al/Mg values in the late Holocene, at the transition from the last glacial period, and during MIS3, indicate lake level highstands and a wet climate in Central Sulawesi. Our findings are in line with earlier studies from Lake Towuti (Russell et al. 2014; Costa et al. 2015; Vogel et al. 2015; Goudge et al. 2017), other studies from Sulawesi (Dam et al. 2001; Hope 2001; Dubois et al. 2014; Wicaksono et al. 2015, 2017), and from the Indo-Pacific Warm Pool region (De Deckker et al. 2002; Reeves et al. 2013), indicating a dry last glacial period. Vegetation around Lake Towuti, which is sensitive to climate rather than tectonics, also shows regional drying during MIS2 and wet conditions during MIS1 and MIS3 (Russell et al. 2014). These results suggest that climate was the dominant factor that shaped sedimentation in Lake Towuti over the last 60,000 years.

Interestingly, the Lake Towuti record indicates a pronounced dry period during the mid-Holocene (6-4 kyr BP) with minima in both the Al/Mg and kaolinite-to-serpentine ratios. This was described previously in a record from Lake Towuti that covered the last 45,000 years, and together with smaller variations during MIS2, was attributed to an 11-kyr, half-precessional signal (Goudge et al. 2017). Our longer, 60,000-year record

suggests that during MIS3, this potential 11-kyr cylicity is less pronounced or absent. This may be a consequence of a more dominant influence of the strong tilt of Earth's axis on northern hemisphere ice sheet extent during MIS3 (Van Meerbeeck et al. 2009; Svendsen et al. 2004; Helmens et al. 2007) and/or the influence of millennial-scale events triggered in the North Atlantic that are not resolved in our data time series (Dansgaard et al. 1993). Alternatively, other mechanisms may be responsible for the pronounced dry period during the mid-Holocene, which would require further investigation.

2.6 Conclusions

Source-to-sink analysis of the geochemistry and clay mineralogy of Lake Towuti provided insights into the modern erosional processes and sediment composition in a tropical lake catchment characterized by ultramafic bedrock composition, lateritic soils, and active tectonics. Mass movement processes, tectonic disturbance of river profiles, and climate-induced remobilisation of fluvial deposits strongly influenced sedimentation at this site. Lower soil horizons can function as a slide plane during mass movement events, mobilising the soil package and contributing substantially to erosion in the steeper parts of this tropical catchment. In the northeastern and western lake catchment such mass movement events may supply material directly to the lake, whereas larger, tectonically disturbed rivers mainly erode and transport bedrock-derived material to the lake. Our analysis of the river profiles, along with spatially explicit analysis of surface sediment composition, added an additional, more process-based understanding of the contribution of tectonic disturbance to the sediment load delivered to the sink. In general, fault movement greatly influences the amount and dispersion of sediment delivered to the sink by disturbed, relative to less-disturbed, river systems.

Although tectonic processes and erosion in the catchment influence the general composition of the lake sediments, this composition is modified by changes in the regional hydroclimate over glacial-interglacial timescales. Based on the understanding of today's lake system, we identified the Al/Mg ratio as a proxy for lake level changes, which provide the dominant sedimentary signal for regional hydroclimate changes. Characterising and understanding the functioning of the modern lake system is crucial for the development and interpretation of sediment proxies, especially in geochemically exceptional lake systems such as Towuti. The complexity of processes described for this tropical lake catchment, in combination with the sampling and analytical approach applied, may help to inform future studies that aim to acquire information on landscape evolution in similar settings.

2.7 Acknowledgements

The Towuti Drilling Project was partially supported by grants from the International Continental Scientific Drilling Program, the US National Science Foundation, the German Research Foundation, the Swiss National Science Foundation (20FI21_153054/1 and 200021_153053/1), Brown University, Genome British Columbia, and the Ministry of Research, Technology, and Higher Education (RISTEK). PT Vale Indonesia, the US Continental Drilling Coordination Office, the GeoForschungszentrum Potsdam and DOSECC Exploration Services are acknowledged for logistical assistance to the project. We further thank Franziska Nyffenegger for support with the geotechnical

analysis, Urs Eggenberger and Christine Lemp for help with the clay and bulk XRD analysis, Elias Kempf for assistance with thin section analysis, as well as Pierre Valla and Romain Delunel for fruitful discussions regarding the geomorphic aspects of the study. This research was carried out with permission from the Ministry of Research and Techonology (RISTEK), the Ministry of Trade of the government of Indonesia, and the Natural Resources Conservation Center (BKSDA) and Government of Luwu Timur of Sulawesi. We also wish to thank two anonymous reviewers and the editors for their helpful comments and suggestions, which improved our manuscript.

2.8 Author contributions

MAM, HV, and AKMH designed the sampling campaign and were responsible for sample acquisition and analyses. JMR, SB, HV, and MM designed and led the Towuti Drilling Project. HV and JMR provided sediment core material. MAM performed lab and GIS analyses (clay and bulk mineralogy, geotechnical and geomorphological parameters). LO and VN provided additional data (WD-XRF and grain size). MAM led the writing of the manuscript and designed the figures. All authors were involved in discussions about the data and contributed to writing and improving the manuscript. Members of the Towuti Drilling Project provided scientific, technical, and logistical support during field sampling and core opening.

2.9 References

Adunoye GO (2014) Fines Content and Angle of Internal Friction of a Lateritic Soil: An Experimental Study. Am J Engin Res 3: 16-21

Bellier O, Sébrier M, Seward D, Beaudouin T, Villeneuve M, Putranto E (2006) Fission track and fault kinematics analyses for new insight into the Late Cenozoic tectonic regime changes in West-Central Sulawesi (Indonesia). Tectonophysics, 413: 201-220. DOI: 10.1016/j.tecto.2005.10.036

Brand NW, Butt CRM, Elias M (1998) Nickel laterites: classification and features. J Aust Geol Geophys 17: 81-88

Casagrande L (1932) Research of Atterberg Limits of Soils. Public Roads 13: 121-136

Chester R, Elderfield H, (1973) An infrared study of clay minerals, 2. The identification of kaolinite-group clays in deep-sea sediments. Chem Geol 12: 281-288

Chukanov NV (2014) Infrared Spectra of Mineral Species. Springer, Dordrecht

Colin F, Nahon D, Trescases JJ, Melfi AJ (1990) Lateritic Weathering of Pyroxenites at Niquelandia, Goias, Brazil: The Supergene Behavior of Nickel. Econ Geol 85: 1010-1023

Costa KM, Russell JM, Vogel H, Bijaksana S (2015) Hydrological connectivity and mixing of Lake Towuti, Indonesia in response to paleoclimatic changes over the last 60,000 years. Palaeogeogr Palaeoclimatol Palaeoecol 417: 467-475. DOI: 10.1016/j.palaeo.2014.10.009

Crowe SA, Jones C, Katsev S, Magen C, O'Neill AH, Sturm A, Canfield DE, Haffner GD, Mucci A, Sundby B, Fowle DA (2008) Photoferrotrophs thrive in an Archean Ocean analogue. Proc Natl Acad Sci USA 105: 15938-43. DOI: 10.1073/pnas.0805313105

Dansgaard W, Johnsen SJ, Clausen HB, Dahl-Jensen D, Gundestrup NS, Hammer CU, Hvidberg CS, Steffensen JP, Sveinbjörnsdottir AE, Jouzel J, Bond G (1993) Evidence for general instability of past climate from a 250-kyr ice-core record. Nature 364: 218-220

Dam RAC, Fluin J, Suparan P, van der Kaars S (2001) Palaeoenvironmental developments in the Lake Tondano area (N. Sulawesi, Indonesia) since 33,000 yr BP. Palaeogeogr Palaeoclimatol Palaeoecol 171: 147-183

De Deckker P, Tapper NJ, van der Kaars S (2002) The status of the Indo-Pacific Warm Pool and adjacent land at the Last Glacial Maximum. Glob Planet Chang 35: 25-35

DIN 18137-1. German Industrial Norm (2010) Baugrund, Untersuchung von Bodenproben. Bestimmung der Scherfestigkeit, Teil 1: Begriffe und grundsätzliche Versuchsbedingungen [Soil, investigation and testing - Determination of shear strength - Part 1: Concepts and general testing conditions]

DIN 18137-3. German Industrial Norm (2002) Baugrund, Untersuchung von Bodenproben. Bestimmung der Scherfestigkeit, Teil 3: Direkter Scherversuch [Soil, investigation and testing - Determination of shear strength - Part 3: Direct shearing test]

Dubois N, Oppo DW, Galy VV, Mohtadi M, van der Kaars S, Tierney JE, Rosenthal Y, Eglinton TI, Lückge A, Linsley BK (2014) Indonesian vegetation response to changes in rainfall seasonality over the past 25,000 years. Nat Geosci 7: 513–517. DOI: 10.1038/ngeo2182

Farmer VC (1974) The infrared spectra of minerals. Mineralogical society monograph 4. Adlard and Son, Dorking, UK.

Golightly JP, Arancibia ON (1979) The chemical composition and infrared spectrum of nickel- and iron-substituted serpentine from a nickeliferous laterite profile, Soroako, Indonesia. Can Mineral 17: 719-728

Goudge TA, Russell JM, Mustard JF, Head JW, Bijaksana S (2017) A 40,000 yr record of clay mineralogy at Lake Towuti, Indonesia: Paleoclimate reconstruction from reflectance spectroscopy and perspectives on paleolakes on Mars. Bull Geol Soc Am 129: 806-819. DOI: 10.1130/B31569.1

Haffner GD, Hehanussa PE, Hartoto D (2001) The biology and physical processes of large lakes of Indonesia: Lakes Matano and Towuti. In: The Great Lakes of the World (GLOW). Michigan State University Press, 183-192

Hasberg AKM, Melles M, Wennrich V, Just J, Held P, Morlock MA, Vogel H, Russell JM, Bijaksana S, Opitz S (2018) Modern sedimentation processes in Lake Towuti, Indonesia, revealed by the composition of surface sediments. Sedimentology. DOI: 10.1111/sed.12503

Helmens KF, Bos JAA, Engels S, Van Meerbeeck CJ, Bohncke SJP, Renssen H, Heiri O, Brooks SJ, Seppä H, Birks HJB, Wohlfarth B (2007) Present-day temperatures in northern Scandinavia during the last glaciation. Geology 35: 987-990. DOI: 10.1130/G23995S1

Hope G (2001) Environmental change in the Late Pleistocene and later Holocene at Wanda site, Soroako, South Sulawesi, Indonesia. Palaeogeogr Palaeoclimatol Palaeoecol 171: 129-145

Jones ES, Hayes GP, Bernardino M, Dannemann FK, Furlong KP, Benz HM, Villaseñor A (2014) Seismicity of the Earth 1900–2012, Java and vicinity. U.S. Geological Survey Open-File Report 2010–1083-N, 1 sheet, scale 1:5,000,000, DOI: 10.3133/ofr20101083N

Kadarusman A, Miyashita S, Maruyama S, Parkinson CD, Ishikawa A (2004) Petrology, geochemistry and paleogeographic reconstruction of the East Sulawesi Ophiolite, Indonesia. Tectonophysics. 392: 55-83. DOI: 10.1016/j.tecto.2004.04.008

Konecky B, Russell JM, Bijaksana S (2016) Glacial aridity in central Indonesia coeval with intensified monsoon circulation. Earth Planet Sci Lett 437: 15-24. DOI: 10.1016/j.epsl.2015.12.037

Madejová J (2003) FTIR techniques in clay mineral studies. Vib Spectrosc 31: 1-10

Marsh E, Anderson E, Gray F (2013) Nickel-Cobalt Laterites - A Deposit Model. In: Mineral Deposit Models of Resource Assessment. U.S. Geological Survey, Reston, USA

Nesbitt HW, Young GM (1982) Early Proterozoic climates and plate motions inferred from major element chemistry of lutites. Nature 299: 715-717

Ogunsanwo O (1988) Basic Geotechnical Properties, Chemistry and Mineralogy of some Laterite Soils from S.W. Nigeria. Bull Int Assoc Engin Geol: 131-135

Omotoso OA, Ojo OJ, Adetolaju ET (2012) Engineering Properties of Lateritic Soils around Dall Quarry in Sango Area, Ilorin, Nigeria. Earth Sci Res 1: 71-81. DOI: 10.5539/esr.v1n2p71

R Development Core Team (2008) R: A language and environment for statistical computing. R Foundation for Statistical Computing. Available at: www.r-project.org (last accessed Feb 13 2017)

Reeves JM, Bostock HC, Ayliffe LK, Barrows TT, De Deckker P, Devriendt LS, Dunbar GB, Drysdale RN, Fitzsimmons KE, Gagan MK, Griffiths ML, Haberle SG, Jansen JD, Krause C, Lewis S, McGregor HV, Mooney SD, Moss P, Nanson GC, Purcell A, van der Kaars S (2013) Palaeoenvironmental change in tropical Australasia over the last 30,000 years – a synthesis by the OZ-INTIMATE group. Quat Sci Rev 74: 97-114. DOI: 10.1016/j.quascirev.2012.11.027

Robinson GW (1922) A new method for the mechanical analysis of soils and other dispersions. J Agric Sci 12: 306-321

Russell JM, Vogel H, Konecky B, Bijaksana S, Huang Y, Melles M, Wattrus N, Costa KM, King JW (2014) Glacial forcing of central Indonesian hydroclimate since 60,000 y BP. PNAS 111: 5100-5105. DOI: 10.1073/pnas.1402373111

Russell JM, Bijaksana S, Vogel H, Melles M, Kallmeyer J, Ariztegui D, Crowe S, Fajar S, Hafidz A, Haffner D, Hasberg A, Ivory S, Kelly C, King J, Kirana K, Morlock M, Noren A, O'Grady R, Ordonez L, Stevenson J, von Rintelen T, Vuillemin A, Watkinson I, Wattrus N, Wicaksono S, Wonik T, Bauer K, Deino A, Friese A, Henny C, Imran, Marwoto R, Ngkoimani LO, Nomosatryo S, Safiuddin LO, Simister R, Tamuntuan G (2016) The Towuti Drilling Project: paleoenvironments, biological evolution, and geomicrobiology of a tropical Pacific lake. Sci Drill 21: 29-40. DOI: 10.5194/sd-21-29-2016

Sagapoa CV, Imai A, Watanabe K (2011) Laterization Process of Ultramafic Rocks in Siruka, Solomon Islands. J Nov Carb Resourc Sci 3: 32-39

SN 670 010. Swiss Norm. Geotechnische Erkundung und Untersuchung - Geotechnische Kenngrössen [Geotechnical exploration and analysis - Geotechnical parameters]. Edition 2011-08

SN 670 816a. Swiss Norm. Mineralische Baustoffe, Schlämmanalyse nach der Aräometermethode [Minerogenic material – Sieving analysis by aerometric method]

SN 670 902-1 (EN 933-1). Swiss Norm. Prüfverfahren für geometrische Eigenschaften von Gesteinskörnungen. Teil 1: Bestimmung der Korngrössenverteilung - Siebverfahren [Testing geometric properties of grains, Part 1: Grain-size distribution – Sieving]. Edition 2013-03

SN 670 345b. Swiss Norm. Böden - Konsistenzgrenzen [Soils – Plasticity Index]

Svendsen JI, Alexanderson H. Astakhov VI, Demidov I, Dowdeswell JA, Funder S, Gataullin V, Henriksen M, Hjort C, Houmark-Nielsen M, Hubberten HW, Ingólfsson Ó, Jakobsson M, Kjær KH, Larsen E, Lokrantz H, Lunkka JP, Lysså A, Mangerud J, Matiouchkov A, Murray A, Möller P, Niessen F, Nikolskaya O, Polyak L, Saarnisto M, Siegert C, Siegert MJ, Spielhagen RF, Stein R (2004) Late Quaternary ice sheet history of northern Eurasia. Quat Sci Rev 23: 1229-1271. DOI: 10.1016/j.quascirev.2003.12.008

Thomas MF (1996) Geomorphology in the tropics. Wiley, Chichester, UK

U.S. Geological Survey (2017) Mineral Commodity Summaries 2017. U.S. Geological Survey, Reston, USA. DOI: 10.3133/70180197

Van Meerbeeck CJ, Renssen H, Roche DM (2009) How did Marine Isotope Stage 3 and Last Glacial Maximum climates differ? - Perspectives from equilibrium simulations. Clim Past 5: 33-51

Vogel H, Russell JM, Cahyarini SY, Bijaksana S, Wattrus N, Rethemeyer J, Melles M (2015) Depositional modes and lake-level variability at Lake Towuti, Indonesia, during the past ~29 kyr BP. J Paleolimnol 54: 359-377. DOI: 10.1007/s10933-015-9857-z

Von Rintelen T, Von Rintelen K, Glaubrecht M, Schubart CD, Herder F (2012) Aquatic biodiversity hotspots in Wallacea: the species flocks in the ancient lakes of Sulawesi, Indonesia. In:

Gower DJ, Johnson K, Richardson J, Rosen B, Rüber L, Williams S (Eds.). Biotic Evolution and Environmental Change in Southeast Asia, Cambridge University Press, Cambridge, UK, pp 291-315

Watkinson IM, Hall R (2016) Fault systems of the eastern Indonesian triple junction: evaluation of Quaternary activity and implications for seismic hazards. In: Cummins PR, Meilano I (Eds.). Geohazards in Indonesia: Earth Science for Disaster Risk Reduction. Geological Society, London, UK, Special Publications: 441, pp 71-120

Weber AK, Russell JM, Goudge TA, Salvatore MR, Mustard JF, Bijaksana S (2015) Characterizing clay mineralogy in Lake Towuti, Indonesia, with reflectance spectroscopy. J Paleolimnol 54: 253-261. DOI: 10.1007/s10933-015-9844-4

Whipple KX, Kirby E, Brocklehurst SH (1999) Geomorphic limits to climate-induced increases in topographic relief. Nature 401: 39-43. DOI: 10.1038/43375

Wicaksono SA, Russell JM, Bijaksana S (2015) Compound-specific carbon isotope records of vegetation and hydrologic change in central Sulawesi, Indonesia, since 53,000 yr BP. Palaeogeogr Palaeoclimatol Palaeoecol 430: 47-56. DOI: 10.1016/j.palaeo.2015.04.016

Wicaksono SA, Russell JM, Holbourn A, Kuhnt W (2017) Hydrological and vegetation shifts in the Wallacean region of central Indonesia since the Last Glacial Maximum. Quat Sci Rev 157: 152-163. DOI: 10.1016/j.quascirev.2016.12.006

Widdowson M (2007) Laterite and Ferricrete. In: Nash DJ, McLaren SJ (Eds.). Geochemical Sediments and Landscapes. Blackwell Publishing, Malden, USA, pp. 46-94

2.10 Supplementary material

Table S2.1 Geomorphological characteristics for all major rivers and their respective catchments around Lake Towuti. Values and catchment boundaries are based on DEM analysis. River slope values are averaged over a horizontal distance of 600 m

River	Catchment size [km^2]	River length [km]	Elevation difference [m]	Mean slope catchment [°]	Max. slope catchment [°]	Mean slope river [°]	Max. slope river [°]	sampled
1 (Timampu)	141	18	540	13.1	63	1.6	8.7	no
2 (Mahalona)	293	43	620	14.5	64	0.8	4.9	yes
3 (unknown)	27	12	600	13.2	54	4	7.8	no
4 (LemoLemo)	52	13	695	16.5	67	3	12.8	yes
5 (Tomerakah)	58	12	400	15.2	55	1.8	6.2	yes
6 (Loeha)	84	21	680	15.5	62	1.9	16.2	yes
7 (Lelebiu)	9	5	150	13.2	41	-	-	yes
8 (unknown)	45	10	310	14.5	50	1.7	7.9	no
9 (Tokolalo)	40	14	510	15.2	51	1.9	10.5	yes
10 (Lantibu)	20	9	690	14.8	47	-	-	yes
11 (Lengke)	49	10	510	12.4	45	2.5	17.5	yes
No permanent river	157	-	-	-	-	-	-	yes

Malili Lakes	Lake surface area [km^2]	Catchment size [km^2] (without lake)
Lake Matano	160.5	295
Lake Mahalona	22.2	205
Lake Towuti	559.9	1144

*Table S2.2 Element concentration for the six individual laterite profiles presented in this study. Concentrations were determined by a) ICP-MS and b) WD-XRF. Lower detection limits for ICP-MS measurements are indicated in row 3. *) Sample SAP2 was taken from a secondary quartz vein*

Sample ID	Profile No.	Profile depth [m]	Laterite horizon	Al	Ca	Cr	Cu	Fe	K	Na	Ni	P	Mg	Mn	Ti	Zn	Zr
				%	%	ppm	ppm	%	%	%	ppm	%	%	ppm	%	ppm	ppm
				0.01	0.01	1	0.1	0.01	0.01	0.001	0.1	0.001	0.01	1	0.001	1	0.1
LAT2	1	0.40	dark red horizon	3.60	0.22	> 10000	83.5	38.40	< 0.01	0.004	9420.0	0.010	7.09	6450	0.061	310	13.0
LAT3	1	1.00	yellow horizon	3.28	< 0.01	> 10000	88.1	38.10	< 0.01	0.004	9560.0	0.004	1.05	6470	0.047	332	7.9
LAT4	1	1.50	yellow horizon	5.24	< 0.01	> 10000	87.2	46.40	< 0.01	0.002	9780.0	0.008	0.86	3070	0.095	346	24.8
LAT5	1	2.20	yellow horizon	2.60	0.02	9650	66.8	24.30	< 0.01	0.007	7560.0	0.003	1.34	5360	0.029	190	3.1
SAP1	1	4.00	saprolite	0.34	0.36	3650	6.9	6.33	< 0.01	0.009	> 10000	0.001	20.10	1020	0.005	64	0.9
SAP2*	1	4.00	saprolite	0.16	0.05	1010	5.6	2.12	0.01	0.006	4420.0	0.001	2.81	406	0.002	34	0.7
BED8 weathered	1	8.00	bedrock	0.71	1.12	2280	16.5	6.23	< 0.01	0.006	3640.0	0.001	29.70	925	0.007	55	0.9
BED8 unweathered	1	8.00	bedrock	0.59	1.22	2430	21.2	6.24	< 0.01	0.005	2290.0	< 0.001	> 30.0	1000	0.007	53	1.0
LAT6a	2	0.10	dark red horizon	3.41	< 0.01	> 10000	84.4	47.30	< 0.01	0.002	> 10000	0.010	0.74	7070	0.137	466	10.7
LAT6b	2	2.00	red horizon	2.93	0.02	> 10000	84.9	48.60	< 0.01	0.002	> 10000	0.007	1.13	8600	0.108	440	6.6
SAP3 weathered	2	2.50	saprolite	2.02	2.41	3190	35.9	6.26	< 0.01	0.167	8460.0	0.002	21.70	820	0.055	240	2.8
SAP3 unweathered	2	2.50	saprolite	1.61	2.38	2030	15.6	5.83	< 0.01	0.136	3690.0	0.002	26.90	954	0.045	58	1.7
BED9	2	3.50	bedrock	0.11	0.02	2060	3.3	5.51	< 0.01	0.005	2310.0	0.001	24.00	710	0.003	59	0.8
LAT7a	3	0.30	dark red horizon	2.87	0.67	6280	45.2	12.30	0.06	0.094	> 10000	0.004	12.80	1970	0.106	120	10.8
LAT7b	3	1.00	yellow horizon	2.17	0.80	7490	34.3	14.90	0.04	0.027	> 10000	0.004	10.80	2670	0.047	123	4.2
BED12	3	8.00	bedrock	0.73	0.69	3560	29.1	5.40	< 0.01	0.012	2000.0	< 0.001	29.20	913	0.008	54	1.1
LAT8c	4	0.05	dark red horizon	5.91	0.66	> 10000	63.3	14.90	0.01	0.051	4490.0	0.018	7.30	6650	0.220	253	13.7
LAT8a	4	0.40	red horizon	4.36	0.31	6700	71.7	33.90	< 0.01	0.033	4810.0	0.005	4.75	3480	0.148	175	13.0
LAT8b	4	1.20	yellow horizon	4.84	0.25	6020	92.5	18.30	< 0.01	0.004	5950.0	0.004	4.13	4360	0.170	119	11.9
BED15	4	15.00	bedrock	2.45	2.51	839	55.7	5.78	< 0.01	0.020	1580.0	0.004	23.20	953	0.110	55	7.8
LAT9a	5	0.20	dark red horizon	5.25	< 0.01	> 10000	61.3	49.10	< 0.01	0.001	7890.0	0.024	0.61	1750	0.111	300	29.9
LAT9b	5	1.50	red horizon	4.20	< 0.01	> 10000	90.0	49.40	< 0.01	0.001	> 10000	0.007	0.61	3850	0.062	340	18.9
LAT9c	5	2.50	yellow horizon	3.73	< 0.01	> 10000	116.0	49.10	< 0.01	0.001	> 10000	0.005	0.62	3110	0.059	375	11.6
LAT10a	6	0.10	dark red horizon	4.58	0.02	> 10000	49.3	34.90	< 0.01	0.003	6390.0	0.009	2.08	5530	0.067	604	10.8
LAT10b	6	1.00	red horizon	8.25	0.01	> 10000	32.0	33.80	< 0.01	0.003	3750.0	0.008	3.22	2740	0.068	740	10.0
LAT10c	6	1.50	red horizon	8.29	< 0.01	> 10000	33.2	32.90	< 0.01	0.003	4220.0	0.008	3.38	3100	0.077	753	11.8
LAT10d	6	2.50	yellow horizon	2.17	0.14	> 10000	106.0	40.90	0.01	0.004	> 10000	0.003	2.25	7910	0.043	589	4.1
LAT10e	6	3.50	saprolite	3.26	0.04	9560	63.4	21.80	0.07	0.016	> 10000	0.003	8.26	6850	0.082	954	9.6
BED18 weathered	6	4.00	bedrock	0.59	0.70	2850	24.7	7.50	< 0.01	0.006	3060.0	< 0.001	> 30.0	934	0.006	98	0.6
BED18 unweathered	6	4.00	bedrock	0.47	0.71	1960	31.9	5.98	< 0.01	0.004	2140.0	< 0.001	> 30.0	971	0.005	55	0.8

Sample ID	Profile No.	Profile depth [m]	Laterite horizon	Al	Ca	Cr	Fe	K	Na	Ni	P	Mg	Mn	Ti	Si	LOI
				%	%	%	%	%	%	%	%	%	%	%	%	%
LAT2	1	0.40	dark red horizon	2.70	0.16	1.59	39.34	0.00	0.02	0.89	0.00	5.28	0.68	0.05	6.91	10.29
LAT3	1	1.00	yellow horizon	2.74	0.01	1.66	41.23	0.00	0.00	0.96	0.00	0.78	0.72	0.05	9.05	10.82
LAT4	1	1.50	yellow horizon	3.92	0.01	2.03	47.75	0.00	0.00	0.94	0.00	0.66	0.30	0.10	2.90	12.72
LAT5	1	2.20	yellow horizon	2.06	0.00	1.02	26.68	0.00	0.00	0.79	0.00	1.00	0.59	0.03	21.25	7.65
SAP1	1	4.00	saprolite	0.28	0.30	0.54	7.04	0.00	0.00	2.57	0.00	18.21	0.11	0.01	21.97	7.51
SAP2*	1	4.00	saprolite	0.20	0.02	0.13	2.13	0.01	0.00	0.44	0.00	2.40	0.04	0.00	41.35	2.51
BED8 weathered	1	8.00	bedrock	0.58	1.05	0.45	6.97	0.00	0.00	0.45	0.00	25.36	0.11	0.01	20.42	0.32
BED8 unweathered	1	8.00	bedrock	0.49	1.01	0.37	6.32	0.00	0.00	0.24	0.00	26.47	0.11	0.01	20.57	-
LAT6a	2	0.10	dark red horizon	4.47	-	1.93	48.18	-	-	0.96	0.01	0.62	0.71	0.18	2.30	11.97
LAT6b	2	2.00	red horizon	3.35	0.02	1.90	49.67	0.01	-	0.99	0.01	0.79	0.89	0.12	2.44	11.19
SAP3 weathered	2	2.50	saprolite	1.62	1.80	0.50	6.98	0.00	0.06	1.08	0.00	19.62	0.09	0.06	19.91	6.98
SAP3 unweathered	2	2.50	saprolite	1.33	1.98	0.36	5.52	0.00	0.05	0.55	0.00	21.13	0.09	0.05	19.93	7.62
BED9	2	3.50	bedrock	0.08	0.01	0.37	6.16	0.00	0.00	0.27	0.00	22.29	0.10	0.01	18.63	13.20
LAT7a	3	0.30	dark red horizon	2.45	0.65	0.93	12.62	0.06	0.04	1.13	0.00	10.47	0.21	0.10	21.51	9.09
LAT7b	3	1.00	yellow horizon	1.96	0.75	1.12	15.67	0.04	0.00	1.06	0.00	9.26	0.30	0.05	21.06	8.46
BED12	3	8.00	bedrock	0.58	0.55	0.57	5.51	0.00	0.00	0.21	0.00	24.64	0.09	0.01	19.43	6.60
LAT8c	4	0.05	dark red horizon	5.26	0.59	1.16	17.19	0.02	0.03	0.46	0.01	6.08	0.79	0.23	16.65	15.43
LAT8a	4	0.40	red horizon	5.20	0.53	0.88	20.90	0.01	0.04	0.59	0.01	7.63	0.49	0.24	15.58	10.61
LAT8b	4	1.20	yellow horizon	4.51	0.35	0.73	21.58	0.01	0.00	0.67	0.00	3.12	0.21	0.19	19.12	11.69
BED15	4	15.00	bedrock	3.40	3.33	0.23	6.64	0.00	0.00	0.17	0.01	17.80	0.09	0.15	17.80	10.82
LAT9a	5	0.20	dark red horizon	3.85	0.01	3.07	50.07	0.00	0.00	0.75	0.01	0.52	0.17	0.11	0.93	13.14
LAT9b	5	1.50	red horizon	3.16	0.01	2.16	51.53	0.00	0.01	0.99	0.00	0.53	0.39	0.07	0.81	13.16
LAT9c	5	2.50	yellow horizon	3.21	0.00	2.22	51.55	0.00	0.00	0.97	0.00	0.57	0.34	0.07	0.79	13.05
LAT10a	6	0.10	dark red horizon	5.09	0.01	9.02	36.08	0.00	0.00	0.60	0.00	1.72	0.53	0.08	4.69	13.35
LAT10b	6	1.00	red horizon	6.34	-	11.51	38.88	0.02	-	0.43	0.01	2.31	0.29	0.08	3.09	7.21
LAT10c	6	1.50	red horizon	6.90	0.01	13.10	36.67	0.00	0.01	0.46	0.00	3.03	0.29	0.09	2.57	7.16
LAT10d	6	2.50	yellow horizon	3.46	0.14	2.88	42.83	0.02	0.00	1.58	0.00	2.08	0.86	0.05	4.40	12.38
LAT10e	6	3.50	saprolite	2.09	0.11	1.38	26.87	0.05	-	1.42	-	5.99	0.82	0.05	16.09	8.39
BED18 weathered	6	4.00	bedrock	0.44	0.60	0.43	7.12	0.00	0.00	0.37	0.00	25.90	0.11	0.01	20.51	0.11
BED18 unweathered	6	4.00	bedrock	0.34	0.52	0.36	6.20	0.00	0.00	0.26	0.00	27.29	0.10	0.01	20.46	-

Figure S2.1 a) Exemplary clay XRD spectra of a surface sediment sample with characteristic peaks for smectite (5.2° 2θ), illite (8.8° 2θ), serpentine (12.24° 2θ), and kaolinite (12.5° 2θ) in the ethylene glycol saturated sample. b) Correlation plots for surface sediment samples and c) for sediment core Co1230: comparison of clay-fraction XRD, clay-fraction mid-infrared FTIRS, and bulk Al and Mg. Correlation method and coefficients are indicated in the top left. Compared to MIR-FTIRS, XRD analysis on oriented clay separates to identify clay minerals in soils and lake sediments is more common. MIR-FTIRS has recently become an established method for the determination of the minerogenic and organic matter content of lake sediments (Rosén and Persson 2006), but is less commonly used for the identification of clay minerals in sediment records. Our results agree well with clay mineralogy analyses by Weber et al. (2015) and Goudge et al. (2017), who used near-infrared spectroscopy to determine the clay mineral content of a surface sediment transect and sediment cores from Lake Towuti. Our data thus show that XRD analysis on oriented clay separates as well as FTIR spectroscopy analysis reliably determine the clay mineralogical content of lake sediments from Towuti, in particular the amount of kaolinite and serpentine, whereas no reliable signal could be obtained for smectites and illite

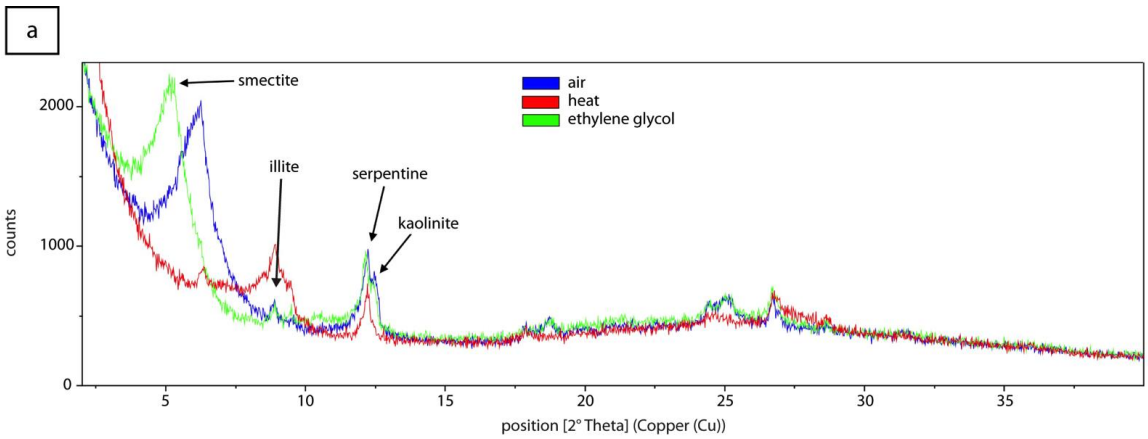

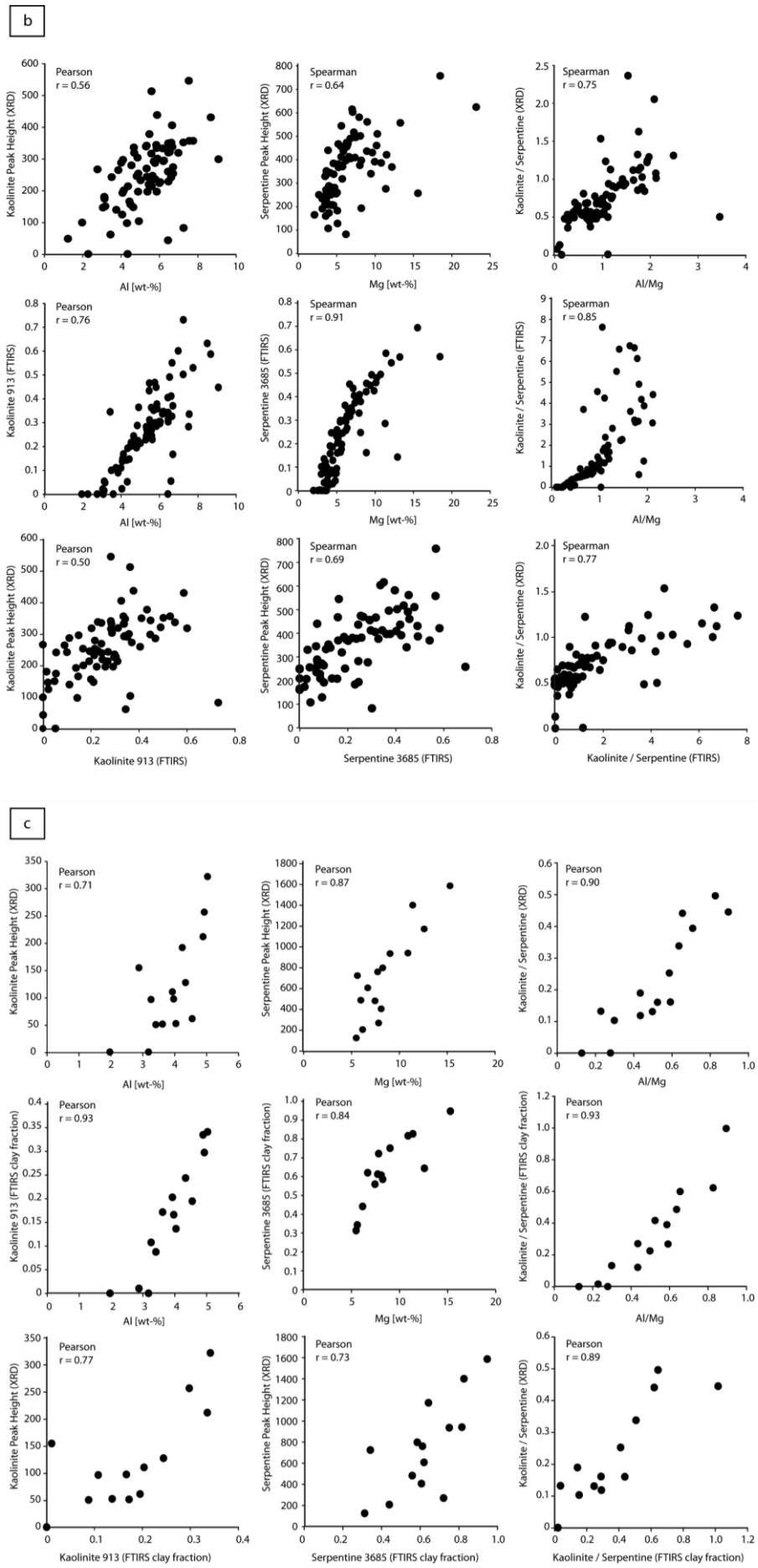
b
Pearson
r = 0.56
Kaolinite Peak Height (XRD)
Al [wt-%]
Spearman
r = 0.64
Serpentine Peak Height (XRD)
Mg [wt-%]
Spearman
r = 0.75
Kaolinite / Serpentine (XRD)
Al/Mg
Pearson
r = 0.76
Kaolinite 913 (FTIRS)
Al [wt-%]
Spearman
r = 0.91
Serpentine 3685 (FTIRS)
Mg [wt-%]
Spearman
r = 0.85
Kaolinite / Serpentine (FTIRS)
Al/Mg
Pearson
r = 0.50
Kaolinite Peak Height (XRD)
Kaolinite 913 (FTIRS)
Spearman
r = 0.69
Serpentine Peak Height (XRD)
Serpentine 3685 (FTIRS)
Spearman
r = 0.77
Kaolinite / Serpentine (XRD)
Kaolinite / Serpentine (FTIRS)
c
Pearson
r = 0.71
Kaolinite Peak Height (XRD)
Al [wt-%]
Pearson
r = 0.87
Serpentine Peak Height (XRD)
Mg [wt-%]
Pearson
r = 0.90
Kaolinite / Serpentine (XRD)
Al/Mg
Pearson
r = 0.93
Kaolinite 913 (FTIRS clay fraction)
Al [wt-%]
Pearson
r = 0.84
Serpentine 3685 (FTIRS clay fraction)
Mg [wt-%]
Pearson
r = 0.93
Kaolinite / Serpentine (FTIRS clay fraction)
Al/Mg
Pearson
r = 0.77
Kaolinite Peak Height (XRD)
Kaolinite 913 (FTIRS clay fraction)
Pearson
r = 0.73
Serpentine Peak Height (XRD)
Serpentine 3685 (FTIRS clay fraction)
Pearson
r = 0.89
Kaolinite / Serpentine (XRD)
Kaolinite / Serpentine (FTIRS clay fraction)

Figure S2.2 a) Average concentration of elements in the three laterite zones, in the saprolite, and in the bedrock. CIA calculation is based on Nesbitt and Young (1982). Colours indicate the five zones: unweathered parent rock (dark green), saprolite zone (light green), and three laterite zones (orange, light red, dark red). Error bars correspond to ± one standard deviation. b) Element concentration of Al, Fe, Mg, and Ti for the six individual laterite profiles presented in this study. Concentrations were determined by ICP-MS, and vertical red lines indicate upper and lower detection limits where applicable. Bedrock type is indicated below the profiles. c) Kaolinite and serpentine concentrations in the laterite horizons based on diagnostic peak integration of FTIR spectra for kaolinite (wavenumbers 900.8-924.6 cm^{-1}; kaolinite 913) and serpentine (3674.9-3694.2 cm^{-1}; serpentine 3685) in absorption units

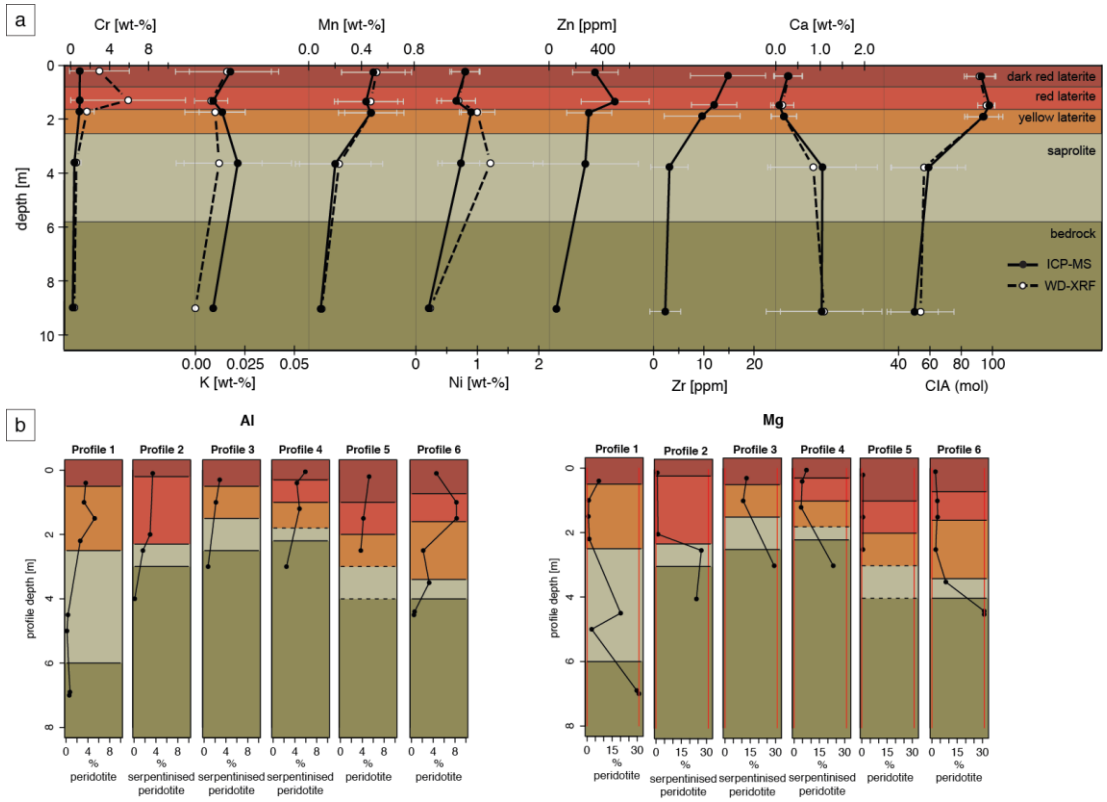

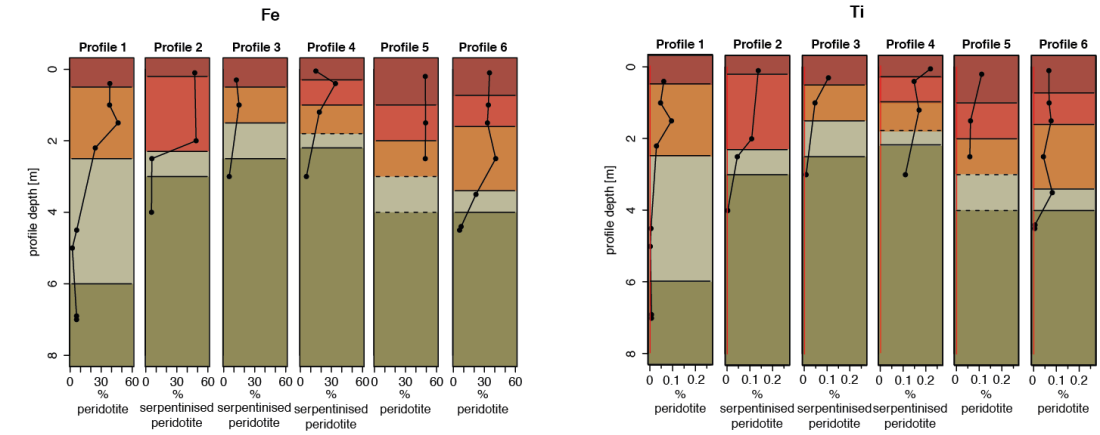
Fe
Ti
Profile 1
Profile 2
Profile 3
Profile 4
Profile 5
Profile 6
profile depth [m]
%
peridotite
serpentinised peridotite

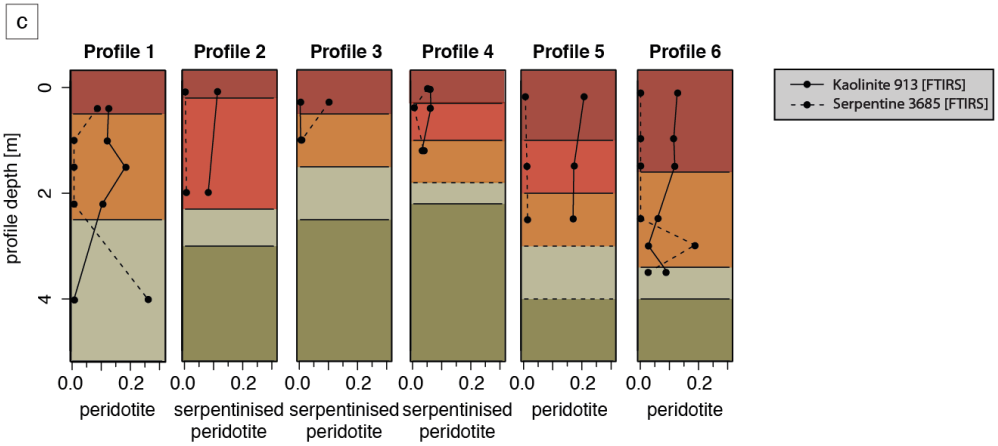
c
Profile 1
Profile 2
Profile 3
Profile 4
Profile 5
Profile 6
profile depth [m]
peridotite
serpentinised peridotite
Kaolinite 913 [FTIRS]
Serpentine 3685 [FTIRS]

Figure S2.3 Microscope images of bedrock thin sections. Left images are in unpolarised light, images to the right are in polarised light. Lowermost images show an olivine grain with a rind of serpentine and possibly magnetite

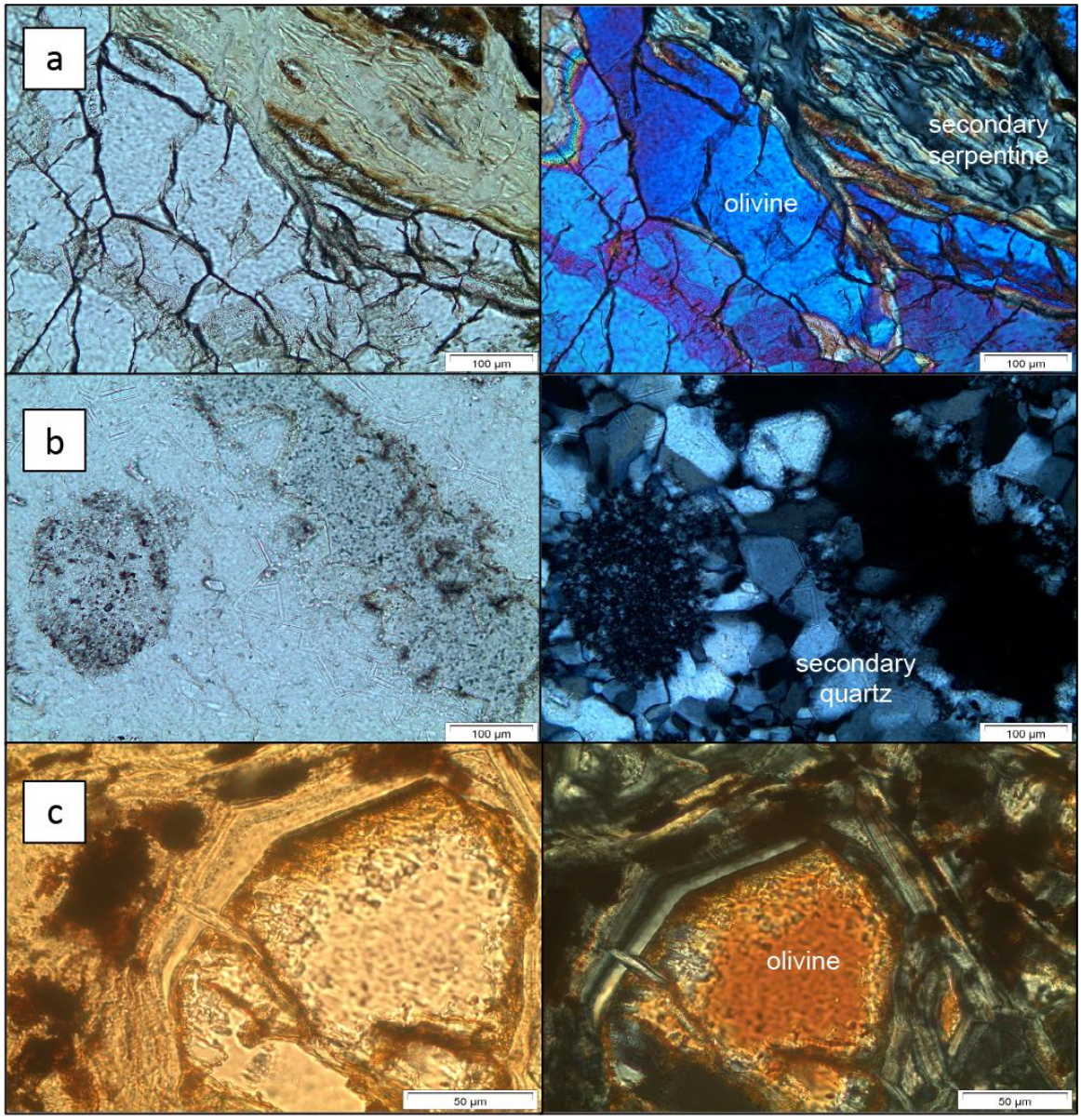

Figure S2.4 Bulk XRD spectra for a) a laterite profile (profile 5) on top of unserpentinised peridotite bedrock, and b) a laterite profile (profile 4) on top of serpentinised peridotite bedrock

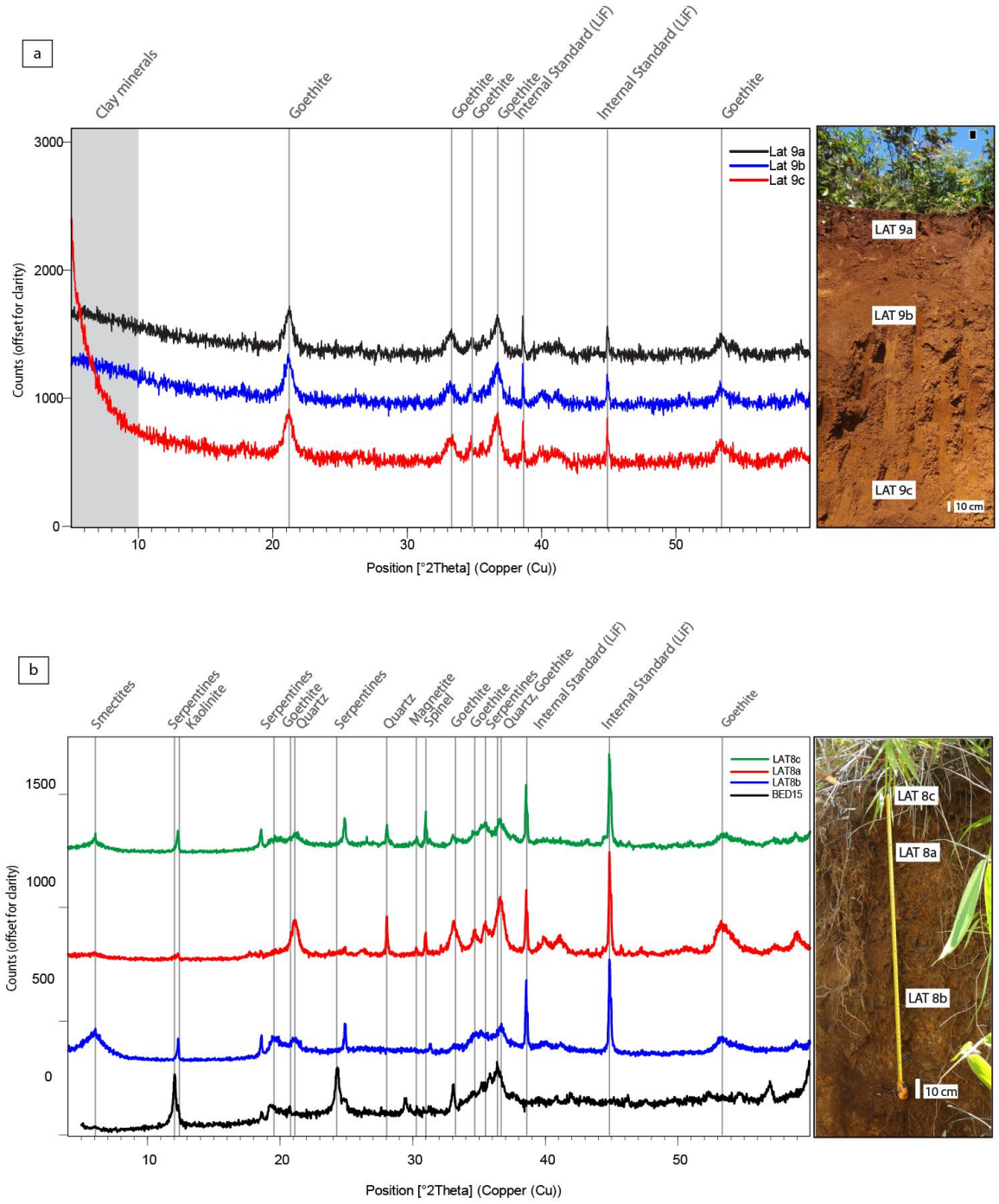

Figure S2.5 Grain-size distribution curves for selected laterite samples based on settling (<0.063 mm), wet (0.063, 0.125, 0.25 mm), and dry (0.5, 1, 2, 4 mm) sieving. Table indicates soil type categorized following the Unified Soil Classification System (USCS). Corresponding geotechnical parameters following Swiss Norm SN 670 010, and parameter values determined on the samples directly

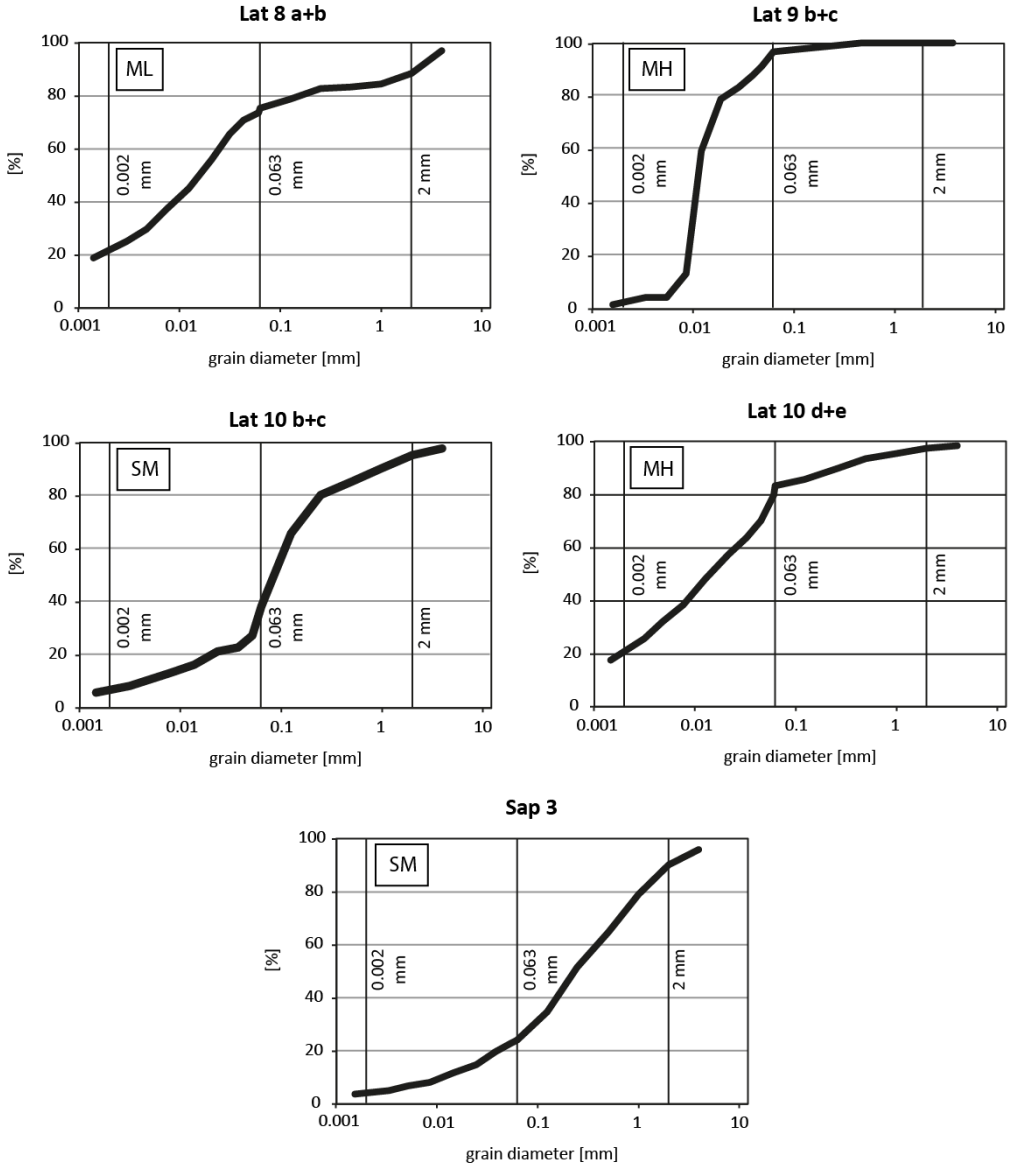

Sample	USCS Classification	Density (ρ)	Water content	ϕ angle	cohesion (c)	Plasticity index (I_P)
		[t m^{-3}]	[wt-%]	[°]	[kN m^{-2}]	[wt-%]
Lat 8 a+b	silt with sand (ML)	1.74 ± 0.18	40.3 ± 6.1	28.8 ± 5.2	54 ± 63	12.3 ± 4.2
	measured	-	44.3	-	-	35.3
Lat 9 b+c	elastic silt (MH)	1.62 ± 0.13	64.8 ± 24.7	25 ± 8	28 ± 25	23.2 ± 7.5
	measured	-	49.5	-	-	20.5
Lat10 b+c	silty sand (SM)	2.07 ± 0.17	18.8 ± 10.8	33.6 ± 1.5	76 ± 73	5.1 ± 4.0
	measured	2.3	17.9	43.8	37.0	not determinable
Lat 10 d+e	elastic silt with sand (MH)	1.62 ± 0.13	64.8 ± 24.7	25 ± 8	28 ± 25	23.2 ± 7.5
	measured	1.5	104.2	26.5	23.0	22.3
Sap 3	silty sand (SM)	2.07 ± 0.17	18.8 ± 10.8	33.6 ± 1.5	76 ± 73	5.1 ± 4.0
	measured	-	9.8	-	-	not determinable

Figure S2.6 Maps of 84 surface sediment samples (colour-coded circles) with background colouring based on kriging interpolation and grey lines representing lake bathymetry with a 20-m line spacing (maximum water depth is ~200 m) for a) Median grain-size diameter (D50) determined by laser diffractometry ('topo-to-raster' interpolation tool was used for the interpolation), b) Chemical Index of Alteration (following Nesbitt and Young 1982), calculation based on ICP-MS measurements. c-f) Element concentrations of Ni, Cr, K, and Ca determined by ICP-MS analysis. g) Kaolinite-to-serpentine ratio determined by FTIRS, h) smectite-to-illite ratio determined by clay XRD. Light blue triangles show the location of the two sediment cores presented in this study, squares represent samples of river suspended load (symbol size is scaled to catchment size; data not available for all parameters)

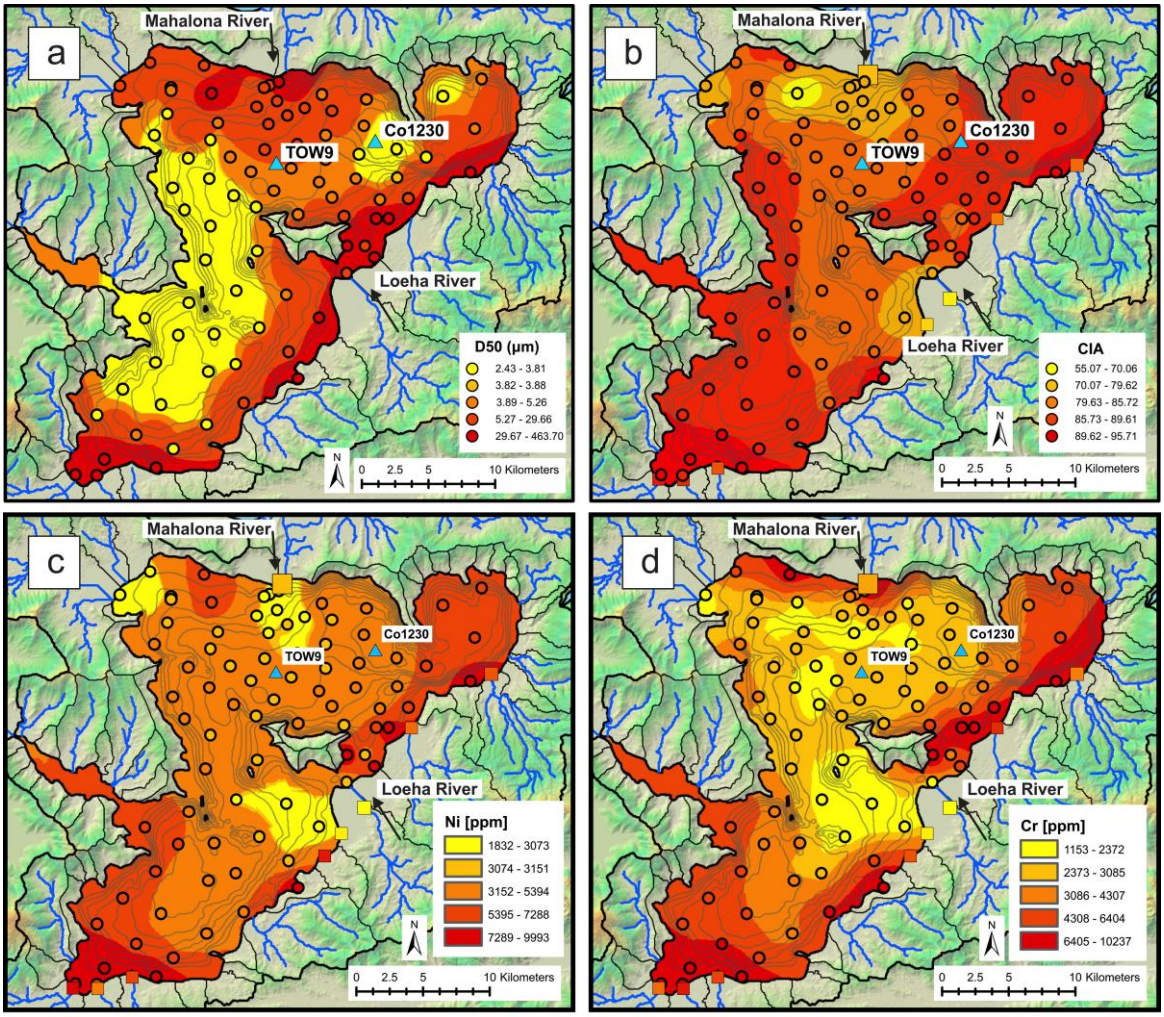

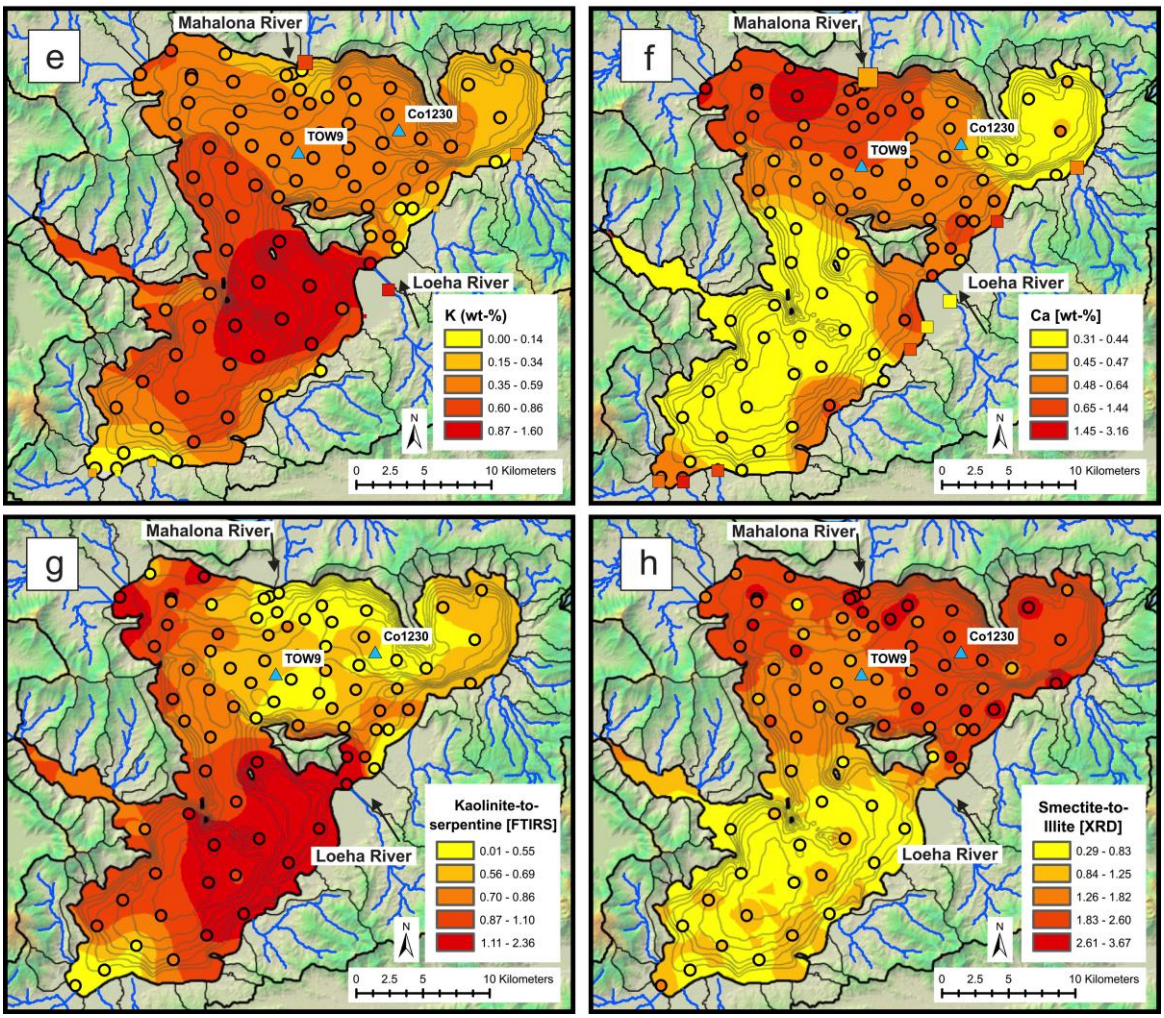
e
Mahalona River
Co1230
TOW9
Loeha River
K (wt-%)
0.00 - 0.14
0.15 - 0.34
0.35 - 0.59
0.60 - 0.86
0.87 - 1.60
N
0 2.5 5 10 Kilometers
f
Mahalona River
Co1230
TOW9
Loeha River
Ca [wt-%]
0.31 - 0.44
0.45 - 0.47
0.48 - 0.64
0.65 - 1.44
1.45 - 3.16
N
0 2.5 5 10 Kilometers
g
Mahalona River
Co1230
TOW9
Loeha River
Kaolinite-to-serpentine [FTIRS]
0.01 - 0.55
0.56 - 0.69
0.70 - 0.86
0.87 - 1.10
1.11 - 2.36
N
0 2.5 5 10 Kilometers
h
Mahalona River
Co1230
TOW9
Loeha River
Smectite-to-Illite [XRD]
0.29 - 0.83
0.84 - 1.25
1.26 - 1.82
1.83 - 2.60
2.61 - 3.67
N
0 2.5 5 10 Kilometers

Figure S2.7 Bulk XRD spectra for a lake surface sediment transect from the Mahalona River mouth to the site of core TOW9 and TDP Site 1

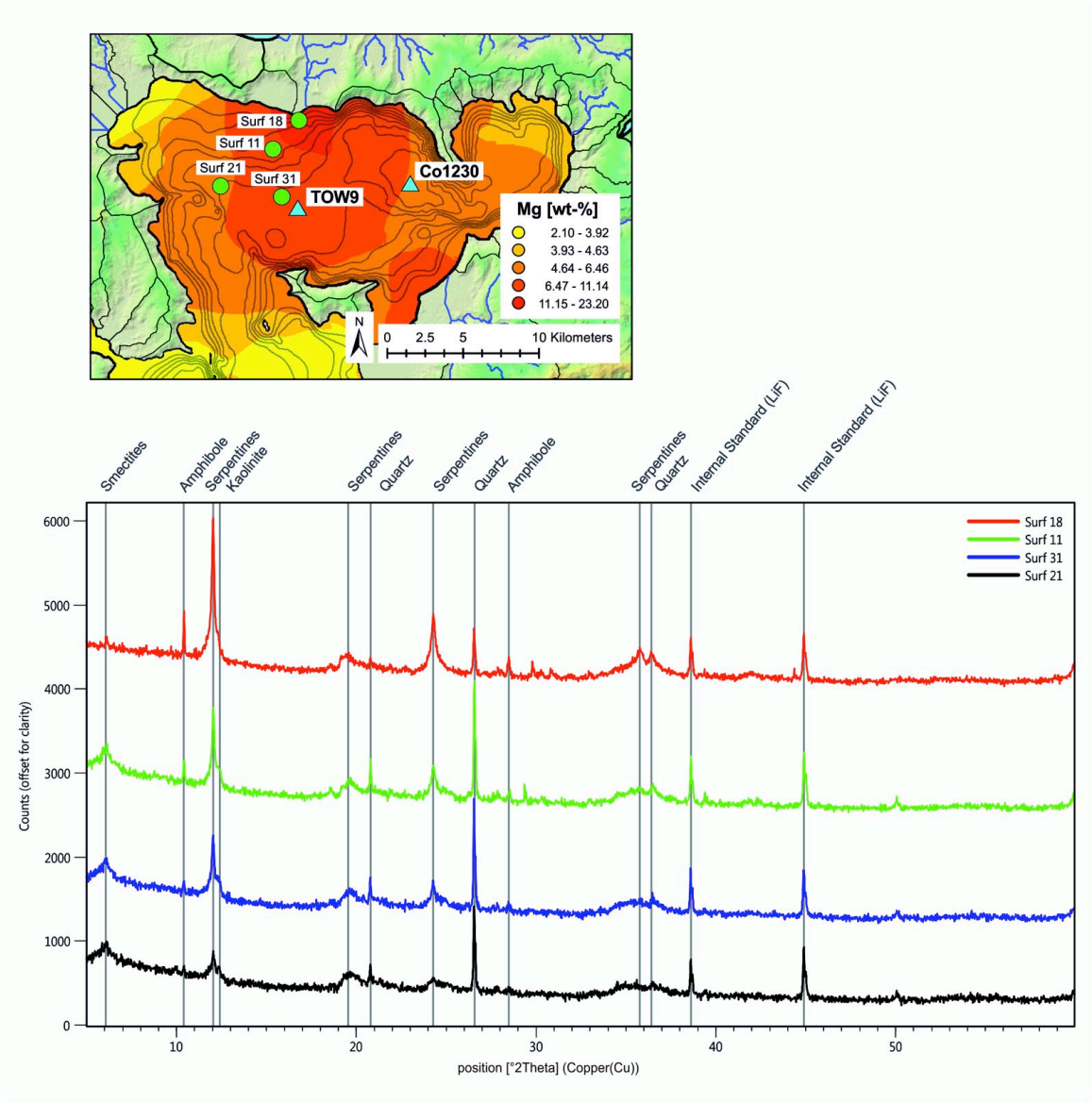

Figure S2.8 XY-plot and ternary diagram showing the element concentration of Al, Mg, and K (concentrations multiplied by 10) in bedrock, saprolite, laterite, river suspended load, surface sediments, and sediment core samples

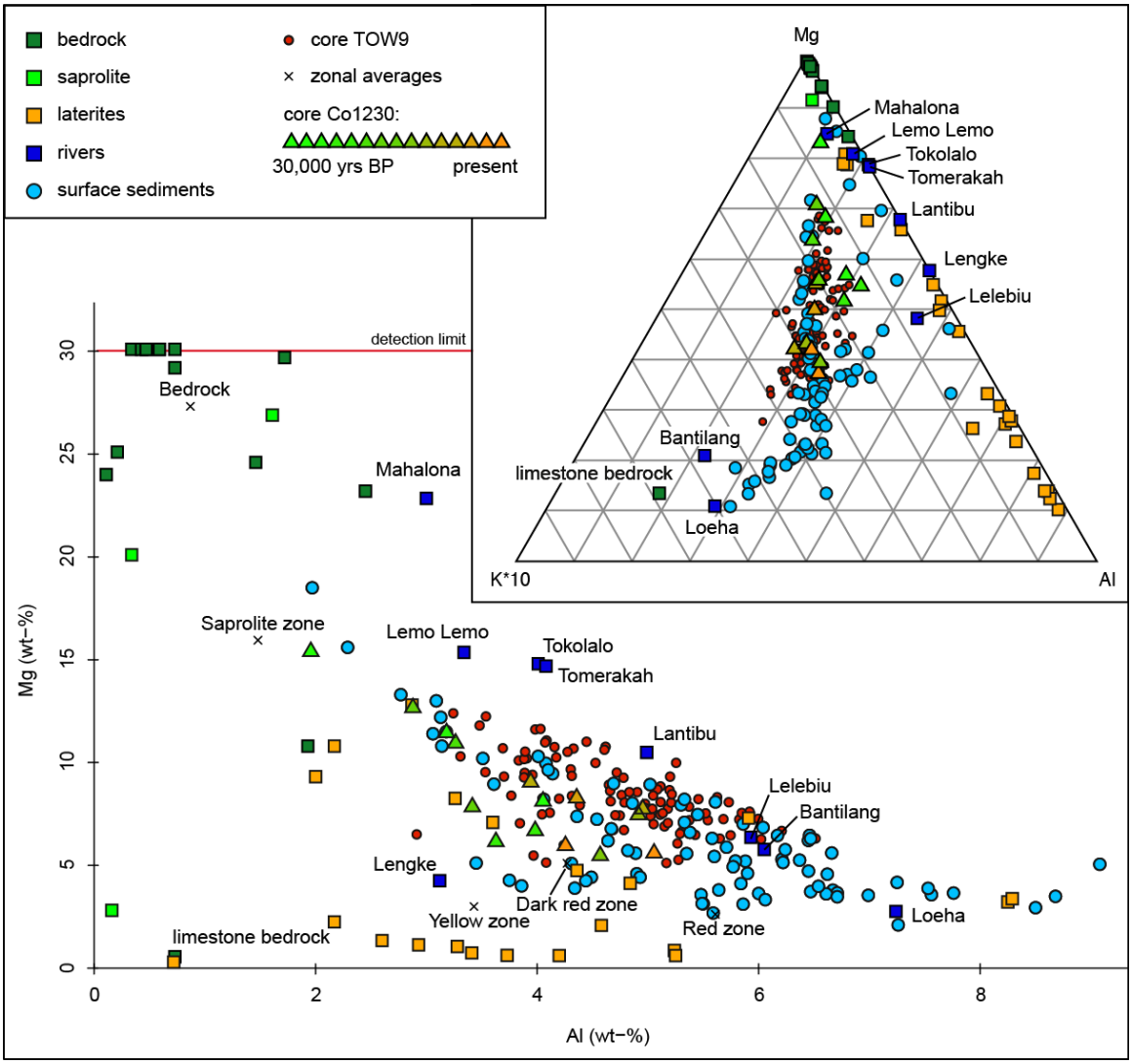

SM References

Rosén P, Persson P (2006) Fourier-transform Infrared Spectroscopy (FTIRS), a new method to infer past changes in tree-line position and TOC using lake sediment. J Paleolimnol 35: 913-923. DOI: 10.1007/s10933-005-5010-8)

CHAPTER 3

Long-term tectonic basin evolution and associated changes in catchment dynamics and depositional environments in tropical Lake Towuti, Indonesia

Marina A. Morlock

in collaboration with

Hendrik Vogel, Daniel Ariztegui, Martin Melles, James M. Russell, Satria Bijaksana & the TDP science team

manuscript draft

3. Long-term tectonic basin evolution and associated changes in catchment dynamics and depositional environments in tropical Lake Towuti, Indonesia

Marina A. Morlock[1]

in collaboration with

Hendrik Vogel[1], Daniel Ariztegui[2], Martin Melles[3], James M. Russell[4], Satria Bijaksana[5] & the TDP science team

[1]*Institute of Geological Sciences and Oeschger Centre for Climate Change Research, University of Bern, 3012 Bern, Switzerland*

[2]*Department of Earth Sciences, University of Geneva, 1205 Geneva, Switzerland*

[3]*Institute of Geology and Mineralogy, University of Cologne, 50674 Cologne, Germany*

[4]*Department of Earth, Environmental, and Planetary Sciences, Brown University, Providence, RI 02912*

[5]*Faculty of Mining and Petroleum Engineering, Institut Teknologi Bandung, Bandung 40132, Indonesia*

This is an early manuscript draft, important data sets (e.g. an age model) were not available in time for completion of this thesis.

3.1 Abstract

Ferruginous lakes Matano and Towuti are part of the ancient Malili Lake System on Sulawesi Island, Indonesia (2.75°S, 121.5°E), which is of great importance to evolutionary studies on adaptive species radiation and endemism. Lake sediment cores of the entire Lake Towuti infill have been recovered in an ICDP project in 2015, offering the unique opportunity to study the environmental and tectonic history of this tropical biodiversity hotspot. Based on core description, mineralogy, grain size, and thin section analysis, we present a general framework of basin evolution and lacustrine sedimentation in Towuti. In the early extensional phase, we find repeated cycles of silting and peat formation, with standing water bodies, swamps and rivers in close proximity. This phase of dynamic habitat changes facilitated adaptation of riverine species to standing water conditions, before a pulse of subsidence established the permanent water body found today, which likely resulted in the initial lake colonisation. Roughly 150,000 years ago, the redirection of today's largest inflow to Lake Towuti, the Mahalona River, with its tributary, the Lampenisu River, greatly increased the supply of serpentine relative to kaolinite to the northern lake basin, creating today's lake system. This drainage reorganisation may correspond to a second colonisation event, which has been suggested by phylogenetics. Large changes in lake trophic state occurred twice in the record, likely related to phosphorous-addition by ash fall. Periodic fluctuations between clay-dominated pelagic fallout sediments and coarser-grained sediments influenced by higher-velocity transport processes may be linked to lake level fluctuations and associated changes in hydroclimate.

Keywords Lake Towuti; depositional environment; Malili Lakes; basin evolution; biodiversity; ancient lakes

3.2 Introduction

Lake Towuti on Sulawesi Island is the largest tectonic lake in Indonesia and one of the oldest lakes in Southeast Asia (Lehmusloto et al., 1997). The lake is part of the Malili Lake System, a biodiversity hotspot and of great importance to evolutionary studies on adaptive radiation (Bramburger et al., 2008; Glaubrecht & von Rintelen, 2008; Herder et al., 2006; von Rintelen et al., 2010; von Rintelen et al., 2012). Despite being hydrologically connected today, each of the Malili lakes has a high number of endemic species distributed amongst several different species flocks (Vaillant et al., 2011). Molecular analyses of snails have suggested several independent colonisations of the lakes by riverine ancestors (von Rintelen et al., 2004) and studies highlight the importance of habitat isolation and resource partitioning for the observed diversification of species (Vaillant et al., 2011). The detailed study of environmental changes in these lakes provides context and can identify external factors influencing biological evolution and endemism in tropical aquatic systems.

In 2015, the International Continental Scientific Drilling Program (ICDP) Towuti Drilling Project (TDP) recovered the entire ~165 m thick sediment sequence down to bedrock from Lake Towuti. Sediments are composed of uninterrupted lacustrine muds present in the upper ~100 m and more heterogeneous alternations of silty-sandy clays and peats in the lower ~65 m (Russell et al., 2016). These sediments offer the unique opportunity to study stages of early lake basin formation and associated changes in fluviolacustrine habitats in an ancient lake setting. The continuous lacustrine sediments are thought to cover the late Pleistocene (Russell et al, 2016; Watkinson & Hall 2016). Earlier studies of Lake Towuti surface sediments (Hasberg et al., 2018; Morlock et al., 2018; Sheppard et al., in review) and short sediment cores (Costa et al., 2015; Goudge et al., 2017; Vogel et al., 2015; Weber et al., 2015) provide detailed descriptions of sedimentation processes in the lake and its catchment today and since the last glacial. These studies suggest that sediment transport and deposition is influenced by tectonics, but that climate-induced changes of the depositional setting were the dominant factor shaping sedimentation in the last 60,000 years (~10 m sediment depth; Morlock et al., 2018). The TDP sediment record can thus contribute significantly to our understanding of the interplay between climatic and tectonic processes and their role in shaping aquatic and terrestrial environments in the humid tropics during the Quaternary.

In this study we provide the lithostratigraphic framework for the 100-m long lacustrine sequence (Unit 1), and the underlying coarser-grained infill (Unit 2) recovered by the ICDP Towuti Drilling Project. For this we utilize mineralogy and grain size results from regularly spaced samples of the TDP Site 1 cores, together with detailed sediment core descriptions and thin section analyses of characteristic lithologies. Our main objectives are: (1) to describe the influence of long-term tectonic basin evolution on catchment dynamics and depositional environments in a tropical setting, (2) to provide a geological perspective on aquatic habitat formation in the ancient lake system, and (3) to differentiate between tectonic and climatic processes that influence changes in lake sediment composition.

3.3 Study Site

Lake Towuti (2.75°S, 121.5°E, 318 m above sea level) is a large (560 km^2) and deep (200 m max. water depth) lake characterised by ferruginous and ultraoligotrophic waters (Figure 3.1; Haffner et al., 2001). In central Sulawesi, three major strike-slip fault systems accommodate the collision between Australia and Sundaland (Asia): the Palu-Koro, Matano, and Lawanopo faults. Lake Towuti is located south of the highly segmented sinistral Matano Fault system, and is bound by several smaller normal faults to the east and west (Figure 3.1; Bellier et al., 2006; Watkinson & Hall, 2016). Several linear fault strands run through the lake and split it into two main and several smaller basins. The catchment of Lake Towuti is dominated by ultramafic rocks from the East Sulawesi Ophiolite complex, with minor occurrences of metasediments and limestones to the East of Lake Towuti and sedimentary melange in the catchments of upstream lakes Mahalona and Matano (Costa et al., 2015; Kadarusman et al., 2004). Today, the lake is thermally stratified below 100 m water depth (Costa et al., 2015), but is suspected to mix occasionally (Hasberg et al., 2018). The main sediment sources to Lake Towuti's deep northern basin are the rivers Mahalona (mafic signature, high abundance of serpentines) and Loeha (more felsic signature), as well as lateritic soil material (mainly kaolinite and Fe-oxides/oxyhydroxides; Hasberg et al., 2018; Morlock et al., 2018).

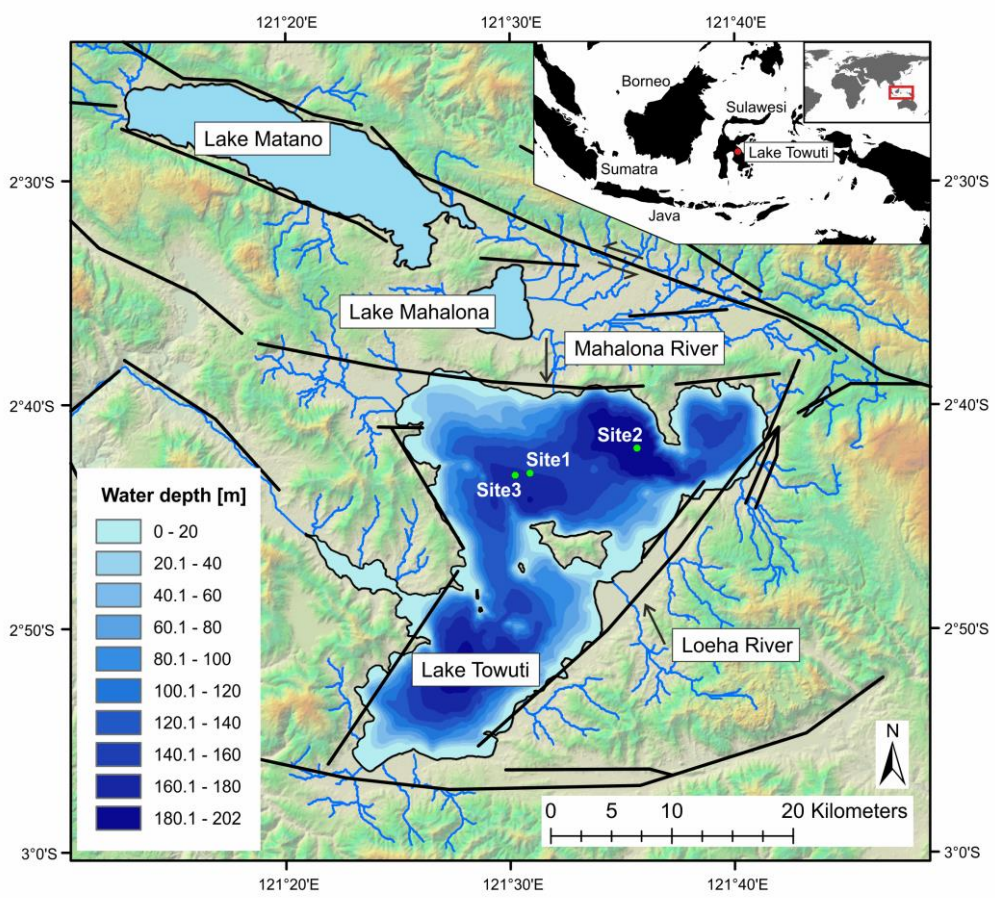

Figure 3.1 Map of the Malili lake system with three TDP drilling locations indicated in Lake Towuti. Tectonic faults in black lines from Watkinson and Hall (2016). Maximum water depths are 590, 73, and 203 m for lakes Matano, Mahalona, and Towuti, respectively (Haffner et al., 2001)

The lake hosts a highly adapted, mostly endemic lake flora and fauna (Haffner et al., 2001; von Rintelen et al., 2012). Previous sediment core studies from Towuti have shown that the lake is sensitive to climate variability on glacial-interglacial timescales (Goudge et al., 2017; Russell et al., 2014; Vogel et al., 2015). In the sediments, these changes are expressed through lake-level induced changes in grain size, bottom water oxygenation, and mineralogy, with coarser, oxic, serpentine-rich sediments indicating dry periods and more fine-grained, anoxic (green), kaolinite-rich sediments deposited during wet periods (Costa et al., 2015; Goudge et al., 2017; Morlock et al., 2018; Russell et al., 2014; Sheppard et al., in review; Vogel et al., 2015; Weber et al., 2015).

3.4 Material and methods

3.4.1 Sample acquisition

In 2015, the ICDP Towuti Drilling Project recovered ~1000 m of sediment cores from three sites in the northern basin of Lake Towuti, using the ICDP Deep Lakes Drilling System (DLDS) operated by DOSECC Exploration Services (Russell et al., 2016). Coring at TDP Site 1 reached bedrock at 162 m below lake floor, consisting of a lithified mafic conglomerate (Russell et al., 2016). All cores were opened, imaged, and described at LacCore, the National Lacustrine Core Facility at the University of Minnesota, USA. The composite section of TDP Site 1 was sampled at 48-cm resolution (276 samples), avoiding event deposits. Samples were integrated over 4 cm of core (~8 cm^3), and material was homogenised before analysis. Smear slides were prepared approximately every 50 cm and examined under the light microscope. Sediments were additionally described based on core images, initial core descriptions and thin sections of characteristic lithologies.

3.4.2 Laboratory analyses

All samples were analysed for clay mineral content by mid-infrared (MIR) Fourier-Transform-Infrared-Spectroscopy (FTIRS). Details on MIR-FTIRS analyses and a comparison to clay X-ray diffraction (XRD) analysis of kaolinite and serpentine in Lake Towuti sediments are described in Morlock et al. (2018). In brief, material for MIR-FTIRS analysis was freeze-dried and 0.011 ±0.0001 g of bulk sediment was mixed and homogenised with 0.5 ±0.0005 g of spectroscopic grade KBr. Samples were analysed at the University of Bern, Switzerland, using a Bruker Vertex 70 equipped with a HTS-XT accessory unit, a liquid nitrogen cooled MCT (Mercury-Cadmium-Telluride) detector, and a KBr beam splitter, in the wavenumber range 3750-520 cm^{-1} at a resolution of 4 cm^{-1}. Characteristic peaks for kaolinite (Chester & Elderfield, 1973; Chukanov, 2014; Farmer, 1974; Madejová, 2003) and serpentine (Chukanov, 2014; Farmer, 1974; Madejová, 2003) were identified. In addition, characteristic peaks for quartz (778 and 798 cm^{-1}), caused by symmetric stretching of SiO_4 (Farmer, 1974; Hahn et al., 2018), and siderite (854-867 cm^{-1}), caused by bending vibrations of the carbonate ion (Chukanov, 2014; Lacey et al., 2016), were identified in the FTIR spectra.

Grain-size distributions of all samples were analysed at the University of Cologne, Germany, with a Beckman Coulter LS13320 laser diffractometer. Bulk samples were treated with 15 ml H_2O_2 (30 %) and ~10ml HCl (10 %) prior to analysis. A few drops of NaOH (1 M) were added to reach a neutral pH before measuring.

Thin sections of representative samples of all main lithologies were analysed under a light microscope. To resolve lateral heterogeneities in geochemistry, selected sections were analysed with an Eagle III µ-XRF spectrometer (Röntgenanalytik Messtechnik GmbH, Germany) at the University of Geneva, Switzerland, at 30 kV, 300 mA, and 10 µs integration time. Each data point reflects the mean element intensity of one measured spot, expressed as counts per second (cps).

3.4.3 Statistics and data analysis

An end-member analysis was performed on the Unit 1 grain-size data set using the Matlab-based software package AnalySize v1.1.2 (Paterson & Heslop, 2015). The algorithm follows the approach of Weltje (1997), which was further developed by Heslop and Dillon (2007). Non-parametric end-members were calculated and three end-members were chosen to best represent the data set. End-member abundances for Unit 2 grain-size data were calculated with end-members predefined by the Unit 1 data set. Three samples were exempt from analysis because their grain-size range lies outside the Unit 1 end-members.

All other statistical analyses were performed in R (R Development Core Team, 2017). All correlation coefficients are Spearman's rank correlation r. Bulk mineralogy from FTIRS was used for a cluster analysis based on Euclidian distances and the complete linkage method. Unless otherwise stated, statistical parameters are given as mean and one standard deviation.

3.5 Results

3.5.1 Stratigraphic units

Based on lithology and seismic profiles (Russell et al., 2016), the Lake Towuti stratigraphic record is divided into two main units (Figure 3.2). The lower part of the record (Unit 2) recovered from the drill core comprises 65 m of coarser-grained, heterogeneous infill, which is overlain by 97-m of fine-grained lacustrine sediments (Unit 1). Based on split core images, core description, thin section analysis, and mineralogy, each main unit is further partitioned into three subunits, 1A-C and 2A-C, respectively (Table 3.1, Figure 3.2 and Figure 3.3). Event layers are omitted from this compilation, but briefly described in the section covering Unit 1 sediments. For Unit 1, three different lithologies (clays, sideritic clays, and diatomaceous oozes) characterise the lacustrine sequence and alternate largely independent of the stratigraphic subunits (Table 3.2, Figure 3.3). These lithologies follow the classification for Unit 1 adopted in Russell et al. (2016).

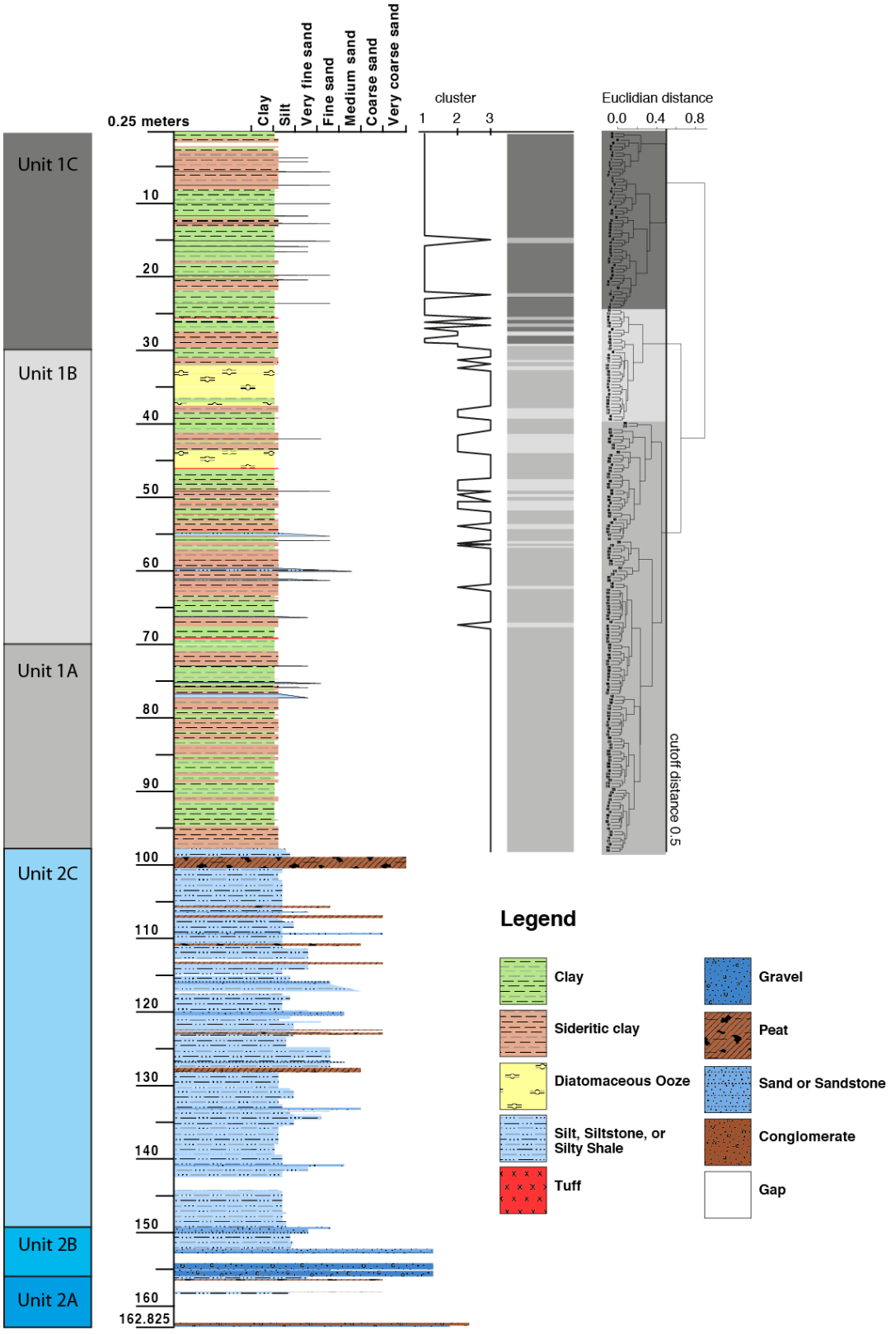

Figure 3.2 Left: Stratigraphic units (this study) and lithostratigraphic column of TDP Site 1 after Russell et al. (2016). Centre: Clusters 1-3 based on bulk FTIRS mineralogy for Unit 1, which subdivide the record in three units of characteristic mineralogy (Unit 1A, 97-70 mcd; Unit 1B, 70-30 mcd; Unit 1C, 30-0 mcd). Right: Dendrogram showing all analysed FTIRS samples and their Euclidian distance, respectively. The three clusters were selected based on a distance greater than 0.5

Table 3.1 Description of stratigraphic units for TDP-Site 1

Core Unit	Interpretation	Depth	Description	Figure 3.3-
Unit 2A	Bedrock and lateritic soil	158-154	Cemented, coarse-grained mafic conglomerate with well-rounded components. Followed by a semi-lithified, iron oxide-rich deposit. Lower part: Fe-rich grains, embedded in a millerite-containing, Ni-, Si-, and Cu-rich matrix. Upper Part: Iron-rich grains (0.5-1 mm), embedded in a Mg-, Si-, and P-rich matrix.	1, 2, Figure 3.4
Unit 2B	Coarse gravel	154-148	Dark grey to black, massive gravelly sand to sandy gravel with clasts up to 7 cm in size. Clasts mostly rounded.	3
Unit 2C	Fill-up sequences	148-97	Clayey-sandy silts, intercalated with peat. Medium bedded, grey to brown in colour. Individual beds are well-sorted and contain occasional siderite nodules. Several such successions are present in Unit 2C. Coarse sections are rich in serpentine, fine-grained sections are kaolinite- and quartz-rich.	4, 6
Unit 1A	Early lake	97-70 mcd	High abundance of kaolinite and quartz, decreasing through the unit. Siderite increasing. Kaolinite and serpentine positively correlated.	Figure 3.7
Unit 1B	Deep lake	70-30 mcd	High abundance of kaolinite, quartz amounts are steady throughout the unit. Serpentine below detection limit.	Figure 3.7
Unit 1C	Modern lake	30-0 mcd	High serpentine abundance, with high-amplitude variations. Kaolinite and serpentine negatively correlated.	Figure 3.7

3.5.2 TDP Site 1, Unit 2

Unit 2A represents the lowest part of the Towuti record, including a section of lithified, mafic conglomerate (bedrock) at 158.7 mcd. Recovery above this conglomerate is poor. The following recovered section at 154.7 mcd contains a 30-cm thick crumbly, reddish brown sediment. Thin section analysis of this layer (154.5 mcd) shows brownish grains (0.5-1 cm in diameter), which are rich in Fe, Cr, and Mn (Figure 3.4). The surrounding matrix is enriched in Mg, Si, and P. This zone is mostly located above, but also partly overlaps a zone with smaller (<1 mm) light-coloured Fe-rich pyroxene grains, which have a Ca-rich rim (Figure 3.4). These grains are embedded in a Ni-, Si-, and Cu-rich matrix, which also contains distinct Ni-S-rich intervals.

Overlying this subunit is a ~1.3-m thick section of alternating coarse, rounded gravels and poorly sorted sands and silts (Unit 2B). Clasts have sizes of up to 7 cm. This subunit sharply transitions to light-coloured clayey silts at 148.7 mcd.

Table 3.2 Description of lithotypes for TDP-Site 1, Unit 1

Core Unit	Lithotype	Description	Figure 3.3-
Unit 1	Sideritic clay	Medium bedded (cm), reddish-grey silty clay with abundant light-coloured siderite-rich layers and siderite mottles. Siderite occurs in patches of fine-grained (~50 µm) crystals, which can be aggregated to larger concretions (0.1-3 mm). Sideritic layers often occur repeatedly within decimetres.	8, 8a
Unit 1	Clay	Structureless, partly medium- to thickly-bedded (cm-dm) grey-green, olive green or very dark green silty clay, characterised by kaolinite and, to a lesser degree, abundant quartz.	9, 9a
Unit 1	Diatomaceous ooze	Diatom-rich sediments, culminating in light-coloured, finely-laminated to thinly-bedded sediments, composed of diatoms and varying amounts of clay flakes within the diatomaceous layers.	10, 10a, Figure 3.8

Unit 2C sediments are primarily composed of clayey-sandy silts intercalated with nine peat deposits, the thickest of which is about 2.5 m thick and marks the transition between Units 1 and 2 (Figure 3.2). This peat deposit is overlain by ~1.10 m of medium bedded, reddish-grey sideritic silt, which at its top is bioturbated (97.9 mcd; Figure 3.3) followed by a sandy layer, which quickly fines upwards towards dark green clay. In general, peat layers gradually transition into clay and silt deposits, which have a light grey-blue to grey-green colour (Figure 3.3). Grain-size patterns of Unit 2C are well described by the three end-members defined on Unit 1 samples (Figure 3.5 and Figure 3.6). Grain size end-member 1 (EM1) is characterised by a negatively skewed unimodal distribution with the main peak at ~7 µm (mean 4.2 µm), and 95 % of the sediment grains between 0.5 and 15 µm (Figure 3.5). Fine-grained EM1 is most abundant close to the uppermost peat layer and between 122 and 117 mcd. End-member scores generally increase from 113 to 103 mcd and are positively correlated with kaolinite and quartz abundance (r=0.64 and r=0.72, respectively, p=0.000, n=37). Grain size end-member 2 (EM2) shows a positively skewed bimodal distribution, with the main peak at 44 µm and a minor peak at 10 µm (Figure 3.5), with 95 % of the grains between 3 and 140 µm (mean 45 µm). Coarse-grained EM2 decreases from 127 to 117 mcd, and scores are positively correlated with serpentine abundance (r=0.70, p=0.017, n=11). Coarse-grained samples are more common around peat deposits. Grain size end-member 3 (EM3) is characterised by a well-sorted unimodal distribution with a maximum at 21 µm (Figure 3.5) and 95 % of the grains between 3 and 35 µm (mean 17 µm). Unimodal EM3 is more variable compared to the other end-members (Figure 3.6). Three samples have coarser grain-sizes than the pre-defined end-members and show a unimodal grain-size distribution between 0.5 and 1 mm (at 109, 113, and 116 mcd, respectively). These coarse samples also have high serpentine abundance.

3.5.3 TDP Site 1, Unit 1

Mineralogy

Cluster analysis of the bulk FTIRS mineralogy divides the data into three clusters of Euclidian distances greater than 0.5 (Figure 3.2). The first cluster is dominant in the upper 30 m of the record, samples between 30 and 70 mcd are alternately associated with clusters 2 and 3, and cluster 3 is dominant in the lowest part of the Unit 1 record. Based on these patterns, Unit 1 is divided into three subunits of characteristic mineralogy.

Unit 1A (97-70 mcd) sediments contain abundant of kaolinite and quartz, followed by a distinct decrease in these minerals along with peaking siderite amounts between 83 and 78 mcd (Figure 3.7). Siderite in this unit is negatively correlated with kaolinite and quartz abundance (r=-0.53 and -0.55, p=0.000, n=66). Kaolinite and serpentine show an overall positive correlation (r=0.42, p=0.005, n=66), but the relationship seems divided into a positively and a negatively correlated section (Figure 3.7). The low number of samples does, however, not allow a robust quantification of the potential negative relationship.

Unit 1B (70-30 mcd) is characterised by abundant kaolinite, which peaks around 38 mcd (Figure 3.7). Quartz amounts are steady throughout this unit and only weakly positively correlated with kaolinite (r=0.41, p=0.000, n=94) compared to units A (r=0.83, p=0.000, n=66) and C (r=0.8, p=0.000, n=63). Serpentine abundance is below detection limit of FTIRS.

Unit 1C (30-0 mcd), in contrast, contains abundant serpentine (Figure 3.7), which shows short-duration high-amplitude variations. Kaolinite content is negatively correlated with serpentine (r=-0.66, p=0.000, n=63). Siderite is negatively correlated with kaolinite and quartz (r=-0.33 and -0.5, p=0.009 and 0.000, n=63, respectively).

Grain size

Grain-size variability occurs largely independent of the mineralogical units. End-member analysis of the grain size data produces three distinct end-members, which describe 94 % of the variance in the data set (11.4° angular deviation). All measured grain sizes in Unit 1 are smaller than 280 µm. Highest abundances of fine-grained EM1 are found around 10, 25, and 96 m composite depth (mcd), with a general decrease in abundance from 96 to 36 mcd (Figure 3.6). Coarse-grained EM2 is antiphased with EM1 and is most abundant at 6, 17, 27, and 52 mcd (Figure 3.6). Unimodal EM3 abundance shows two distinct peaks at 36.5 and 44.8 mcd (Figure 3.6). Smear slide and thin section analyses show very high (>80 %) concentrations of planktonic diatoms in this part of the record (Figure 3.8), with occasional clay-rich lenses and very few pyrite grains.

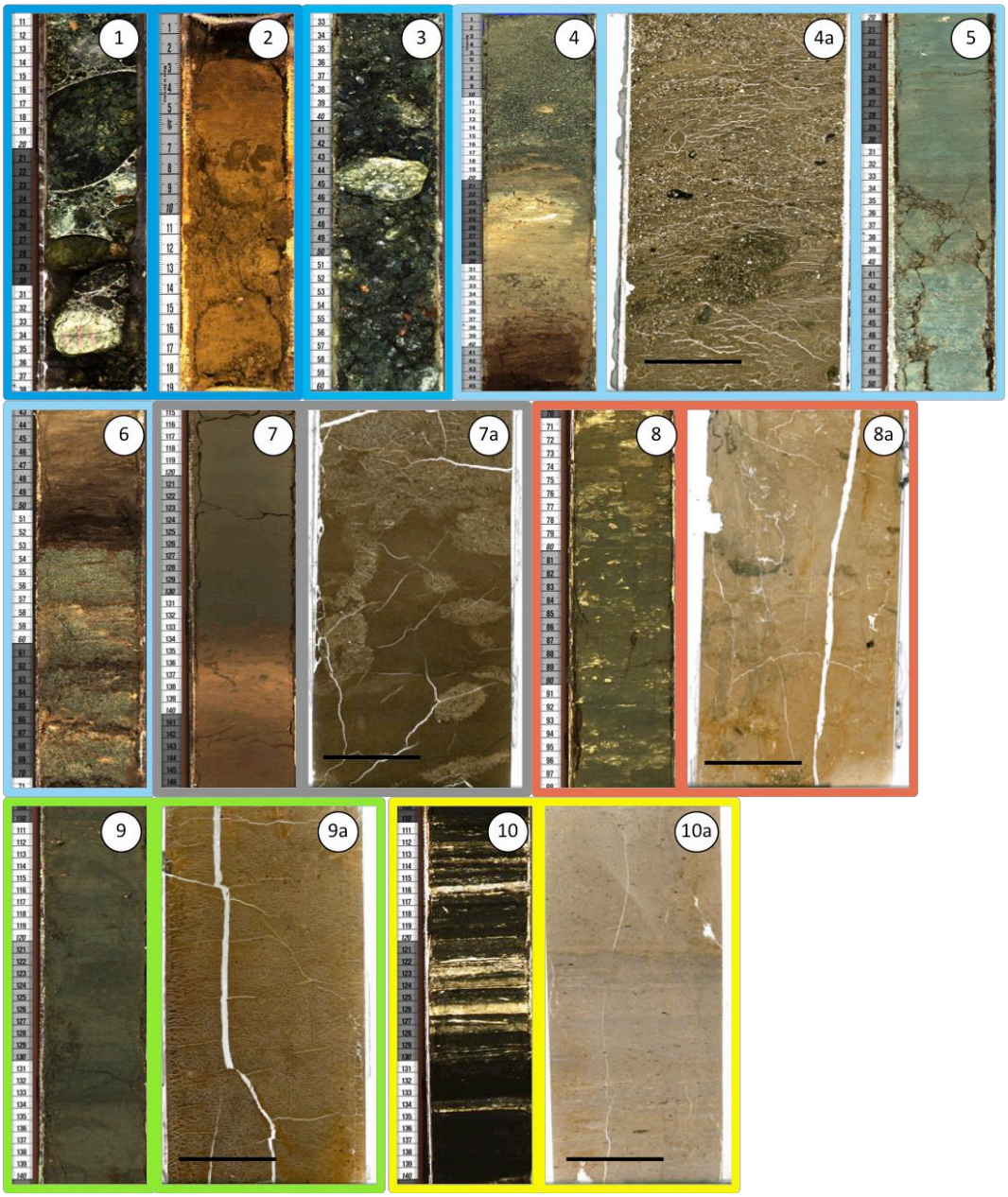

Figure 3.3 Core and thin section images of TDP-Site 1 main stratigraphic units (1-6) and main Unit 1 lithologies (7-10). Brightness enhanced by 40 %, frame colours follow colouring in Figure 3.2. Black bars in thin section images are 1 cm. (1) Mafic conglomerate bedrock. (2) Overlying laterite soil. (3) Coarse gravel in Unit 2. (4) Peat (bottom) transitioning first to fine-, then to coarser-grained sediments. (4a) Thin section image of a coarse-grained section in a peat-sand-sequence. (5) Light-blue clay in Unit 2. (6) Unit 2 sequence of peat and sand deposition. (7) Last indication for shallow-water deposition with burrow structures at the transition Unit 1-Unit 2. (7a) Thin section image of this transition, with burrow structures. (8) Slightly reddish-grey to dark grey sideritic clay, corresponding to enhanced lake mixing. (8a) Thin section image of a characteristic sideritic clay section, siderite appears black in the image. (9) Dark olive green clay, corresponding to deposition in a stratified water column. (9a) Thin section image of a characteristic clay section, clays are mostly structureless. (10) Diatomaceous ooze indicating eutrophic lake water. (10a) Thin section image of a diatomaceous layer showing fine laminations in the diatomaceous sequence

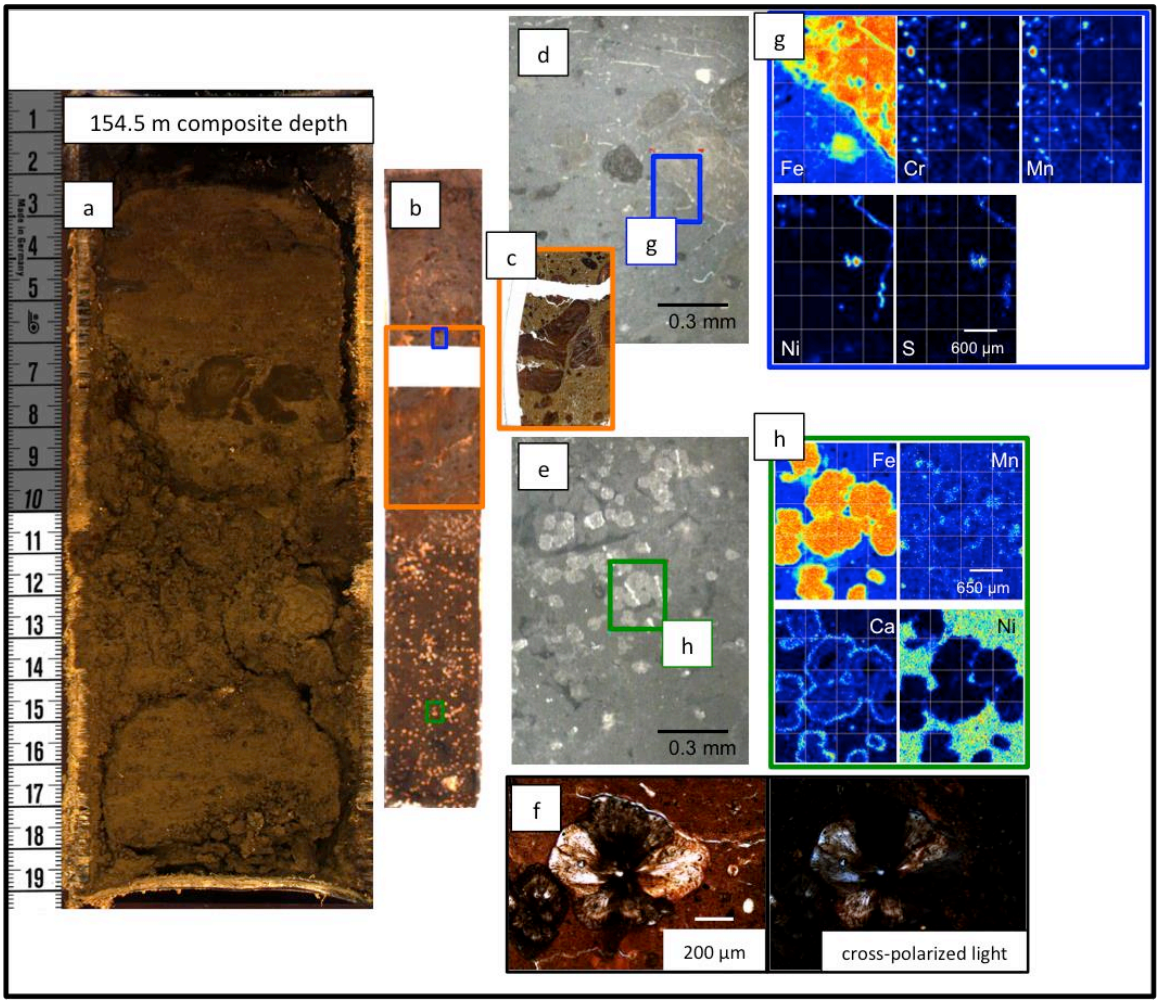

Figure 3.4 Buried laterite at 154.5 m composite depth: Images of (a) sediment core, (b) polished core section, (c) thin section, (d and e) reflected-light and (f) transmitted-light microscopic section, (g and h) µ-XRF maps. Colour-coded boxes show the locations of respective detailed views

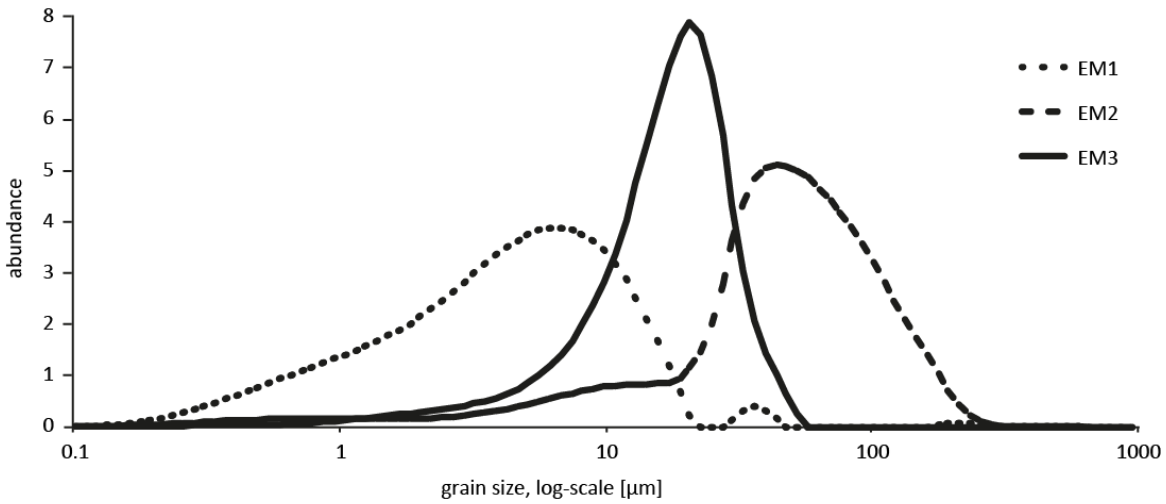

Figure 3.5 Calculated grain size distribution curves for the three end-members based on grain size measurements of regular-spaced samples from TDP Site 1 Unit 1 cores

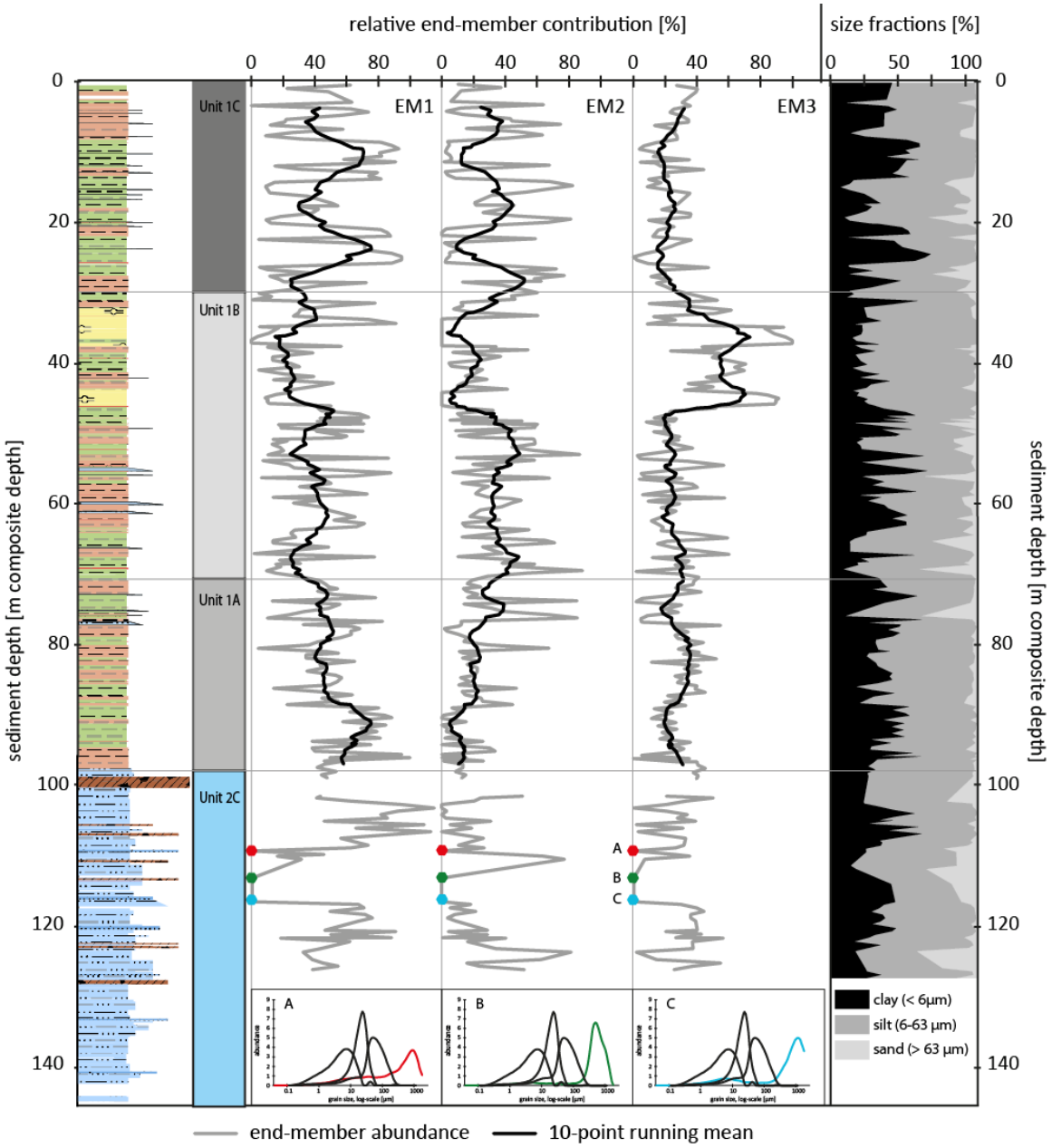

Figure 3.6 Relative contribution of the three grain-size end-members to the measured grain size distribution curves determined on regular-spaced samples from TDP Site 1 cores. Right: Grain-size classes (clay, silt, sand) for each sample

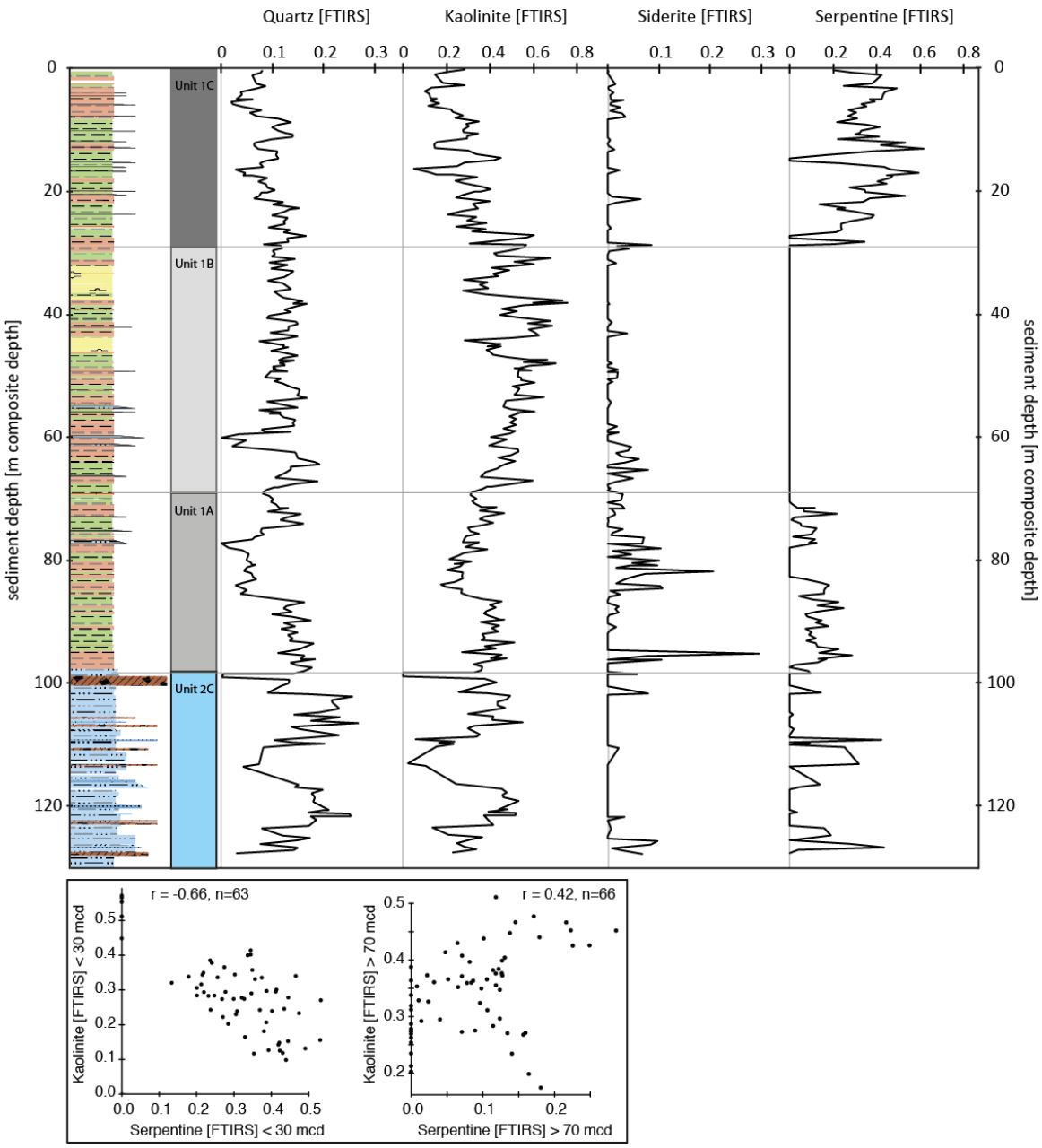

Figure 3.7 Mineralogy determined on regular-spaced samples from TDP Site 1 cores by FTIR spectroscopy. Lower panels show crossplots of kaolinite and serpentine for samples from 0-30 and 70-97 m composite depth, respectively

Event layers

Two types of event layers are present in the Towuti record: tephra deposits and normally graded silts. The deposits jointly make up ~4 m of the lacustrine record. In total, 18 tephra deposits could be identified in the record, which appear as 1-40 cm thick, partly semi-lithified deposits. Normally graded silts (19 deposits) occur in beds with thicknesses between 1 and 55 cm in the upper 97 m of the Towuti record.

Authigenic minerals

Siderite ($FeCO_3$) and millerite (NiS) occur irregularly, but are present throughout the sediment record (Figure 3.9). Abundance generally increases with depth in the upper 97 m, with highest concentrations below 70 mcd. Siderite and millerite occur in all lacustrine lithologies, but large siderite concretions are more abundant in reddish sediments and millerite often occurs close to or within these concretionary sideritic horizons. Siderite concretions are commonly between 0.1 and 3 mm in diameter, and various sizes may be found within the same sideritic band. Millerite occurs more sporadic and aggregates are commonly smaller than siderite (<100 µm), but can occasionally have sizes of up to 0.5 mm.

Vivianite ($Fe(PO_4)_2$) is sporadically observed at several core intervals, particularly at 19.9, 22.8, 27.0, and 50 mcd. At 22.8 mcd, vivianite is present as a distinct, about 2-cm thick layer of grains embedded in the sediment matrix. At 27.0 mcd, occasional vivianite grains are mottled in the sediment matrix over several cm. The vivianite concretion at 50 mcd is ~5 cm long and ~2 cm wide and is covered by a 1 cm thick siderite-cemented turbidite deposit (Vuillemin et al., in prep.). In the thin section at 19.9 mcd, vivianite occurs as three distinct, 1-2 mm thick layers just above a 4-cm thick tephra deposit (Figure 3.10). The first horizon occurs directly above the tephra deposit, and each of the three horizons is covered by a 3-8 mm thick detrital clastic, normally-graded layer. Within the horizons, vivianite occurs in patches of fine-grained minerals (Figure 3.10), which appear dark blue under the light microscope. Micro-XRF mapping of the section show that the vivianite horizons are enriched in Fe and P, and that their chemistry is distinctly different from the underlying tephra deposit (Figure 3.10).

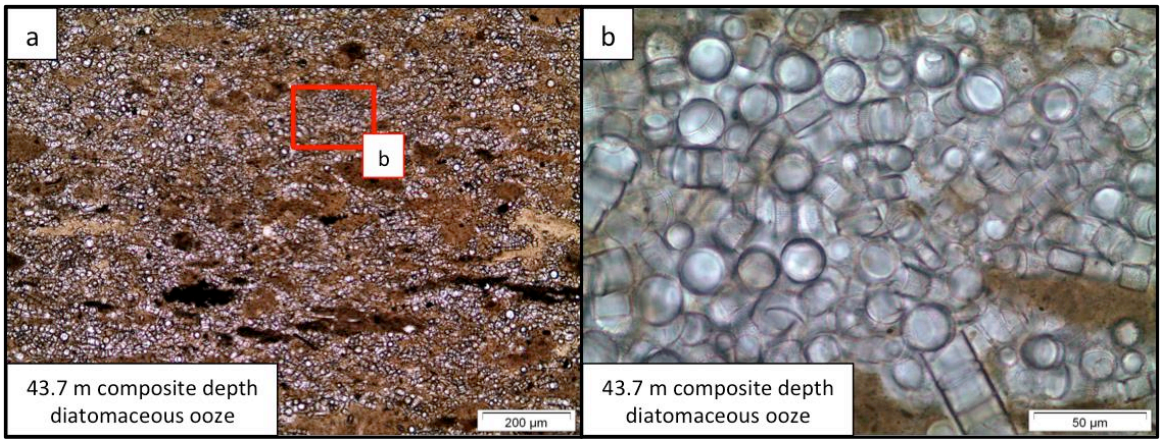

Figure 3.8 Transmitted-light microscope images of thin sections from diatomaceous ooze sediments

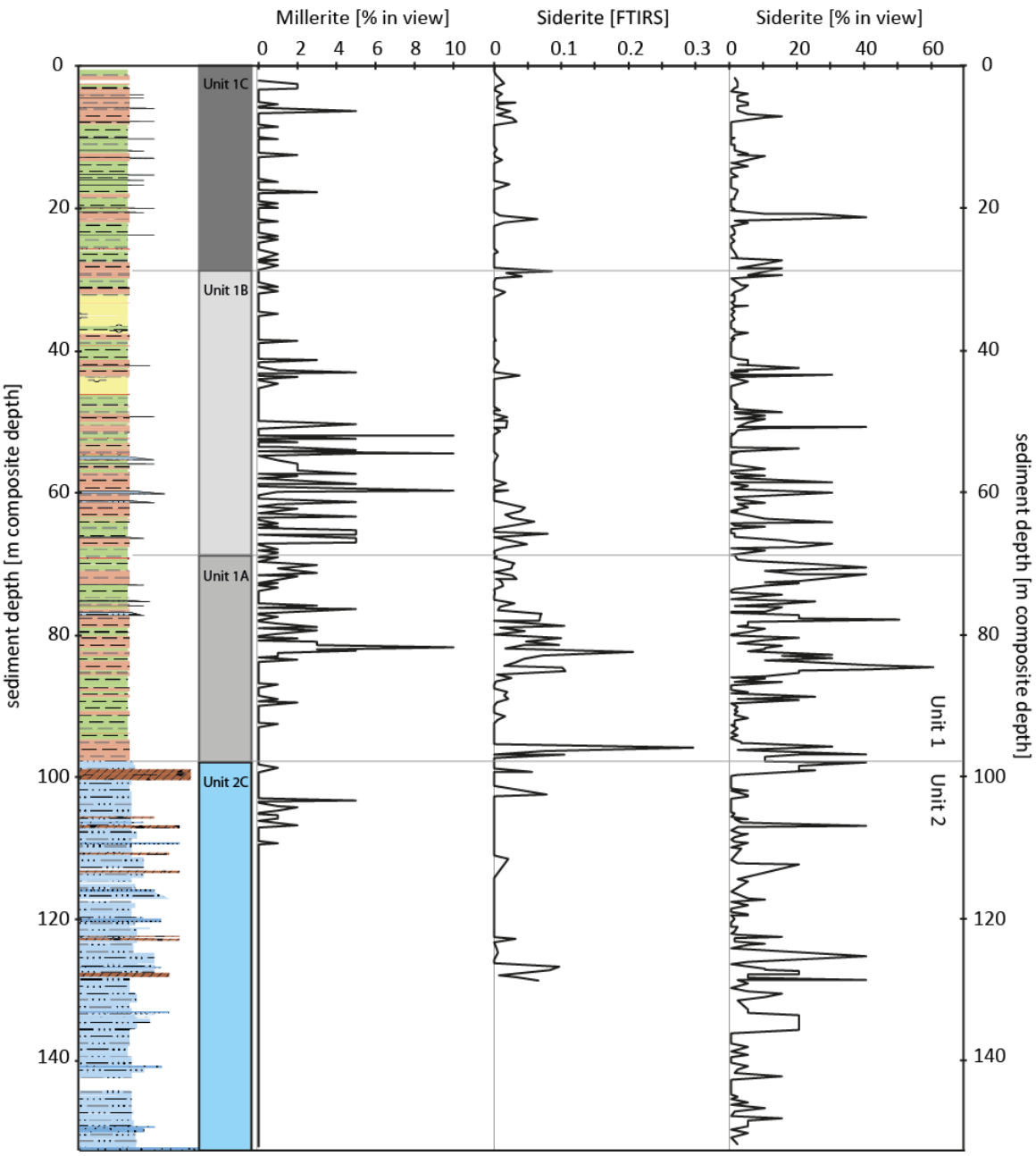

Figure 3.9 Millerite and siderite content determined on smear slides and FTIRS measurements of siderite determined on regular-spaced samples from TDP Site 1 cores, respectively

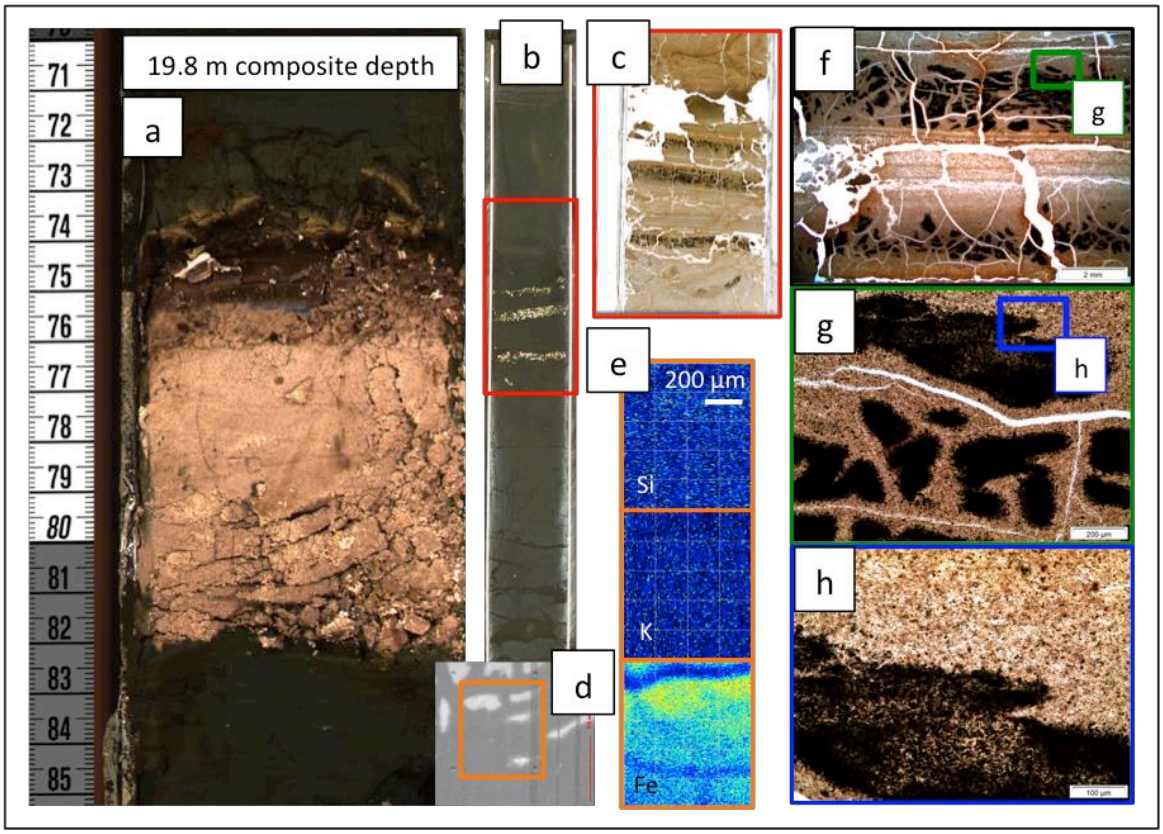

Figure 3.10 Tephra and overlaying vivianite layers at 19.8 m composite depth: Images of (a) sediment core, (b) polished core section, (c, f-h) thin section, (d) reflected-light microscopic section, (e) µ-XRF maps. Colour-coded boxes show the respective location of more detailed views

3.6 Discussion

3.6.1 Tectonic basin evolution

Laterite formation (Unit 2A)

Drilling at TDP Site 1 reached bedrock at 158.7 mcd at hole 1B, consisting of a lithified mafic conglomerate (Russell et al., 2016). Bedrock is covered by a reddish brown crumbly sediment, which contains a zone of strongly weathered pyroxene crystals, surrounded by secondary serpentines in the lower part, and overlain by Fe-oxides/oxyhydroxides (Figure 3.4). This zoning, although in a contracted fashion, resembles the laterites developed on ultramafic bedrock found in the lake's catchment today (Morlock et al., 2018), with weathering of bedrock components and secondary mineral formation in the saprolite zone and high concentrations of iron oxides/oxyhydroxides in the lateritic horizons. Based on the presence of *in situ* weathering features, e.g. in pyroxene crystals, and the chemical zonation, we argue that soil formation rather than erosion predominated at the coring site during this initial stage of basin formation.

Initial subsidence (Unit 2B)

Above this paleosol, ~1.3 m of coarse, rounded gravel indicate a switch from soil formation on bedrock to subsidence and accumulation of fluvially transported sediments in a topographic depression. Based on 2D-seismic profiles, the coring location TDP-Site

1 lies in a basin confined by normal faults, which show displacement in the sediments associated to Unit 2 (Appendix I, Figure I.1.3). The deposition of well-rounded gravels suggests subsidence, creation of accommodation space, and the redirection of rivers following tectonic activity along these faults. Absence of sediments associated with soil erosion speaks against neo-formation of rivers close to the coring site.

A dynamic landscape (Unit 2C)

Initial subsidence at the coring site was followed by the deposition of clay- to silt-sized clastic sediments, which dominate the record a mere ~2 m above the paleosol horizon. The generally fine-grained nature of the sediments suggests deposition in a low-energy environment and the existence of standing water bodies already in these early stages of basin formation. Mineralogy in the fine-grained deposits indicates kaolinite and secondary quartz from the surrounding laterites as the main sediment source. Exposed metasedimentary rocks and corresponding soils could have further contributed to this fine-grained quartz-rich sedimentation. Today these lithologies are only present at the margins of Lake Towuti's catchment, e.g. along the Loeha River, but lateral and vertical displacement along the Matano Fault and associated smaller faults throughout the Quaternary may have exposed metasedimentary rocks closer to the coring site. The clay deposits are intercalated with coarser serpentine-rich intervals, which indicate river incision into the ultramafic bedrock occurred in response to tectonic subsidence and increasing hydrologic gradients. These coarse-grained intervals occur repeatedly through Unit 2, amongst others above and below the peat layers. This indicates that new accommodation space was created repeatedly, flooding the peat bogs and allowing for fluvial or fluviolacustrine sediment deposition on top of the organic material. Once this new accommodation space was sufficiently filled with clastic sediments, fine-grained lake sedimentation and peat formation continued. Hence, already during early basin formation, successive fill-up of tectonically-formed accommodation space by siliciclastics and organic sediments (peat) occurred.

Establishment of a permanent lake (Unit 1A)

The last indication of shallow-water deposition under oxic conditions is found at 97.9 mcd, where burrow structures indicate bioturbation by worms or roots, followed by a ~10 cm-thick sand-rich layer. The following 97.8 m of the sediment record are dominated by clay and silt, indicating continuous lacustrine deposition. Sedimentation rates in the upper 10 m of the record average ~20 cm/1000 years (kyr; Russell et al., 2014), which suggests a Pleistocene age for the entire lacustrine succession. Mineralogy shows that there were substantial changes in sediment provenance and depositional environments during the lake's history. In the lowest part of the succession (Unit 1A) high clay content indicates low transport energies at the coring site, suggesting a rapid increase in lake surface area, i.e. a pulse of basin extension and subsidence shortly (0.85 m) after the last peat formation, shifting the coring site to a distal position in the lake. During the early continuous lake phase, active subsidence probably led to a lowering of the base level and upslope knick-point propagation in existing rivers and/or the formation of new creeks and rivers. Knick-point propagation and the newly forming rivers around Lake Towuti eroded both laterites and bedrock-derived material. High amounts of kaolinite and quartz indicate erosion and transport of strongly weathered laterite soils to the lake, whereas elevated serpentine content relative to Unit 2 indicates river incision into the serpentinised peridotite bedrock, which could best be explained by continued basin

subsidence. Between 83 and 58 mcd, abundant siderite marks an interval of strong post-depositional alteration, which partly overprints the mineralogical signature at time of deposition.

A stable, deep lake (Unit 1B)

The formation of the lake was followed by a phase of a stable, deep water body (Unit 1B). Serpentine is largely absent (below the sensitivity of the FTIRS analysis), either indicating no major tectonic disturbance with little bedrock incision or hydrodynamic sorting with the coring location sufficiently distal to major river deltas. Sediment composition in Unit 1B in comparison to Unit 1C and today suggests a very much reduced or absent influence of the Mahalona River with its strong Mg-serpentine-rich sediment load. Kaolinite dominates sediment mineralogy, suggesting predominant erosion and/or transport of strongly weathered material from the lateritic soils to the coring location. Moderately high, but constant amounts of quartz further suggest a component of more felsic material. Based on mineralogy of the surface sediments today, the Loeha River is the main source of felsic minerals to the lake (Hasberg et al., 2018; Morlock et al., 2018). With a much more limited or absent Mahalona River, sediments from the Loeha River could have had a stronger influence on sedimentation at the coring location during this phase. The more pronounced increase in kaolinite relative to quartz, however, rather points towards lateritic soil material as the main sediment source. Laterites around Lake Towuti have occasional secondary quartz veins running through the profiles, which could account for moderate quartz concentrations in the lake sediments (Morlock et al., 2018).

Fundamental change in hydrology (Unit 1C)

At 30 mcd, mineralogy changes abruptly to abundant serpentine and less common kaolinite in the sediment, and both minerals are negatively correlated in this unit (Unit 1C, roughly 150 kyr-today). In today's lake system, the Mahalona/Lampenisu River system is the most important source of serpentine-rich material to the northern lake basin (Costa et al., 2015) because of persistent tectonic perturbation of the Lampenisu River by the Matano fault (Morlock et al., 2018). A moderate modification to the catchment topography would terminate the direct connection of the Lampenisu River to Lake Towuti. Based on today's DEM, the topographic gradient between the large alluvial plain of the Lampenisu River, Lake Mahalona, and Lake Towuti is smaller than DEM resolution (30 m), and the relative difference between the alluvial plain of the Lampenisu River and the drainage system to the east of the river is approximately 220 m. Located within the tectonically active area of Central Sulawesi with rapid slip rates along the Matano fault, which has been active throughout the Quaternary (Bellier et al., 2006), various topographic changes seem possible over the proposed time scales. Solely based on today's DEM it is not possible, however, to distinguish between several scenarios: i) The Lampenisu River formerly drained into Lake Mahalona until erosion or a tectonic pulse allowed the direct connection to Lake Towuti. ii) Lakes Mahalona and Towuti were formerly combined into a large lake extending north of Towuti's modern limit and material transported by the Lampenisu River did not reach the TDP coring sites until tectonic disturbance split the lakes. iii) The Lampenisu River formerly drained to the east, away from the Malili Lake system or even served as an outflow, with the entire Malili lake system draining east. Yet, regardless of the scenario, there is clear evidence that today's dominance of the Mahalona/Lampenisu River is limited to the upper 30 m of the

sediment succession (Unit 1C) and the connection of the river system to Lake Towuti significantly changed the sedimentation patterns in the lake. There is no indication that the Mahalona/Lampenisu River system was directly connected to Lake Towuti earlier, during deposition of Unit 1B, and it is difficult to infer the palaeo-topography during deposition of Unit 1A.

3.6.2 Changes in aquatic habitats

The temporal and lateral inhomogeneity within Unit 2 sediments and between the different drill holes at Site 1 (Russell et al., 2016) suggests that the early Towuti basin was topographically diverse with aquatic environments ranging from swamps, standing water bodies, and fluvial systems in close spatial and temporal proximity. Conditions in the early extensional phase of the basin may have been similar to the large alluvial plains along the lower river courses of Towuti's main rivers today, where serpentine-rich fluvial gravels are deposited in direct proximity to the active river course, whereas the currently inactive plain is covered by swamps and silting, abandoned meanders (oxbow lakes). Biological habitats thus changed repeatedly in the early phase of basin formation. Diverse substrates (rocks, mud, leaf litter) were available for snails and riverine species had the opportunity to adapt to standing water conditions. Indeed, molecular analyses of snails and shrimps indicate that the species relate back to a common riverine ancestor (von Rintelen et al., 2010; von Rintelen et al., 2004).

Following this initial phase of basin formation, rapid flooding of the landscape led to the establishment of a permanent lake. The initially shallow lake, as indicated by burrow structures, with low-energy deposition, as indicated by high clay content of the sediments around 97 mcd, favoured morphological or physiological traits adapted to lacustrine conditions. This likely resulted in the initial lake colonisation by riverine species. Continued lake deepening and steepening of the slopes above and below the water table, indicated by the overall increase of coarse-grained EM2 between 97 and 36 mcd, may have constantly decreased and/or extended the distance between areas covered by shallow-water habitats, which would have promoted the isolation of populations. Adaptation to changes in shallow-water habitats has also been suggested for snails, where a close link between substrate and radular morphology has been observed (von Rintelen et al., 2004). Several studies from the Malili Lake system highlight the importance of habitat isolation and resource partitioning for the observed diversification of species (Vaillant et al., 2011).

Molecular analyses of snails, crabs, and shrimps suggest several independent colonisations of the Malili Lakes by riverine species (von Rintelen et al., 2010; von Rintelen et al., 2012; von Rintelen et al., 2004). Data for shrimps indicates that one colonisation event led to subsequent radiation into 14 species, whereas the second colonisation did not radiate into different species. The species is described to be a generalist, whereas species of the first colonisation clade have specialised on different substrates (e.g. wood, leaf litter, rocks; von Rintelen et al., 2010). In view of the tectonic basin evolution, an initial colonisation likely corresponds to the establishment of a permanent lake. Further colonisation events are more difficult to discern. If diversity within this species flock is assumed to relate to radiation age, the second colonisation event may be more recent, e.g. related to the connection of the Mahalona/Lampenisu River System to Lake Towuti. From the sediment record it remains ambiguous whether this event also changed the drainage direction of the lake system, i.e. from draining east

through the Mahalona/Lampenisu System to draining west through the Larona River. If this is what occurred, such an event could have offered new colonisation opportunities to the lake system.

3.6.3 Change in trophic lake state

Two distinct diatom-rich intervals occur in the lacustrine sediment record of Lake Towuti, corresponding to grain-size EM 3. These occurrences culminate in sediments that consist almost entirely of planktonic diatoms (Figure 3.8), indicating eutrophication and algal blooms in the lake. This raises the question of reasons for such drastic changes in trophic state in tropical lakes. The lake nowadays is ultraoligotrophic (Lehmusloto et al., 1997) and no diatoms are present (or preserved) at any other depth in the core. Only few benthic species have been found in littoral environments in the lake today (Haffner et al., 2001; Hasberg et al., 2018; Lehmusloto et al., 1997). One of the reasons for today's ultraoligotrophy is that essentially all of the bioavailable phosphorus is scavenged by prevalent iron oxyhydroxides during transport in rivers or in the oxygenated epilimnion. As a result, little phosphorus is bioavailable in the lake today. Data from upstream Lake Matano shows low phosphorus and nitrogen concentration in the epilimnion (50.2 and 55 mm/L, respectively), and corresponding low phytoplankton density (0.013 mg/L; Sabo et al., 2008).

Fundamentally changing the trophic status of such a large lake requires the addition or release of large amounts of nutrients, together with less efficient scavenging of these nutrients in the water column. Closely associated to the diatom oozes (~30 cm below) are tephra deposits. These events may have sufficiently changed nutrient recycling in the lake and nutrient supply in the catchment to sustain large populations of diatoms. Weathering of phosphorous-bearing volcanic ash in the catchment could have released substantial amounts of phosphorus. The phosphorus cycle in lakes is strongly coupled to lake water oxygenation (Stumm & Morgan, 1996). In a permanently stratified lake, phosphorus gets rapidly removed from the oxic water column, accumulates in the hypolimnion and can precipitate in authigenic minerals (Stumm & Morgan, 1996). In Lake Towuti, phosphorus in the sediments is bound in vivianite ($Fe(PO_4)_2$), which is found at several depths in the lacustrine record. Specifically, three vivianite layers occur directly above a tephra deposit at 19.8 mcd (Figure 3.10), suggesting a direct link between ash fall and phosphorus deposition Thin turbidite deposits (3-8 mm) on top of the vivianite layers can prevent release of the phosphorus if oxygen reaches the sediment-water interface at a later stage. Hence, if phosphorous-bearing ash fall occurs in times of permanent lake water stratification, the added phosphorus may not become bioavailable, as is the case in today's lake system. This suggests that the influence of ash fall on changes in trophic state is closely linked to hydroclimatic boundary conditions. The sediment record contains 18 tephra deposits, but diatomaceous oozes overlay just two of these ashes. Tephra chemistry, which is currently being analysed, could also have an influence on how ash fall affects lake status and sedimentation. Another factor contributing to the diatomaceous oozes in the sediment record could be diatom speciation. Today, the Malili Lake System is characterised by a high degree of diatom endemism, most of which are benthic diatoms (Bramburger et al., 2008). Small-scale variations in the abiotic environment and stochastic disturbance events have been suggested to mainly drive diatom species evolution in the lakes (Bramburger et al., 2008). Hence it seems possible that disturbance to the system due to ash fall in the lake

and its catchment may have contributed to the success of the planktonic diatoms, which are nearly absent in the lake today. Ash fall and associated changes in lake trophic state may have also contributed to the diversification and adaptive radiation in other species, e.g. in substrate dwellers such as shrimps, crabs, and snails. Deposition of large amounts of ash in the littoral zone of the lake may have substantially changed turbidity and substrate type, reducing rocky areas and increasing areas covered by mud and leaf litter, if ash fall induces leaf shedding in the catchment.

3.6.4 Sediment deposition and lake level fluctuations

Despite changes in basin hydrology, fine- and coarser-grained sediments alternate throughout the upper 97 m of the sediment record. EM1 sediments with a mean grain size of 4.2 µm likely represent hemi-pelagic sedimentation. In contrast, coarser-grained EM2 sediments are more strongly influenced by high-energy transport processes. Such processes could involve lateral transport by hyperpycnal and interflows and/or turbidity currents associated with mass movements from slopes around the deep northern basin. In a 20-m long sediment record covering 30 kyr close to the Mahalona River Delta and TDP Site 2, similar variations in grain-size patterns in pelagic sediments have been described by Vogel et al. (2015). The authors relate these variations to climate-dependent lake level fluctuations. Dry periods induce lake-level low stands, which increase hydrologic gradients and river incision in the catchment, while decreasing the distance between river delta and coring site, allowing coarser-grained material to reach the deep basin. In contrast, pelagic sediment rain is the dominant sedimentation process during wet phases, with reduced hydrologic gradients and decreased river incision (Vogel et al., 2015). Their findings have been confirmed by more detailed studies on basin-wide grain-size patterns (Hasberg et al., 2018) and source-to-sink analyses in the Towuti catchment (Morlock et al., 2018; Sheppard et al., in review). Despite severe changes in catchment morphology, our analyses suggest that changes in depositional modes controlling grain-size patterns are applicable to the entire lacustrine record of TDP Site 1. A minor influence of basin evolution can be seen in the long-term decrease of the fine-grained EM1 between 96 and 36 mcd. This indicates that inter- and underflows (EM2) became more important relative to the pelagic sediment rain, likely as a result of long-term basin slope steepening above and/or below the water table or as a result of delta progradation towards the coring site. In the catchment, increased slope angles allow for the erosion of more coarse-grained material and higher transport energies of the rivers, whereas steep slopes in the lake itself enable the mobilisation and transport of coarser-grained sediments into the deep lake basin.

3.7 Conclusion

The sediment record of Lake Towuti, recovered by the ICDP Towuti Drilling Project in 2015, consists of two main sedimentary units, which split the record into an early lake phase (~65 m) and a continuous lacustrine phase in the upper 97 m. This sediment succession allows studying the tectonic, climatic, and biological evolution in a unique tropical setting. We find that in the early extensional phase, repeated cycles of fill-up of newly formed accommodation space culminating with peat formation reflect the dynamic landscape evolution of the basin. In this period, standing water bodies were present in close spatial and temporal proximity to swamps and rivers, offering diverse

habitats to aquatic organisms. During this phase, riverine species may have had the opportunity to adapt to standing water conditions. A pulse of subsidence then established the permanent water body found today, which likely resulted in the initial colonisation by riverine species. Further colonisation events are more difficult to discern, but a potential second event may be related to the connection of the Mahalona/Lampenisu River System to Lake Towuti roughly 150,000 years ago. For the late Quaternary, the record of continuous lacustrine sedimentation provides a detailed archive of tectonic changes in the catchment as well as climate-induced lake-level fluctuations. The former are well described by changes in mineralogy, particularly associated to the connection of the Lampenisu River to Lake Towuti around 30 mcd, which severely changed the lake hydrology and sediment composition. Varying grain-size patterns, which fluctuate between clay-dominated pelagic rain sediments and coarser-grained sediments influenced by higher-velocity transport processes, may be linked to lake-level fluctuations and associated changes in hydroclimate. The alternation of these depositional processes was interrupted by two distinct intervals characterized by sediments predominantly composed of diatom frustules, which indicate high primary productivity in the nowadays ultraoligotrophic lake. These events seem related to increased phosphorous availability, potentially linked to ash fall.

3.8 Acknowledgements

The Towuti Drilling Project was partially supported by grants from the International Continental Scientific Drilling Program, the US National Science Foundation, the German Research Foundation, the Swiss National Science Foundation (20FI21_153054/1 and 200021_153053/1), Brown University, Genome British Columbia, and the Ministry of Research, Technology, and Higher Education (RISTEK). PT Vale Indonesia, the US Continental Drilling Coordination Office, the GeoForschungszentrum Potsdam and DOSECC Exploration Services are acknowledged for logistical assistance to the project. We further thank Björn Stelbrink and Thomas von Rintelen for fruitful discussions about the biologic evolution in the Malili Lake System and Jebril Hadi for help with sample embedding and thin section preparation. This research was carried out with permission from the Ministry of Research and Techonology (RISTEK), the Ministry of Trade of the government of Indonesia, and the Natural Resources Conservation Center (BKSDA) and Government of Luwu Timur of Sulawesi.

3.9 Author Contributions

MAM sampled at LacCore, conducted laboratory analyses, wrote the manuscript and designed the figures. HV provided support for analyses, was involved in discussions and commented on the manuscript. DA supervised µXRF analyses. JMR, SB, HV, and MM designed and led the Towuti Drilling Project. JMR and HV developed the sediment stratigraphy. MAM, HV, JMR, and SB participated in fieldwork and core opening. Members of the Towuti Drilling Project provided scientific, technical, and logistical support during field sampling and core opening.

3.10 References

Bellier O, Sébrier M, Seward D, Beaudouin T, Villeneuve M, Putranto E. (2006). Fission track and fault kinematics analyses for new insight into the Late Cenozoic tectonic regime changes

in West-Central Sulawesi (Indonesia). Tectonophysics, 413(3-4), 201-220. doi: 10.1016/j.tecto.2005.10.036

Bramburger AJ, Hamilton PB, Hehanussa PE, Haffner GD. (2008). Processes regulating the community composition and relative abundance of taxa in the diatom communities of the Malili Lakes, Sulawesi Island, Indonesia. Hydrobiologia, 615(1), 215-224. doi: 10.1007/s10750-008-9562-2

Chester R, Elderfield H. (1973). An infrared study of clay minerals. The identification of kaolinite-group clays in deep-sea sediments. Chemical Geology, 12, 281-288.

Chukanov NV. (2014). Infrared spectre of mineral species - extended library (Vol. 1). Dordrecht: Springer.

Costa KM, Russell JM, Vogel H, Bijaksana S. (2015). Hydrological connectivity and mixing of Lake Towuti, Indonesia in response to paleoclimatic changes over the last 60,000years. Palaeogeography, Palaeoclimatology, Palaeoecology, 417, 467-475. doi: 10.1016/j.palaeo.2014.10.009

Farmer VC. (1974). The infrared spectra of minerals. Dorking, UK: Adlard and Son.

Glaubrecht M, von Rintelen T. (2008). The species flocks of lacustrine gastropods: Tylomelania on Sulawesi as models in speciation and adaptive radiation. Hydrobiologia, 615(1), 181-199. doi: 10.1007/s10750-008-9568-9

Goudge TA, Russell JM, Mustard JF, Head JW, Bijaksana S. (2017). A 40,000 year record of clay mineralogy at Lake Towuti, Indonesia: Paleoclimate reconstruction from reflectance spectroscopy and perspectives on paleolakes on Mars. Geological Society of America Bulletin.

Haffner GD, Hehanussa PE, Hartoto D. (2001). The biology and physical processes of large lakes of Indonesia: Lakes Matano and Towuti. In: Munawar M, Hecky RE (Eds.) The Great Lakes of the World (GLOW): Food-web, health and integrity (pp. 183-192). Leiden, The Netherlands: Backhuys Publishers.

Hahn A, Vogel H, Andó S, Garzanti E, Kuhn G, Lantzsch H, Schüürman J, Vogt C, Zabel M. (2018). Using Fourier transform infrared spectroscopy to determine mineral phases in sediments. Sedimentary Geology, 375, 27-35. doi: 10.1016/j.sedgeo.2018.03.010

Hasberg AKM, Melles M, Wennrich V, Just J, Held P, Morlock MA, Vogel H, Russell JM, Bijaksana S, Opitz S. (2018). Modern sedimentation processes in Lake Towuti, Indonesia, revealed by the composition of surface sediments. Sedimentology.

Herder F, Nolte AW, Pfaender J, Schwarzer J, Hadiaty RK, Schliewen UK. (2006). Adaptive radiation and hybridization in Wallace's Dreamponds: evidence from sailfin silversides in the Malili Lakes of Sulawesi. Proc Biol Sci, 273(1598), 2209-2217. doi: 10.1098/rspb.2006.3558

Heslop D, Dillon M. (2007). Unmixing magnetic remanence curves withouta prioriknowledge. Geophysical Journal International, 170(2), 556-566. doi: 10.1111/j.1365-246X.2007.03432.x

Kadarusman A, Miyashita S, Maruyama S, Parkinson CD, Ishikawa A. (2004). Petrology, geochemistry and paleogeographic reconstruction of the East Sulawesi Ophiolite, Indonesia. Tectonophysics, 392(1-4), 55-83. doi: 10.1016/j.tecto.2004.04.008

Lacey JH, Leng MJ, Francke A, Sloane HJ, Milodowski A, Vogel H, Baumgarten H, Zanchetta G, Wagner B. (2016). Northern Mediterranean climate since the Middle Pleistocene: a 637 ka stable isotope record from Lake Ohrid (Albania/Macedonia). Biogeosciences, 13(6), 1801-1820. doi: 10.5194/bg-13-1801-2016

Lehmusloto P, Machbub B, Terangna N, Rusmiputro S, Achmad F, Boer L, Brahmana SS, Priadi B, Setiadji B, Sayuman O, Margana A. (1997). National Inventory of the Major Lakes and Reservoirs in Indonesia. General limnology, Expedition Indodanau Technical Report. Bandung and Helsinki.

Madejová J. (2003). FTIR techniques in clay mineral studies. Vibrational Spectroscopy, 31, 1-10.

Morlock MA, Vogel H, Nigg V, Ordoñez L, Hasberg AK, Melles M, Russell JM, Bijaksana S. (2018). Climatic and tectonic controls on source-to-sink processes in the tropical, ultramafic catchment of Lake Towuti, Indonesia. Journal of Paleolimnology. doi: 10.1007/s10933-018-0059-3

Paterson GA, Heslop D. (2015). New methods for unmixing sediment grain size data. Geochemistry, Geophysics, Geosystems(16), 4494-4506. doi: 10.1002/2015GC006070

Russell JM, Bijaksana S, Vogel H, Melles M, Kallmeyer J, Ariztegui D, Crowe S, Fajar S, Hafidz A, Haffner D, Hasberg A, Ivory S, Kelly C, King J, Kirana K, Morlock M, Noren A, O'Grady R, Ordonez L, Stevenson J, von Rintelen T, Vuillemin A, Watkinson I, Wattrus N, Wicaksono S, Wonik T, Bauer K, Deino A, Friese A, Henny C, Imran, Marwoto R, Ngkoimani LO, Nomosatryo S, Safiuddin LO, Simister R, Tamuntuan G. (2016). The Towuti Drilling Project: paleoenvironments, biological evolution, and geomicrobiology of a tropical Pacific lake. Scientific Drilling, 21, 29-40. doi: 10.5194/sd-21-29-2016

Russell JM, Vogel H, Konecky B, Bijaksana S, Huang Y, Melles M, Wattrus N, Costa KM, King JW. (2014). Glacial forcing of central Indonesian hydroclimate since 60,000 y BP. PNAS, 111(14), 5100-5105. doi: 10.1073/pnas.1402373111

Sabo E, Roy D, Hamilton PB, Hehanussa PE, McNeely R, Haffner GD. (2008). The plankton community of Lake Matano: factors regulating plankton composition and relative abundance in an ancient, tropical lake of Indonesia. Hydrobiologia, 615(1), 225-235. doi: 10.1007/s10750-008-9560-4

Sheppard RY, Milliken RE, Russell JM, Vogel H, Melles M, Bijaksana S, Morlock MA, Hasberg AKM. (in review). Spectroscopic Analysis of Iron Cycling in a Terrestrial Ultramafic Lake and its Implications for Martian Sedimentary Systems. Submitted to Chemical Geology.

Stumm W, Morgan JJ. (1996). Aquatic Chemistry. Chemical Equilibria and Rates in Natural Waters (3 ed.). New York: John Wiley & Sons.

Team RDC. (2017). R: A language and environment for statistical computing: R Foundation for Statistical Computing. Retrieved from Available at: http://www.r-project.org.

Vaillant JJ, Haffner GD, Cristescu ME. (2011). The ancient lakes of Indonesia: towards integrated research on speciation. Integr Comp Biol, 51(4), 634-643. doi: 10.1093/icb/icr101

Vogel H, Russell JM, Cahyarini SY, Bijaksana S, Wattrus N, Rethemeyer J, Melles M. (2015). Depositional modes and lake-level variability at Lake Towuti, Indonesia, during the past ~29 kyr BP. Journal of Paleolimnology, 54(4), 359-377. doi: 10.1007/s10933-015-9857-z

von Rintelen K, Glaubrecht M, Schubart CD, Wessel A, Von Rintelen T. (2010). Adaptive radiation and ecological diversification of Sulawesi's ancient lake shrimps. Evolution, 64(11), 3287-3299. doi: 10.1111/j.1558-5646.2010.01043.x

von Rintelen T, von Rintelen K, Glaubrecht M, Schubart CD, Herder F. (2012). Aquatic biodiversity hotspots in Wallacea: the species flocks in the ancient lakes of Sulawesi, Indonesia. In: D J Gower, K Johnson, J Richardson, B Rosen, L Rüber & S Williams (Eds.) Biotic Evolution and Environmental Change in Southeast Asia (pp. 291-315). Cambridge: Cambridge University Press.

von Rintelen T, Wilson AB, Meyer A, Glaubrecht M. (2004). Escalation and trophic specialization drive adaptive radiation of freshwater gastropods in ancient lakes on Sulawesi, Indonesia. Proc Biol Sci, 271(1557), 2541-2549. doi: 10.1098/rspb.2004.2842

Vuillemin A, Kemnitz H, Wirth R, Schüssler JA, Schleicher AM, Friese A, Lücke A, Henny C, Crowe SA, Kallmeyer J, Russell JM, Bijaksana S, Vogel H. (in prep.). Vivianite formation in phosphorus-limited ferruginous Lake Towuti, Indonesia.

Watkinson IM, Hall R. (2016). Fault systems of the eastern Indonesian triple junction: evaluation of Quaternary activity and implications for seismic hazards. In: Cummins PR, Meilano I (Eds.) Geohazards in Indonesia: Earth Science for Disaster Risk Reduction. (Vol. 441, pp. 71-120). London, UK: Geological Society, London, Special Publications.

Weber AK, Russell JM, Goudge TA, Salvatore MR, Mustard JF, Bijaksana S. (2015). Characterizing clay mineralogy in Lake Towuti, Indonesia, with reflectance spectroscopy. Journal of Paleolimnology, 54(2-3), 253-261. doi: 10.1007/s10933-015-9844-4

Weltje GJ. (1997). End-Member Modeling of Compositional Data: Numerical-Statistical Algorithms for Solving the Explicit Mixing Problem. Mathematical Geology, 29(4), 503-549.

CHAPTER 4

Temporal and spatial variability of siderite formation in ferruginous sediments

Marina A. Morlock, Hendrik Vogel, Jebril Hadi, Anneleen Foubert, Daniel Ariztegui, Martin Melles, James M. Russell, Satria Bijaksana & the TDP science team

under review in Geology

4. Temporal and spatial variability of siderite formation in ferruginous sediments

Marina A. Morlock*[1,2], Hendrik Vogel[1,2], Jebril Hadi[1], Anneleen Foubert[3], Daniel Ariztegui[4], Martin Melles[5], James M. Russell[6], Satria Bijaksana[7] & the TDP science team[8]

[1]*Institute of Geological Sciences, University of Bern, 3012 Bern, Switzerland*

[2]*Oeschger Centre for Climate Change Research, University of Bern, 3012 Bern, Switzerland*

[3]*Department of Geosciences, University of Fribourg, 1700 Fribourg, Switzerland*

[4]*Department of Earth Sciences, University of Geneva, 1205 Geneva, Switzerland*

[5]*Institute of Geology and Mineralogy, University of Cologne, 50674 Cologne, Germany*

[6]*Department of Earth, Environmental, and Planetary Sciences, Brown University, Providence, RI 02912, USA*

[7]*Faculty of Mining and Petroleum Engineering, Institut Teknologi Bandung, Bandung 40132, Indonesia*

[8]*See Chapter 4.11.1 (Appendix A) for full list of contributors to the Towuti Drilling Project*

**corresponding author: marina.morlock@geo.unibe.ch*

4.1 Abstract

Post-depositional mineral formation in sediments challenges their use as paleoenvironmental archives. Particularly controversial is the use of iron carbonates in banded iron formations for reconstructing Archean ocean chemistry. Increasing evidence suggests that ancient ferruginous sediments were strongly altered by post-depositional mineral formation. In this study we use high-resolution X-ray computed micro-tomography (µCT) images, µ-X-ray fluorescence (µXRF) mapping, and thin section analysis to study the distribution and formation of siderite in Pleistocene sediments from ferruginous Lake Towuti, Indonesia, a modern Archean ocean analogue. These analyses allow us for the first time to visualize fragile 3D structures *in situ* related to authigenic and early diagenetic mineral formation in ferruginous sediments. In many cases we observe siderite confined to sedimentary bedding planes, indicating synsedimentary formation. However, we also find clear evidence for post-depositional siderite formation, including siderite concretions linked to fault-controlled vertical fluid advection. We also identified structures in which siderite potentially was precipitated by microbial activity. All structures occur repeatedly in the 100 m long soft sediment record and sometimes in close, or even overlapping relation to each other, suggesting siderite in these sediments contains a mixed signal of different mineral formation generations and processes. Our results highlight the importance of the thorough identification and characterization of different mineral formation modes using detailed sedimentology, particularly with respect to ancient ocean chemistry reconstructions.

4.2 Introduction

Lacustrine and marine sediments contain powerful records of environmental change, but are also affected by diagenetic overprinting that challenge paleoenvironmental analyses. Particularly controversial is the use iron carbonates from banded iron formations (BIFs; Johnson et al., 2013; Lyons et al., 2014). These sediments are alternating siderite- and silicate-rich marine deposits dating back to the Archean Eon (Posth et al., 2011), when oceans might have been ferruginous and oxygen-poor (Canfield et al., 2008). It remains ambiguous whether siderite and other iron mineral phases precipitated in near-chemical equilibrium with Precambrian seawater, enabling the reconstruction of ocean oxygenation and/or atmospheric CO_2 composition (Planavsky et al., 2009; Rouxel et al., 2005), whether they primarily record diagenetic processes in the sediment (Craddock and Dauphas, 2011; Heimann et al., 2010; Johnson et al., 2013), or a combination of the two (Planavsky et al., 2012; Steinhoefel et al., 2010). In unconsolidated sediments, sequential growth of concretions after sediment deposition suggests several phases of siderite precipitation and growth at depth (Hounslow, 2001; Lim et al., 2004; Sapota et al., 2006). Simulations of diagenetic sediment overprinting (Posth et al., 2013) and in situ isotope analyses in BIF samples (Li et al., 2013) support the hypothesis of multiple siderite formation steps and mechanisms through space and time. In consequence, recent studies have focused on higher spatial resolution isotope measurements in BIFs to characterize the degree of variability (Heimann et al., 2010; Li et al., 2013; Steinhoefel et al., 2010). This cannot, however, address the temporal and spatial interplay of mineral formation mechanisms acting in unconsolidated sediments, the initial environment in which the siderite was formed.

Here we present 3D imaging of siderite-rich sediments from ferruginous Lake Towuti, Indonesia, using X-ray computed micro-tomography (µCT) visualization to investigate siderite formation in unconsolidated sediments during and after deposition. Samples cover a 100-m-long continuous lacustrine sediment record, facilitating the detailed description of siderite occurrences in recent and long-buried sediments. The identification and study of syn- and post-depositional structures related to siderite occurrence allows understanding different siderite formation modes in these ferruginous sediments. Establishing such relationships can help to address uncertainties in the environmental interpretation of siderite in BIFs.

4.3 Material and methods

Large (560 km^2) and deep (200 m max. water depth) tectonic Lake Towuti (2.75°S, 121.5°E; Figure 4.1) is located in the East Sulawesi Ophiolite complex (Indonesia). Its lake water and sediments are metal- and particularly iron-rich, but poor in sulfur and nutrients (Costa et al., 2015; Haffner et al., 2001). The Towuti Drilling Project recovered cores of the entire sediment infill to bedrock (162 m below lake floor) in 2015, including ~100 m of lacustrine sediments covering ~600,000 years (Russell et al., 2016).

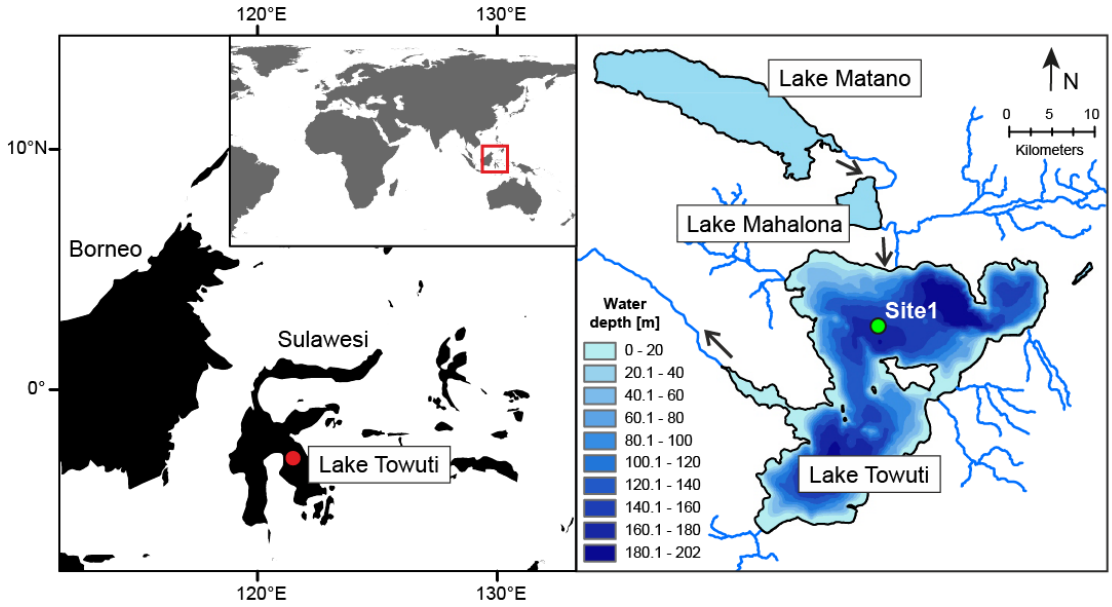

Figure 4.1 Location of Lake Towuti on Sulawesi Island, Indonesia (left side and inset), and close-up of Lake Towuti (with bathymetry (20 m spacing), coring location indicated by green circle) and upstream lakes Matano and Mahalona

Upon core opening, ten sections representing the main lithofacies from the lacustrine record of TDP Site 1 were sampled by pressing aluminum frames (15x2x1 cm) into the soft sediment. Sediment-filled frames, stored in vacuumed bags (Appendix B (Chapter 4.11.2) Figure S4.1), were imaged with a multi-scaled Bruker-Skyscan 2211 µCT scanner. Samples were scanned using an open X-ray source with diamond-window target (settings: 80-120 kV, 60-200 µA, 6 Mp flatpanel detector, voxel resolution 6-25 µm, 1° rotation steps). Images were reconstructed with InstaRecon reducing beam hardening and ring artifacts, and initially segmented using CT-An and CT-Vox (Bruker Skyscan software). Advanced segmentation and 3D visualization for high-density mineral phases have been performed with Avizo (ThermoFisher Scientific). Imaged sections have a vertical extent of ~1-3 cm. Sections were then freeze-dried, vacuum-embedded in epoxy resin and polished to a surface quality of 6 µm. Geochemical composition was analyzed on an X-ray fluorescence (XRF) core scanner (ITRAX, Cox Ltd., Sweden; settings: Cr-tube, 30 kV, 50 mA, 50 s integration time, 1 mm resolution) and selected sections additionally mapped with an Eagle III µXRF spectrometer (Röntgenanalytik Messtechnik GmbH, Germany; settings: 30 kV, 300 mA, 10 µs integration time). Thin sections were prepared from polished 3-cm pieces and analyzed under a light microscope. Locations and analyses performed on the sediment sections are summarized in Figure 4.2 and Table S4.1.

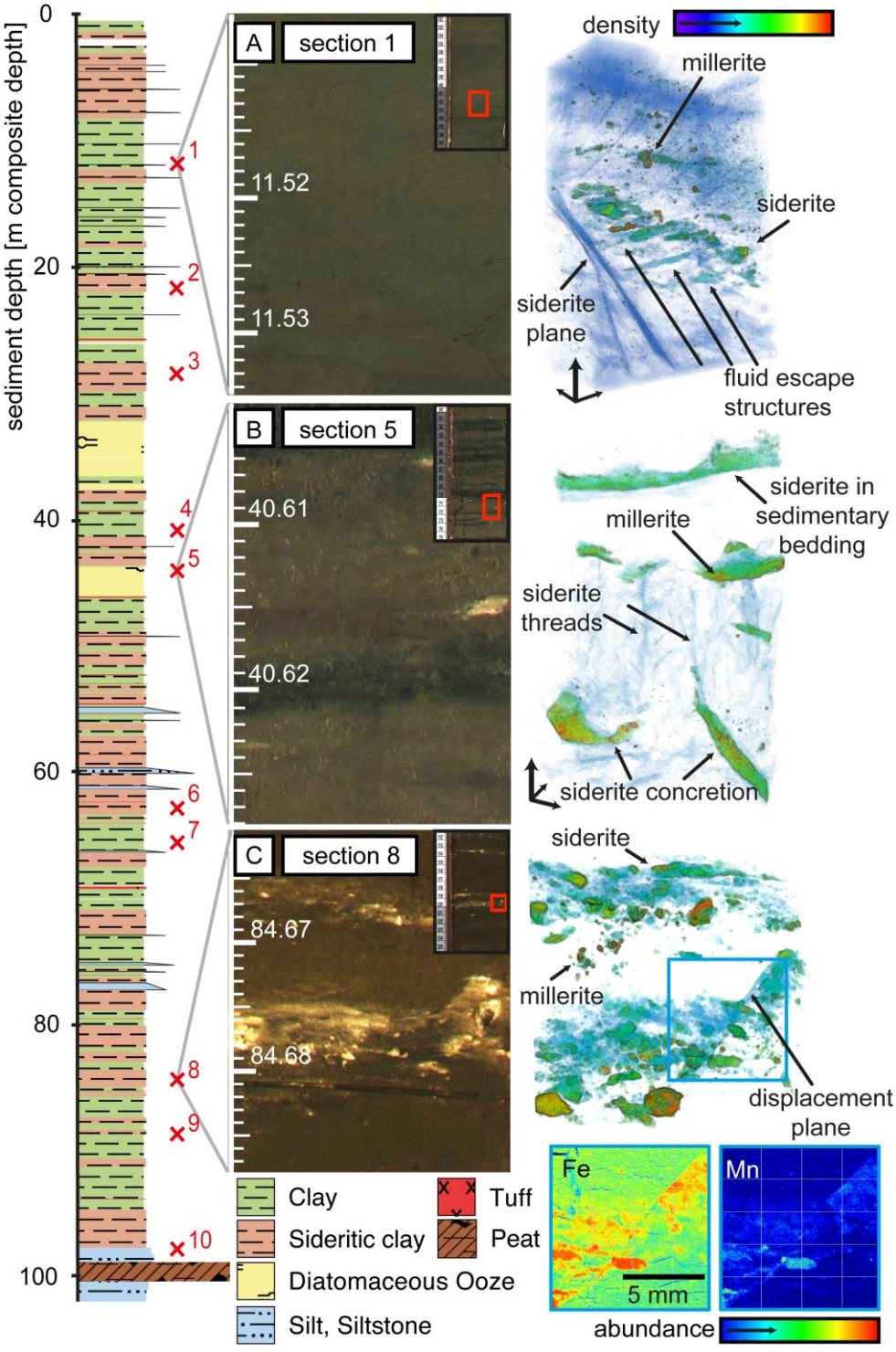

Figure 4.2 Sediment core image and corresponding X-ray computed micro-tomography (µCT) visuali-zation of unprocessed, unconsolidated sediments (A-C). Siderite and millerite are present in all samples (red: millerite, green/blue: siderite, background sediments transparent). Left: Stratigraphy after Russell et al. (2016) with red crosses indicating locations of µCT scanned samples. Bottom right: elemental maps (based on µXRF mapping) of section indicated in C by the blue box

4.4 Siderite and millerite in Lake Towuti sediments

Siderite, the only carbonate present in Lake Towuti sediments (Tamuntuan et al., 2015), occurs sporadically throughout the record, with its abundance generally increasing with depth (Russell et al., 2016). Siderite is the most common high-density mineral in the lacustrine sediments, embedded in a phyllosilicate-rich sediment matrix. Abundance and size of the concretionary, aggregated siderite crystals depends on lithology, with clear preference for reddish-gray clays (lithology sideritic clay in Figure 4.2). Individual siderite concretions are commonly between 0.1 and 3 mm in diameter, and various sizes occur within the same sideritic layer (Figure 4.2). Siderite is absent from the catchment soils, which are instead enriched in iron oxides, mainly goethite and hematite. These oxides are delivered to the lake, where ferric iron may be reduced at the oxycline or at the redox front in the sediments, as has been observed in upstream Lake Matano (Crowe et al., 2008). Hence, reduction of Fe^{3+} from (oxyhydr)oxide minerals in the sediment can be an important process for siderite formation.

Thin section analyses show that the high-density authigenic mineral millerite (NiS) is also present in the lacustrine record (Figure S4.2), with highest abundance between 50 and 80 m composite depth (mcd). Millerite occurs more sporadically and aggregates are smaller compared to siderite (<100 µm), but can occasionally have sizes of ~0.5 mm (e.g. sections 1 and 5). Millerite appears as radiating acicular crystals (Figure S4.2C), and often, but not solely, it is associated with siderite, forming chain-like structures that surround siderite concretions (Figure S4.2A). In consequence, we suggest that millerite forms post-depositionally in Lake Towuti sediments. In metal-rich lakes, millerite formation in the sediment has been proposed to be tightly coupled to bacterial sulfate reduction, where nickel reacts with the produced sulfur to form millerite (Ferris et al., 1987). Despite low sulfur concentrations in the lake, viable sulfate reducing bacteria have been found in Lake Towuti sediments (Vuillemin et al., 2016). As nickel has a more pronounced chalcophile character compared to iron and the solubility of millerite is lower than pyrite, most sulfur in Lake Towuti sediments is likely bound to nickel, inhibiting the formation of pyrite.

4.5 3D visualisation of siderite and millerite in ferruginous sediments

CT imaging has long been recognized as a powerful tool in geosciences (Duliu, 1999; Mees et al., 2003), and recent advances in resolution have facilitated multiple applications of the technique (Cnudde and Boone, 2013). In Lake Towuti, high density contrasts between pelagic sediments ($\rho \approx 2.2$ g/cm^3), siderite ($\rho \approx 3.9$ g/cm^3), and millerite ($\rho \approx 5.4$ g/cm^3) facilitate the 3D visualization of these phases by high-resolution µCT scanning.

Micro-CT scans of Lake Towuti sediments reveal discrete patches of high-density material embedded in a low-density matrix at all depths. In thin sections, siderite and millerite are identified in areas corresponding to these high-density patches, and geochemical data shows enrichments in Fe and Mn in sideritic areas (Figure 4.2C and Figure 4.3), and Ni and S where millerite is present (Figure S4.2A and Figure S4.3). Millerite, having a higher density, occupies the brightest colors (gray scale values 251-255; Figure S4.3), whereas siderite, having a lower density, appears slightly darker (gray scale values ~190-250), and matrix sediments appear darkest (gray scale values <100), corresponding with the lowest densities. Siderite quantified as volume-% based on the

segmentation analysis are in general agreement with Fe and Mn peaks in the XRF data, but absolute abundance varies (Figure S4.3B), highlighting differences between 2D surface scans and 3D volumetric calculations of a heterogeneous sample. High-resolution µCT imaging of unprocessed sediments thus allows the visualization, detailed analysis, and quantification of high-density components in lake sediments, in particular the study of siderite in ferruginous sediments.

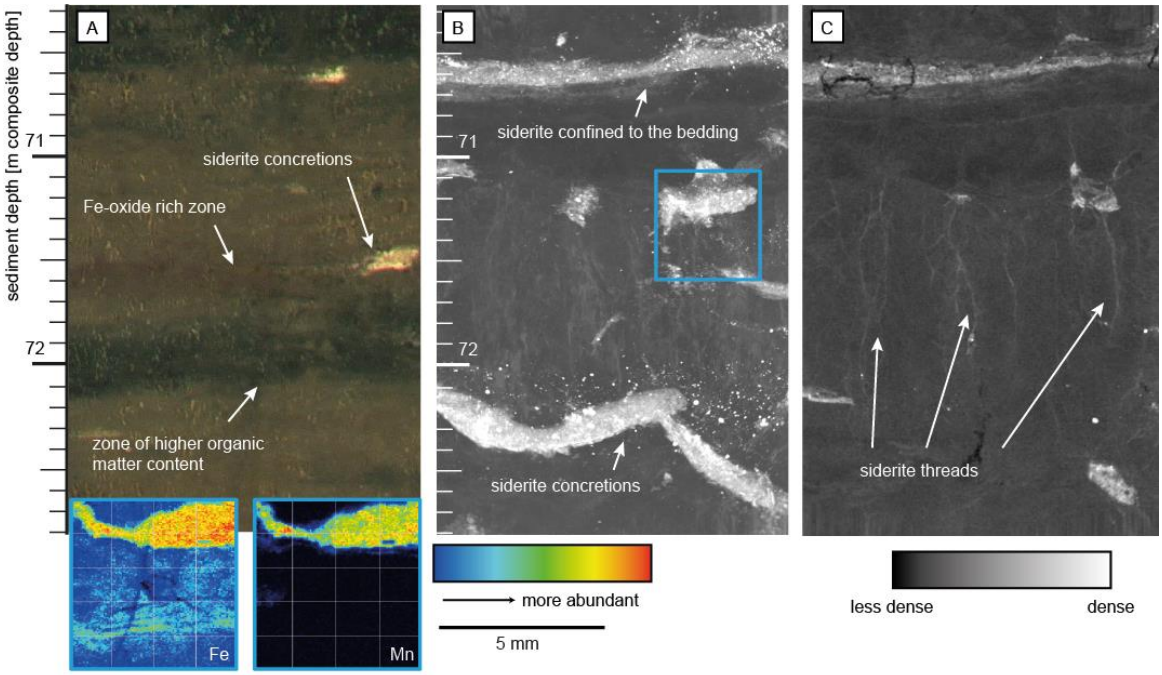

Figure 4.3 Core image (A), composite µCT gray scale image (B), and individual µCT gray scale slice image (C) for sediment section 5 (40.6 m composite depth). Bottom panels show elemental maps (based on µXRF mapping) for blue box region. Siderite is visualized in light colors in gray scale µCT images

4.6 Syn- and post-depositional siderite formation structures

Micro-CT images visualize multiple structures that provide clear evidence for syn- and post-depositional siderite precipitation in the sediment. Multiple modes can be distinguished, which can be attributed to different formation processes. Siderite already occurs at shallow depths in the sediment (Tamuntuan et al., 2015), suggesting a very early formation phase. These siderite concretions commonly line up with the sedimentary bedding (e.g. Figure 4.2B), indicating formation at the sediment-water interface or within the uppermost centimeters of the sediment, bounded by under- and overlying clayey sediments. Siderite crystals may, however, continue to grow at depth, as is suggested by a general increase in siderite abundance with sediment depth (Russell et al., 2016) and observed chemical zonation in siderite (see last paragraph of this section).

At several locations, fine-grained siderite is precipitated on sedimentary structures such as displacement planes from micro-faulting (Figure 4.2A and C, Figure S4.3A and D, Appendix C (Chapter 4.11.3; Electronic Supplementary Material) Movie S4.1-S4.3). Displacement planes are clearly post-depositional, possibly linked to sediment consolidation or earthquake-induced ruptures, the latter of which regularly occur in the tectonically active area of Central Sulawesi. Fluid advection and localization

along the fault planes then results in siderite precipitation on the displacement surface (Movie S4.1-S4.3). Potential fluid escape structures, conjugate to the displacement surface, connect to larger siderite concretions, possibly initiating or enhancing their growth by direction and localization of fluid flow (Figure 4.2A and Movie S4.1). Interestingly, these processes are observed at various depths (10 to 80 mcd) and in both main lithologies of the Towuti sediments, green clays and reddish-gray clays, the latter of which commonly contains siderite formed along bedding planes. Thus, it seems that diagenetic siderite formation along fluid flow planes is not significantly influenced by siderite abundance from other formation modes or time since deposition (i.e. sediment depth).

Similar structures of µm-thick (sub-)vertical siderite-filled conduits (siderite threads) also occur in sediments that do not show heterogeneities likely to focus fluid advection (Figure 4.2B and Figure 4.3, Movie S4.4 and Movie S4.5). These structures stand perpendicular to the sedimentary bedding and resemble fungal mycelium structures of very fine, branched threads. The structures penetrate multiple bedding planes, including a layer of iron oxides, and connect to larger siderite concretions, which are present in areas of higher organic matter content above and below. There is no direct evidence for microbial or fungal activity, but the appearance of the siderite threads and lack of physical heterogeneities perpendicular to the sedimentary bedding (i.e. in direction of the threads) point towards a biological origin of these structures. Using iron oxides as electron acceptors, microbial dissimilatory iron reduction (DIR) liberates Fe^{2+}, which together with HCO_3^- ions from organic matter can precipitate as siderite. Similar to structures linked to displacement surfaces, this process potentially initiates and/or enhances the growth of connected larger siderite concretions. Although they appear similar to synsedimentary siderite, these siderite concretions may at least partly be influenced by post-sedimentary formation or growth. This post-sedimentary signal can be related to abiotic (e.g. linked to fluid advection) and biotic (e.g. through microbial DIR) processes.

Lastly, siderite forms coatings around centers that are chemically similar to the background sediments (Figure S4.3C and D, Movie S4.3 bottom center and Movie S4.6). These coatings occur at several depths, but no such case was visible in thin sections. Therefore, it remains unclear what causes these coatings to form and what makes the nucleus different from the surrounding material. The coatings show a zonation with Mn-rich siderite closer to the nucleus and Fe enriched towards the rim (Figure S4.3C). This has been observed in discrete siderite aggregates and is attributed to continued siderite growth under chemical pore water evolution (Hounslow, 2001; Lim et al., 2004; Mortimer et al., 1997).

4.7 Siderite: recorder of a paleoenvironmental or diagenetic signal?

We find evidence for syn- and post-sedimentary siderite formation modes in unconsolidated sediments, co-occurring at various depths, and including vertical migration of chemical components perpendicular to the initial sediment structure. Particularly intriguing is the spatial heterogeneity and mixing of observed structures, where syn- and post-sedimentary siderites occur within one 3-cm long µCT section. Our results suggest that high spatial variability can be expected for siderite chemical and isotopic compositions within small sediment intervals. Vice versa, bulk samples contain an unknown and varying degree of signal mixing. Samples with a complex formation

history could therefore lead to erroneous conclusions about the environmental conditions during formation. On top of that, fragile post-depositional siderite structures connected to larger siderite aggregates can induce or influence crystal growth in these aggregates and change their chemical and isotopic signature through time. The fragile structures, however, do not preserve during “bulk” sediment sample processing, impeding the identification of different formation and/or growth histories in processed samples. Similarly, sediment consolidation and diagenetic overprint may cover the signals of post-depositional mineral formation processes, which can, for example, explain the significant iron isotope variability over mm to cm scales reported by Heimann et al. (2010) in a South African BIF.

The structures observed in Lake Towuti sediments strongly support the hypothesis that post-depositional processes alter iron carbonates from ferruginous sediments already prior to lithification and may explain the observed high spatial heterogeneity in siderite isotopic compositions. With respect to the current discussion on iron carbonates in BIFs our results suggest that interpretations from iron isotopes in bulk samples could be erroneous. Our results highlight a method to identify different formation processes, which might help to disentangle the effects of several formation generations on siderite geochemistry and isotopes.

4.8 Acknowledgements

The Towuti Drilling Project was supported by grants from the International Continental Drilling Program, the US National Science Foundation, the German Research Foundation, the Swiss National Science Foundation (20FI21_153054/1 and 200021_153053/1), Brown University, Genome British Columbia, and the Ministry of Research, Technology, and Higher Education (RISTEK). PT Vale Indonesia, the US Continental Drilling Coordination Office, the GeoForschungszentrum Potsdam and DOSECC Exploration Services are acknowledged for logistical assistance. We thank Christoph Neururer for help with µCT image acquisition and processing and Martin Wille for discussions on iron chemistry. This research was carried out with permission from the Ministry of Research and Technology (RISTEK), the Ministry of Trade of the Republic of Indonesia, and the Natural Resources Conservation Center (BKSDA) and Government of Luwu Timur of Sulawesi.

4.9 Author contributions

MAM and HV designed the study; MAM sampled at LacCore, conducted laboratory analyses, led manuscript writing and designed the figures. JH designed and led sample embedding. AF provided and operated the µCT scanner. DA supervised µXRF analyses. JMR, SB, HV, and MM designed and led the Towuti Drilling Project. MAM, HV, JMR, and SB participated in fieldwork and core opening. All authors discussed about the data and contributed to writing the manuscript. Members of the Towuti Drilling Project provided scientific, technical, and logistical support during field sampling and core opening.

4.10 References

Canfield DE, Poulton SW, Knoll AH, Narbonne GM, Ross G, Goldberg T, Strauss H. (2008). Ferruginous conditions dominated later neoproterozoic deep-water chemistry. Science, 321, 949-952.

Cnudde V, Boone MN. (2013). High-resolution X-ray computed tomography in geosciences: A review of the current technology and applications. Earth-Science Reviews, 123, 1-17.

Costa KM, Russell JM, Vogel H, Bijaksana S. (2015). Hydrological connectivity and mixing of Lake Towuti, Indonesia in response to paleoclimatic changes over the last 60,000 years. Palaeogeography, Palaeoclimatology, Palaeoecology, 417, 467-475.

Craddock PR, Dauphas N. (2011). Iron and carbon isotope evidence for microbial iron respiration throughout the Archean. Earth and Planetary Science Letters, 303, 121-132.

Crowe SA, O'Neill AH, Katsev S, Hehanussa PE, Haffner GD, Sundby B, Mucci A, Fowle DA. (2008). The biogeochemistry of tropical lakes: A case study from Lake Matano, Indonesia. Limnology Oceanography, 53, 319-331.

Duliu OG. (1999). Computer axial tomography in geosciences: an overview. Earth-Science Reviews, 48, 265-281.

Ferris FG, Fyfe WS, Beveridge TJ. (1987). Bacteria as nucleation sites for authigenic minerals in a metal-contaminated lake sediment. Chemical Geology, 63, 225-232.

Haffner GD, Hehanussa PE, Hartoto D. (2001). The biology and physical processes of large lakes of Indonesia: Lakes Matano and Towuti, In: Munawar M, Hecky RE (Eds.) The Great Lakes of the World (GLOW): Food-web, health and integrity. Leiden, The Netherlands, Backhuys Publishers, 183-192.

Heimann A, Johnson CM, Beard BL, Valley JW, Roden EE, Spicuzza MJ, Beukes NJ. (2010). Fe, C, and O isotope compositions of banded iron formation carbonates demonstrate a major role for dissimilatory iron reduction in ~2.5Ga marine environments. Earth and Planetary Science Letters, 294, 8-18.

Hounslow MW. (2001). The crystallographic fabric and texture of siderite in concretions: implications for siderite nucleation and growth processes. Sedimentology, 48, 533-557.

Johnson CM, Ludois JM, Beard BL, Beukes NJ, Heimann A. (2013). Iron formation carbonates: Paleoceanographic proxy or recorder of microbial diagenesis?. Geology, 41, 1147-1150.

Li W, Huberty JM, Beard BL, Kita NT, Valley JW, Johnson CM. (2013). Contrasting behavior of oxygen and iron isotopes in banded iron formations revealed by in situ isotopic analysis. Earth and Planetary Science Letters, 384, 132-143.

Lim DI, Jung HS, Yang SY, Yoo HS. (2004). Sequential growth of early diagenetic freshwater siderites in the Holocene coastal deposits, Korea. Sedimentary Geology, 169, 107-120.

Lyons TW, Reinhard CT, Planavsky NJ. (2014). The rise of oxygen in Earth's early ocean and atmosphere. Nature, 506, 307-315.

Mees F, Swennen R, Van Geet M, Jacobs P. (2003). Applications of X-ray computed tomography in the geosciences. Geological Society, London.

Mortimer RJG, Coleman ML, Rae JE. (1997). Effect of bacteria on the elemental composition of early diagenetic siderite: implications for palaeoenvironmental interpretations. Sedimentology, 44, 759-765.

Planavsky N, Rouxel O, Bekker A, Shapiro R, Fralick P, Knudsen A. (2009). Iron-oxidizing microbial ecosystems thrived in late Paleoproterozoic redox-stratified oceans. Earth and Planetary Science Letters, 286, 230-242.

Planavsky N, Rouxel OJ, Bekker A, Hofmann A, Little CTS, Lyons TW. (2012). Iron isotope composition of some Archean and Proterozoic iron formations. Geochimica et Cosmochimica Acta, 80, 158-169.

Posth NR, Köhler I, Swanner ED, Schröder C, Wellmann E, Binder B, Konhauser KO, Neumann U, Berthold C, Nowak M, Kappler A. (2013). Simulating Precambrian banded iron formation diagenesis. Chemical Geology, 362, 66-73.

Posth NR, Konhauser KO, Kappler A. (2011). Banded Iron Formations. In: Reitner J, Thiel V (Eds.) Encyclopedia of Geobiology. Dordrecht, Springer, 92-103.

Rouxel O, Bekker A, Edwards KJ. (2005). Iron Isotope Constraints on the Archean and Paleoproterozoic Ocean Redox State. Science, 307, 1088-1091.

Russell JM, Bijaksana S, Vogel H, Melles M, Kallmeyer J, Ariztegui D, Crowe S, Fajar S, Hafidz A, Haffner D, Hasberg A, Ivory S, Kelly C, King J, Kirana K, Morlock M, Noren A, O'Grady R, Ordonez L, Stevenson J, von Rintelen T, Vuillemin A, Watkinson I, Wattrus N, Wicaksono S, Wonik T, Bauer K, Deino A, Friese A, Henny C, Imran, Marwoto R, Ngkoimani LO, Nomosatryo S, Safiuddin LO, Simister R, Tamuntuan G. (2016). The Towuti Drilling Project: paleoenvironments, biological evolution, and geomicrobiology of a tropical Pacific lake. Scientific Drilling, 21, 29-40.

Sapota T, Aldahan A, Al-Aasm IS. (2006). Sedimentary facies and climate control on formation of vivianite and siderite microconcretions in sediments of Lake Baikal, Siberia. Journal of Paleolimnology, 36, 245-257.

Steinhoefel G, von Blanckenburg F, Horn I, Konhauser KO, Beukes NJ, Gutzmer J. (2010). Deciphering formation processes of banded iron formations from the Transvaal and the Hamersley successions by combined Si and Fe isotope analysis using UV femtosecond laser ablation. Geochimica et Cosmochimica Acta, 74, 2677-2696.

Tamuntuan G, Bijaksana S, King J, Russell J, Fauzi U, Maryunani K, Aufa N, Safiuddin LO. (2015). Variation of magnetic properties in sediments from Lake Towuti, Indonesia, and its paleoclimatic significance. Palaeogeography, Palaeoclimatology, Palaeoecology, 420, 163-172.

Vuillemin A, Friese A, Alawi M, Henny C, Nomosatryo S, Wagner D, Crowe SA, Kallmeyer J. (2016). Geomicrobiological Features of Ferruginous Sediments from Lake Towuti, Indonesia. Frontiers in Microbiology, 7, art. 1007.

4.11 Supplementary material

4.11.1 Appendix A. Full list of contributors to the Towuti Drilling Project

Jens Kallmeyer[1], Sean Crowe[2], Silvia Fajar[3], Abdul Hafidz[3], Doug Haffner[4], Ascelina K.M. Hasberg[5], Sarah Ivory[6,7], Christopher Kelly[7], John King[8], Kartika Kirana[3], Anders Noren[9], Ryan O'Grady[9], Luis Ordoñez[10], Janelle Stevenson[11], Thomas von Rintelen[12], Aurèle Vuillemin[1,13], Ian Watkinson[14], Nigel Wattrus[15], Satrio Wicaksono[7], Thomas Wonik[16], Kohen Bauer[2], Alan Deino[17], André Friese[1], Cynthia Henny[18], Imran[19], Ristiyanti Marwoto[18], La Ode Ngkoimani[20], Sulung Nomosatryo[5], La Ode Safiuddin[20], Rachel Simister[2], and Gerald Tamuntuan[21]

[1]Helmholtz Centre Potsdam, GFZ German Research Center for Geosciences, Telegrafenberg, Building C, 14473 Potsdam, Germany

[2]Department of Microbiology and Immunology, University of British Columbia, Vancouver, BC, Canada

[3]Faculty of Mining and Petroleum Engineering, Institut Teknologi Bandung, Jalan Ganesa 10, Bandung, 50132, Indonesia

[4]Great Lakes Institute for Environmental Research, University of Windsor, Windsor, Ontario, N9B 3P4, Canada

[5]Institute for Geology and Mineralogy, University of Cologne, Zülpicher Str. 49a/b, 50674 Cologne, Germany

[6]Department of Geosciences, Penn State University, State College, PA, USA

[7]Department of Earth, Environmental, and Planetary Sciences, Brown University, 324 Brook St., Providence, RI, 02912, USA

[8]Graduate School of Oceanography, University of Rhode Island, Narragansett, RI, 02882, USA

[9]LacCore, Dept. of Earth Science, University of Minnesota, Minneapolis, MN, 55455, USA

[10]Department of Earth Sciences, University of Geneva, rue des Maraichers 13, 1205 Geneva, Switzerland

[11]School of Culture, History and Language, Australia National University, Acton, ACT 2601, Australia

[12]Museum für Naturkunde, Leibniz Institute for Evolution and Biodiversity Science, Invalidenstr. 43, 10115 Berlin, Germany

[13]Department of Earth and Environmental Sciences, Paleontology and Geobiology, Ludwig-Maximilians Universität München, Richard-Wagner-Str. 10, 80333 Munich, Germany

[14]Dept. of Earth Sciences, Royal Holloway University of London, Egham, Surrey TW20 0EX, UK

[15]Large Lakes Observatory, University of Minnesota Duluth, Duluth, MN, 55812, USA

[16]Leibniz Institute for Applied Geophysics, Stilleweg 2, 30655 Hanover, Germany

[17]Berkeley Geochronology Center, Berkeley, CA, 94709, USA

[18]Research Center for Limnology, Indonesian Insitute of Sciences (LIPI), Jl. Raya Bogor m 46, Cibinong, West Java, Indonesia

[19]Geological Department, Universitas Hasanuddin, Kampus UNHAS Tamalanrea, Makassar, 90245, Indonesia

[20]Faculty of Earth Sciences and Technology, Haluoleo University, Kampus Baru Unhalu Anduoonoho, Kendari, 93232, Indonesia

[21]Department of Physics, Faculty of Mathematics and Natural Sciences, Sam Ratulangi University, Jl. Kampus Unsrat, Manado, 95114, Indonesia

4.11.2 Appendix B. Supplementary Figures

Figure S4.1 Five-step workflow for µCT and thin section sample preparation

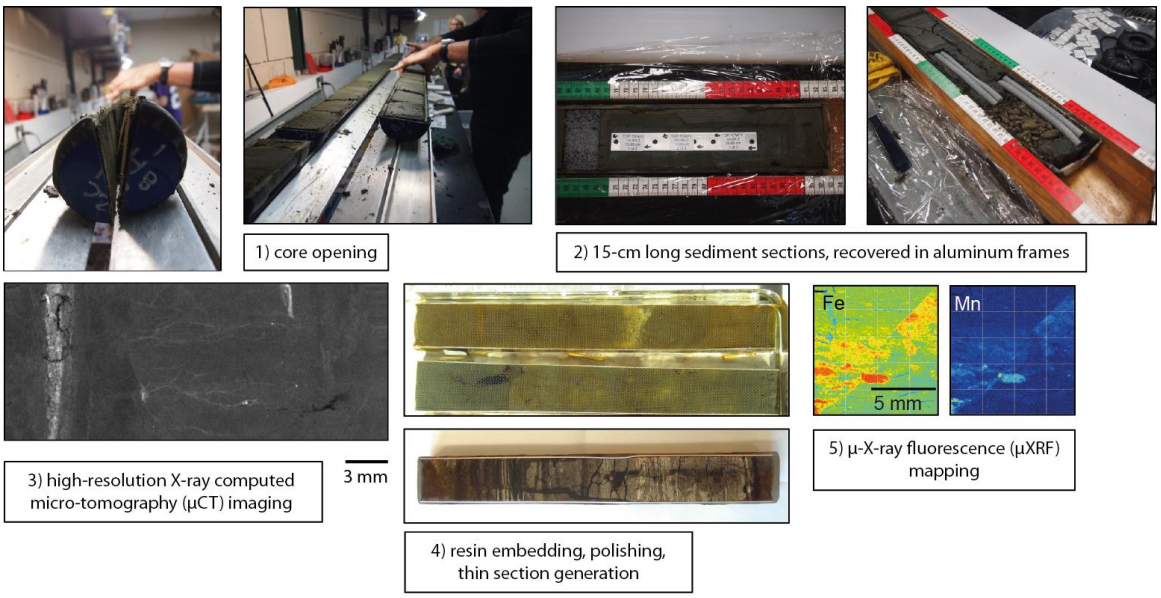

Figure S4.2 Exemplary microscope images of siderite patches (A), individual siderite crystals (B) and millerite (C) co-occurring in a sample at 40.6 m composite depth

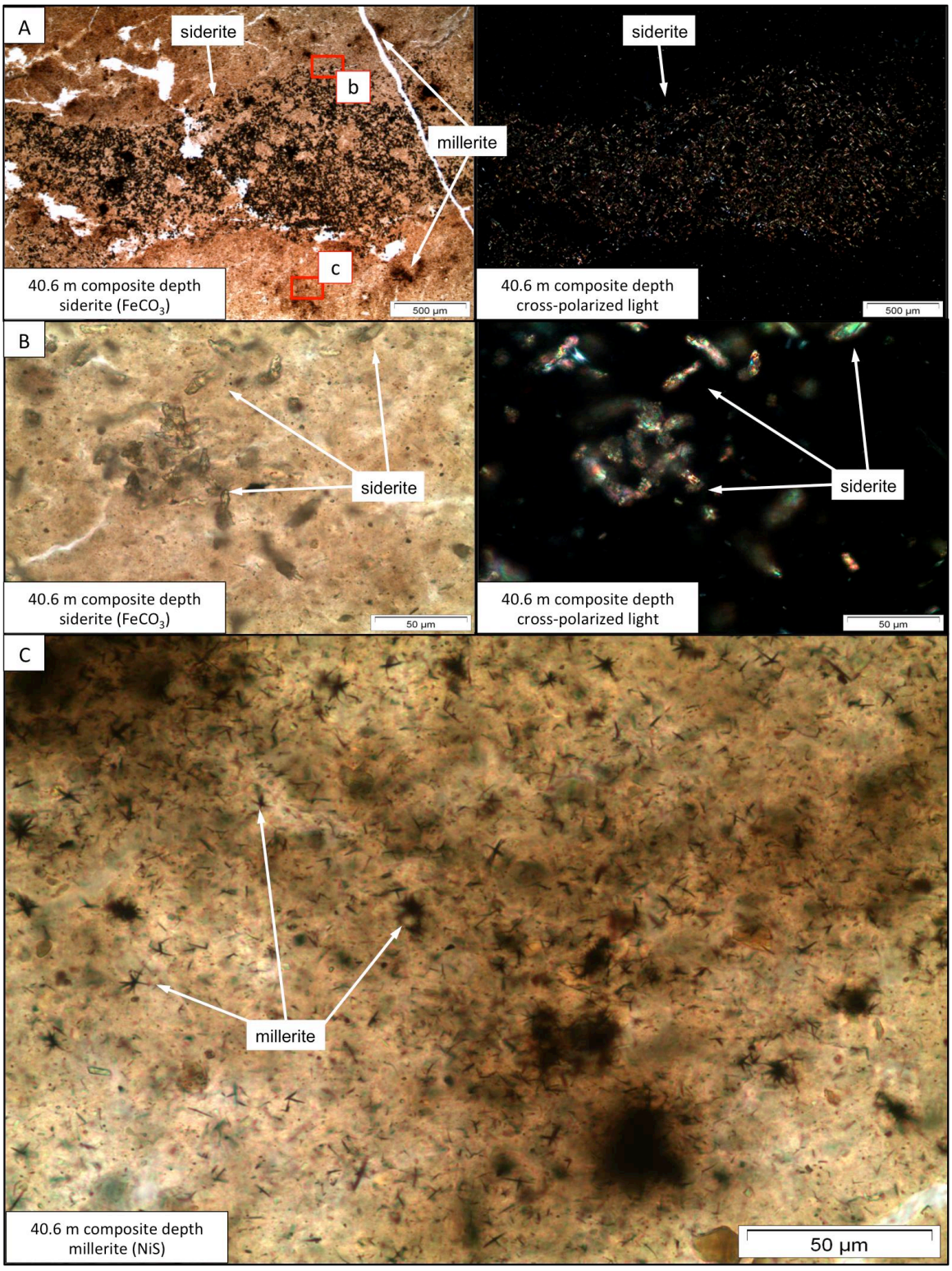

Figure S4.3 (A) and (D): Core images (two left panels), individual µCT gray scale slice image (right two panels), and elemental maps (based on µXRF measurements; small panels). Siderite and millerite are present in all samples (light colors in gray scale µCT images). (B): Core images (two left panels), µCT gray scale image (right panel), and total XRF counts for Fe and Mn (Cr-tube measurements) for polished 15-cm section compared to siderite volume calculated by image slice based on µCT measurements. (C): Core images (two left panels), microscope image of polished section and elemental maps (based on µXRF measurements; small panels)

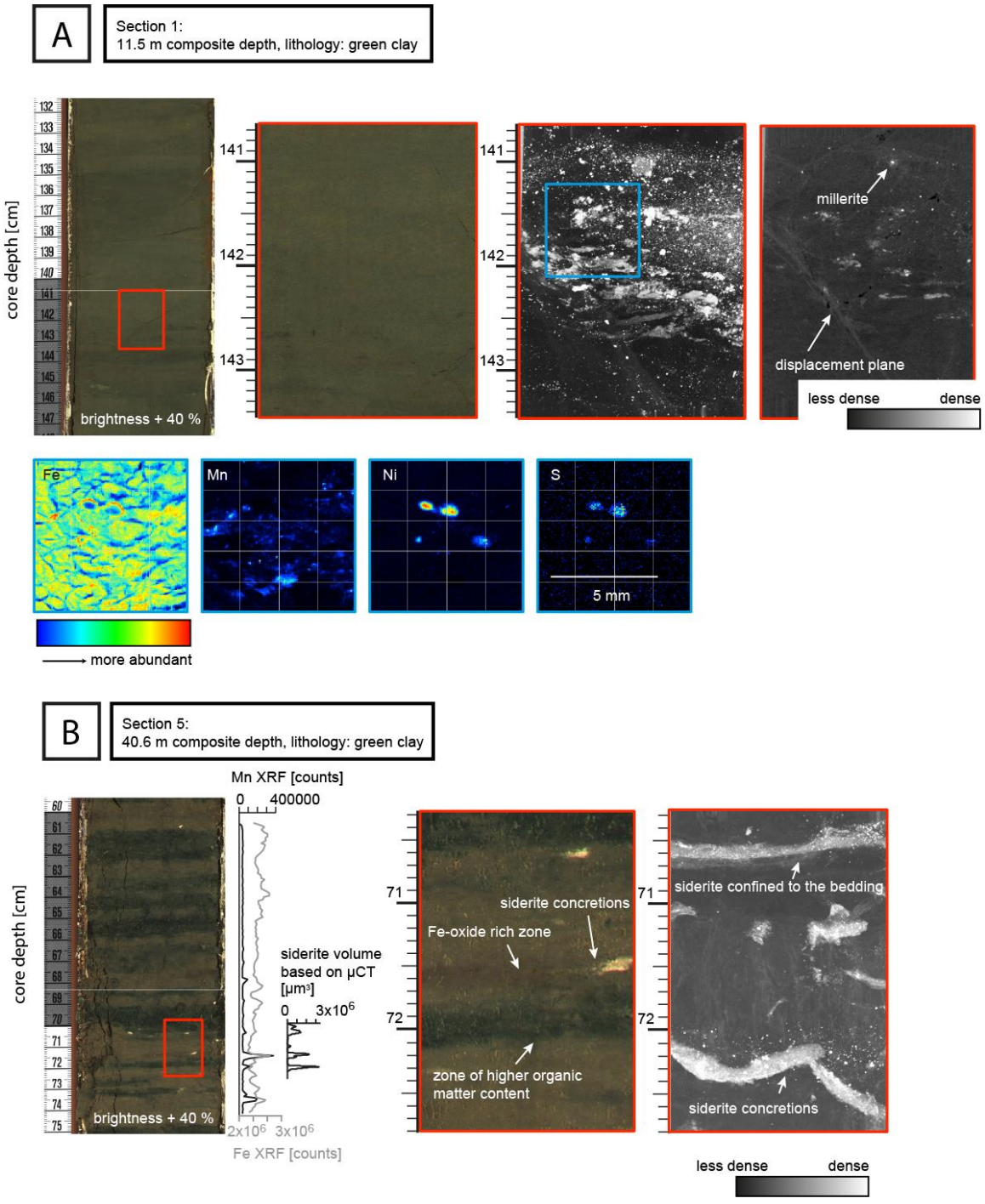

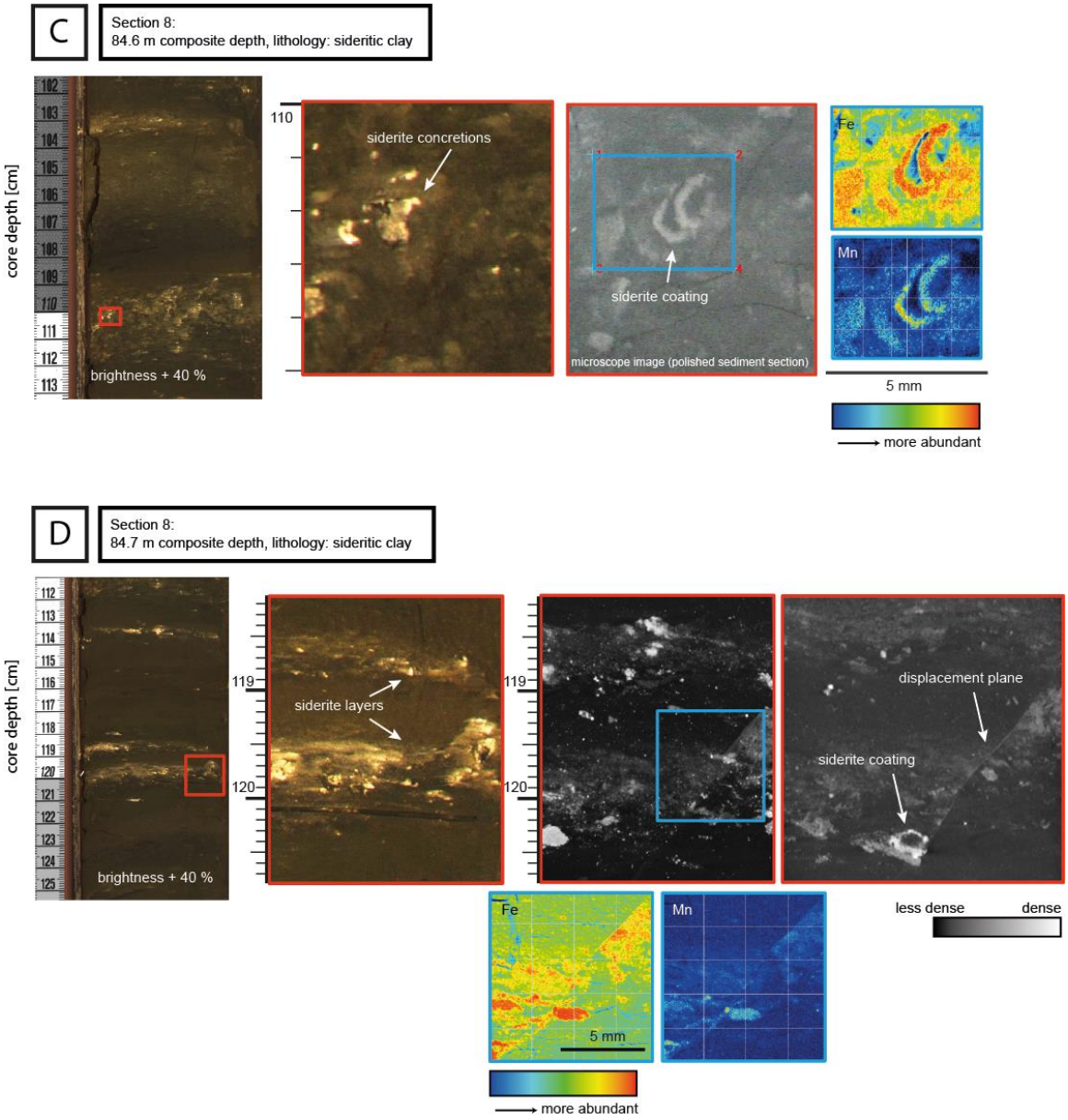
C
Section 8:
84.6 m composite depth, lithology: sideritic clay
core depth [cm]
brightness + 40 %
siderite concretions
siderite coating
microscope image (polished sediment section)
Fe
Mn
5 mm
more abundant
D
Section 8:
84.7 m composite depth, lithology: sideritic clay
core depth [cm]
brightness + 40 %
siderite layers
displacement plane
siderite coating
Fe
Mn
5 mm
less dense
dense
more abundant

Table S4.1 Sample names, locations, and performed analyses for the ten sediment sections, respectively

Sample ID	Composite core depth (sample top) [mcd]	Core	Sample top core depth [cm]	Sample bottom core depth [cm]	Main lithology	µCT	µXRF	XRF Cr-tube	XRF Mo-tube	Thin section
Sec1	11.40	TDP-TOW15-1B-5H-2	132	147	clay	yes	yes	yes	yes	yes
Sec2	14.86	TDP-TOW15-1A-6H-6	2	17	clay	yes	yes	yes	-	-
Sec3	21.43	TDP-TOW15-1A-9H-2	70	85	sideritic clay	yes	yes	yes	-	-
Sec4	36.16	TDP-TOW15-1B-14H-2	112	127	diatomaceous ooze	yes	yes	yes	-	yes
Sec5	40.48	TDP-TOW15-1A-17H-1	60	75	clay	yes	yes	yes	yes	yes
Sec6	43.79	TDP-TOW15-1A-18H-1	84	99	diatomaceous ooze	yes	yes	yes	-	yes
Sec7	65.53	TDP-TOW15-1A-30H-3	43	58	clay	yes	yes	yes	-	yes
Sec8	84.59	TDP-TOW15-1A-37H-2	110	125	sideritic clay	yes	yes	yes	-	yes
Sec9	88.53	TDP-TOW15-1A-39H-1	52	67	sideritic clay	yes	yes	yes	yes	yes
Sec10	97.87	TDP-TOW15-1A-42H-2	108	123	red clay	yes	yes	yes	yes	yes

4.11.3 Appendix C. Micro-CT movies (Electronic supplementary material)

Movie S4.1 Three-dimensional (3D) X-ray computed micro-tomography (µCT) visualization of sediment section 1 (11.4 m composite depth). Siderite appears in green/blue, millerite in red, background sediments are transparent. 3D volume visualizes siderite precipitated on a displacement plane and along associated fluid escape structures. See Fig. 2A for scale
see folder: Chapter 4 - Supplementary Movies
Movie_S4.1_Section1_3DVolume_Morlock_2018_PhD_Thesis.mp4

Movie S4.2 Three-dimensional (3D) X-ray computed micro-tomography (µCT) visualization of sediment section 8 (84.6 m composite depth). Siderite appears in green/blue, millerite in red, background sediments are transparent. 3D volume visualizes siderite concretions in two distinct layers. The lower of these layers is cut by a displacement plane, with siderite precipitated on the plane. See Fig. 2C for scale
see folder: Chapter 4 - Supplementary Movies
Movie_S4.2_Section8_3DVolume_Morlock_2018_PhD_Thesis.mp4

Movie S4.3 Sequence of X-ray computed micro-tomography (µCT) gray scale images of sediment section 8 (84.6 m composite depth), cut parallel to the sedimentary bedding. Millerite occupies the brightest, i.e. highest-density fraction of the visualization (gray scale values 251-255), siderite appears slightly darker (gray scale values ~190-250) and matrix sediments appear darkest (gray scale values <100). Images show fine siderite precipitated on the displacement plane cutting through the lower layer of siderite concretions. Bottom central part further shows a siderite coating with its center similar to the surrounding background sediments. See Fig. 2C for scale
see folder: Chapter 4 - Supplementary Movies
Movie_S4.3_Section8_Flythrough_Morlock_2018_PhD_Thesis.mov

Movie S4.4 Three-dimensional (3D) X-ray computed micro-tomography (μCT) visualization of sediment section 5 (40.5 m composite depth). Siderite appears in green/blue, millerite in red, background sediments are transparent. 3D volume visualizes several modes of siderite formation within one sample. Topmost siderite layer appears confined to the sedimentary bedding, below are siderite concretions, which are connected by very fine, branched threads of siderite. These may indicate microbial siderite precipitation. See Fig. 2B for scale
see folder: Chapter 4 - Supplementary Movies
Movie_S4.4_Section5_3DVolume_Morlock_2018_PhD_Thesis.mp4

Movie S4.5 Sequence of X-ray computed micro-tomography (μCT) gray scale images of sediment section 5 (40.5 m composite depth), cut parallel to the sedimentary bedding. Millerite occupies the brightest, i.e. highest-density fraction of the visualization (gray scale values 251-255), siderite appears slightly darker (gray scale values ~190-250) and matrix sediments appear darkest (gray scale values <100). Images show fine vertical structures interpreted as siderite, which connect larger siderite concretions above and below the threads. See Fig. 2B for scale
see folder: Chapter 4 - Supplementary Movies
Movie_S4.5_Section5_Flythrough_Morlock_2018_PhD_Thesis.mov

Movie S4.6 Sequence of X-ray computed micro-tomography (μCT) gray scale images of sediment section 3 (21.4 m composite depth), cut parallel to the sedimentary bedding. Millerite occupies the brightest, i.e. highest-density fraction of the visualization (gray scale values 251-255), siderite appears slightly darker (gray scale values ~190-250) and matrix sediments appear darkest (gray scale values <100). Images show several examples of siderite coating with centers similar to the surrounding background sediments
see folder: Chapter 4 - Supplementary Movies
Movie_S4.6_Section3_Flythrough_Morlock_2018_PhD_Thesis.mp4

CHAPTER 5

Sedimentation processes in tropical Lake Towuti: Palaeoenvironmental insights from end-member modelling of high-resolution XRF core-scanning data

Marina A. Morlock, Hendrik Vogel, James M. Russell, Flavio S. Anselmetti, Martin Melles & Satria Bijaksana

manuscript in preparation, under review with co-authors

5. Sedimentation processes in tropical Lake Towuti: Palaeoenvironmental insights from end-member modelling of high-resolution XRF core-scanning data

Marina A. Morlock*[1], Hendrik Vogel[1], James M. Russell[2], Flavio S. Anselmetti[1], Martin Melles[3] & Satria Bijaksana[4]

[1]*Institute of Geological Sciences and Oeschger Centre for Climate Change Research, University of Bern, 3012 Bern, Switzerland*

[2]*Department of Earth, Environmental, and Planetary Sciences, Brown University, Providence, RI 02912*

[3]*Institute of Geology and Mineralogy, University of Cologne, 50674 Cologne, Germany*

[4]*Faculty of Mining and Petroleum Engineering, Institut Teknologi Bandung, Bandung 40132, Indonesia*

to be submitted to Sedimentology

5.1 Abstract

Lacustrine and marine sediments often record a complex history of environmental change, but it can be challenging to separate different environmental processes in a sediment record. Recently, X-ray fluorescence (XRF) core scanning has become a standard technique in sediment-core processing, facilitating the generation of geochemical data sets down to a spatial resolution of 200 µm. To fully exploit such high-resolution records, we applied end-member modelling to an XRF core-scanning data set. End-member modelling is a statistical tool to unmix data into characteristic structures of - in this case- similar elemental composition. Analogous to grain-size analysis, where end-member modelling is more frequently applied, the underlying concept is that different sedimentary processes are reflected in characteristic elemental compositions, e.g. terrestrial influx is characterised by variations in Al and Ti concentrations. We present a study of sediments from tropical Lake Towuti (2.75°S, 121.5°E), one of the oldest and deepest lakes in Indonesia. Cores of the entire sediment infill have been recovered in the ICDP Towuti Drilling Project in 2015, including a 100-m-long lacustrine sequence that we XRF-scanned at 0.5 cm resolution. The end-member analysis reveals six end-members, which are interpreted to represent changes in climatic, tectonic and post-sedimentary processes as well as lake productivity. The three dominant end-members correspond to climatic and post-sedimentary processes identified in earlier studies on short (10 m) sediment cores from the same lake. The three other end-members represent processes not encountered in the short record. Based on the end-member scores, a high-resolution stratigraphic column of the sediment sequence can be generated. In our example, this stratigraphy shows general similarity to visual core descriptions, but provides a more detailed picture of transient and overlapping processes in the sediment. End-member analysis thus allows a detailed and objective description of sediment sequences and their respective sedimentological units beyond visual description.

Keywords XRF core scanner; stratigraphy; geochemistry; lake sediments; Lake Towuti; end-member analysis

5.2 Introduction

In the last decade, X-ray fluorescence (XRF) core scanning has become a standard technique to non-destructively assess the geochemical composition of sediments (Croudace & Rothwell, 2015). Fast and reliable determination of elements between Mg and U in the periodic table has facilitated the analysis of long sediment sequences at high spatial resolution. XRF core scanning in general and long sequences in particular entail a series of challenges such as X-ray tube drift, changing matrix effects due to lithology changes, and varying signal attenuation due to variable water content with sediment depth. Several approaches to correct for these effects have been suggested (Chen et al., 2016; Hennekam & de Lange, 2012; Löwemark et al., 2011; Lyle et al., 2012; Ohlendorf et al., 2015; Weltje & Tjallingii, 2008). With these corrections XRF core scanning provides a reliable and consistent record of high-resolution quantitative geochemical information, which can, for example, be used for palaeoenvironmental reconstructions (Rothwell & Croudace, 2015).

To describe XRF data sets, statistical methods such as clustering and PCA are commonly applied (Rothwell & Croudace, 2015), but interpretation of the results can be challenging in complex systems. End-member modelling is a statistical approach to separate a multivariate data set into characteristic groups with similar patterns (Heslop & Dillon, 2007; Weltje, 1997). In geosciences, end-member modelling has mostly been used with grain-size data, following the idea that different transport processes result in characteristic grain-size patterns (Dietze et al., 2012; Paterson & Heslop, 2015). Similarly, different processes influencing sedimentation can have characteristic geochemical compositions and data distributions, e.g. caused by mineral sorting by different transport processes or secondary mineral formation. Recently, Beuscher et al. (2017) successfully applied end-member modelling to a geochemical data set from a Mediterranean sediment record to reconstruct climate variability during the Holocene, but the authors do not provide details on their approach and do not compare their results to more widely applied techniques.

In this study we present a record of geochemical composition of a 100-m-long sedimentary record from Lake Towuti, Indonesia, determined by XRF scanning. The lake is located in a complex geologic setting in Central Sulawesi, where dynamic environmental and tectonic processes shape the landscape (Morlock et al., 2018). It is therefore challenging to consistently separate the different lithologies and processes by visual core description. Hence, we perform end-member modelling of XRF scanning data to extract high-resolution information about processes influencing lake sediment composition in our record. Based on the end-members, we generate a chemostratigraphic column of the sediment record. The combination of XRF scanning and statistical tools such as end-member modelling provides a powerful instrument for high-resolution analyses of long sediment sequences.

5.3 Material and Methods

5.3.1 Study site and sample acquisition

Large (560 km^2) and deep (200 m max. water depth) Lake Towuti (2.75°S, 121.5°E, 318 m a.s.l.) is located in the humid tropics on the island of Sulawesi, Indonesia (Figure 5.1). Cores of the complete sediment infill were recovered in 2015 by the International Continental Scientific Drilling Program (ICDP) Towuti Drilling Project (TDP;

Russell et al., 2016). The upper 100 m of sediment consist of uninterrupted lacustrine facies (Russell et al., 2016), covering part of the Pleistocene. The main lithological units are alternating green-grey and red-grey clays, with occasional occurrence of tephra and turbidite layers. Diatom oozes are present at two distinct intervals in the core (Russell et al. 2016). Mineralogy is dominated by phyllosilicates and Fe-oxides / Fe-oxyhydroxides, both of which are abundant in catchment soils, and serpentine phases from the ultramafic bedrock (Morlock et al., 2018). Several authigenic minerals are present in the sediments, with siderite ($FeCO_3$) being very abundant (Morlock et al., in review; Russell et al., 2016; Vuillemin et al., in press).

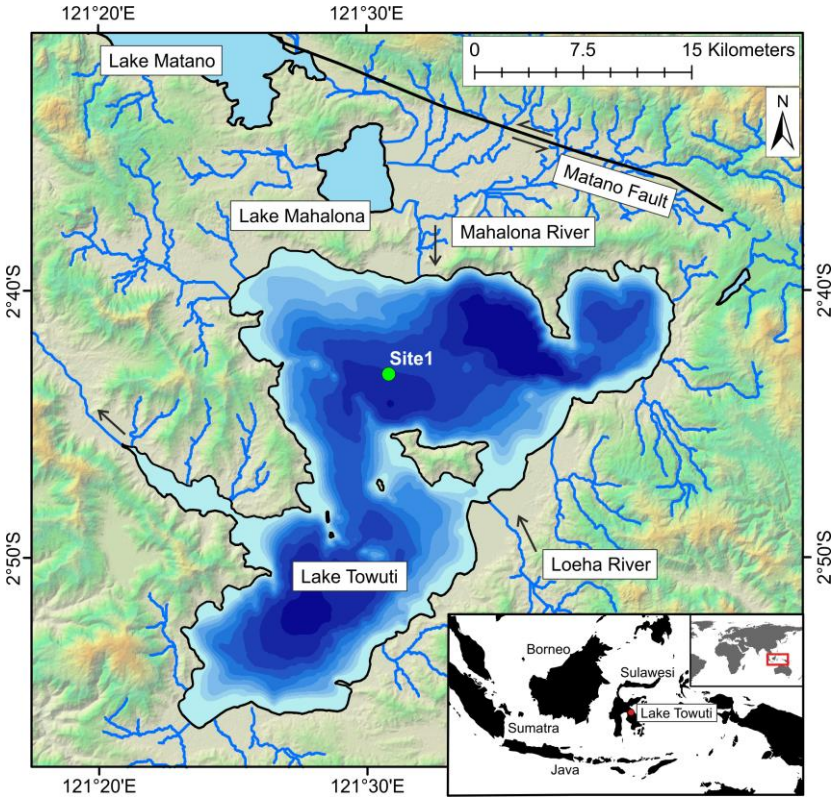

Figure 5.1 Location of Lake Towuti with bathymetry (20 m spacing), and upstream lakes Matano and Mahalona. Green circle indicates the coring location TDP Site 1

5.3.2 Geochemical analyses

Following core splitting at the National Lacustrine Core Facility (LacCore) in Minnesota, USA, a composite for TDP Site 1 was established based on visual alignment of lithologic features, supported by point sensor magnetic susceptibility measurements, in the program suite CoreWall (Correlator and Corelyzer, LacCore). This composite was sampled at 48-cm resolution (188 samples in the upper 100 m). Each sample is an integration of 4 cm of sediment (~8 cm^3). For all samples, concentrations of major elements (Al, Ca, Fe, K, Mg, Mn, Ni, P, Si, and Ti) were determined on dried, homogenised material by Inductively Coupled Plasma Atomic Emission Spectrometry (ICP-AES) at Brown University, USA. Samples were combined with lithium metaborate flux in graphite crucibles and fused at 1050°C for 10–12 min. After dissolution in 10 % HNO_3 and stirring for 30 min, samples were filtered and diluted for analysis on a Jobin Yvon JY2000 by ICP-AES at Brown University. Concentration data are calibrated to fluxed standard reference materials (NIST1646a, BIR-1, MESS-3, DTS-2B, SGR-1, NIST2702, MAG-1, SDO-1, NIST2711, BHVO-2). All samples were also analysed for their mineralogic composition by mid-infrared (MIR) Fourier-Transform-Infrared-

Spectroscopy (FTIRS). Details on MIR-FTIRS analyses and a comparison to clay X-ray diffraction (XRD) analysis of Lake Towuti sediments are given in Morlock et al. (2018).

In total, 106 split core sections of the upper ~100 m composite from TDP Site 1 were scanned on an XRF core scanner (ITRAX, Cox Ltd., Sweden) equipped with a chromium anode X-ray tube (Cr-tube) set to 30 kV, 50 mA, and 50 s integration time at 5 mm resolution at the University of Bern, Switzerland. Measurements were repeated with a molybdenum anode X-ray tube (Mo-tube) with the same settings to better resolve elements with high atomic numbers. Before each core, a site-specific standard (10 x 10 x 0.5 cm), prepared from dried and homogenised Lake Towuti sediment recovered in 2010, was measured to assess changes in X-ray source intensity. Sections of uneven core surface that affected XRF performance, gaps, and event layers were removed from the data set during post-processing. Event layers (tephra and turbidites) were also removed from the final depth scale (i.e. a constant depth was assumed for event layers). To correct for biases in the XRF data set, e.g. changes in interstitial water, a potential water film between core surface and covering foil, or grain size variations, discrete, dried, and homogenised samples from TDP Site 1 were measured (Supplementary Material [SM] Figure S5.1). Core surface scans were corrected for each element individually based on a linear regression model between dried homogenised sample measurements and their corresponding core scans. A detailed description of the correction and XRF scanning procedure is provided in Appendix II of this thesis.

5.3.3 Data analyses

Several end-member modelling algorithms have been developed for geoscientific applications (Dietze et al., 2012; Paterson & Heslop, 2015; Weltje, 1997). End-members describe a mixed data set as a combination of end-member loadings and scores. End-member loadings describe the contribution of the elements to each end-member. Scores quantify the relative contribution of each end-member to a sample, i.e. describe the relative contribution of each identified end-member (process) to the sediment composition through time or space. Mathematically, data sets for end-member modelling are required to be nonnegative and have a constant sum (sum-to-one; Paterson & Heslop, 2015). Details on the mathematical background of end-member modelling and a comparison of different approaches is summarised in Paterson and Heslop (2015) and Weltje (1997). If end-members are unknown *a priori*, no unique solution exists to the end-member computations. Therefore, besides mathematical validity, it is important to ensure that the final end-members are reasonable in a geologic context (Weltje, 1997).

Using the corrected XRF data set, we performed end-member modelling using the R package EMMAgeo (version 0.9.4), which was developed by Dietze et al. (2012) for end-member modelling of grain-size data. Elemental abundance (XRF counts of dry sediment) were used instead of grain-size bins for each of the ~18,000 XRF data points. XRF data were divided by the total counts of the respective X-ray tube and divided by the sum of all selected elements to fulfil the sum-to-one criterion. The algorithm of EMMAgeo is based on PCA, eigenvector rotation, variable scaling, and nonnegative least square estimation (Dietze et al., 2012). The algorithm is fastest in comparison to other methods (see Paterson & Heslop, 2015 for details), an important advantage when considering large data sets. The total number of end-members (EMs) is based on optimising the mean total explained variance and assessing a meaningful number of processes identified in the context of a data set (Dietze et al., 2012; Heslop & Dillon,

2007; Weltje, 1997), in this case Lake Towuti sediments. On the same data set, a principal component analysis (PCA) was performed on the data correlation matrix for comparison. A stratigraphic column of the XRF end-member data set was produced using the stratiplot function in the R package analogue (Simpson & Oksanen, 2016). For each XRF data point, the end-member with highest score determines the colouring of the respective line in the stratigraphic column. In correlation calculations, all coefficients are Spearman's rank correlation r.

5.4 Results

5.4.1 Generating a long XRF scanning record

Site-specific sediment standard measurements prior to each measured core section show a linear trend in tube aging, with opposing signs for light and heavy elements, respectively (SM Figure S5.2). Based on these measurements, a linear regression correction was applied to the wet XRF counts in the sediment-core sequence. In a second step, continuous sediment-core scans were corrected through linear regression of the wet counts to measurements of the discrete samples (Appendix II). Based on correlation between wet and dry XRF measurements and correlation of XRF core scans to ICP-AES measurements (where available), 19 elements (Mg, Al, Si, P, S, K, Ca, Sc, Ti, V, Cr, Mn, Fe, Co, Ni, Cu, Zn, Sr, Zr) were selected for further analysis.

5.4.2 End-member modelling and PCA

A total of six EMs were chosen to best represent the data set, minimising mean relative total error, while all end-members have a clear environmental context in the setting of Lake Towuti. The model explains 75 % of the sample variance. Parameters and characteristics of all end-members are summarised in Table 5.1. Figure 5.2 and Figure 5.3 show element abundance in each EM and EM scores for each measurement point, respectively. The end-member-based stratigraphic column representing the highest end-member score in each sample, respectively, is shown in Figure 5.4. In PCA, the first four principal components explain 75.4 % of the data set variance (PC1 31.5 %, PC2 22.0 %, PC3 12.5 %, PC4 9.5 %; SM Figure S5.3).

Table 5.1 Parameters and characteristics of the six end-members

End-members	Characteristic elements	Explained variance [%]	Interpretation	Positive correlation to mineralogy
EM1	Al, Ti, K, Zr	46.7	Soil erosion / Loeha River	kaolinite, quartz
EM2	Ni, Cr, Sc	28.4	Bedrock erosion / oxic water column	siderite
EM3	Si, Sr, P, Cu	11.6	Diatom productivity	-
EM4	Fe	7.9	Redox conditions	siderite, serpentine
EM5	Mn, Co	3.5	Post-sedimentary mineral formation	siderite
EM6	Mg, Ca	1.7	Tectonic basin evolution	serpentine

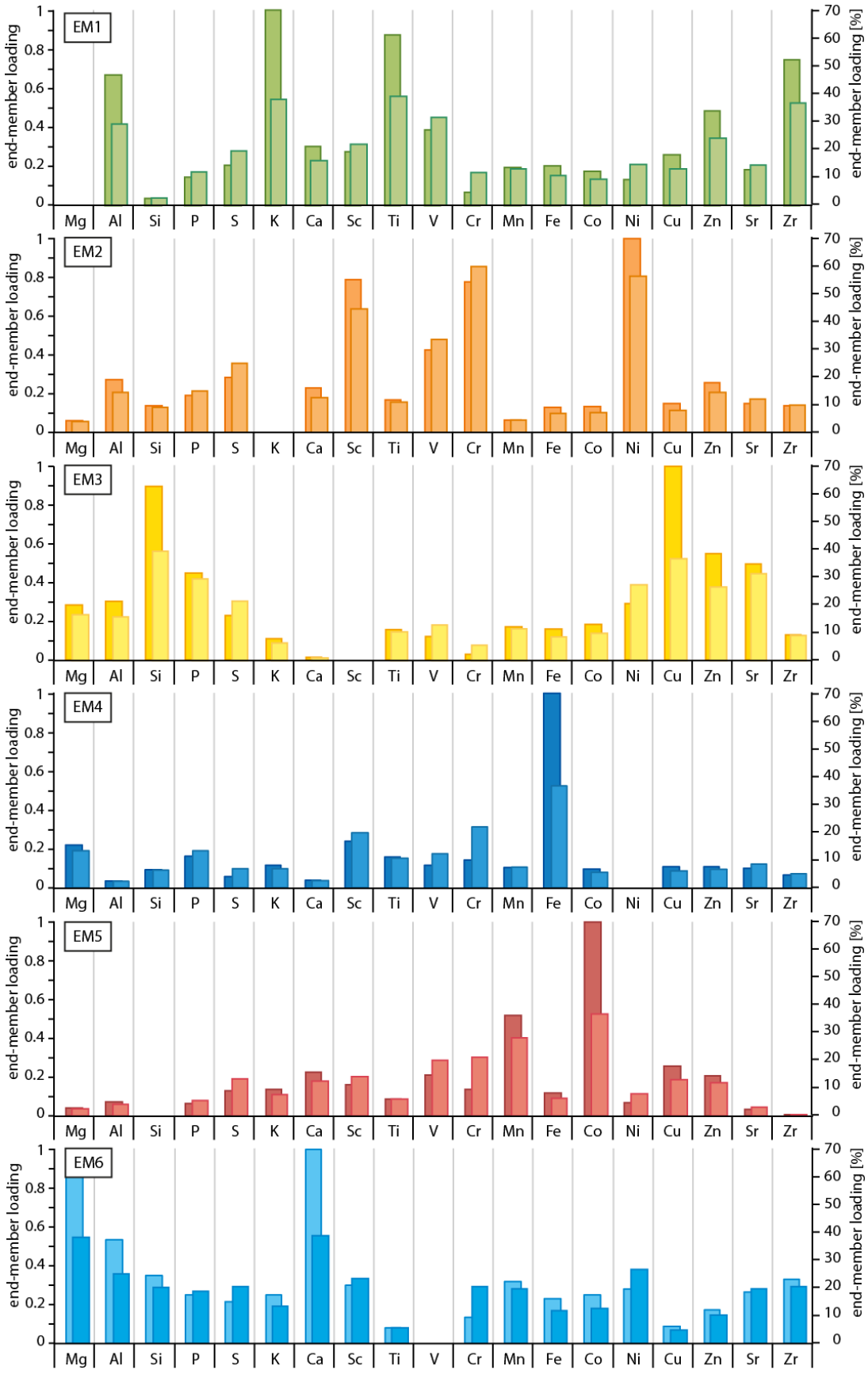

Figure 5.2 Element abundance in each of the six end-members calculated from the Towuti XRF data set. Bars on the left correspond to absolute end-member loadings, right bars correspond to relative end-member loading, scaled to 100 % for each element

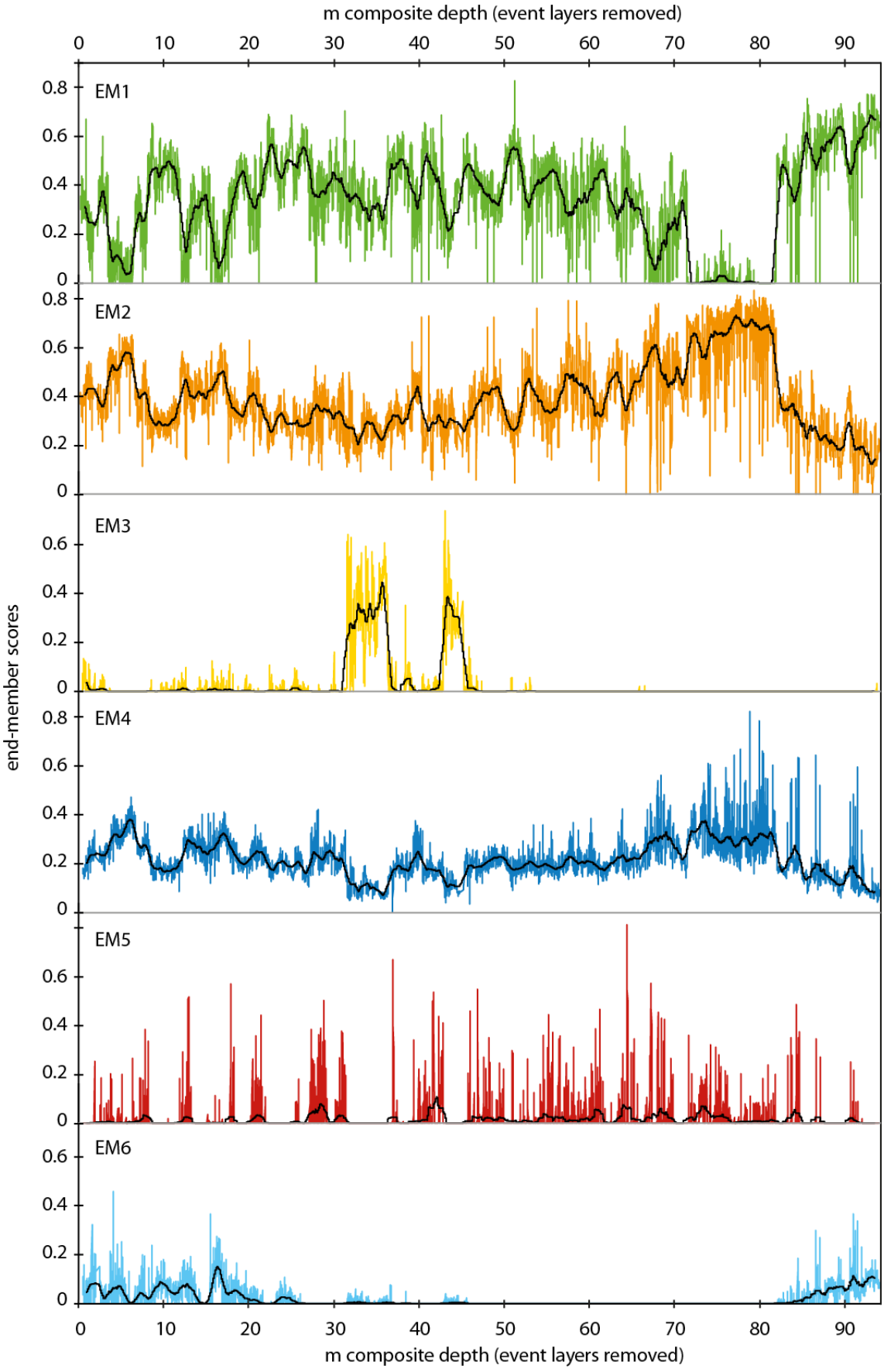

Figure 5.3 End-member scores for all six end-members calculated from the Towuti XRF data set. Black line indicates 200-point running mean (i.e. mean over ~1 m of core)

5.4.3 End-member description and interpretation

The first end-member (EM1) is characterised by high abundance (more than ~30 % element loading) of K, Ti, Zr, and Al, (Figure 5.2A), i.e. data points with high EM1 scores are particularly rich in K, Ti, Zr, and Al. EM1 explains 46.7 % of the model variance and scores are positively correlated with quartz and kaolinite content of discrete sediment samples (r=0.83 and 0.59, respectively, p=0, n=197; SM Figure S5.4). Analyses of catchment samples show that laterite soils, developed on ultramafic bedrock, are, relative to bedrock, enriched in Al and Ti, and to a smaller extent in K (Morlock et al., 2018). These soils, together with material from the Loeha River, which drains a catchment of more felsic bedrock to the East of the lake, provide the most important contribution of Al, K, Ti, and Zr to the deep northern lake basin (Costa et al., 2015; Hasberg et al., 2018; Morlock et al., 2018). These two sources (soils and the Loeha river) deliver fine-grained sediments that are rich in kaolinite and quartz (Morlock et al., 2018). EM1 is therefore interpreted to represent a mixture of these two sources to the coring location. Previous studies on short sediment cores covering the last 60,000 years have shown that sedimentation of soil and Loeha material is enhanced in phases of lake-level high stands, e.g. during the relatively wet Holocene period (Costa et al., 2015; Morlock et al., 2018; Vogel et al., 2015). EM1 scores are negatively correlated to PCA component 1 (r=-0.78, p=0, n=17322).

EM2 is characterised by a high abundance of Cr, Ni, and Sc (Figure 5.2B) and explains 28.4 % of the model variance. Samples with high EM2 scores are antiphased to samples with high EM1 scores (Figure 5.3A and B). Cr and Ni are enriched in rivers draining ultramafic bedrock relative to metasedimentary rivers (Costa et al., 2015) and are components in mafic minerals from the bedrock and saprolite zone, e.g. pyroxenes and (secondary) serpentines (Kadarusman et al., 2004; Morlock et al., 2018). In the last 60,000 years, increased hydrologic gradients and a shorter distance between lake shore and coring site during dry periods increased the delivery of bedrock-derived material to the deep northern lake basin (Costa et al., 2015; Morlock et al., 2018; Vogel et al., 2015). Further, Costa et al. (2015) suggest that bottom-water oxygenation is higher during phases of lake level low stands, increasing the sedimentation of redox-sensitive elements like Fe, Cr, and Co in the basin. Hence, EM2 is interpreted to represent increased (ultramafic) bedrock erosion in combination with increased metal deposition in a more oxygenated water column during lake-level low stands. EM2 sediments are positively correlated to PCA component 1 (r=0.77, p=0, n=17322).

EM3 sediments are particularly enriched in Si, Cu, Sr, and P (Figure 5.2C). EM3 explains 11.6 % of the model variance, and high EM3 scores occur at two distinct intervals in the record (Figure 5.3C), which coincide with the diatomaceous ooze described in the sediment stratigraphy from Russell et al. (2016). Sediments with high EM3 scores show high concentrations of diatoms. EM3 is therefore interpreted to represent phases of high diatom abundance in the sediments. EM3 scores are positively correlated to PCA component 2 (r=0.48, p=0, n=17322).

EM4 is characterised by a high Fe content and explains 7.9 % of the model variance (Figure 5.2D). End-member scores are positively correlated to siderite and serpentine (r=0.57 and 0.24, respectively, p=0, n=179), correlate negatively with quartz and kaolinite (r=-0.71 and -0.51, respectively, p=0, n=179; SM Figure S5.4), and co-vary with EM2. Fe deposition depends on water-column oxygenation and redox conditions at the sediment-water interface, as well as Fe diagenesis and mineral formation in the

sediment column. Similar to EM2, EM4 is thus interpreted to record changes in lake-water oxygenation. While EMs 2 and 4 show similar long-term trends in the down-core sequence (Figure 5.3), variability of the two sequences differs on shorter time scales. This is also seen in the original XRF data for Fe and Ni (SM Figure S5.5) as well as in the ICP-AES data set (not shown). Possible reasons for these patterns are briefly touched upon in the discussion section. EM4 scores are positively correlated to PCA component 1 (r=0.89, p=0, n=17322).

EM5 sediments are rich in Mn and Co (Figure 5.2E). EM5 explains 3.5 % of the model variance and shows sharp peaks across the 100 m long record (Figure 5.3E). Samples with high EM5 scores are positively correlated to siderite abundance (r=0.65, p=0, n=179). Siderite is a common Fe- and Mn-rich mineral in Lake Towuti sediments, related to post-sedimentary alteration of iron oxides (Morlock et al., in review; Vuillemin et al., 2016), and can also incorporate Co in its structure. Siderite distribution in the sediment is highly heterogeneous. Therefore, EM5 sediments are interpreted to represent siderite-rich intervals in the sediment record. EM5 scores are positively correlated to PCA component 1 (r=0.44, p=0, n=17322) and PCA component 4 (r=0.46, p=0, n=17322).

EM6 is characterised by a dominant signal in Mg and Ca, with minor components of Al, Mn, Si, Sr, and Zr (Figure 5.2F). It explains 1.9 % of the model variance and shows highest scores in the top 30 and lowest 10 m of the record (Figure 5.3F). Scores are positively correlated to serpentine abundance (r=0.68, p=0, n=179) and correlate negatively with kaolinite (r=-0.49, p=0, n=179; SM Figure S5.4). Comparison to the original XRF data set shows that Mg abundance characterises the upper 30 m of the record, while Ca abundance leads the pattern in the lowest 10 m. In modern sedimentation, the main tributary to the northern basin, the Mahalona River, is the main source of Mg-rich serpentines to the lake (Hasberg et al., 2018; Morlock et al., 2018). Dynamic tectonics in the area together with a marked decrease in serpentine abundance in the sediments below 30 m depth (data not shown) suggest that this source, the Mahalona River, did not always directly contribute to sedimentation in Lake Towuti. The importance of EM6 in the upper part of the record is thus interpreted to represent the influence of the Mahalona River on lake sedimentation at the coring site. In the lowest part of the record, peat underlies the earliest lake sediments at 100 m sediment depth. The decreasing scores of EM6 between 95 and 80 m are interpreted to represent the opening of the basin and initial formation of a permanent lake, when drainage reorganisation, river incision into the Mg-serpentine-rich bedrock and more felsic Ca-rich bedrock components dominated sedimentation relative to kaolinite-rich laterites. EM6 scores are positively correlated to PCA component 3 (r=0.50, p=0, n=17322).

5.5 Discussion

5.5.1 End-member modelling as a tool for sedimentology

Up to now, clustering and PCA are more common statistical methods used on XRF data sets (Rothwell & Croudace, 2015). As opposed to clustering, end-member analysis can account for several processes influencing one data point, and hence allows for the description of gradual transitions in sediment composition. As an example, tectonic changes in the upper and lower part of the record can be isolated from climate-driven processes without excluding the tectonically influenced parts of the record from

the climate interpretation. End-member modelling is well suited as a sedimentological tool if stratigraphic units have contrasting elemental compositions, but little grain-size variation. Large differences in grain size will have a strong effect on XRF scanning quality, making the generation of high-quality data sets difficult. As opposed to visual core descriptions, core oxidation only plays a minor role in influencing the modelling results.

The six processes separated by end-member modelling in Lake Towuti are reflected in PCA axes 1-4 (SM Figure S5.3). PC1 separates metals (Fe, Cr, Mn, Co, PC1 positive (PC+)) from the remaining data set (PC1-). PC2 separates diatoms and the Mahalona (Si, Sr, and Mg, PC2+) from laterite/Loeha input and the metals (Al, Ti, Ca, and Ni, Cr, Fe, PC2-). Based on PCA crossplots, it is possible to identify different depositional processes and sources (metals (PC1+/PC2-), siderite (PC1+), laterite/Loeha (PC1-/PC2-) and diatoms/Mahalona (PC1-/PC2+) for PC axes 1 and 2). Downcore, however, the influence of these processes over time cannot be visualised separately. This exemplifies issues with interpreting PCA results in complex systems with multiple depositional processes such as Lake Towuti. With the exception of the diatom oozes, all PCA axes contain a mixture of sedimentation processes (SM Figure S5.3), making a process-based interpretation of downcore changes difficult. End-member modelling extracts the variability of one or a group of elements, relative to all other elements. It includes a PCA but performs additional steps in the calculation process, resulting in a more easily interpretable data set, which identifies important sedimentation processes across the lacustrine record. Particularly in complex systems with multiple sediment sources and influencing processes, end-member modelling is clearly better suited than PCA. In simple lake systems with only few contributing sources, e.g. siliciclastic input and organic-rich sedimentation, PCA commonly generates satisfactory results.

5.5.2 Comparison between visual core description and end-member analysis

Specifically, four end-members (EMs 1-3 and 5) describe the processes that dominate lake sedimentation (i.e. have highest end-member scores) and are hence represented in the XRF-based stratigraphic column (Figure 5.4). The other two end-members (EMs 4 and 6, representing iron and tectonics, respectively) don't reach the highest score in any sample. The general pattern of the end-member based record compares well with the stratigraphic column based on visual core description (Russell et al., 2016; Figure 5.4). However, particularly in the central part of the record, where higher-frequency changes occur, the two methods deviate. A direct comparison between visual core description and EM-based lithologies for all XRF data points (Figure 5.4B-G) shows that generally, sediments visually classified as 'diatomaceous ooze' have high scores of diatom-EM3, whereas coarser-grained sediments (classified as 'silt') are strongly associated with tectonic EM6. Tectonic disturbance, e.g. to river courses will cause river incision and slope erosion, mobilising coarser-grained material from the catchment. More difficult to separate visually are sediments represented by EMs 1, 2, 4, and 5. Visually described sideritic clays are more frequently associated with end-members representing siderite (EM5), iron oxides (EM4), and metal oxides (EM2). Siderite is the only iron carbonate present in Lake Towuti and can thus easily be identified on the core surface and in smear slides, but besides discrete layers of siderite, the lithologic unit 'sideritic clay' also includes more reddish-grey sediments surrounding sideritic layers. The presence of iron and metal oxides can be inferred from sediment

colour, but colour changes may be difficult to systematically assess through a 100 m-long core sequence. This also applies to the second main lithology, ‘clay’, which appear darker and more olive green to grey compared to more reddish-grey ‘sideritic clay’ (Russell et al., 2016). EM2, representing input from laterites and the Loeha River, generally has higher scores in sediments attributed to ‘clay’. The good agreement between EM2 sediments and visually classified ‘silt’ (Figure 5.4) can be explained by early basin subsidence, which caused the initial erosion and mobilisation of lateritic material prior to bedrock incision. In general, in the complex setting of Lake Towuti, a tropical lake located in a tectonically active area, geochemical variations in sediment composition provide a similar, but more detailed picture of sedimentation processes compared to the visual core description.

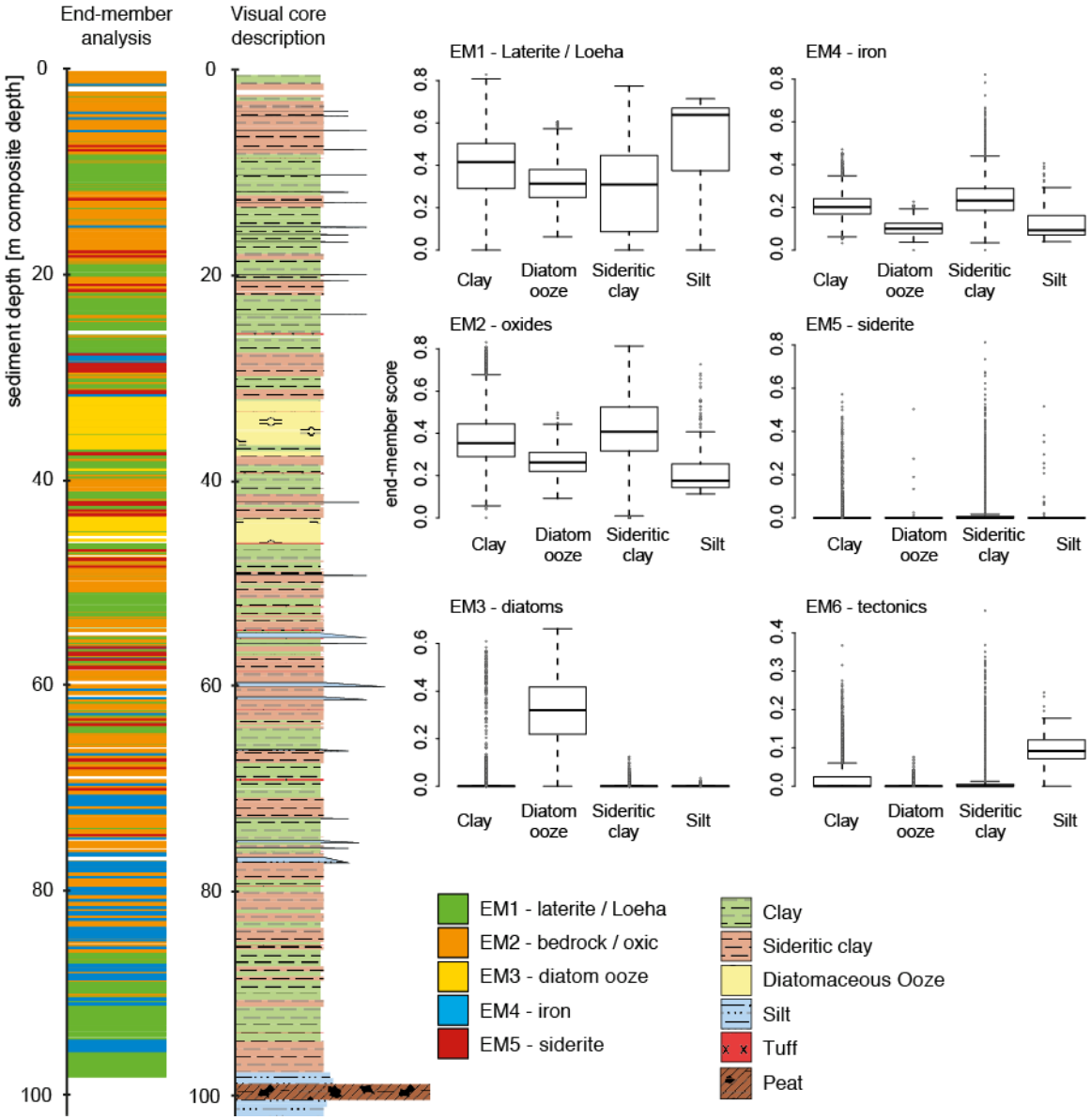

Figure 5.4 Stratigraphic column based on end-member analysis (left) and visual core description (centre). EM-based stratigraphic column is generated by colouring each XRF data point according to its highest-score end-member. Boxplots to the right show agreement of the end-member and visual lithologies for all 17322 XRF data points

5.5.3 The Lake Towuti sediment record

Previous studies on modern and past sediments from Lake Towuti have described a complex interaction between climatic and tectonic processes that influence lake sedimentation today and during the last 60,000 years (10 m long record; Goudge et al., 2017; Hasberg et al., 2018; Morlock et al., 2018; Russell et al., 2014; Vogel et al., 2015). The main drivers of sedimentation are climatically controlled lake-level fluctuations, which cause the alternate deposition of slightly coarser-grained Mg-serpentine-rich clays during lake-level low stands and darker green clays enriched in Al-phyllosilicates and quartz derived from the catchment soils and the Loeha river during lake-level high stands. The former lithology is further characterised by marked sideritic bands related to syn- and post-sedimentary siderite formation (Morlock et al., in review; Russell et al., 2016). Our end-member analysis performed on the XRF data set identifies processes, which reflect changes in climate (EMs 1 and 2), lake productivity (EM3), redox processes (EM4), post-sedimentary sediment alteration (EM5) and tectonics (EM6). Amongst these are the three main drivers for sedimentation in the upper 10 m of the record (wet and dry periods, and siderite), which are now shown to also characterise sedimentation over the entire ~100-m-long sediment record (EMs 1, 2, and 5). The heterogeneous siderite occurrence in the record particularly highlights the benefits of high-resolution XRF scanning in combination with end-member modelling, which allows a detailed description of heterogeneous lithologies throughout the 100 m record.

In addition, three other processes are identified, which did not act as primary drivers of sediment composition in the most recent sediments. These processes are related to long-term tectonic changes to the catchment (EM3), to redox-processes (EM4), and episodic diatom blooms in the lake (EM6). In the modern lake system, tectonic processes were identified to only indirectly modify sediment composition through regulating river incision and slope angles in the lake catchment (Morlock et al., 2018). Yet, in the tectonically active area of central Sulawesi, long-term changes in basin subsidence and catchment hydrology are expected (Watkinson & Hall, 2016).

High diatom abundance in EM3, culminating in sediments that consist almost entirely of diatoms, indicates algal blooms in the modern oligotrophic lake. No diatoms are present (or preserved) at any other depth in the core (Russell et al., 2016) and only few benthic species have been found in littoral environments in the lake today (Haffner et al., 2001; Hasberg et al., 2018; Lehmusloto et al., 1997). To this point, it remains uncertain what caused the diatomaceous oozes to form and why they occur at only two distinct intervals in the lacustrine record (see Chapter 3).

Redox-processes in ferruginous and metal-rich Lake Towuti are complex. End-members 2 (Cr, Ni), 4 (Fe), and 5 (Mn, Co) all represent redox-sensitive elements and end-member scores co-vary through the record. Yet, down-core variability of the respective elements is sufficiently different to separate them into several end-members. Mn and Co get concentrated in siderite, which abundantly forms in Fe-oxide-rich sediment horizons of Lake Towuti sediments. Siderite abundance is strongly influenced by post-depositional mineral formation and growth (Morlock et al., in review; Vuillemin et al., in press), i.e. to a large degree this end-member represents a post-depositional signal. Fe-rich EM4 and Cr- and Ni-rich EM2 show a similar overall trend through the 100 m sequence (Figure 5.3), but small-scale variability differs between the two end-members and their most prominent elements (SM Figure S5.5). The different variability in Fe relative to Ni and Cr could be explained by several mechanisms involving

differential deposition, redox processes in the water column or post-depositional sediment alteration. Further analyses are currently underway to get a more in-depth understanding of element recycling in Lake Towuti.

5.6 Conclusion

Long, high-resolution geochemical data sets can now easily be generated through XRF scanning of sediment-core records. End-member modelling provides a tool to make use of these large data sets, allowing for a quantitative, objective, and consistent description of sedimentological units throughout the XRF sequence. For Lake Towuti sediments, end-member modelling separates processes related to climate (EMs 1 and 2), diatom productivity (EM 3), redox processes (EM4), post-sedimentary mineral formation (EM 5), and tectonics (EM 6). Lake-level fluctuations, which change lake-water oxygenation and fluvial transport in the catchment, are identified as the main drivers in sedimentation through the 100-m long lacustrine record. These changes were modulated by long-term tectonic basin subsidence and a prominent change in river connectivity recorded at 30 m sediment depth. Distinct intervals of high diatom abundance and post-sedimentary mineral alteration also play a role in sediment composition. Sediment stratigraphy across the 100-m record generally matches the initial visual core description, but shows more detailed variations, particularly in the central part of the record. We show that the combination of high-resolution XRF core scanning and end-member modelling can serve as a tool to adequately describe the palaeoenvironmental significance of complex sedimentation systems.

5.7 Acknowledgements

The Towuti Drilling Project was partially supported by grants from the International Continental Drilling Program, the US National Science Foundation, the German Research Foundation, the Swiss National Science Foundation (20FI21_153054/1 and 200021_153053/1), Brown University, Genome British Columbia, and the Ministry of Research, Technology, and Higher Education (RISTEK). PT Vale Indonesia, the US Continental Drilling Coordination Office, the GeoForschungs-Zentrum Potsdam and DOSECC Exploration Services are acknowledged for logistical assistance to the project. We further thank Elisabeth Dietze for constructive comments and discussions on end-member modelling and Martin Wille for discussions on metal chemistry. This research was carried out with permission from the Ministry of Research and Technology (RISTEK), the Ministry of Trade of the Republic of Indonesia, and the Natural Resources Conservation Center (BKSDA) and Government of Luwu Timur of Sulawesi.

5.8 Author contributions

JMR, SB, HV, and MM designed and led the Towuti Drilling Project. MAM, HV, JMR, MM, and SB participated in fieldwork and core opening. JMR and HV developed the sediment stratigraphy. MAM and HV designed the study; MAM performed XRF scans and post-processing, HV assisted with XRF post-processing, FSA provided XRF scanning facilities and support, JMR provided ICP-AES data. MAM led the writing of the manuscript and designed the figures. All authors were involved in discussions about the

data and contributed to writing and improving the manuscript. The authors declare no conflict of interest.

5.9 References

Beuscher S, Krüger S, Ehrmann W, Schmiedl G, Milker Y, Arz H, Schulz H. (2017). End-member modelling as a tool for climate reconstruction - An Eastern Mediterranean case study. PLoS ONE, 12(9), e0185136. doi: 10.1371/journal.pone.0185136

Chen Q, Kissel C, Govin A, Liu Z, Xie X. (2016). Correction of interstitial water changes in calibration methods applied to XRF core-scanning major elements in long sediment cores: Case study from the South China Sea. Geochemistry, Geophysics, Geosystems, 17(5), 1925-1934. doi: 10.1002/2016gc006320

Costa KM, Russell JM, Vogel H, Bijaksana S. (2015). Hydrological connectivity and mixing of Lake Towuti, Indonesia in response to paleoclimatic changes over the last 60,000years. Palaeogeography, Palaeoclimatology, Palaeoecology, 417, 467-475. doi: 10.1016/j.palaeo.2014.10.009

Croudace IW, Rothwell RG. (2015). Micro-XRF Studies of Sediment Cores. Application of a non-destructive tool for the environmental sciences. Dordrecht: Springer.

Dietze E, Hartmann K, Diekmann B, Ijmker J, Lehmkuhl F, Opitz S, Stauch G, Wünnemann B, Borchers A. (2012). An end-member algorithm for deciphering modern detrital processes from lake sediments of Lake Donggi Cona, NE Tibetan Plateau, China. Sedimentary Geology, 243-244, 169-180. doi: 10.1016/j.sedgeo.2011.09.014

Goudge TA, Russell JM, Mustard JF, Head JW, Bijaksana S. (2017). A 40,000 year record of clay mineralogy at Lake Towuti, Indonesia: Paleoclimate reconstruction from reflectance spectroscopy and perspectives on paleolakes on Mars. Geological Society of America Bulletin.

Haffner GD, Hehanussa PE, Hartoto D. (2001). The biology and physical processes of large lakes of Indonesia: Lakes Matano and Towuti. In: Munawar M, Hecky RE (Eds.) The Great Lakes of the World (GLOW): Food-web, health and integrity (pp. 183-192). Leiden, The Netherlands: Backhuys Publishers.

Hasberg AKM, Melles M, Wennrich V, Just J, Held P, Morlock MA, Vogel H, Russell JM, Bijaksana S, Opitz S. (2018). Modern sedimentation processes in Lake Towuti, Indonesia, revealed by the composition of surface sediments. Sedimentology.

Hennekam R, de Lange G. (2012). X-ray fluorescence core scanning of wet marine sediments: methods to improve quality and reproducibility of high-resolution paleoenvironmental records. Limnology and Oceanography: Methods, 10(12), 991-1003. doi: 10.4319/lom.2012.10.991

Heslop D, Dillon M. (2007). Unmixing magnetic remanence curves withouta prioriknowledge. Geophysical Journal International, 170(2), 556-566. doi: 10.1111/j.1365-246X.2007.03432.x

Kadarusman A, Miyashita S, Maruyama S, Parkinson CD, Ishikawa A. (2004). Petrology, geochemistry and paleogeographic reconstruction of the East Sulawesi Ophiolite, Indonesia. Tectonophysics, 392(1-4), 55-83. doi: 10.1016/j.tecto.2004.04.008

Lehmusloto P, Machbub B, Terangna N, Rusmiputro S, Achmad F, Boer L, Brahmana SS, Priadi B, Setiadji B, Sayuman O, Margana A. (1997). National Inventory of the Major Lakes and Reservoirs in Indonesia. General limnology, Expedition Indodanau Technical Report. Bandung and Helsinki.

Löwemark L, Chen HF, Yang TN, Kylander M, Yu EF, Hsu YW, Lee TQ, Song SR, Jarvis S. (2011). Normalizing XRF-scanner data: A cautionary note on the interpretation of high-resolution records from organic-rich lakes. Journal of Asian Earth Sciences, 40(6), 1250-1256. doi: 10.1016/j.jseaes.2010.06.002

Lyle M, Oliarez Lyle A, Gorgas T, Holbourn A, Westerhold T, Hathorne E, Kimoto K, Yamamoto S. (2012). Data report: raw and normalized elemental data along the Site U1338 splice from X-ray fluorescence scanning. doi: 10.2204/iodp.proc.320321.203.2012

Morlock MA, Vogel H, Hadi J, Foubert A, Ariztegui D, Melles M, Russell JM, Bijaksana S. (in review). Temporal and spatial Variability of Siderite formation in ferruginous Sediments. submitted to Geology.

Morlock MA, Vogel H, Nigg V, Ordoñez L, Hasberg AK, Melles M, Russell JM, Bijaksana S. (2018). Climatic and tectonic controls on source-to-sink processes in the tropical, ultramafic catchment of Lake Towuti, Indonesia. Journal of Paleolimnology. doi: 10.1007/s10933-018-0059-3

Ohlendorf C, Wennrich V, Enters D. (2015). Experiences with XRF-Scanning of Long Sediment Records. 17, 351-372. doi: 10.1007/978-94-017-9849-5_13

Paterson GA, Heslop D. (2015). New methods for unmixing sediment grain size data. Geochemistry, Geophysics, Geosystems(16), 4494-4506. doi: 10.1002/ 2015GC006070

Rothwell RG, Croudace IW. (2015). Twenty Years of XRF Core Scanning Marine Sediments: What Do Geochemical Proxies Tell Us? In: Croudace IW & Rothwell RG (Eds.) Micro-XRF Studies of Sediment Cores. Application of a non-destructive tool for the environmental sciences (pp. 25-102). Dordrecht: Springer.

Russell JM, Bijaksana S, Vogel H, Melles M, Kallmeyer J, Ariztegui D, Crowe S, Fajar S, Hafidz A, Haffner D, Hasberg A, Ivory S, Kelly C, King J, Kirana K, Morlock M, Noren A, O'Grady R, Ordonez L, Stevenson J, von Rintelen T, Vuillemin A, Watkinson I, Wattrus N, Wicaksono S, Wonik T, Bauer K, Deino A, Friese A, Henny C, Imran, Marwoto R, Ngkoimani LO, Nomosatryo S, Safiuddin LO, Simister R, Tamuntuan G. (2016). The Towuti Drilling Project: paleoenvironments, biological evolution, and geomicrobiology of a tropical Pacific lake. Scientific Drilling, 21, 29-40. doi: 10.5194/sd-21-29-2016

Russell JM, Vogel H, Konecky B, Bijaksana S, Huang Y, Melles M, Wattrus N, Costa KM, King JW. (2014). Glacial forcing of central Indonesian hydroclimate since 60,000 y BP. PNAS, 111(14), 5100-5105. doi: 10.1073/pnas.1402373111

Simpson GL, Oksanen J. (2016). analogue: Analogue and Weighted Averaging Methods for Palaeoecology. Retrieved from https://github.com/gavinsimpson/analogue

Vogel H, Russell JM, Cahyarini SY, Bijaksana S, Wattrus N, Rethemeyer J, Melles M. (2015). Depositional modes and lake-level variability at Lake Towuti, Indonesia, during the past ~29 kyr BP. Journal of Paleolimnology, 54(4), 359-377. doi: 10.1007/s10933-015-9857-z

Vuillemin A, Friese A, Alawi M, Henny C, Nomosatryo S, Wagner D, Crowe SA, Kallmeyer J. (2016). Geomicrobiological Features of Ferruginous Sediments from Lake Towuti, Indonesia. Front Microbiol, 7, 1007. doi: 10.3389/fmicb.2016.01007

Vuillemin A, Horn F, Friese A, Winkel M, Alawi M, Wagner D, Henny C, Orsi WD, Crowe SA, Kallmeyer J. (in press). Metabolic potential of microbial communities from ferruginous sediments. Environmental Microbiology. doi: 10.1111/1462-2920.14343

Watkinson IM, Hall R. (2016). Fault systems of the eastern Indonesian triple junction: evaluation of Quaternary activity and implications for seismic hazards. In: Cummins PR, Meilano I (Eds.) Geohazards in Indonesia: Earth Science for Disaster Risk Reduction. (Vol. 441, pp. 71-120). London, UK: Geological Society, London, Special Publications.

Weltje GJ. (1997). End-Member Modeling of Compositional Data: Numerical-Statistical Algorithms for Solving the Explicit Mixing Problem. Mathematical Geology, 29(4), 503-549.

Weltje GJ, Tjallingii R. (2008). Calibration of XRF core scanners for quantitative geochemical logging of sediment cores: Theory and application. Earth and Planetary Science Letters, 274(3-4), 423-438. doi: 10.1016/j.epsl.2008.07.054

5.10 Supplementary Material

Figure S5.1 Sample holder and setup for sequential XRF scans of dry, homogenised samples

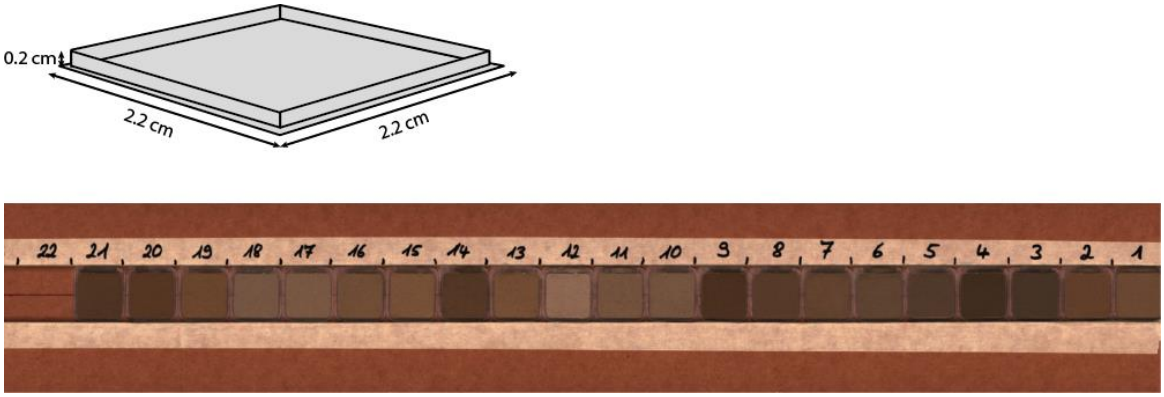

Figure S5.2 XRF measurements of Si before and after tube aging correction for Cr- and Mo-tubes, respectively. Correction is <5 % of the total counts

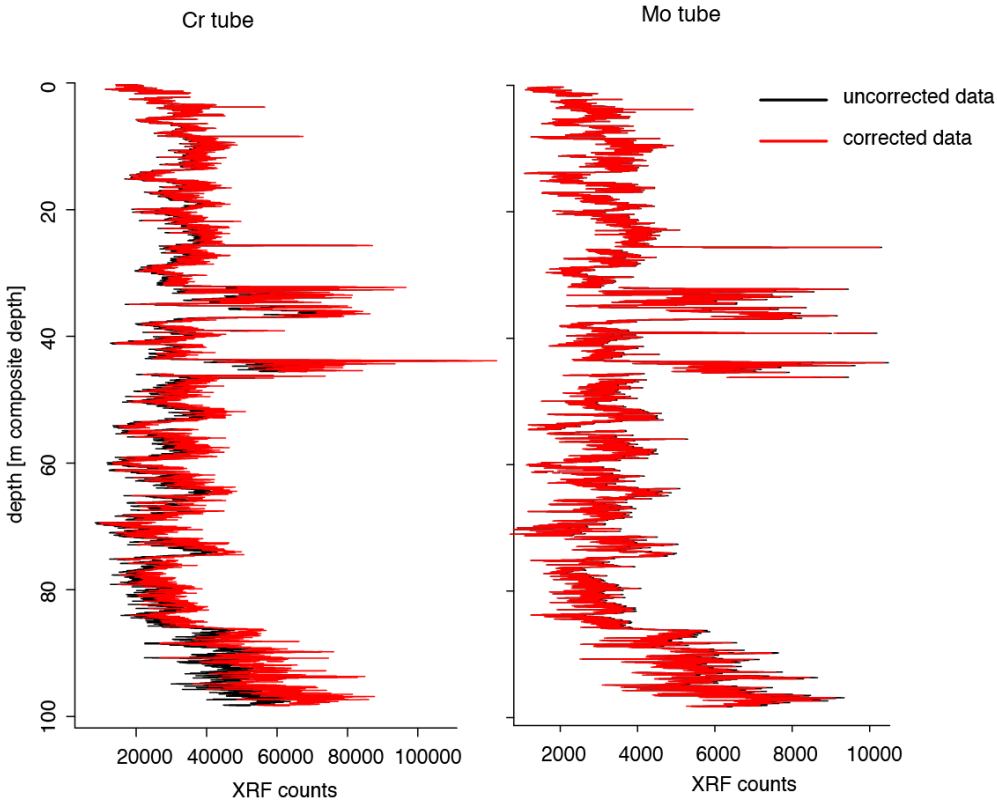

Figure S5.3 a) Crossplots and b) explained variance of principal components, calculated on the standardised XRF data set. c) Element loadings for PC axes 1-4. Table shows correlation coefficient r between the first eight principal components (explaining 91 % of the data set variance) and the six end-members. Highest correlation in red

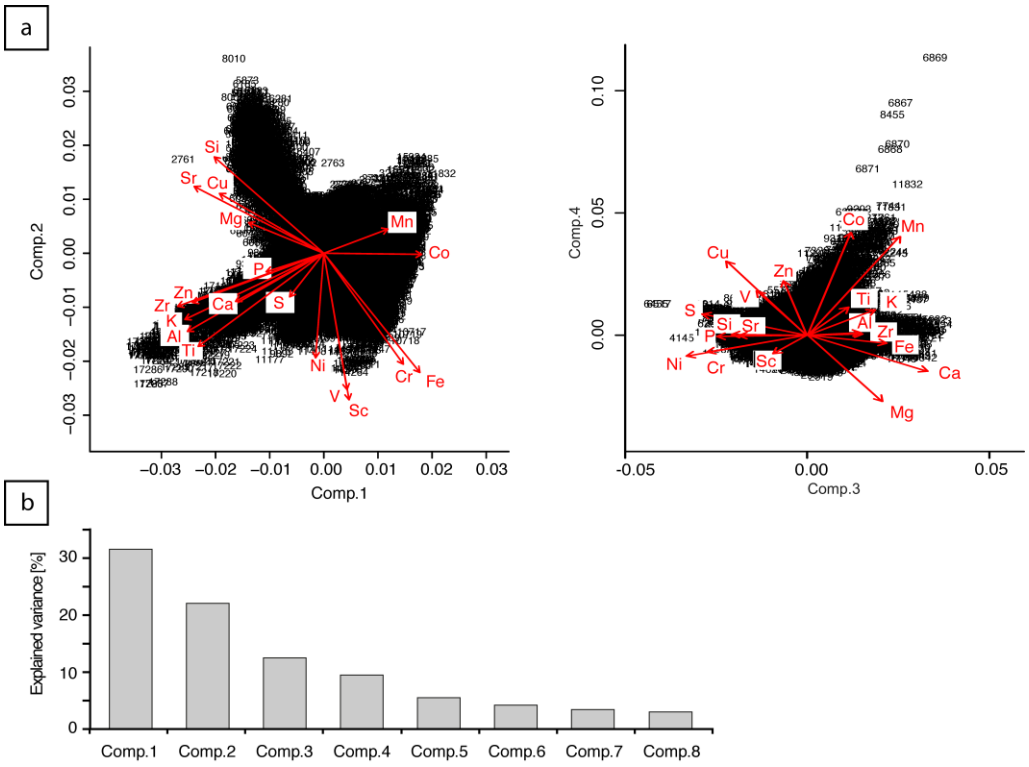

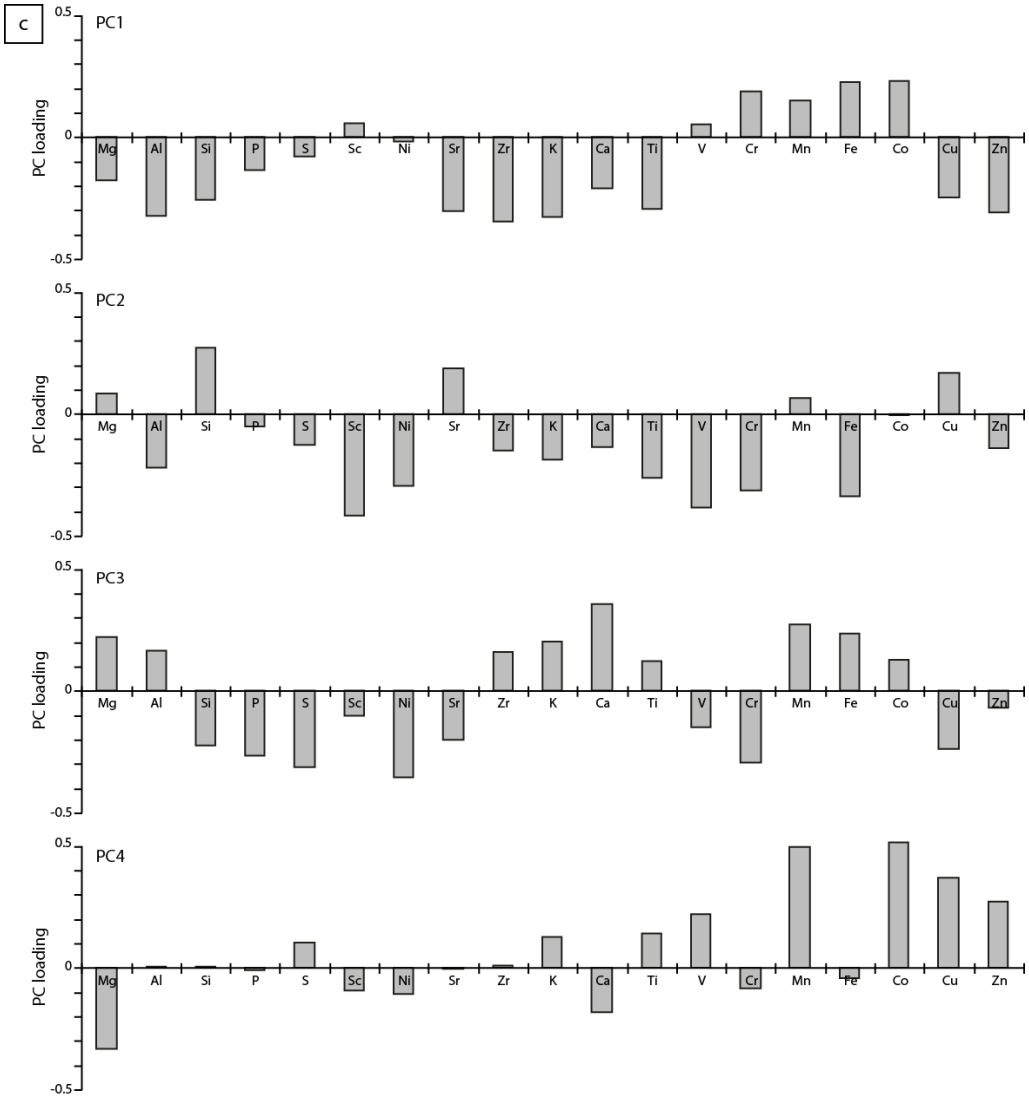

r	EM1	EM2	EM3	EM4	EM5	EM6
	Laterite	Oxides	Diatoms	Iron	Siderite	Tectonics
PC1	-0.78	0.77	-0.38	0.89	0.44	-0.34
PC2	-0.25	-0.17	0.48	0.19	0.14	0.16
PC3	0.32	-0.41	-0.32	0.13	0.27	0.50
PC4	0.23	-0.32	0.18	-0.35	0.46	-0.43
PC5	-0.35	0.07	0.08	0.08	0.21	0.39
PC6	-0.02	0.05	0.02	0.02	-0.03^{+}	0.15
PC7	0.21	-0.2	-0.12	0.03	-0.02	-0.27
PC8	0.11^{+}	-0.02	-0.06	0.08	-0.10	0.20

$^{+}$ significant at $p<0.05$, all others significant at $p<0.01$
Spearman's Rank Correlation, n=17322

Figure S5.4 Correlation between XRF-based end-members (averaged over the 4-cm sampling area) and mineralogy based on FTIRS analysis on 179 discrete homogenised samples. Table shows correlation coefficient r between the six end-members and mineralogy

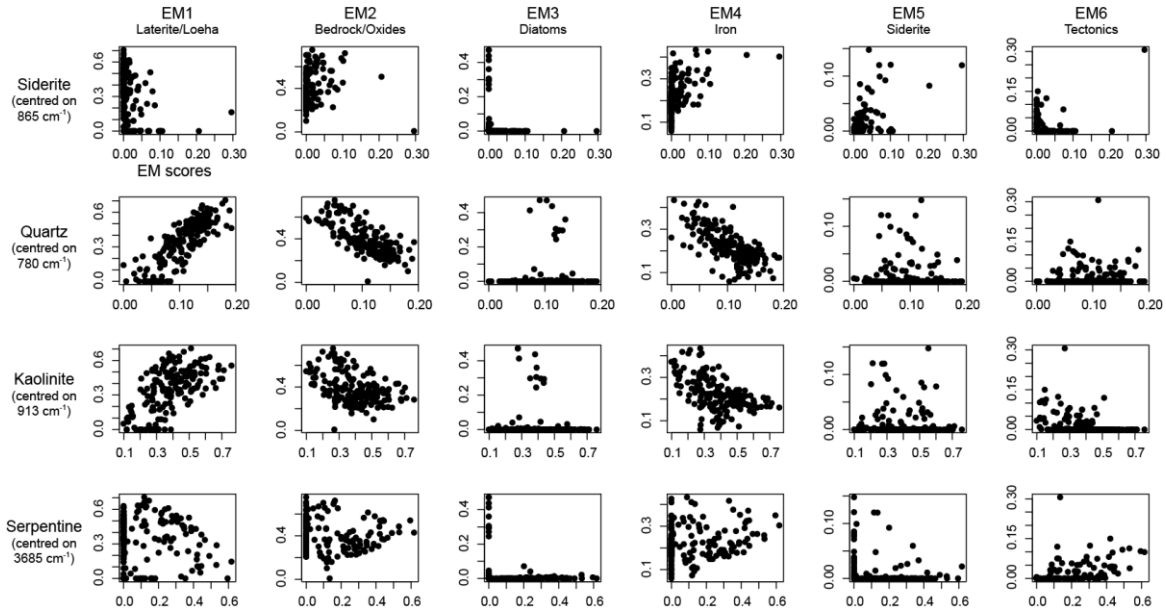

r	EM1	EM2	EM3	EM4	EM5	EM6
	Laterite	Oxides	Diatoms	Iron	Siderite	Tectonics
Siderite	-0.52*	0.46*	-0.35*	0.57*	0.65*	-0.16^{+}
Quartz	0.83*	-0.74*	0.02	-0.71*	-0.25*	-0.12
Kaolinite	0.59*	-0.40*	-0.11	-0.51*	-0.02	-0.49*
Serpentine	-0.07	0.05	0.08	0.24*	-0.15^{+}	0.68*

* significant at p<0.01; $^{+}$ significant at p<0.05
Spearman's Rank Correlation, n=179

Figure S5.5 Comparison between Fe and Ni XRF core scans for 60-90 m composite depth. Coloured lines are 200 point running means (averaging over ~1 m of core), grey lines are 0.5-cm spaced XRF measurements

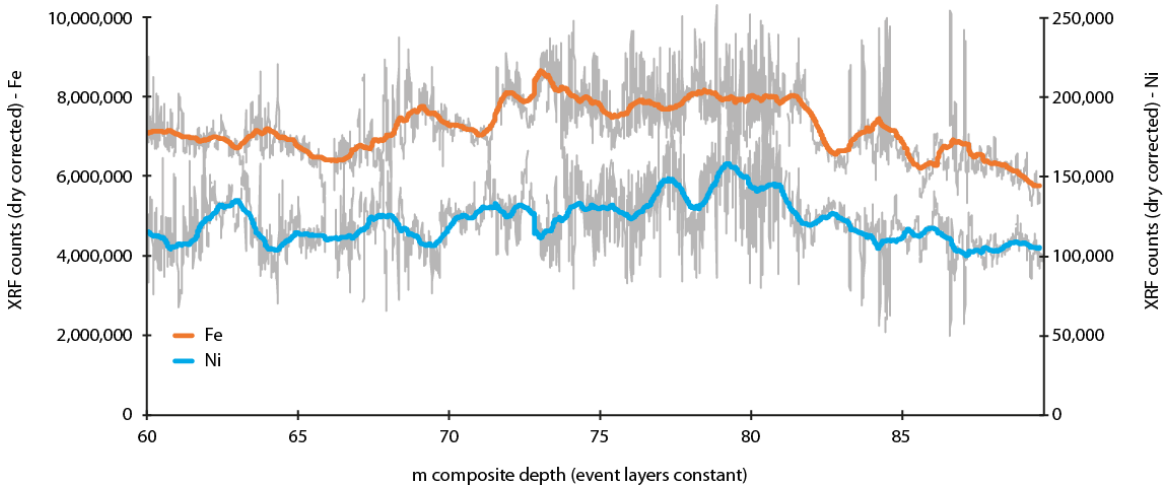

Chapter 6

Conclusions and Outlook

6. Conclusions and outlook

6.1 Conclusions

This thesis provides a detailed description of source-to-sink processes in modern Lake Towuti and its catchment, characterises depositional modes and their variability through the Pleistocene sediment record, and provides novel insight into the distribution and formation types of authigenic minerals forming in the sediments. The results show that the detailed study of long-lived lake systems, in combination with new methodological approaches and interdisciplinary cooperation, can add new perspectives to various fields of geoscientific research. The Pleistocene record of Lake Towuti is particularly valuable, because long, continuous, terrestrial archives, which record palaeoenvironmental and palaeoclimatic changes, are rare in the Southeast Asian tropics.

In Chapter 2, a source-to-sink approach is adopted to characterise processes in the modern catchment of Lake Towuti. Complementary studies on the surface sediments of Lake Towuti characterise lake-internal processes and iron transport and cycling in the modern system (Appendix Chapters I.2 and I.3). Few studies have previously looked at transport and erosion of soils and sediments in the Southeast Asian humid tropics. The detailed study of the modern catchment and associated processes provides an important contribution to defining the baseline status and variability of ecosystems and landscapes in Central Sulawesi in the recent past and on glacial-interglacial time scales. Geotechnical analyses from Lake Towuti's catchment show that the lower laterite horizons have lowest stability and can function as slide planes to mobilise the entire soil package during mass movement events. The overall composition of modern sediments across the lake is strongly influenced by tectonic disturbance of river courses, which enhances bedrock abrasion and promotes slope instabilities in some of the river catchments. The study identifies the two large and most tectonically influenced rivers Mahalona and Loeha as the dominant sediment sources to coring location TDP-Site 1. Differences in sediment composition and loading of these rivers influence the Al/Mg ratio in the deep basin, which in turn can be related to climate-induced lake level fluctuations. This is the main driver of sedimentation changes during the last 60,000 years, highlighting the potential for a long climate record at Lake Towuti. In proxy-based research, it is fundamental to ensure a thorough understanding of the modern system before inferring changes that occurred in the past. This is particularly applicable to palaeolimnology, because each lake is a unique system with its individual hydrology, geochemistry, climate and mixing regime. In extensive projects such as those in the framework of the ICDP (but not limited to these), studies of the modern setting have already proven their scientific value (Nolan & Brigham-Grette, 2006; Stockhecke et al., 2012; Vogel et al., 2010) and will hopefully be part of any larger lake coring project in the future. It is therefore strongly recommended to include the characterisation of the modern system into the science plan for large (lake) coring projects.

In Chapter 3, the stratigraphic sequence of the entire sedimentary basin infill of Lake Towuti is depicted and analysed to reconstruct long-term basin evolution, particularly with respect to changes in catchment dynamics and depositional environments. Early basin subsidence was characterised by repeated cycles of silting and peat formation, with standing water bodies in close proximity to rivers and swamps. The establishment of a permanent lake likely corresponds to the initial colonisation by

riverine species, which are the common ancestor of many lacustrine species found in the Malili Lakes today. The connection of the Mahalona and Lampenisu River System to Lake Towuti at 30 m (~150,000-180,000 years) is the largest change in hydrology seen in the lacustrine record and may correspond to a second colonisation event of the lake. Like in many ancient lakes, the exceptional flora and fauna of Lake Towuti raises questions about endemism, rates of diversification, and adaptive radiation of species over geologic times. Together with a reliable age-depth model, at least for stratigraphic Unit 1, the reconstruction of lake connectivity and changes in depositional environments through time can add important information to the interpretation of biologic evolution in the lake.

In Chapter 4, the application of µCT imaging in a new, sedimentological context allowed the identification and visualisation of siderite formation modes, contributing to the overall project aim of studying the response of microbial activity, biogeochemical processes, and their products at depth in the sediment to environmental variations over long time scales. Our analyses showed that syn- and postsedimentary siderite formation modes co-occur at small spatial scales. This observation offers an additional explanation for the high spatial variability of siderite geochemistry and isotope composition observed in banded iron formations. Modern systems on Earth, which resemble conditions elsewhere in time or space, can provide important insights into these otherwise inaccessible systems. Through hypothesis testing in the analogous system, parameters such as formation conditions can be constrained. In case of Lake Towuti, this provides a better understanding of mineral assemblages identified on Mars (Appendix I.3) and the role of early diagenesis in ferruginous early oceans (Chapter 4). In addition, our analyses show that µCT analysis is a powerful tool to study unprocessed sediments and variations in high-density minerals therein. Recent advances in CT resolution and computational power now available at reasonable cost make this a valuable tool for future studies of unconsolidated sediments.

In Chapter 5, the combination of high-resolution XRF core scanning with end-member modelling has proven highly successful in describing the lithological variations throughout the lacustrine sequence. With increasing size of geoscientific data sets and growing availability of high-resolution techniques such as XRF core scanning, it is important to develop techniques, which make the best use of these large data sets. End-member modelling is applicable to a wide range of depositional environments and can help to generate an objective, quantitative, and consistent characterisation of processes that determine composition in long sediment successions. At the same time it is fundamental to maintain high data quality, e.g. through validation of the scanning data by comparison to/correction by more precise XRF measurements of dried, homogenised samples or ICP measurements (Appendix II). With this procedure, systematic biases in the original XRF data set such as water content and matrix effects can be reduced or eliminated. For Lake Towuti, end-member modelling is shown to adequately separate tectonic, climatic, and post-sedimentary processes in the XRF data set and thus provides a useful tool to isolate specific processes from a complex record. The resulting record offers many applications for a detailed study of the sediments. Climate-induced lake level fluctuations, which change lake water oxygenation and fluvial transport in the catchment, are identified as the main drivers influencing sedimentation throughout the 100-m-long lacustrine record. Once a reliable age-depth model is established for the cores, the data set will be valuable in aswering some of the main target questions of the TDP investigations. Specifically, forcings and feedbacks of orbital-scale climatic changes in

Central Sulawesi can be identified and studied in detail. The high resolution of the data set will also facilitate more detailed insights, e.g. into the system response to large volcanic eruptions, specifically related to trophic state and aquatic productivity, or the local and regional climate response to millennial-scale events triggered in the North Atlantic.

The results of this thesis and generally of the Towuti Drilling Project highlight the merits of scientific collaboration across continents and disciplines. As recently pointed out by a review of scientific drilling projects in ancient lakes, interdisciplinary approaches are of increasing importance to advancing research in the individual fields (Wilke et al., 2016). If scientific efforts are combined to overcome logistical, planning, and communication challenges, this thesis shows that the detailed study of one lake system can contribute to advancing our understanding in various fields of research.

6.2 Outlook

6.2.1 Climate variability in the Indo-Pacific Warm Pool

Climate dynamics in the tropics are tightly coupled to the volume and extent of northern hemisphere glaciations and their direct impact on atmospheric circulation (Mohtadi et al., 2011; Turney et al., 2004) as well as to changes in regional and seasonal insolation strength modulated by changes in Earth's orbital parameters (Clement et al., 2004; Verschuren et al., 2009). A long climate record from East-African Lake Malawi further suggests an influence of atmospheric CO_2 concentrations and wind-blown dust on tropical climate dynamics over glacial-interglacial time scales (Johnson et al., 2016). These forcings exert varying control on deep atmospheric convection and land-sea temperature contrasts with subsequent changes in ENSO (Liu et al., 2014; Turney et al., 2004) and the monsoon systems (Konecky et al., 2016; Mohtadi et al., 2011; Wang et al., 2008). For Southeast Asia, the influence of the last northern hemisphere glaciation on the East-Asian monsoon and its southern hemisphere counterpart, the Australian-Indonesian monsoon, has been widely described in recent years (Eroglu et al., 2016; Wang et al., 2008). The climate of the last glacial maximum (LGM) is characterised by drier conditions in most parts of tropical and subtropical Asia (De Deckker et al., 2002; Partin et al., 2007; Reeves et al., 2013; Russell et al., 2014). Yet, very few records exist from equatorial Southeast Asia, despite the regions importance in heat transfer and its substantial supply of atmospheric moisture to the global climate (Chiang, 2009; Pierrehumbert, 1999). Recently, particular focus has also been on disentangling large-scale orbital forcings from millennial-scale changes, which seem to be much more locally constrained (Griffiths et al., 2009). However, climate reconstructions in tropical continental archives are often discontinuous (Wang et al., 2008) and mostly do not cover time scales long enough to reliably evaluate the varying influence of orbital, ice sheet, and greenhouse gas forcing during the Quaternary period. Thus, time series spanning several glacial-interglacial cycles from sites sensitive to hydroclimatic change in equatorial Southeast Asia are required.

At the low-latitude location of Lake Towuti (2°S), the twice-annual passage of the ITCZ controls annual rainfall patterns. Sediment core studies from Lake Towuti, covering the last 60,000 years (60 kilo years; kyr), showed that the sediments are sensitive to climate variability (Costa et al., 2015; Goudge et al., 2017; Morlock et al., 2018; Russell et al., 2014; Vogel et al., 2015). These studies suggest that on orbital time scales, rainfall

patterns in Central Sulawesi are influenced by northern hemisphere glacial extent and precessional forcing on insolation (Goudge et al., 2017; Morlock et al., 2018; Russell et al., 2014). The promise to extend this record to the period covered by the long TDP cores could not met in time for completion of this thesis work, because analyses to establish a reliable age-depth model are still in progress. Preliminary age estimates are only available through ^{14}C dating in the upper 10 m, suggesting relatively constant sedimentation rates in that part of the record. This relationship, together with preliminary interpretation of palaeomagnetic intensity variations in the upper 30 m of the record, suggests an age of ~180 kyr at 30 mcd. During this period, mineralogy and geochemistry do not indicate large changes in provenance und depositional environments relative to the 60-kyr record (Chapter 3). It can therefore generally be assumed that the climate indicators identified in the upper 10 m are applicable to this period. This provides the basis for an initial outlook on climate-controlled variations in Lake Towuti sediments. Figure 6.1 shows the two main end-members of the XRF data set (Chapter 5), representing laterite erosion/Loeha River input (EM1) and the deposition of metal oxides (EM2), plotted against the preliminary age-depth relationship for the upper 30 m of the record. High EM1 scores were shown to correspond to lake-level high stands and a wet climate, while high EM2 scores characterise periods of lake-level low stands and a dry climate.

Across the 180-kyr record, the two end-members show antiphased, quasi-cyclic variations (Figure 6.1A), with amplitudes and frequencies comparable to the 60-kyr record. Based on the shorter record, it has been suggested that climate in Central Sulawesi exhibits a strong non-linear response to glacial climate forcing, with wet conditions in the Holocene and marine isotope stage (MIS) 3, and a dry MIS2 (Russell et al., 2014). Comparison of the extended 180-kyr Towuti record to globally stacked benthic foraminifera $\delta^{18}O$ as an indicator for global ice volume (Figure 6.1B) confirms the observation that there is no linear response of Central Sulawesi hydroclimate to global ice volume. Rather, the two end-members show pronounced higher-frequency variability. At the current stage of the age model, it is difficult to discern the exact frequency of this quasi-cyclic variability in the Towuti record. It seems that cyclicity may have varied across the record. This suggests that climate sensitivity in the Indo-Pacific Warm Pool changed under different orbital configurations, ice sheet volume and extent, and atmospheric greenhouse gas concentrations. In the last 70 kyr, variability in the record could correspond to changes in obliquity (~40 kyr cyclicity; Figure 6.1A and E), while thereafter frequency variability broadly corresponds to a precessional forcing (~23 kyr cyclicity; Figure 6.1A and D). This may indicate that climate in Central Sulawesi was sensitive to local insolation or interhemispheric gradients (Figure 6.1C), forced by precession, at times where precession shows high amplitude variations and ice sheet extent and volume is reduced, e.g. around 100 kyr BP, whereas at times of low variability in precession, e.g. in the last 70 kyr BP, an obliquity signal may influence local climate. A precessional influence on the response of tropical hydroclimate to obliquity forcing has been suggested by climate modelling for the African summer monsoon (Tuenter et al., 2003). The influence of precession and obliquity on low latitude climate is discussed in the following paragraphs. It has to be noted, however, that uncertainty of these patterns in the Lake Towuti record is high, because of (substantial) uncertainties of the current age model and the short observation period relative to cyclicity.

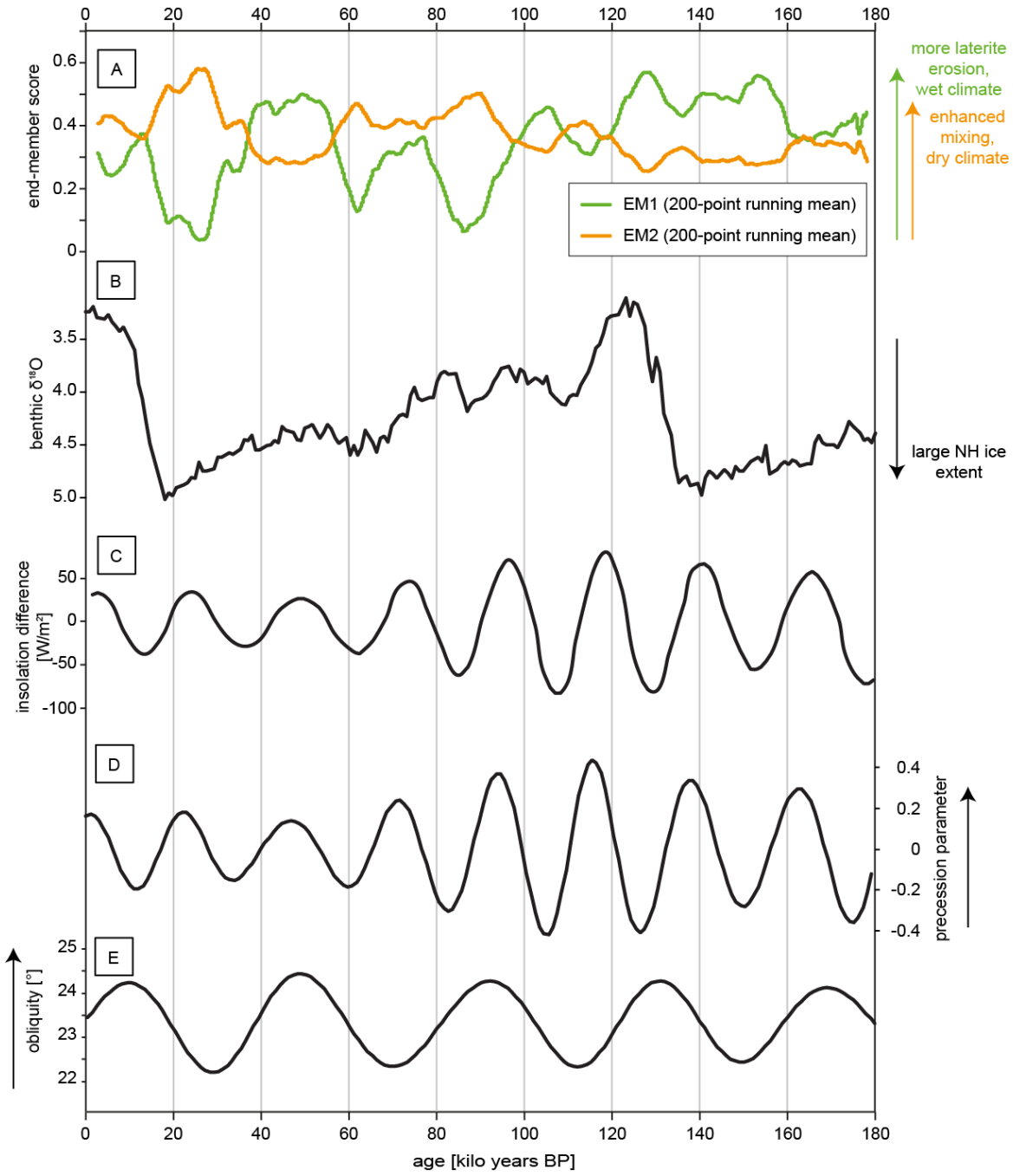

Figure 6.1 (A) Scores for XRF end-members 1 (laterite/Loeha) and 2 (metal oxides) plotted against a preliminary age-depth model for the lacustrine sequence of Lake Towuti. (B) LR04 stack of $\delta^{18}O$ measurements from benthic foraminifera as a proxy for global ice volume. Data from Lisiecki and Raymo (2005). (C) Difference between 30°N June insolation and 30°S December insolation as a measure for interhemispheric gradients and the amplitude of seasonal ITCZ shifts. (D) Precession parameter after Laskar et al. (2004) using its standard definition. (E) Obliquity forcing after Laskar et al. (2004)

A precessional signal in the Towuti record would be in line with observations and modelling results from northern and southern tropical regions, suggesting that precession is an important driver in climate variability at low latitudes (Clement et al.,

2004; Holbourn et al., 2005; Kutzbach et al., 2007; Tachikawa et al., 2011; Wyrwoll et al., 2007). Precessional forcing strongly alters seasonal insolation, which controls the position of the ITCZ and monsoon strength. Hence, this insolation variability is closely linked to the difference between 30°N June insolation and 30°S December insolation (Figure 6.1C), which is a measure for interhemispheric gradients and the amplitude of seasonal ITCZ shifts. Climate response to precession is zonally asymmetric, because of the differential thermodynamic response over land and oceans. This changes circulation patterns, which has a strong influence on convection, monsoon circulation and consequently hydroclimate in the tropics (Clement et al., 2004). At times when precessional variability dominates the Towuti record, sediment composition suggests that climate in the Indo-Pacific Warm Pool was wet when northern hemisphere summer insolation was high, e.g. at around 11 kyr BP.

At times when the Towuti record shows variability on time scales comparable to an obliquity forcing, the record suggests that climate in the Indo-Pacific Warm Pool was wet during phases of high obliquity. Climate variability paced by obliquity-driven insolation changes has been suggested for both the eastern and western tropical Pacific during the Early Pleistocene (de Garidel-Thoron et al., 2005; Lawrence et al., 2006; Medina-Elizalde & Lea, 2005), but an influence on tropical climate during the Late Pleistocene is less widely described. Yet, Clemens and Prell (2003) suggest that precessional and obliquity forcing can trigger a comparable or even dominant response in low latitude climate, which is also seen in a speleothem record from southern China (Clemens et al., 2010). Similar to precession, high obliquity forcing increases northern hemisphere summer insolation and hence is expected to increase monsoon strength. Clemens and Prell (2003) suggest that in addition, internal climate feedbacks amplify the obliquity signal, resulting in obliquity forcing accounting for a greater amount of variance in Southeast Asian records. They propose that high seasonal insolation variability in the southern hemisphere under high obliquity increases latent heat export from the subtropical Indian ocean. This further amplifies monsoon strength at low latitudes. In contrast, under high precessional forcing these two hemispheric mechanisms are out of phase, i.e. high northern hemisphere summer insolation coincides with low southern hemisphere summer insolation and latent heat export from the southern hemisphere is maximal during northern hemisphere winter. Once an age model is established for the entire lacustrine sequence from Lake Towuti, a more reliable evaluation of the timing, cyclicity and underlying mechanisms of hydroclimate variability in Central Sulawesi can be provided.

Previous studies on Lake Towuti sediments (Goudge et al., 2017) and several studies from the tropics (Clement et al., 2004; Partin et al., 2007; Turney et al., 2004; Verschuren et al., 2009) have also described a half-precessional signal (~11 kyr cyclicity), suggesting that low-latitude climate is sensitive to rainfall intensity linked to the twice-annual passage of the Intertropical Convergence Zone (ITCZ). With the current age model, it is difficult to investigate such high-frequency signals (Figure 6.2). The high-resolution XRF record from Lake Towuti in combination with a reliable age model will, however, allow to further explore the influence of higher frequency forcings. The continuous lacustrine sediment record from Lake Towuti can thus contribute to a more detailed understanding of climate in the Indo-Pacific Warm Pool, which is crucial for accurate modelling of future climates.

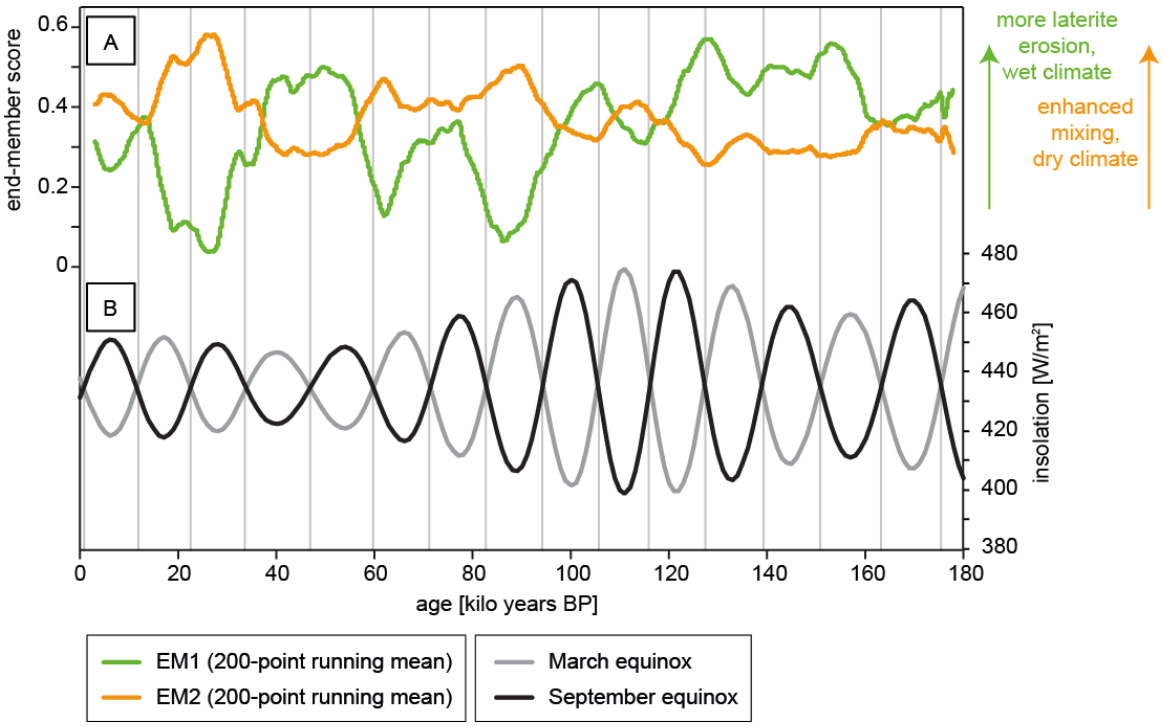

Figure 6.2 (A) Time series of EM1 residuals after linear detrending. (B) Daily insolation at the location of Lake Towuti (2°S) for March and September equinox, respectively

6.2.2 Other open questions

In the last three years since coring Lake Towuti, large data sets from sedimentology, geochemistry, and geomicrobiology have been acquired. Out of the many specific questions that are currently under study, I would like to highlight two topics, which have not yet been fully addressed and understood.

Firstly, the unique occurrence of the two diatomaceous oozes at around 35 and 40 m composite depth is still puzzling. As mentioned earlier, no algal blooms are present (or preserved) at any other depth in the core and only few benthic species have been found in littoral environments in the lake today. This raises the question of factors triggering high primary productivity in the lake, which today is classified as ultraoligotrophic. External modifications to the system, e.g. through phosphorus input by ash fall (as proposed in chapter 3) could explain the diatom occurrences. Nutrient recycling, resource allocation and utilisation, and adaptation of species may also play an important role. Exploring these avenues in more detail, e.g. by studying the lake system response to the 18 tephra deposition events using high-resolution XRF scans and thin sections, can provide insights into ecosystem resilience, potential tipping points and species adaptation to disturbance. This also requires putting further constraints on the tectonic, climatic, and hydrologic boundary conditions during the occurrence of the diatom oozes. Again, this requires close interdisciplinary collaboration of sedimentologists, geochemists, and biologists.

Secondly, many analyses have addressed biogeochemical cycles in this ferruginous system, particularly focussing on iron, phosphorous and sulphur. These data sets include iron isotopes, pore water chemistry, sedimentary DNA, and the characterisation of organic matter. The synthesis of these investigations together with the detailed description of authigenic minerals and the high-resolution XRF data set

presented in this thesis can result in a detailed, process-based understanding of element cycling in ferruginous systems. Element mobilisation and redeposition after burial, the identification of different formation mechanisms and the role of microbes in these processes can contribute to current research in natural systems on Earth and Mars.

6.2.3 Beyond Lake Towuti

High-resolution geoscientific data sets are now available at relatively low cost, e.g. through XRF core scanning or µCT imaging. The results of this thesis provide examples of how to take advantage of such large data sets. End-member modelling may be applied to informative high-resolution data sets from sedimentary records, particularly in complex systems where multiple processes influence sedimentation. Micro-CT imaging can help to identify fragile sedimentary structures in unprocessed sediments, e.g. prior to geomicrobiological analyses under sterile conditions. In both cases, handling large data sets while maintaining high quality is challenging, but crucial to ensure a sound analysis.

6.3 References

Chiang JCH. (2009). The Tropics in Paleoclimate. Annual Review of Earth and Planetary Sciences, 37(1), 263-297. doi: 10.1146/annurev.earth.031208.100217

Clemens SC, Prell WL. (2003). A 350,000 year summer-monsoon multi-proxy stack from the Owen Ridge, Northern Arabian Sea. Marine Geology, 201(1-3), 35-51. doi: 10.1016/s0025-3227(03)00207-x

Clemens SC, Prell WL, Sun Y. (2010). Orbital-scale timing and mechanisms driving Late Pleistocene Indo-Asian summer monsoons: Reinterpreting cave speleothemδ18O. Paleoceanography, 25(4), n/a-n/a. doi: 10.1029/2010pa001926

Clement AC, Hall A, Broccoli AJ. (2004). The importance of precessional signals in the tropical climate. Climate Dynamics, 22(4), 327-341. doi: 10.1007/s00382-003-0375-8

Costa KM, Russell JM, Vogel H, Bijaksana S. (2015). Hydrological connectivity and mixing of Lake Towuti, Indonesia in response to paleoclimatic changes over the last 60,000years. Palaeogeography, Palaeoclimatology, Palaeoecology, 417, 467-475. doi: 10.1016/j.palaeo.2014.10.009

De Deckker P, Tapper NJ, van der Kaars S. (2002). The status of the Indo-Pacific Warm Pool and adjacent land at the Last Glacial Maximum. Global and Planetary Change, 35, 25-35.

de Garidel-Thoron T, Rosenthal Y, Bassinot F, Beaufort L. (2005). Stable sea surface temperatures in the western Pacific warm pool over the past 1.75 million years. Nature, 433, 294-298.

Eroglu D, McRobie FH, Ozken I, Stemler T, Wyrwoll KH, Breitenbach SF, Marwan N, Kurths J. (2016). See-saw relationship of the Holocene East Asian-Australian summer monsoon. Nat Commun, 7, 12929. doi: 10.1038/ncomms12929

Goudge TA, Russell JM, Mustard JF, Head JW, Bijaksana S. (2017). A 40,000 year record of clay mineralogy at Lake Towuti, Indonesia: Paleoclimate reconstruction from reflectance spectroscopy and perspectives on paleolakes on Mars. Geological Society of America Bulletin.

Griffiths ML, Drysdale RN, Gagan MK, Zhao JX, Ayliffe LK, Hellstrom JC, Hantoro WS, Frisia S, Feng Y-X, Cartwright I, Pierre ES, Fischer MJ, Suwargadi BW. (2009). Increasing Australian-Indonesian monsoon rainfall linked to early Holocene sea-level rise. Nature Geoscience, 2, 636-639. doi: 10.1038/ngeo605

Holbourn A, Kuhnt W, Kawamura H, Jian Z, Grootes P, Erlenkeuser H, Xu J. (2005). Orbitally paced paleoproductivity variations in the Timor Sea and Indonesian Throughflow variability during the last 460 kyr. Paleoceanography, 20(3), n/a-n/a. doi: 10.1029/2004pa001094

Johnson TC, Werne JP, Brown ET, Abbott A, Berke M, Steinman BA, Halbur J, Contreras S, Grosshuesch S, Deino A, Scholz CA, Lyons RP, Schouten S, Damste JS. (2016). A progressively wetter climate in southern East Africa over the past 1.3 million years. Nature, 537(7619), 220-224. doi: 10.1038/nature19065

Konecky B, Russell J, Bijaksana S. (2016). Glacial aridity in central Indonesia coeval with intensified monsoon circulation. Earth and Planetary Science Letters, 437, 15-24. doi: 10.1016/j.epsl.2015.12.037

Kutzbach JE, Liu X, Liu Z, Chen G. (2007). Simulation of the evolutionary response of global summer monsoons to orbital forcing over the past 280,000 years. Climate Dynamics, 30(6), 567-579. doi: 10.1007/s00382-007-0308-z

Laskar J, Robutel P, Joutel F, Gastineau M, Correia ACM, Levrard B. (2004). A long-term numerical solution for the insolation quantities of the Earth. Astronomy & Astrophysics, 428(1), 261-285. doi: 10.1051/0004-6361:20041335

Lawrence KT, Liu Z, Herbert TD. (2006). Evolution of the eastern tropical Pacific through Plio-Pleistocene glaciation. Science, 312(5770), 79-83. doi: 10.1126/science.1120395

Lisiecki LE, Raymo ME. (2005). A Pliocene-Pleistocene stack of 57 globally distributed benthic δ18O records. Paleoceanography, 20(1), n/a-n/a. doi: 10.1029/2004pa001071

Liu Z, Lu Z, Wen X, Otto-Bliesner BL, Timmermann A, Cobb KM. (2014). Evolution and forcing mechanisms of El Nino over the past 21,000 years. Nature, 515(7528), 550-553. doi: 10.1038/nature13963

Medina-Elizalde M, Lea DW. (2005). The Mid-Pleistocene Transition in the Tropical Pacific. Science, 310, 1009-1012. doi: 10.1126/science.1115933

Mohtadi M, Oppo DW, Steinke S, Stuut J-BW, De Pol-Holz R, Hebbeln D, Lückge A. (2011). Glacial to Holocene swings of the Australian-Indonesian monsoon. Nature Geoscience, 4. doi: 10.1038/ngeo1209

Morlock MA, Vogel H, Nigg V, Ordoñez L, Hasberg AK, Melles M, Russell JM, Bijaksana S. (2018). Climatic and tectonic controls on source-to-sink processes in the tropical, ultramafic catchment of Lake Towuti, Indonesia. Journal of Paleolimnology. doi: 10.1007/s10933-018-0059-3

Nolan M, Brigham-Grette J. (2006). Basic hydrology, limnology, and meteorology of modern Lake El'gygytgyn, Siberia. Journal of Paleolimnology, 37(1), 17-35. doi: 10.1007/s10933-006-9020-y

Partin JW, Cobb KM, Adkins JF, Clark B, Fernandez DP. (2007). Millennial-scale trends in west Pacific warm pool hydrology since the Last Glacial Maximum. Nature, 449(7161), 452-455. doi: 10.1038/nature06164

Pierrehumbert RT. (1999). Subtropical Water Vapor As a Mediator of Rapid Global Climate Change. In: Clark PU, Webb RS, Keigwin LD (Eds.) Mechanisms of Global Climate Change at Millennial Time Scales (Vol. 112, pp. 339-361). Washington DC: American Geophysical Union.

Reeves JM, Bostock HC, Ayliffe LK, Barrows TT, De Deckker P, Devriendt LS, Dunbar GB, Drysdale RN, Fitzsimmons KE, Gagan MK, Griffiths ML, Haberle SG, Jansen JD, Krause C, Lewis S, McGregor HV, Mooney SD, Moss P, Nanson GC, Purcell A, van der Kaars S. (2013). Palaeoenvironmental change in tropical Australasia over the last 30,000 years – a synthesis by the OZ-INTIMATE group. Quaternary Science Reviews, 74, 97-114. doi: 10.1016/j.quascirev.2012.11.027

Russell JM, Vogel H, Konecky B, Bijaksana S, Huang Y, Melles M, Wattrus N, Costa KM, King JW. (2014). Glacial forcing of central Indonesian hydroclimate since 60,000 y BP. PNAS, 111(14), 5100-5105. doi: 10.1073/pnas.1402373111

Stockhecke M, Anselmetti FS, Meydan AF, Odermatt D, Sturm M. (2012). The annual particle cycle in Lake Van (Turkey). Palaeogeography, Palaeoclimatology, Palaeoecology, 333-334, 148-159. doi: 10.1016/j.palaeo.2012.03.022

Tachikawa K, Cartapanis O, Vidal L, Beaufort L, Barlyaeva T, Bard E. (2011). The precession phase of hydrological variability in the Western Pacific Warm Pool during the past 400 ka. Quaternary Science Reviews, 30(25-26), 3716-3727. doi: 10.1016/j.quascirev.2011.09.016

Tuenter E, Weber SL, Hilgen FJ, Lourens LJ. (2003). The response of the African summer monsoon to remote and local forcing due to precession and obliquity. Global and Planetary Change, 36(4), 219-235. doi: 10.1016/s0921-8181(02)00196-0

Turney CSM, Kershaw AP, Clemens SC, Branch N, Moss PT, Fifield LK. (2004). Millennial and orbital variations of El Nino/Southern Oscillation and high-latitude climate in the last glacial period. Nature, 428, 306-310.

Verschuren D, Sinninghe Damste JS, Moernaut J, Kristen I, Blaauw M, Fagot M, Haug GH, members Cp. (2009). Half-precessional dynamics of monsoon rainfall near the East African Equator. Nature, 462(7273), 637-641. doi: 10.1038/nature08520

Vogel H, Russell JM, Cahyarini SY, Bijaksana S, Wattrus N, Rethemeyer J, Melles M. (2015). Depositional modes and lake-level variability at Lake Towuti, Indonesia, during the past ~29 kyr BP. Journal of Paleolimnology, 54(4), 359-377. doi: 10.1007/s10933-015-9857-z

Vogel H, Wessels M, Albrecht C, Stich HB, Wagner B. (2010). Spatial variability of recent sedimentation in Lake Ohrid (Albania/Macedonia). Biogeosciences, 7(10), 3333-3342. doi: 10.5194/bg-7-3333-2010

Wang Y, Cheng H, Edwards RL, Kong X, Shao X, Chen S, Wu J, Jiang X, Wang X, An Z. (2008). Millennial- and orbital-scale changes in the East Asian monsoon over the past 224,000 years. Nature, 451(7182), 1090-1093. doi: 10.1038/nature06692

Wilke T, Wagner B, Van Bocxlaer B, Albrecht C, Ariztegui D, Delicado D, Francke A, Harzhauser M, Hauffe T, Holtvoeth J, Just J, Leng MJ, Levkov Z, Penkman K, Sadori L, Skinner A, Stelbrink B, Vogel H, Wesselingh F, Wonik T. (2016). Scientific drilling projects in ancient lakes: Integrating geological and biological histories. Global and Planetary Change, 143, 118-151. doi: 10.1016/j.gloplacha.2016.05.005

Wyrwoll K-H, Liu Z, Chen G, Kutzbach JE, Liu X. (2007). Sensitivity of the Australian summer monsoon to tilt and precession forcing. Quaternary Science Reviews, 26(25-28), 3043-3057. doi: 10.1016/j.quascirev.2007.06.026

Appendix I

Co-authored Papers and Manuscripts

During the four years as a PhD student I contributed to two other publications and one submitted manuscript. These are included here in Appendix I, accompanying the main thesis.

The first publication summarises the drilling operations, highlights first results of initial core logging, visual sediment and smear slide descriptions, and presents a preliminary lithostratigraphy for the three TDP coring sites. In 2015, I participated in the drilling operations on Lake Towuti, working in the field laboratory (MSCL core scanning, smear slide descriptions, core sorting and storage) and on the drilling barge. I also took part in the two core splitting and sampling parties at LacCore, the National Lacustrine Core Facility at the University of Minnesota, USA, in autumn 2015 and winter 2016, where I was mostly responsible for core imaging, colour reflectance spectrophotometer measurements and subsampling.

The second publication focuses on a set of 84 surface sediment samples from Lake Towuti to study lake-internal processes based on physical, chemical, mineralogical and biological constituents in the sediments. I contributed to this by joining the sampling campaign, prior to the deep drilling in 2015, and providing geochemical data of the surface sediment samples as well as relevant catchment parameters. I was actively involved in discussions about modern processes in Lake Towuti and contributed to improving of the manuscript.

The third manuscript uses a subset of 42 surface sediment samples from the lake to characterise iron and iron-bearing minerals in the lake. The manuscript draws the comparison to environments on Mars, highlighting yet another area of research where the study of Lake Towuti sediments can contribute to an advanced process understanding. Similar to the second publication, I contributed to this by joining the fieldwork, providing material and supplementary geochemical and mineralogical data of surface sediments, bedrock and soils and through discussions and comments on the manuscript text.

The Towuti Drilling Project: paleoenvironments, biological evolution, and geomicrobiology of a tropical Pacific lake

James M. Russell, Satria Bijaksana, Hendrik Vogel, Martin Melles, Jens Kallmeyer, Daniel Ariztegui, Sean Crowe, Silvia Fajar, Abdul Hafidz, Doug Haffner, Ascelina Hasberg, Sarah Ivory, Christopher Kelly, John King, Kartika Kirana, **Marina Morlock**, Anders Noren, Ryan O'Grady, Luis Ordonez, Janelle Stevenson, Thomas von Rintelen, Aurele Vuillemin, Ian Watkinson, Nigel Wattrus, Satrio Wicaksono, Thomas Wonik, Kohen Bauer, Alan Deino, André Friese, Cynthia Henny, Imran, Ristiyanti Marwoto, La Ode Ngkoimani, Sulung Nomosatryo, La Ode Safiuddin, Rachel Simister, and Gerald Tamuntuan

published in Scientific Drilling 2016

Modern sedimentation processes in Lake Towuti, Indonesia, revealed by the composition of surface sediments

Ascelina K. M. Hasberg, Satria Bijaksana, Peter Held, Janna Just, Martin Melles, **Marina A. Morlock**, Stephan Opitz, James M. Russell, Hendrik Vogel, and Volker Wennrich

published in Sedimentology 2018

Characterization of Iron in Lake Towuti Sediment

Rachel Y. Sheppard, Ralph E. Milliken, James M. Russell, M. Darby Dyar, Elizabeth C. Sklute, Hendrik Vogel, Martin Melles, Satria Bijaksana, **Marina A. Morlock**, and Ascelina K. M. Hasberg

under review in Chemical Geology

I.1. The Towuti Drilling Project: paleoenvironments, biological evolution, and geomicrobiology of a tropical Pacific lake

published in Scientific Drilling 21, 29-40, 2016, doi:10.5194/sd-21-29-2016

James M. Russell[1], Satria Bijaksana[2], Hendrik Vogel[3], Martin Melles[4], Jens Kallmeyer[5], Daniel Ariztegui[6], Sean Crowe[7], Silvia Fajar[2], Abdul Hafidz[2], Doug Haffner[8], Ascelina Hasberg[4], Sarah Ivory[1], Christopher Kelly[1], John King[9], Kartika Kirana[2], **Marina Morlock[3]**, Anders Noren[10], Ryan O'Grady[10], Luis Ordonez[6], Janelle Stevenson[11], Thomas von Rintelen[12], Aurele Vuillemin[5], Ian Watkinson[13], Nigel Wattrus[14], Satrio Wicaksono[1], Thomas Wonik[15], Kohen Bauer[7], Alan Deino[16], André Friese[5], Cynthia Henny[17], Imran[18], Ristiyanti Marwoto[17], La Ode Ngkoimani[19], Sulung Nomosatryo[5], La Ode Safiuddin[19], Rachel Simister[7], and Gerald Tamuntuan[20]

[1]Department of Earth, Environmental, and Planetary Sciences, Brown University, 324 Brook St., Providence, RI, 02912, USA, [2]Faculty of Mining and Petroleum Engineering, Institut Teknologi Bandung, Jalan Ganesa 10, Bandung, 50132, Indonesia, [3]Institute of Geological Science & Oeschger Center for Climate Change Research, University of Bern, Baltzerstrasse 1+3, 3012 Bern, Switzerland , [4]Institute for Geology and Mineralogy, University of Cologne, Zülpicher Str. 49a/b, 50674 Cologne, Germany, [5]Helmholtz Centre Potsdam, GFZ German Research Center for Geosciences, Telegrafenberg, Building C, 14473 Potsdam, Germany, [6]Department of Earth Sciences, University of Geneva, rue des Maraichers 13, 1205 Geneva, Switzerland, [7]Department of Microbiology and Immunology, University of British Columbia, Vancouver, BC, Canada, [8]Great Lakes Institute for Environmental Research, University of Windsor, Windsor, Ontario, N9B 3P4, Canada, [9]Graduate School of Oceanography, University of Rhode Island, Narragansett, RI, 02882, USA, [10]LacCore, Dept. of Earth Science, University of Minnesota, Minneapolis, MN, 55455, USA, [11]School of Culture, History and Language, Australia National University, Acton, ACT 2601, Australia, [12]Museum für Naturkunde, Leibniz Institute for Evolution and Biodiversity Science, Invalidenstr. 43, 10115 Berlin, Germany, [13]Dept. of Earth Sciences, Royal Holloway University of London, Egham, Surrey TW20 0EX, UK, [14]Large Lakes Observatory, University of Minnesota Duluth, Duluth, MN, 55812, USA, [15]Liebniz Institute for Applied Geophysics, Stilleweg 2, 30655 Hanover, Germany, [16]Berkeley Geochronology Center, Berkeley, CA, 94709, USA, [17]Research Center for Limnology, Indonesian Insitute of Sciences (LIPI), Jl. Raya Bogor m 46, Cibinong, West Java, Indonesia, [18]Geological Department, Universitas Hasanuddin, Kampus UNHAS Tamalanrea, Makassar, 90245, Indonesia, [19]Faculty of Earth Sciences and Technology, Haluoleo University, Kampus Baru Unhalu Anduoonoho, Kendari, 93232, Indonesia, [20]Department of Physics, Faculty of Mathematics and Natural Sciences, Sam Ratulangi University, Jl. Kampus Unsrat, Manado, 95114, Indonesia

Correspondence to: James M. Russell (james_russell@brown.edu)

I.1.1 Abstract

The Towuti Drilling Project (TDP) is an international research program, whose goal is to understand long-term environmental and climatic change in the tropical western Pacific, the impacts of geological and environmental changes on the biological evolution of aquatic taxa, and the geomicrobiology and biogeochemistry of metal-rich, ultramafic-hosted lake sediments through the scientific drilling of Lake Towuti, southern

Sulawesi, Indonesia. Lake Towuti is a large tectonic lake at the downstream end of the Malili lake system, a chain of five highly biodiverse lakes that are among the oldest lakes in Southeast Asia. In 2015 we carried out a scientific drilling program on Lake Towuti using the International Continental Scientific Drilling Program (ICDP) Deep Lakes Drilling System (DLDS). We recovered a total of ~1018 m of core from 11 drilling sites with water depths ranging from 156 to 200 m. Recovery averaged 91.7 %, and the maximum drilling depth was 175 m below the lake floor, penetrating the entire sedimentary infill of the basin. Initial data from core and borehole logging indicate that these cores record the evolution of a highly dynamic tectonic and limnological system, with clear indications of orbital-scale climate variability during the mid-to late Pleistocene.

I.1.2 Introduction

The Towuti Drilling Project (TDP) is an international research program, whose objective is to understand long-term environmental and climatic change in the tropical western Pacific, the impacts of geological and environmental changes on the biological evolution of aquatic taxa, and the geomicrobiology and biogeochemistry of metal-rich, ultramafic-hosted lake sediment. To accomplish this goal, the TDP recovered over 1000 m of sediment core from the floor of Lake Towuti, the largest tectonic lake in Southeast Asia. Analysis of these cores is just beginning, but will provide a new long, high-resolution record of tropical western Pacific paleohydrology during the Pleistocene, information on the age and history of the lake and the limnological conditions that gave rise to Towuti's endemic fauna and flora, and new insight into the microbial processes operating at depth in Towuti's sediments and their effects on sediment mineralogy and biogeochemistry.

Lake Towuti is a large tectonic lake at the downstream end of the Malili lake system (Figure I.1.1), a set of five ancient, tectonic lakes that have formed over the past ~1.5 million years on the island of Sulawesi, Indonesia (Haffner et al., 2001; Lehmusluoto et al., 1995; Russell and Bijaksana, 2014). These are the oldest lakes in Indonesia and are thought to contain the longest continuous terrestrial records of climate in the Indo-Pacific Warm Pool (IPWP), a vast pool of warm surface waters in the western tropical Pacific. The IPWP exerts enormous influence on global climate through its interactions with the El Niño-Southern Oscillation (ENSO), the Australasian monsoons, and the Intertropical Convergence Zone (ITCZ; Chiang, 2009; Clement et al., 2001; Seager and Battisti, 2007) and through its influence on the concentration of atmospheric water vapor - the Earth's most important greenhouse gas (Pierrehumbert, 1999, 2000). Our ability to make accurate predictions about future climate, and in particular future precipitation, thus rests on our understanding of the tropical Pacific climate under different climate boundary conditions than today. Global climate models exhibit significant inter-model differences in their simulations of recent and future precipitation change over the IPWP (Kumar et al., 2013; Meehl et al., 2007), as do simulations of IPWP precipitation under glacial boundary conditions (DiNezio et al., 2011; DiNezio and Tierney, 2013), motivating scientific drilling at Lake Towuti.

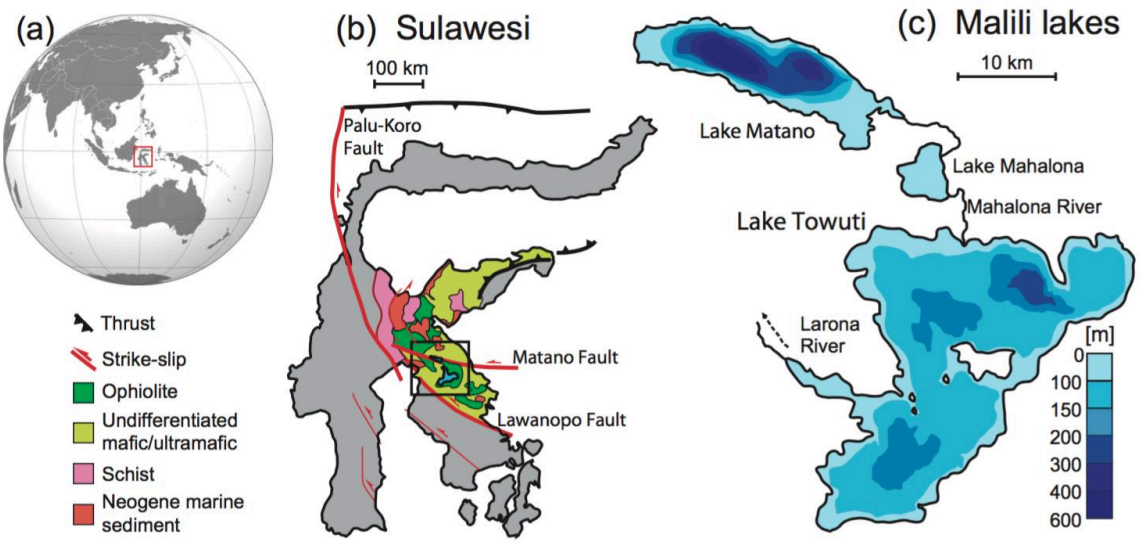

Figure I.1.1 Overview map of the study area showing (a) the location of Sulawesi in the Indo-Pacific region, (b) the regional geology of Sulawesi (modified after Kadarusman et al., 2004), and (c) the configuration of the Malili lake system

In recent years the global lakes drilling program under the auspices of the International Continental Scientific Drilling Program (ICDP) has made substantial contributions to understanding Pliocene-Pleistocene climate variability, including multiple paleoclimate records from the northern and southern tropics. These records, together with many long speleothem data sets, have highlighted the importance of 21 000-year cycles in subtropical rainfall, indicating strong forcing of the strength of the monsoons by orbital precession (e.g., Fritz et al., 2007; Hodell et al., 2007; Scholz et al., 2007; Wang et al., 2008). Despite these advances, we lack long records of terrestrial paleoclimate from equatorial regions and particularly the Indo-Pacific. Previous sedimentary records from Lake Towuti span the last ~60 kyr BP, and contain an intriguing record of past climate that differs markedly from that of the subtropics (Russell et al., 2014). In particular, we observed grassland expansion, lowered lake levels, and strong drying during the last glacial maximum (LGM) relative to both marine isotope stage 3 (~30-60 kyr BP) and the Holocene (Costa et al., 2015; Konecky et al., 2016; Russell et al., 2014; Vogel et al., 2015). The strong glacial-interglacial signal at Lake Towuti challenges the hypothesis that tropical hydroclimate is predominantly controlled by precessional orbital forcing, with little influence of glacial-interglacial changes in climate boundary conditions (Carolin et al., 2013; Meckler et al., 2012). A critical goal of TDP is, therefore, to obtain a continuous sedimentary record to document orbital-scale patterns of climate change spanning as many glacial-interglacial cycles as possible to test and differentiate the forcings that govern Indo-Pacific rainfall variations.

Lake Towuti is not simply a repository of information on past climate. The lake is situated within the East Sulawesi Ophiolite (Figure I.1.1; Kadarusman et al., 2004; Monnier et al., 1995), the third largest ophiolite in the world, which releases iron, chromium, and other metals that catalyze biogeochemical activity by a unique and diverse microbial community in the lake and its sediments (Crowe et al., 2008). Lake Towuti's sediments are extremely Fe rich and thus stand out as an end-member microbial habitat. The prevalence of Fe-rich sedimentary rock units in the Precambrian suggests that ferruginous conditions were a prominent feature of the deep ocean

throughout the Earth's history (Poulton and Canfield, 2011), and with mounting evidence for Fe-rich Martian soils and lake sediments dominated by ultramafic weathering products (e.g., Ehlmann et al., 2008), the study of an active biosphere in environments such as Towuti is timely and critical. Moreover, Towuti's pelagic microbial ecology, biogeochemistry, and sediment mineralogy are tightly linked to climate variations through varying lake mixing regimes, soil erosion, and weathering (Costa et al., 2015; Tamuntuan et al., 2015). These processes are directly or indirectly responsible for the production and deposition of many paleoclimate proxies, and postdepositional alteration of those proxies is often linked to the activity of sedimentary microorganisms. In light of these issues, a critical component of the TDP is to investigate the microbial community at depth and its effects on iron mineralogy, carbon, and metal cycling using a variety of state-of-the-art geochemical, molecular genetic, and isotopic tools.

Towuti is surrounded by one of the most diverse tropical rainforests on Earth, and harbors endemic species flocks of fish, snails, shrimp, crabs, and other organisms. Identifying the role of past environmental change in governing the evolution and biogeographical range of these organisms will be crucial for identifying conservation priorities and strategies to cope with anthropogenic climate change and land use. In terms of its flora, Sulawesi lies within one of the world's most biologically complex and diverse regions and is home to fundamentally important faunal and floristic boundaries such as the famed Wallace Line (which separates fauna of Australian and Asian origin). The regional phytogeography is controlled by these diverse geological origins and by subsequent modification by climate variations, particularly the glacial-interglacial cycles, which have influenced the connectivity between adjacent islands as well as drought tolerance and resilience of the regional flora (Cannon et al., 2009; van Welzen et al., 2011). Understanding the past dynamics of these forest communities therefore is critical for our understanding of their response to future change. Faunally, the Malili lakes offer by far the most outstanding example of lacustrine biological evolution in Southeast Asia, with parallel adaptive radiations of gastropods (Rintelen et al., 2004), crabs (Schubart et al., 2008), shrimps (Rintelen et al., 2010), and fishes (Herder et al., 2006). Genetic and morphological data indicate multiple colonizations of the lakes in several of these groups; a high level of endemism within each lake, suggesting allopatric speciation despite the presence of riverine connections among the lakes; and intralacustrine diversification through shifting trophic structure suggesting ecological speciation (Rintelen et al., 2012). These faunal data thus have strong links to the climatic, limnological, and geological evolution of Lake Towuti. Drilling in Lake Towuti will document the environmental and climatic context that shaped the evolution of these unique lacustrine and terrestrial ecosystems, and their resilience to long-term environmental change.

These outstanding characteristics motivated the TDP, under the auspices of the ICDP. Through continuous coring of the entire sedimentary sequence of Lake Towuti, the project aims to

1. reconstruct long-term hydrologic change in central Indonesia in order to understand the processes controlling long-term climate change in the tropical western Pacific;
2. discover the micro-organisms living in Towuti's metal-rich sediments, and determine their impacts on the lake's sediments and biogeochemistry;
3. evaluate the history and stability of Sulawesi's lush rainforests, and the impacts of past climate change on these ecosystems;

4. document the age of Lake Towuti, its long-term limnological history, and the environmental background shaping the diversification of Towuti's endemic flora and fauna.

I.1.3 Study Site

Lake Towuti is located near the Equator (2.75 S, 121.5 E; Figure I.1.1 and Figure I.1.2) at 318 m above sea level in central Sulawesi, Indonesia. The island of Sulawesi has a complex tectonic history. At the large scale, a complex zone of deformation extends across central Sulawesi and absorbs the collision of Australia with Asia (Sundaland). Three major sinistral strike-slip fault systems accommodate this motion: the Palu-Koro, Matano, and Lawanopo faults. Lake Towuti and neighboring lakes occupy small transtensional basins along the Matano Fault. Northeast of Sulawesi, the Molucca Sea subduction zone accommodates convergence between the Philippine Sea Plate and Sundaland, giving rise to extensive volcanic fields in northern Sulawesi (Hamilton, 1988).

Sulawesi is composed of four elongate "arms", which broadly correspond to lithotectonic units (Hamilton, 1979). The southeast arm, which houses Lake Towuti, is dominated by the highly tectonized East Sulawesi Ophiolite, which is inter-thrust with Mesozoic and Cenozoic sediments. These rocks are comprised of ultramafic mantle peridotites (lherzolites and harzburgites), cumulate gabbros, and basalts of normal mid-ocean ridge composition (Kadarusman et al., 2004; Monnier et al., 1995). The ophiolites have sourced large lateritic nickel deposits that have attracted the mining industry since the beginning of the 1970s, with active operations and extensive infrastructure in the region currently operated by PT Vale Indonesia (a subsidiary of Vale SA).

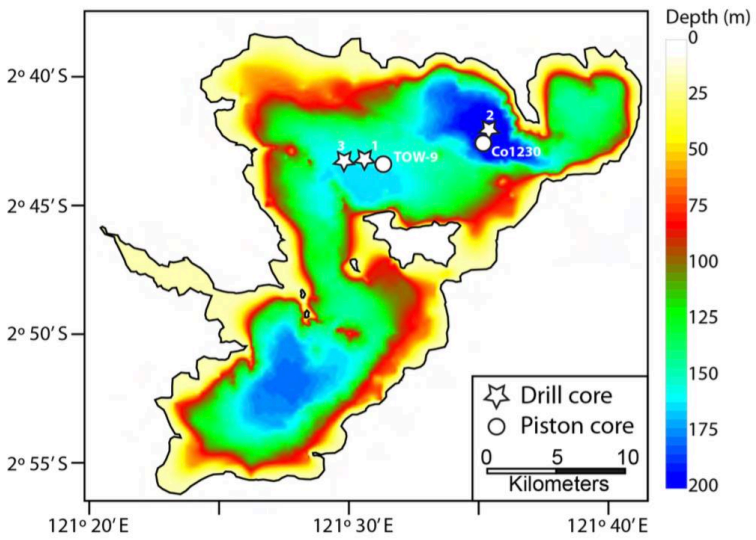

Figure I.1.2 A bathymetric map of Lake Towuti showing the location of core sites discussed in the text

The three largest of the Malili lakes, Matano, Mahalona, and Towuti, are connected with surface outflow from Matano to Mahalona to Towuti via the Mahalona River, the largest river inflow to the lake (Figure I.1.2). Lake Towuti is the largest of the Malili lakes, with a surface area of 560 km^2 and a maximum water depth of 200 m (Haffner et al., 2001; Lehmusluoto et al., 1995). A chain of islands divides the lake into two basins: a larger northern basin that contains the deepest part of the lake, and a

smaller southern basin. Lake Towuti is presently hydrologically open with outflow to the southwest through the Larona River, which flows to the Bay of Bone.

Lake Towuti experiences a tropical humid climate. The region receives ~2700 mm yr^{-1} of precipitation, with a wet season from December-May, during which strong north-easterly flow, warm sea surface temperatures (SSTs), and local convective activity (Hendon, 2003) maintain precipitation at >250 mm $month^{-1}$. Precipitation falls below 150 mm month 1 from August-October, when southeasterly flow and cool SSTs suppress regional convection. This circulation and precipitation seasonality is characteristic of much of southern Sumatra, southern Borneo (Kalimantan), Java, and the Moluccas (Hendon, 2003), suggesting our record should represent climate change across a broad swath of central and southern Indonesia (Aldrian and Susanto, 2003; Konecky et al., 2016).

Towuti's surface water temperatures vary between ~29 and 31°C. The lake water column is thermally stratified, with seasonal mixing to a depth of ~100 m (Costa et al., 2015). Lake Towuti is relatively dilute (210 µS cm^{-1}) and circumneutral (pH ~7.8) with a chemistry dominated by Mg and HCO_3 (Haffner et al., 2001; Lehmusluoto et al., 1995). The lake is among the least productive tropical lakes on Earth (ultraoligotrophic), likely due to low nutrient delivery from intensely weather soils and sedimentary PO_4^{3-} trapping by very high Fe concentrations. The surface waters are well-oxygenated, but hypoxic to anoxic conditions exist below ~120 m depth allowing for the development of ferruginous conditions with very low concentrations of dissolved sulfur.

I.1.4 Core site selection

Site selection for the TDP was guided by three surveys carried out between 2007 and 2013 that collected over 1000 km of seismic reflection data and piston cores that document the nature of the upper 10–20 m of Towuti's sediment column. Seismic data include "CHIRP" data acquired with an Edgetech™ 216s Towfish with a topside 3200XS collection system, and both single channel and multichannel data collected using a Bolt™ 5 in^3 airgun and a 150 m long Geometrics™ GeoEel solid digital streamer with 24 channels.

The seismic data revealed two major sedimentary units in Lake Towuti (Figure I.1.3; Russell and Bijaksana, 2012). Unit 1 consists of a well-stratified sequence that extends from the lake floor down to ~100 m sub-bottom, and is characterized by parallel acoustic reflectors that can be traced across most of the basin. These reflectors do not exhibit obvious geometric relationships such as angular contacts that would indicate large lake-level changes, suggesting stable, continuous, fine-grained sediment deposition in Towuti's deep basins. Some of the thickest Unit 1 accumulations are found in the deepest basin of Lake Towuti, located near the northern shore of the lake. This basin receives distal deltaic sediments derived from the Mahalona River, which drains the upstream lakes Matano and Mahalona.

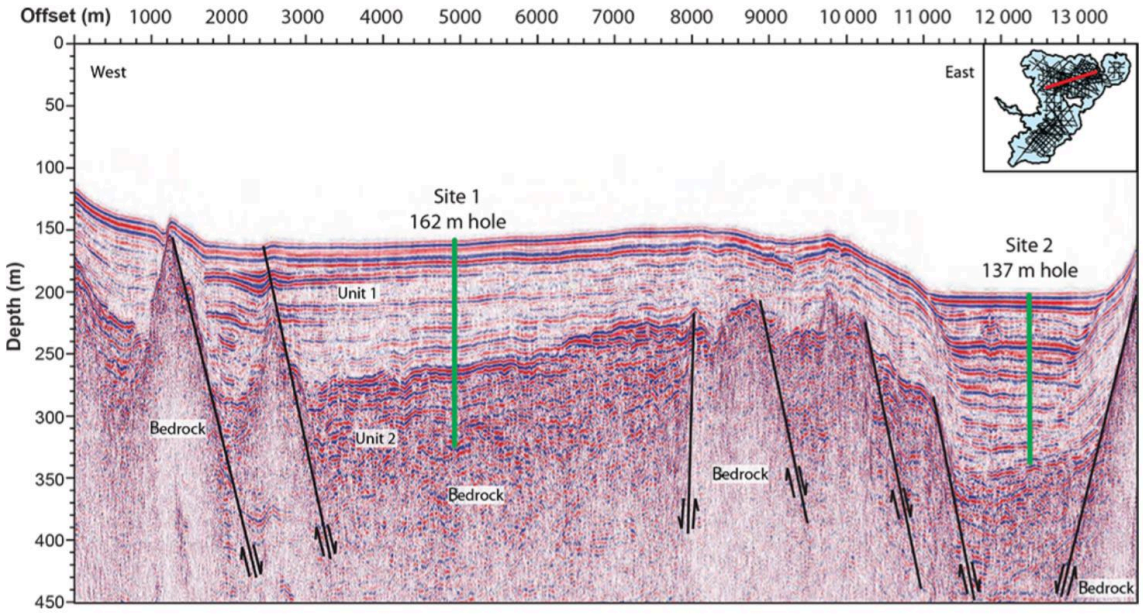

Figure I.1.3 Seismic reflection profile oriented WSW–ENE over Lake Towuti's northern basin (see inset for line position) crossing TDP Sites 1 and 2. Thick green lines show the borehole depths for TDP-TOW15-1B and TDP-TOW15-2A. Seismic Units 1, 2, and bedrock are labeled, and major faults are indicated by thin black lines.

Our piston coring survey sampled only the uppermost sediments of Unit 1, but confirmed the observations from our seismic reflection data. A core collected at site TOW-9 (Figure I.1.2) documented continuous, fine-grained sedimentation in the central part of Towuti's northern basin, with sedimentation rates of ~5.5 kyr m^{-1} during the past ~60 kyr BP (Russell et al., 2014). We found very frequent distal deltaic turbidites in the deepest part of the lake (Site Co1230, Figure I.1.2), particularly during lake-level low stands that remobilize delta topset beds and force deltaic progradation (Vogel et al., 2015). Elsewhere, the piston cores generally consisted of fine-grained clays interbedded with more or less frequent turbidites. Turbidites increased in frequency and thickness with proximity to the Mahalona River delta, but were also common near shorelines or in the deepest parts of sub-basins within the lake, perhaps originating from seismically induced failure of poorly consolidated sediments in this tectonically active basin.

Unit 1 is underlain by Unit 2, a more poorly stratified unit that varies between a few tens to ~150 m in thickness. Unit 2 is characterized by a range of sediment types, from continuous, sub-parallel reflectors to short, discontinuous reflectors. Prior to drilling, Unit 2 was interpreted to reflect alternating fluvial and lacustrine sedimentation that occurred during the initial stages of formation of Lake Towuti. Drilling Unit 2 could provide insight into Lake Towuti's age, processes of basin formation, and the early lake stages, which is information critical to understanding the biological evolution of Towuti's endemic fauna.

Based upon these data, we selected three primary drilling sites, between 156 and 200 m water depth, and with drilling targets between ~130 and ~175 m sub-bottom. Our primary goals in selecting drilling sites were to recover

1. high-quality continuous sections with as few turbidites as possible through Unit 1 for paleoclimate, paleolimnological, and geomicrobiological studies;

2. a distal record of the Mahalona River system to monitor changes in deltaic sedimentation forced by lake-level changes and possible changes in the river system itself signaling changes in the hydrological connectivity of lakes Towuti, Mahalona, and Matano;
3. as long a section as possible through Unit 2, preferably at sites containing more lacustrine than fluvial sedimentation (fine-grained deposits).

Site 1 is TDP's primary drilling target, located in the central part of Towuti's northern basin in ~156 m water depth (Figure I.1.4a). This "master site" is located close to our piston coring site TOW-9, which has yielded high-quality paleoclimatic and paleolimnologic reconstructions. The site is located upslope of slightly deeper areas of the lake on the northern edge of Loeha Island, and south of a large WNW– ESE trending intrabasin fault that limits sediment inputs from the Mahalona River, and thus contains few turbidites. Site 1 is well-suited to address most of our key studies in paleoclimate, paleolimnology, paleoecology, and geomicrobiology. Seismic data over Site 1 show that Unit 1 is approximately 100 m thick, and piston cores suggest the site is undisturbed by turbidites or other event deposits. Seismic data also imaged approximately at least 75 m of sediment in Unit 2, including two intervals marked by roughly parallel acoustic reflectors centered at ~115 and ~160 m depth, indicating relatively well-stratified sediments. Our primary goals at Site 1 were to obtain overlapping triplicated cores through the upper ~100 m, to obtain 100 % recovery of Unit 1, and to recover as complete a section as possible of Unit 2 including cores to bedrock if possible.

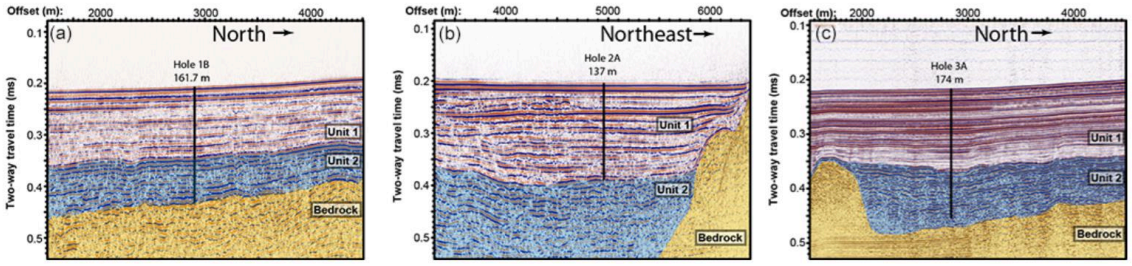

Figure I.1.4 Expanded seismic reflection sections over the TDP core Sites 1 (a), 2 (b), and 3 (c), with seismic Units 1 and 2, and bedrock labeled. Black lines show the positions and depths of TDP-TOW15-1B, TDP-TOW15-2A, and TDP-TOW15-3A

Site 2 is located in the deepest part of Lake Towuti at 200 m water depth (Figure I.1.4b). Piston core Co1230 indicates that this site receives distal deltaic sediments derived from the Mahalona River, and seismic reflection data indicated a major change in the acoustic character of the sediments at ~65 m depth that could reflect the beginning of distal deltaic sedimentation from the Mahalona River. The principle objectives of drilling this location were therefore to provide a record of lake-level changes and/or major changes in the hydrological connection between lakes Towuti, Mahalona, and Matano through study of these distal deltaic deposits. Changes in the amount and style of clastic sedimentation, together with sediment provenance studies, at Site 2 may provide relatively direct insight into the history of hydrological connectivity between the Malili lakes, with important implications for the biological, hydrological, and geological evolution of Lake Towuti. Seismic reflection data suggested ~130 m of well-stratified lacustrine sediment at this site, so our goal was to recover duplicate overlapping cores to the Unit 1-Unit 2 boundary.

Site 3 was originally proposed for Towuti's southern basin to provide a sedimentary sequence unaffected by sedimentological changes associated with the evolution of the Mahalona River, in order to test the reproducibility of our reconstructions of terrestrial weathering and sediment supply obtained from Site 1. The long transit times to Towuti's southern basin, combined with equipment failures, forced us to relocate Site 3. An alternate site was selected to the west of Site 1 in 159 m water depth (Figure I.1.4c). Seismic data suggested that this site could have the most continuous lacustrine sedimentation through the time period represented by Unit 2, as the site is located in a small structural sag that may have allowed for continuous lacustrine conditions while other sites in the basin were dry. Our goal at this site was to obtain overlapping duplicated cores as deeply as possible.

I.1.5 Drilling, logging, and on-site geomicrobiological operations

Drilling in a remote part of central Indonesia was a difficult logistical undertaking. Major logistical activities began in September 2014, when we shipped 14 containers of drilling equipment and supplies from the United States of America to the town of Sorowako, Sulawesi Selatan, Indonesia; initiated research permit applications and paperwork; began on-site construction of a dock and crane pad from which we could launch the drilling barge; and developed agreements with PT Vale Indonesia for local logistical support including the use of cranes, housing, and assistance with environmental, health, and safety planning. We shipped the GFZ "Buglab" to Sorowako to support on-site sample processing for geomicrobiological investigations, as well as borehole logging equipment from the Leibniz Institute for Applied Geophysics (LIAG), Hanover, Germany. Logistical preparations were completed in May 2015, when the drilling team arrived and set up on-site analytical facilities and the drilling barge on Lake Towuti's shore.

Drilling commenced at Site 1 on 23 May 2015 using the ICDP Deep Lakes Drilling System (DLDS) operated by DOSECC Exploration Services. Boreholes were drilled using PQ (122.6 mm hole, 66 mm core) diameter drill string, which uses the hydraulic piston corer (HPC) for soft sediment and the "Alien" rotating corer to recover more resistant lithologies; attempts to recover more resistant lithologies with the Extended Nose Corer (EXN) resulted in poor core recovery and quality. All cores were recovered into standard butyrate liners. Geophysical downhole logging data, including natural gamma radiation, magnetic susceptibility (MS), electrical resistivity, temperature, acoustic velocity, vertical seismic profiles, and borehole diameter and dip, were measured at varying depth resolutions in a subset of holes.

A multisensor core logger (MSCL; Geotek Ltd.) was used to collect magnetic susceptibility (MS) and *p* wave velocity data on whole cores in an on-site laboratory immediately after drilling, though the *p* wave velocity data were of low-quality due to gas expansion in most cores. At Hole 1A, also known as the "bughole", a fluid contamination tracer was used to aid geomicrobiological sampling. Samples were collected from cores from Hole 1A immediately upon recovery on the drilling barge to measure trace and redox-sensitive gas concentrations (such as methane), and over 450 samples were subsequently processed in the BugLab for analyses of pore-water chemistry, cell counting and microbial finger-printing, experiments on microbial turnover and processes, and organic geochemistry.

Upon conclusion of drilling operations, cores were shipped via air freight to LacCore, the National Lacustrine Core Facility at the University of Minnesota, USA, for full processing, description, scanning, and subsampling. There, physical properties for whole cores were analyzed via MSCL-S to obtain *p* wave velocity, gamma density, loop MS, electrical resistivity, and natural gamma radiation data at intervals of 2-4 cm. After splitting, cores were logged using an MSCL-XYZ to obtain high-resolution MS and color reflectance spectrophotometry at 0.5 cm resolution. Split cores were cleaned and scanned with a GeotekTM Geotek Single Track Core Imaging System (MSCL-CIS) digital linescan imager. Visual core description and smear slide analyses were carried out to classify the sediment into major compositional units, and subsamples were extracted at intervals coordinated to obtain stratigraphically equivalent samples for sedimentological, geochemical, and paleoecological parameters. All cores received identical treatment except cores from Hole 1C, which were left in Indonesia to aid in educational and outreach activities, and cores from Hole 1A, many of which were completely sampled in the field leaving no material for logging nor core description.

I.1.6 Initial coring and core description results

TDP drilled 11 boreholes in total (Table I.1.1), although several of these were relatively short due to twist offs that broke drilling rods, or other equipment malfunctions. In total we drilled ~1228m of sediment and recovered ~1018m of core within the intervals where coring was attempted, resulting in a recovery of 91.7 % (Figure I.1.5). Recovery was generally very high through the upper ~100 m of sediment (Unit 1), but much lower in Unit 2 due to the presence of coarse-grained unconsolidated lithologies. We acquired borehole logging data from three holes, though not all parameters were logged at all depths due to borehole collapse in shallow unconsolidated sediment. Attempts to collect vertical seismic profiles at Site 1 were unsuccessful due to equipment malfunction, and were not repeated at other sites.

Six boreholes were drilled at Site 1 yielding approximately 524m of core. Drilling commenced at Site 1A on 23 May 2015, and penetrated ~115 m reaching ~10 m below the Unit 1-Unit 2 boundary. Our geomicrobiology team did extensive sampling of this core in the field. The majority of the core consists of relatively soft clays that were cored with the HPC; however, we encountered four relatively hard beds between ~25 and 70 m sub-bottom that required drilling with the Alien tool. These hard beds were later determined to be tephras, which, despite their deposition as airfall, were frequently semi-lithified. Drilling the soft sediments surrounding these tephras with the Alien tool resulted in significant homogenization and contamination of these cores, as revealed by our contamination tracer, will be published elsewhere. We subsequently adjusted our drilling strategy to maximize recovery of the tephras while minimizing disturbance of the soft clays. Drilling was terminated in this hole upon encountering the first resistant sand bed, in order to start a new hole to ensure duplication of the upper 100 m of the sediment column.

Our second hole, 1B, was our deepest hole at Site 1, extending to 162 m below lake floor (m b.l.f.). The upper ~115 m b.l.f. was very similar to Hole 1A, but the lower ~46 m b.l.f. consisted of a variety of coarser-grained lithologies that resulted in relatively low recovery. Coring was terminated at ~162 m b.l.f. after coring ~0.40 m of bedrock, which consisted of a lithified mafic conglomerate that appears similar to Eocene-aged deposits that occasionally outcrop in the region.

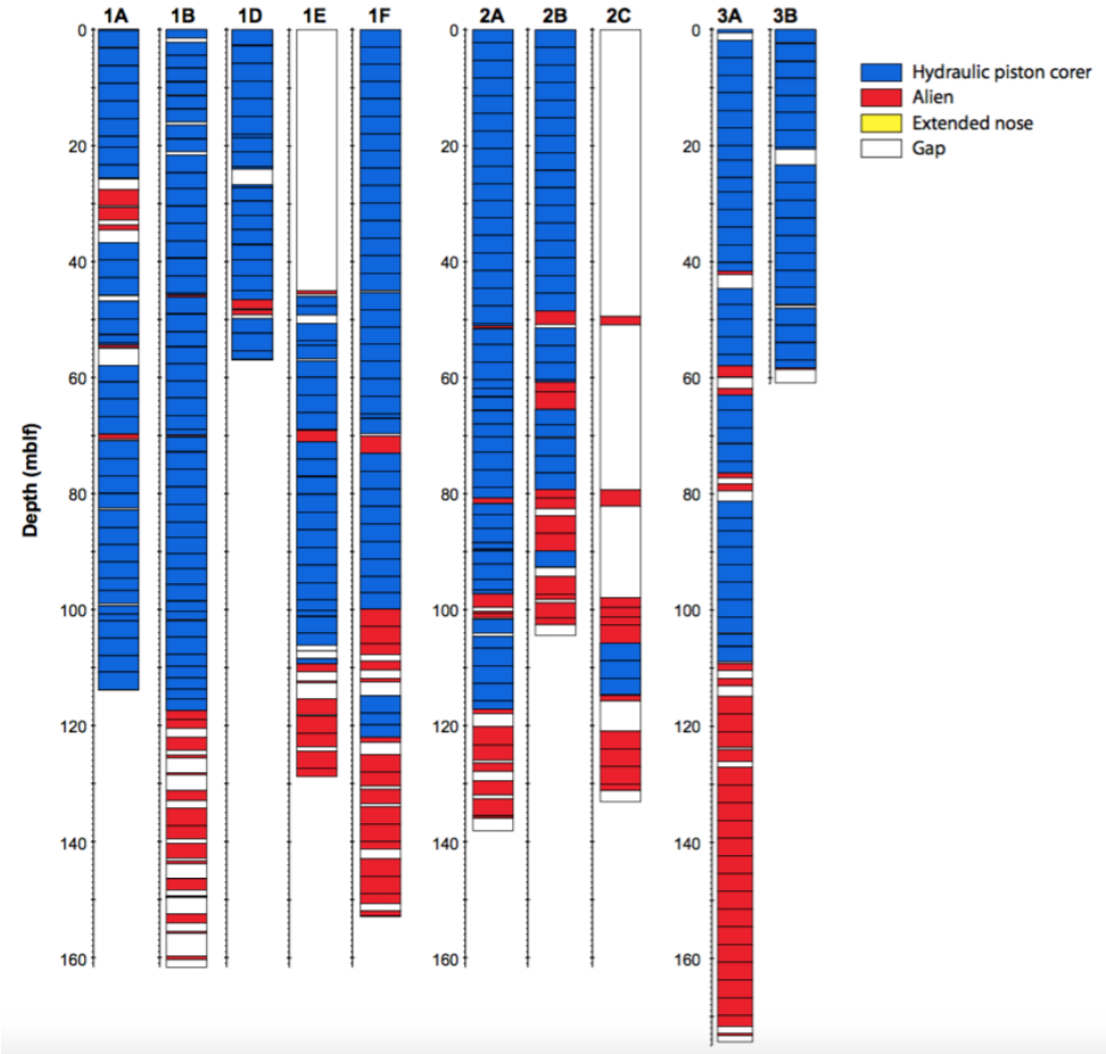

Figure I.1.5 Core recovery from the TDP drill sites in Lake Towuti. Colors indicate the various tools used to recover cores from all TDP sites except 1C. White boxes indicate intervals that were not recovered

While drilling Hole 1B, we began to experience problems with the hydraulic power system of the drilling rig, and after completing Hole 1B, we completely lost rig function. Drilling operations had to be shut down for 18 days in order to replace the main hydraulic pumps of the rig. We then repositioned the drill rig and cored a short hole, 1C, which extended only ~5.5 m b.l.f. After correcting additional hydraulic problems identified while drilling this hole, we drilled three additional holes at Site 1 (1D, 1E, and 1F). Hole 1D extends ~54 m b.l.f. with excellent recovery, and was terminated due to a stuck tool. We repositioned and reamed to ~45 m b.l.f. with a non-coring assembly (NCA) at Hole 1E, and then cored the interval from 45 to ~129 m b.l.f. with 91 % recovery. In light of the various equipment issues and difficulties recovering sediments around tephras in Unit 1 and coarse sediments in Unit 2, we drilled a sixth and final hole, 1F. This hole extends to ~154 m b.l.f., with nearly 95 % recovery, and was terminated when we encountered gravel that, based on 1B, cap a bedrock–soil–fluvial sequence. Holes 1B and 1F were successfully logged for various geophysical parameters, though barge movement and borehole collapse prevented logging of the upper ~20 m of sediment.

Table I.1.1 Summary information about TDP drill sites. Drilled depth indicates the bottom depth of each hole; % recovery indicates the meters of core recovered within the depth intervals where coring was attempted, and thus excludes intervals drilled with a non-coring assembly

Labels	Water depth (m)	Core length (m)	Drilled depth (m b.l.f.)	Recovery (%)	Borehole logging	Remarks
Site 1						
TDP-TOW15-1A	156	105.837	113.58	93.2	N	Geomicrobio Site
TDP-TOW15-1B	156	137.871	161.7	85.3	Y	
TDP-TOW15-1C	156	4.455	5.64	79.0	N	Rig failure
TDP-TOW15-1D	156	53.21	53.91	98.7	N	Ended in twist off
TDP-TOW15-1E	156	76.19	128.72	91.0	N	Continuation of 1D
TDP-TOW15-1F	156	145.965	154.06	94.7	Y	
Site 2						
TDP-TOW15-2A	201	134.515	137.58	97.8	Y	
TDP-TOW15-2B	201	103.918	104.55	99.4	N	Ended in twist off
TDP-TOW15-2C	201	34.175	133.21	82.9	N	Continuation of 2B
Site 3						
TDP-TOW15-3A	159	166.08	174.09	95.4	N	
TDP-TOW15-3B	159	55.3	60.88	90.8	N	Ended in twist off
TOTAL		1017.5	1227.9			

Core 1F is the most complete section from Site 1 and its lithology is representative of the section recovered from this site (Figure I.1.6). The basal sediments consist of a variety of lithologies including alternating gravels, poorly to well-sorted sands, silts, clayey silts, and peats. This unit is capped by a ~2.5 m thick woody peat at ~100 m b.l.f., which correlates to the transition from Unit 2 to Unit 1 in seismic reflection data. The upper 100 m of sediments consist largely of alternating thinly bedded to massive dark reddish-gray to dark-green gray clays. Normally graded silts (turbidites) are relatively rare but more common in the lower ~50 m of this interval, and we discovered ~14 light gray tephras that range from ~1 to ~40 cm thickness and are scattered through the upper ~95 m. The source of these tephras is currently under investigation, but they likely derive from the Tondano caldera system in northern Sulawesi, which is the closest tephra source to Lake Towuti. We also observed two 3-5m thick intervals of laminated to medium-bedded diatomaceous ooze. Diatoms are not a significant part of the pelagic phytoplankton in the present-day lake (Haffner et al., 2001; Lehmusluoto et al., 1995), suggesting that these intervals mark major changes in the biogeochemical functioning of Lake Towuti.

Three holes were drilled at Site 2 to obtain a record of the evolution of the Mahalona River delta. Hole 2A reached ~134 m b.l.f. with ~98 % recovery, though there was significantly more gas expansion at Site 2 than at Site 1, which contributed significantly to the high apparent recovery. Coring was terminated when we reached sandy gravel, interpreted to correspond to the Unit 1-Unit 2 boundary observed in seismic reflection data (Figure I.1.4b). Hole 2B extended to ~105 m b.l.f., and ended in a twist off of the drilling rod. We repositioned and in Hole 1C reamed down to 100 m using a NCA, with spot coring to close coring gaps in 2A and 2B. We then cored from ~100 to ~133 m with 83 % recovery.

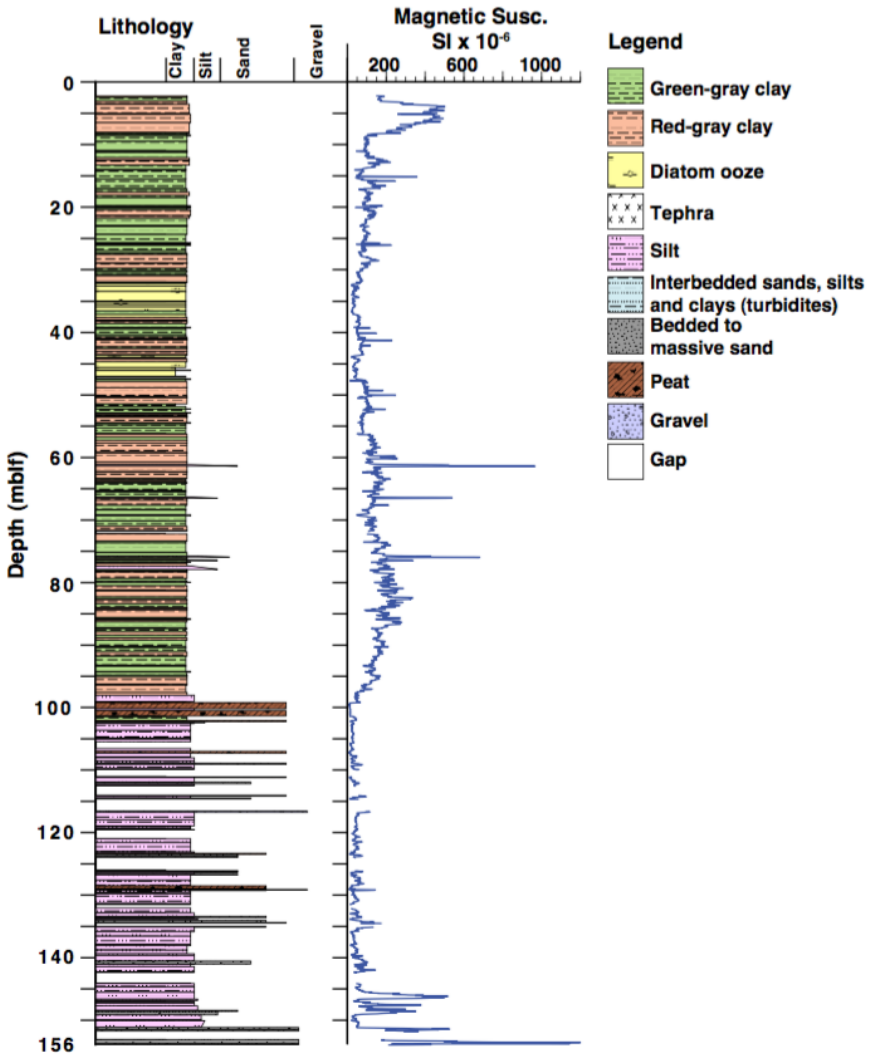

Figure I.1.6 Summary stratigraphy of core TDP-TOW15-1F, based on initial core descriptions. Lithology data are based upon visual and smear slide descriptions, and are rendered in PSICAT. Magnetic susceptibility data measured on the whole (unsplit) core from the Geotek MSCL are shown in the central panel, and at far right is the key to the lithologic symbols. Blank (white) areas indicate zones with no recovery

Hole 2A provides the most complete and representative stratigraphy from Site 2. The upper ~71 m of this core consist of 1-80 cm thick normally graded silts (Figure I.1.7), reflecting deposition by turbidity currents, interbedded with dark reddish to greenish-gray silty clay, whereas the lower 64 m consists largely of alternating thinly bedded to massive dark reddish-gray to dark-green gray clays similar to Site 1. We observe multiple tephra beds as well as two intervals of diatomaceous ooze, similar to Site 1. The tephras are much thicker than observed at Site 1, likely reflecting enhanced re-working of tephra from the Mahalona Delta and steep slopes bordering the basin.

We drilled our deepest hole of the project at Site 3, where Hole 3A reached ~174 m b.l.f. with over 95 % core recovery. Drilling at 3A was terminated when we encountered gravel near the contact with bedrock (Figure I.1.8). We began a second hole, 3B, which ended in a twist-off while trying to drill through a tephra at ~61 m depth. Due to time and budgetary constraints, we were not able to drill a third hole at Site 3 and

concluded the project. Hole 3A, however, contains an excellent record of sedimentation at this site. Unit 1 at Site 3 is similar to that of Site 1, but is slightly expanded (~10 % thicker) and contains much more frequent turbidites, particularly in the lower ~50 m. Peats are less common in Unit 2 of Site 3 than at Site 1, and the sediments are generally finer grained, resulting in better recovery. These observations are consistent with our interpretation of the seismic reflection data that places Site 3 in a small structural basin that supported more continuous lacustrine sedimentation during the early stages of formation of Lake Towuti basin.

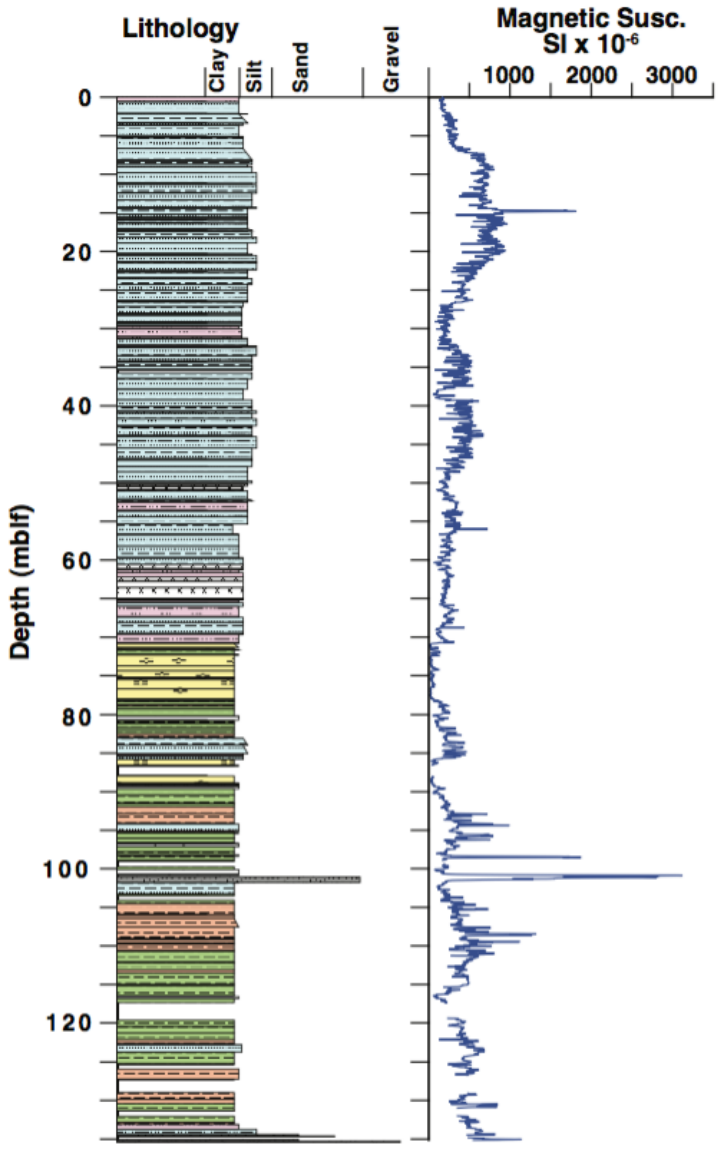

Figure I.1.7 Summary stratigraphy of core TDP-TOW15-2A, based on initial core descriptions, and magnetic susceptibility data measured on the whole (unsplit) core from the Geotek MSCL. The key to the lithologic symbols is given in Figure I.1.6

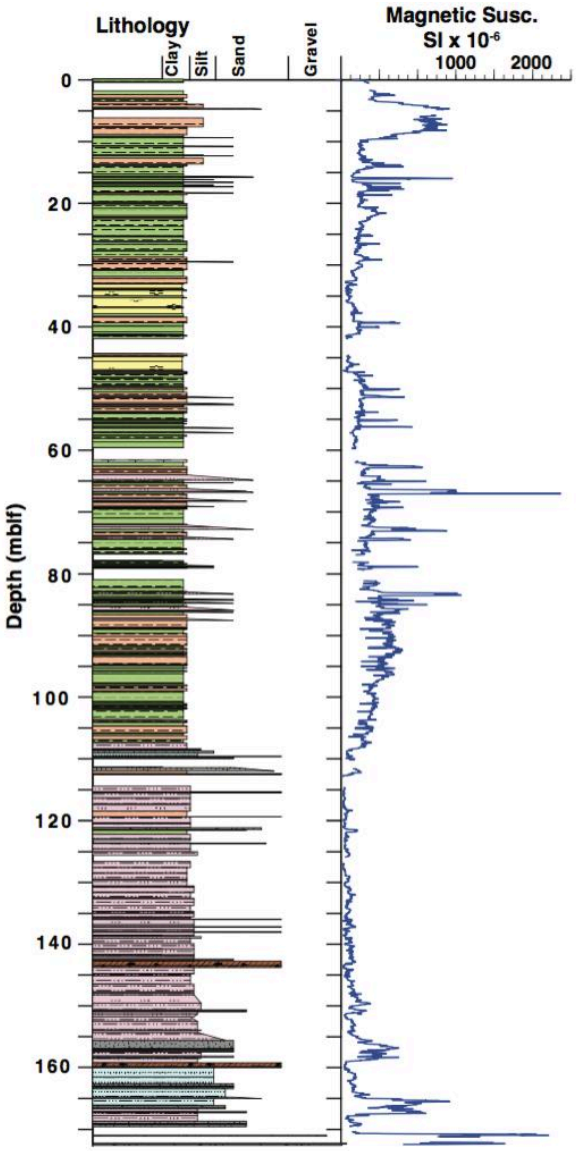

Figure I.1.8 Summary stratigraphy of core TDP-TOW15-3A based on initial core descriptions, and magnetic susceptibility data measured on the whole (unsplit) core from the Geotek MSCL. The key to the lithologic symbols is given in Figure I.1.6

I.1.7 Conclusions

The TDP cores record the evolution of a highly dynamic tectonic and limnological system. Sediments in Unit 2 represent a mixture of lacustrine, fluvial, and terrestrial sediments deposited during the initial stages of extension and subsidence of the Lake Towuti basin. Comparison of Unit 2 sediments between Sites 1 and 3, or even between different holes drilled at Site 1, suggest Unit 2 is highly spatially variable over short distances, perhaps reflecting a variety of lake, swamp, and riverine environments that existed simultaneously in a large, slowly subsiding swampy plain. The rapid transition from Unit 2, which represents sedimentation near base level, to Unit 1, which represents sedimentation permanently below base level, suggests rapid fault movement and creation of accommodation space.

We interpret Unit 1 to represent sedimentation in a generally deep lake, with red/green alternations reflecting climate-driven transitions in lake level and mixing (Costa et al., 2015). Unit 1 sediments are quite similar at Sites 1 and 3, but differ substantially at Site 2, where the upper ~70 m of sediment predominantly consists of distal deltaic

sedimentation. This supports our interpretation of the seismic reflection data and could indicate relatively recent establishment of the Mahalona River.

Magnetic susceptibility profiles from Lake Towuti show very similar patterns at all three sites, and show generally excellent correlation to borehole profiles (Figure I.1.9). These data, together with tephras, biogenic opal beds, and other distinct beds, allow for a preliminary correlation of cores from the three holes. This correlation highlights the relatively rapid influx of sediment to the upper 70 m of Site 2 relative to Sites 1 and 3, likely reflecting the rapid influx of sediment from the Mahalona River to the core site during this time. Interestingly, the basal sediments of Site 2 appear to be younger than those at Sites 1 and 3, despite the fact that Site 2 currently lies n deeper water than the other sites. This could suggest relatively fast subsidence of the northernmost part of the lake relative to the central part of the basin, perhaps reflecting recent changes in fault motion.

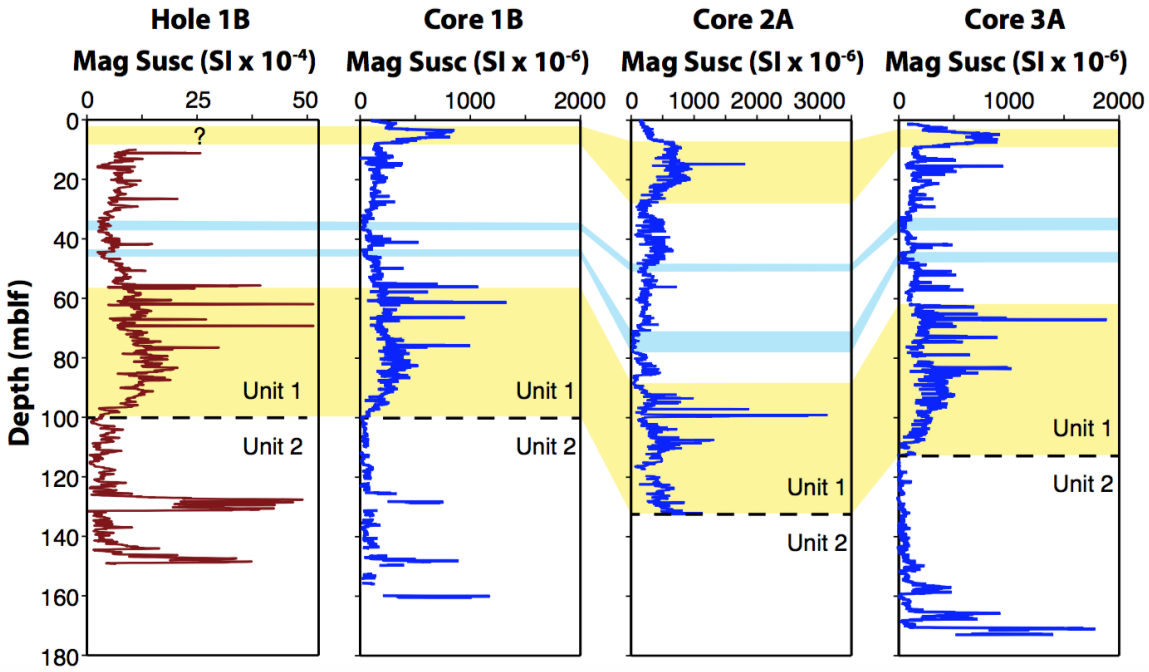

Figure I.1.9 Magnetic susceptibility data from borehole logging of Hole 1B as well as MS data of cores 1B, 2A, and 3A. Yellow shading indicates correlative high magnetic susceptibility features in each site, whereas blue shading indicates correlative low susceptibility features. The dashed line marks the interpreted boundary between Seismic Unit 1 and 2; note that this boundary appears younger in core 2A than at sites 1 and 3

Our analysis of these cores is just beginning and includes an array of geochronological, sedimentological, geochemical, geophysical, and biological methods. The geochronology is being assembled through a combination of $^{40}Ar/^{39}Ar$ ages on tephras, paleomagnetic, luminescence, and ^{14}C dating. State of the art isotopic, organic geochemical, and elemental methods are being applied to understand the climate history of the tropical western Pacific and the evolving biogeochemistry of the basin. Analyses of the pore fluid chemistry, Fe-mineralogy, and microbial communities in the sediments will reveal the nature of the deep biosphere that inhabits these iron-rich sediments, and fossil pollen and fossil diatoms will reveal the dynamics of the evolving terrestrial and aquatic

biota in central Sulawesi. Ultimately, through interactions between these groups we will try to unravel the coupled tectonic, biologic, and climatic evolution of this unique system.

I.1.8 Data availability

Cores and project data are archived at the National Lacustrine Core Repository, USA and are under a 2-year moratorium during which time only project scientists have access. The data will become publicly available in 2018, but could, through request to LacCore, be made available earlier to other individuals on a case-by-case basis.

I.1.9 Acknowledgements

This research was carried out with partial support from the International Continental Scientific Drilling Program (ICDP), the U.S. National Science Foundation (NSF), the German Research Foundation (DFG) the Swiss National Science Foundation (SNSF), PT Vale Indonesia, the Ministry of Research, Education, and Higher Technology of Indonesia (RISTEK), Brown University, the GFZ German Research Centre for Geosciences, the Natural Sciences and Engineering Research Council of Canada (NSERC), and Genome British Columbia. We thank PT Vale Indonesia, the US Continental Scientific Drilling and Coordination Office, and US National Lacustrine Core Repository, and DOSECC Exploration Services for logistical support. The research was carried out with permissions from RISTEK, the Ministry of Trade of the Republic of Indonesia, the Natural Resources Conservation Center (BKSDA), and the Government of Luwu Timur of Sulawesi. We thank Andy Cohen and Christine Lane for helpful comments on a previous version of this paper.

Edited by: U. Harms
Reviewed by: A. S. Cohen and C. S. Lane

I.1.10 References

Aldrian, E. and Susanto, R. D.: Identification of three dominant rainfall regions within Indonesia and their relationship to sea surface temperature, Int. J. Climatol., 23, 1435–1452, 2003.

Cannon, C. H., Morley, R. J., and Bush, A. B. G.: The current rainforests of Sundaland are unrepresentative of their biogeographic past and highly vulnerable to disturbance, P. Natl. Acad. Sci. USA, 106, 11188-11193, 2009.

Carolin, S. A., Cobb, K. M., Adkins, J. F., Clark, B., Conroy, J. L., Lejau, S., Malang, J., and Tuen, A. A.: Varied response of western Pacific hydrology to climate forcings over the last glacial period, Science, 340, 1564–1566, 2013.

Chiang, J. C. H.: The tropics in paleoclimate, Annu. Rev. Earth Pl. Sc., 37, 20.21–20.35, 2009.

Clement, A. C., Cane, M. A., and Seager, R.: An orbitally-driven tropical source for abrupt climate change, J. Climate, 14, 2369– 2375, 2001.

Costa, K., Russell, J. M., Vogel, H., and Bijaksana, S.: Hydrologial connectivity and mixing of Lake Towuti, Indonesia in response to paleoclimatic change over the last 60,000 years, Palaeogeogr. Palaeocl., 417, 467–475, 2015.

Crowe, S. A., O'Neill, A. H., Katsev, S., Hehanussa, P. E., Haffner, G. D., Sundby, B., Mucci, A., and Fowle, D. A.: The biogeochemistry of tropical lakes: a case study from Lake Matano, Indonesia, Limnol. Oceanogr., 53, 319–331, 2008.

DiNezio, P. N. and Tierney, J. E.: The effect of sea level on glacial Indo-Pacific climate, Nat. Geosci., 6, 485–491, 2013.

DiNezio, P. N., Clement, A. C., Vecchi, G. A., Soden, B. J., Broccoli, A. J., Otto-Bliesner, B., and Braconnot, P.: The response of the Walker Circulation to LGM forcing: Impilcations for detection in proxies, Paleoceanography, 26, PA3217, doi:10.1029/2010PA002083, 2011.

Ehlmann, B. L., Mustard, J. F., Fassett, C. I., Schon, S. C., Head, J. W., DesMarais, D. J., Grant, J. A., Murchie, S. L., and the CRISM team: Clay mineralogy and organic preservation potential of lacustrine sediments from a Martian delta environment, Nature Geoscience, 1, 355–358, 2008.

Fritz, S. C., Baker, P. A., Seltzer, G. O., Ballantyne, A., Tapia, P. M., Cheng, H., and Edwards, R. L.: Quaternary glaciation and hydrologic variation in the South American tropics as reconstructed from the Lake Titicaca drilling project, Quaternary Res., 68, 410–420, 2007.

Haffner, G. D., Hehanussa, P. E., and Hartoto, D.: The biology and physical processes of large lakes of Indonesia: Lakes Matano and Towuti, in: The Great Lakes of the World (GLOW): Food-Web, Health, and Integrity: Leiden, edited by: Munawar, M. and Hecky, R. E., The Netherlands, Blackhuys, 129–155, 2001.

Hamilton, W.: Tectonics of the Indonesian region, U.S.G.S. Professional Paper, 1078, 345 pp., 1979.

Hamilton, W. B.: Plate tectonics and island arcs, Geologic Society of America Bulletin, 100, 1503–1327, 1988.

Hendon, H. H.: Indonesian rainfall variability: impacts of ENSO and local air-sea interaction, J. Climate, 16, 1775–1790, 2003.

Herder, F., Nolte, A. W., Pfänder, J., Schwarzer, J., Hadiaty, R. K., and Schliewen, U. K.: Adaptive radiation and hybridization in Wallace's dreamponds: evidence from sailfin silversides in the Malili lakes, P. Roy. Soc. Lond. B, 273, 2209–2217, 2006.

Hodell, D. A., Anselmetti, F. S., Ariztegui, D., Brenner, M., Curtis, J. H., Gilli, A., Grzesik, D., Guilderson, T. J., Müller, A. D., Bush, M. B., Correa-Metrio, A., Escobar, J., and Kutterolf, S.: An 85-ka record of climate change in lowland central America, Quaternary Sci. Rev., 27, 1152–1165, 2007.

Kadarusman, A., Miyashita, S., Maruyama, S., Parkinson, C. D., and Ishikawa, A.: Petrology, geochemistry, and paleogeographic reconstruction of the East Sulawesi ophiolite, Indonesia, Tectonophysics, 392, 55–83, 2004.

Konecky, B. L., Russell, J. M., and Bijaksana, S.: Glacial aridity in central Indonesia coeval with intensified monsoon circulation, Earth Planet. Sc. Lett., 437, 15–24, 2016.

Kumar, S., Merwade, V., Kinter, J. L., and Niyogi, D.: Evaluation of temperature and precipitation trends and long-term persistence in CMIP5 Twentieth-Century Climate Simulations, J. Climate, 26, 4168–4185, 2013.

Lehmusluoto, P., Machbub, B., Terangna, N., Rusmiputro, S., Achmad, F., Boer, L., Brahmana, S. S., Priadi, B., Setiadji, B., Sayuman, O., and Margana, A.: National inventory of the major lakes and reservoirs in Indonesia, General limnology.: FAOFINNIDA, 1995.

Meckler, A. N., Clarkson, M. O., Cobb, K. M., Sodemann, H., and Adkins, J.: Interglacial hydroclimate in the tropical west Pacific through the late Pleistocene, Science, 336, 1301–1304, 2012.

Meehl, G. A., Stocker, T., Collins, W. D., Friedlingstein, P., Gaye, A. T., Gregory, J. M., Kitoh, A., Knutti, R., Murphy, J. M., Noda, A., Raper, S. C. B., Watterson, I. G., Weaver, A. J., and Zhao, Z.-C.: Global Climate Projections, in: Climate Change 2007: The Physical Science Basis. Contribution of Working Group I to the Fourth Assessment of the Intergovernmental Panel on Climate Change: New York, USA, edited by: Solomon, S., Qin, D., Manning, M., Chen, Z., Marquis, M., Averyt, K. B., Tignor, M., and Miller, D. J., Cambridge University Press, 747–845, 2007.

Monnier, C., Girardeau, J., Maury, R. C., and Cotten, J.: Back-arc basin origin for the East Sulawesi ophiolite (eastern Indonesia): Geology, 23, 851–854, 1995.

Pierrehumbert, R. T.: Subtropical water vapor as a mediator of rapid global climate changes, in: Mechanisms of global climate change at millennial time scales, edited by: Clark, P. U.,

Webb, R. S., and Keigwin, L. D., Geophysical monograph series v. 112, Washington DC, American Geophysical Union, 339–361, 1999.

Pierrehumbert, R. T.: Climate change and the tropical Pacific: the sleeping dragon wakes, P. Natl. Acad. Sci. USA, 97, 1355–1358, 2000.

Poulton, S. W. and Canfield, D. E.: Ferruginous Conditions: A Dominant Feature of the Ocean through Earth's History, Elements, 7, 107–112, 2011.

Rintelen, T. V., Wilson, A. B., Meyer, A., and Glaubrecht, M.: Escalation and trophic specialization drive adaptive radiation of viviparous freshwater gastropods in the ancient lakes on Sulawesi, Indonesia, Proc. Roy. Soc. Lond. B, 271, 2541–2549, 2004.

Rintelen, T. V., Rintelen, K. V., Glaubrecht, M., Schubart, C., and Herder, F.: Aquatic biodiversity hotspots in Wallacea – the species flocks in the ancient lakes of Sulawesi, Indonesia, in: Biotic evolution and environmental change in southeast Asia Cambridge, edited by: Gower, D. J., Johnson, K. G., Richardson, J. E., Rosen, B. R., Rüber, L., and Williams, S. T., Cambridge University Press, 2012.

Russell, J. and Bijaksana, S.: The Towuti Drilling Project: Paleoenvironments, Biological Evolution, and Geomicrobiology of a Tropical Pacific Lake, Sci. Dril., 14, 68–71, doi:10.2204/iodp.sd.14.11.2012, 2012.

Russell, J. M., Vogel, H., Konecky, B. L., Bijaksana, S., Huang, Y., Melles, M., Wattrus, N., Costa, K., and King, J. W.: Glacial forcing of central Indonesian hydrolclimate since 60,000 yr B.P., P. Natl. Acad. Sci. USA, 111, 5100–5105, 2014.

Scholz, C., Johnson, T. C., Cohen, A. S., King, J. W., Peck, J. A., Overpeck, J. T., Talbot, M. R., Brown, E. T., Kalindekafe, L., Amoako, P. Y. O., Lyons, R. P., Shanahan, T., Castañeda, I. S., Heil, C. W., Forman, S. L., McHargue, L. R., Beuning, K. R. M., Gomez, J., and Pierson, J.: East African megadroughts between 135 and 75 thousand years ago and bearings on early-modern human origins, P. Natl. Acad. Sci. USA, 42, 16416–16421, 2007.

Schubart, C. D., Santl, T., and Koller, P.: Mitochondrial patterns of intra- and interspecific differentiation among endemic freshwater crabs of ancient lakes in Sulawesi, Contrib. Zool., 77, 83–90, 2008.

Seager, R. and Battisti, D. S.: Challenges to our understanding of the general circulation: abrupt climate change, in: Global Circulation of the Atmosphere, edited by: Schneider, R. R. and Sobel, A. H., Princeton, Princeton University Press, 331–371, 2007.

Tamuntuan, G., Bijaksana, S., King, J. W., Russell, J. M., Fauzi, U., Maryuanani, K., Aufa, N., and Safiuddin, L. O.: Variation of magnetic properties in sediments from Lake Towuti, Indonesia, and its paleoclimatic significance, Palaeogeogr. Palaeocl., 420, 163–172, 2015.

van Welzen, P. C., Parnell, J. A. N., and Slik, J. W. F.: Wallace's line and plant distributions: two or three phytogeographical areas and where to group Java?, Biological Journal of the Linnaen Society, 103, 541–545, 2011.

Vogel, H., Russell, J. M., Cahyarini, S. Y., Bijaksana, S., Wattrus, N., Rethemeyer, J., and Melles, M.: Depositional modes and lake-level variability at Lake Towuti, Indonesia during the past ~29 kyr BP, J. Paleolimnol., 54, 359–377, 2015.

Wang, Y., Cheng, H., Edwards, R. L., Kong, X., Shao, X., Chen, S., Wu, J., Jiang, X., Wang, X., and An, Z.: Millennial- and orbital-scale changes in the East Asian monsoon over the past 224,000 years, Nature, 451, 1909–1093, 2008.

I.2. Modern sedimentation processes in Lake Towuti, Indonesia, revealed by the composition of surface sediments

Ascelina K. M. Hasberg[1], Satria Bijaksana[2], Peter Held[1†], Janna Just[1], Martin Melles[1], **Marina A. Morlock[3]**, Stephan Opitz[4], James M. Russell[5], Hendrik Vogel[3], Volker Wennrich[1]

published in Sedimentology 2018, doi: 10.1111/sed.12503

[1]*Institute of Geology and Mineralogy, University of Cologne, Zülpicher Str. 49a, 50674 Cologne, Germany (E-mail: hasberg.ascelina@uni-koeln.de)*

[2]*Faculty of Mining and Petroleum Engineering, Institut Teknologi Bandung, Jalan Ganesa 10, Bandung, 40291, Indonesia*

[3]*Institute of Geological Sciences & Oeschger Centre for Climate Change Research, University of Bern, Baltzerstr. 1+3, 3012 Bern, Switzerland*

[4]*Geographical Institute, University of Cologne, Zülpicher Str. 45, 50674 Cologne, Germany*

[5]*Department of Earth, Environmental, and Planetary Sciences, Brown University, 324 Brook St. BOX, 1846, Providence, RI 02912, USA*

Correspondence to: Ascelina K. M. Hasberg (hasberg.ascelina@uni-koeln.de)

I.2.1 Abstract

Lake Towuti on Sulawesi Island, Indonesia, is located within the heart of the Indo-Pacific Warm Pool (IPWP). This tropical lake is surrounded by ultramafic (ophiolitic) rocks and lateritic soils that create a unique ferruginous depositional setting. In order to understand modern sediment deposition in Lake Towuti, a set of 84 lake surface sediment samples was collected from across the entirety of the lake and samples were analyzed for their physical, chemical, mineralogical and biological constituents. End-member analyses were carried out to elucidate modern sediment origin, transport and depositional processes. This study found that allochthonous sediment, characterized by the concentrations of the elements Mg, Fe, Si and Al, as well as the clay and serpentine minerals, is dominated by fluvial supply from five distinct source areas. Granulometric data and the occurrence of organic matter of terrestrial origin suggest that in the southern and northeastern parts of the lake the near-shore sediments may additionally be influenced by mass wasting. This at least is partly due to the particularly steep slopes in these areas. Furthermore, sediment composition suggests that sediment transport into deeper parts of the lake, particularly in the northern basin, is partly controlled by gravitational and density-driven processes such as turbidity currents. Directional sediment transport by persistent lake currents, in contrast, appears less important. Organic matter deposition in the ultraoligotrophic lake, albeit limited, is dominated by autochthonous production, but with some contribution of fluvial and gravitational supply. Biogenic silica deposition, primarily from diatom frustules and sponge spicules, is very limited and is concentrated in only a few areas close to the shoreline that are characterized by shallow waters, but away from the areas of high suspension loads at the mouths of the major inlets. The results of this study build upon current and published work on short piston cores from Lake Towuti. Conversely, the results will support the

interpretation of the depositional history and past climatic and environmental conditions derived from the composition of much longer records, which were obtained by the Towuti Drilling Project (TDP) in May 2015 and are currently under investigation.

Keywords Indo-Pacific Warm Pool (IPWP), Lake Towuti, modern sedimentation, provenance analysis, redox conditions, tropical lake.

I.2.2 Introduction

The Indo-Pacific Warm Pool (IPWP) is the most extensive warm water mass in the world´s oceans, and houses the largest zone of deep atmospheric convection on Earth. The IPWP impacts global climate through its influence on the concentration of atmospheric water vapour, the Earth's most important greenhouse gas (Pierrehumbert, 1999), and through interactions with the El Niño-Southern Oscillation (ENSO), the Australian-Asian monsoons and the Intertropical Convergence Zone (ITCZ; Clement et al., 2001; Chen and Cane 2008; Chiang 2009). Lake Towuti on Sulawesi Island, Indonesia, is the largest tectonic lake in Southeast Asia, and sits at the heart of the IPWP. Lake Towuti has very high rates of biological endemism, with species flocks of fishes, snails and shrimp, among others (von Rintelen et al., 2011). Despite this endemism, Towuti is one of the least productive tropical lakes on Earth. Lake Towuti is located in a unique catchment, the East Sulawesi Ophiolite belt, and lateritic soils, providing ferruginous metal substrates that feed a diverse, exotic microbial community in the lake and its sediments.

Given this extraordinary setting the Towuti Drilling Project (TDP) of the International Continental Scientific Drilling Program (ICDP) recovered over 1000 m of sediment core from three sites in the northern basin of Lake Towuti to investigate: (i) the understanding of the long-term environmental and climatic change in the tropical western Pacific; (ii) the impacts of geological and environmental changes on the biological evolution of aquatic taxa; and (iii) the geomicrobiology and biogeochemistry of metal-rich, ultramafic-hosted lake sediment (Russell et al., 2016).

The multi-disciplinary investigation of ICDP lake cores will strongly benefit from a thorough understanding of modern processes of sediment formation in this area under known environmental and climatic conditions. The most important triggering factors of sediment formation like fluvial input, terrestrial run-off and authigenic formation vary significantly in each lake. This has been shown for ICDP projects on Lake Ohrid in Macedonia/Albania and Lake El´gygytgyn in the Russian Arctic (Vogel et al., 2010; Wennrich et al., 2013). These studies have highlighted an important role for lake circulation and lateral transport in controlling and to some extent homogenizing spatial patterns of clastic and chemical sediment deposition within these lakes, as well as a role for organic matter, iron oxides and metal adsorption in chemical sedimentation. These findings helped to develop chemical tracers for tectonic and lake circulation changes (e.g. Wennrich et al., 2013). Previous work on Lake Towuti by Costa et al. (2015), Weber et al. (2015), and Goudge et al. (2017) investigated the chemical and mineralogical composition of river inputs to the lake, and developed potential tracers for sediment inputs from the largest river entering the lake, the Mahalona River. However, those studies were limited by very low areal coverage (only one sediment transect in the northern lake basin; Figure I.2.1), and did not investigate spatial gradients in organic matter or other patterns of chemical sedimentation. It is possible that the low-latitude

setting and ultraoligotrophic status of Lake Towuti limit the effects of in-lake circulation and organic matter production on the spatial patterns of sediment infill in Lake Towuti; however, this has yet to be tested through comprehensive sampling and analysis.

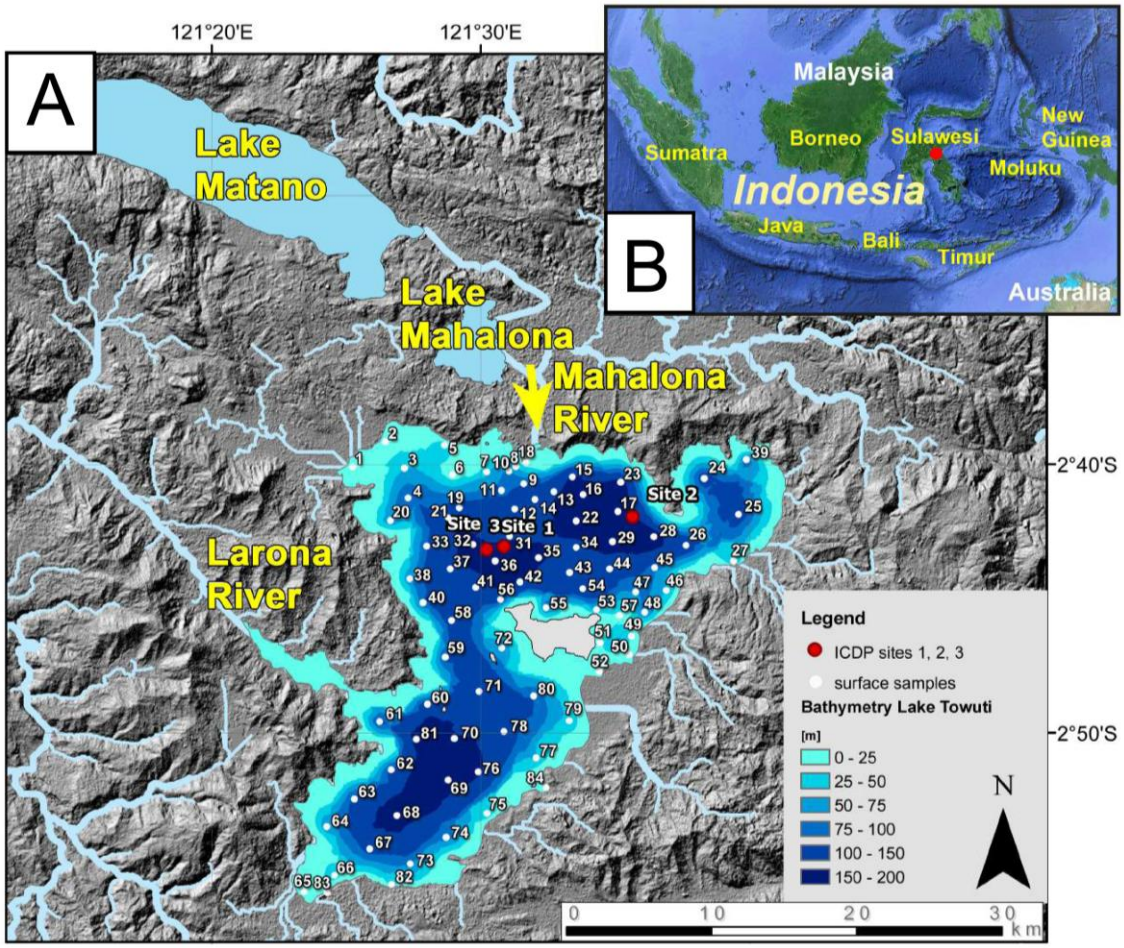

Figure I.2.1 (A) Digital Elevation Model (DEM) of the Lake Towuti area showing the lakes Matano and Mahalona further upstream, the major inlets, the outlet Larona River, the lake bathymetry, and the sampling sites. (B) Location of Lake Towuti (red dot) on Sulawesi Island, southeastern Asia

In this study, 84 lake surface sediment samples were collected from Lake Towuti to document patterns of sedimentation over the entire lake basin. These samples were investigated for a variety of physical, mineralogical and chemical attributes. The results presented here shed new light on the modern sedimentary processes operating in Lake Towuti and complement studies, which focus on modern weathering processes in the lake catchment and potential analogues to iron-rich lake sediments observed on Mars. Furthermore, this study provides information concerning potential impact of anthropogenic activity during recent decades on the composition of the surface sediments in Lake Towuti, in particular the impacts of extensive nickel mining to the northwest of the lake (PT Vale, 2017), population increase in expanding villages (Robinson, 1986), as well as increased deforestation and farming in the lake catchment (Dechert et al., 2004).

I.2.3 Study site

Lake Towuti is part of the Malili Lake System, a chain of five lakes in the centre of Sulawesi Island, northeastern Indonesia (2.5°S, 121.5°E; Figure I.2.1). The three largest of these lakes are connected by surface outflow from Lake Matano via Lake Mahalona to Lake Towuti, with the latter located at 319 m above sea level and draining into the Bay of Bone via the Larona River. The 561.1 km^2 large, and ca 200 m deep Lake Towuti occupies a transtensional basin (Lehmusluoto et al., 1995; Haffner et al., 2001) situated at the junction of the Eurasian, Caroline-Philippine and Indo-Australian tectonic plates (Hamilton, 1979; Spakman and Hall, 2010). Frequent earthquakes (168 between 2010 and 2016), including several above magnitude five, highlight modern tectonic activity (Watkinson and Hall, 2016). Moreover, subduction under North Sulawesi leads to an extensive volcanic field on the island's northern arm, which has been active since the Miocene (Hamilton et al., 1979).

The majority of Lake Towuti´s catchment area (1280 km^2) consists of mafic to ultramafic bedrock of the East Sulawesi Ophiolite belt, the third largest ophiolite complex in the world (Figure I.2.2; Monnier et al., 1995; Kadarusman et al., 2004). The ophiolites around Lake Towuti are composed primarily of serpentinized (lherzolite) and unserpentinized peridotites (harzburgite, dunite; Kadarusman et al., 2004; Figure I.2.2), as well as minor gabbros, dolerites and basalts. The peridotites are intensely weathered and form laterites several metres thick, including nickeliferrous oxisol soils with an FeO content of about 60 % (Golightly and Aranabia, 1979; Kadarusman et al., 2004). Additionally, the ophiolite is interthrusted by Mesozoic and Cenozoic sediments and metasediments (Silver et al., 1983; Kadarusman et al., 2004).

Lake Towuti is roughly separated into a northern and a southern basin by a large island and a series of subaquatic ridges ascending to ca 125 m water depth (Russell et al., 2016; Figure I.2.1). The largest tributary is the Mahalona River, which forms a large delta in the northern part of the lake (the Mahalona Delta) and exerts a strong influence on sedimentation in the northern basin (Costa et al., 2015; Vogel et al., 2015; Weber et al., 2015; Goudge et al., 2017). Today, Lake Towuti is ultra-oligotrophic and dilute (conductivity 210 µS/cm), with a circumneutral pH (ca 7.8), and the water chemistry is dominated by Mg and HCO_3^- ions (Lehmusluoto et al., 1995; Haffner et al., 2001; Vuillemin et al., 2016). The lake is thermally stratified, with seasonal mixing occurring down to ca 100 m and surface water temperatures between 29°C and 31°C (Costa et al., 2015).

The climate at Lake Towuti is tropical humid, exhibiting a mean annual air temperature of 26°C with monthly averages varying by less than 1°C (Costa et al., 2015). Precipitation averages ca 2700 mm/year, with its maximum and minimum in March/April and in October, respectively, governed by the seasonal influences of the ITCZ and the Australian-Indonesian Summer Monsoon (AISM; Konecky et al., 2016). During the wet season from December to May, when precipitation can exceed 250 mm/month, the ITCZ passes over the region, northerly winds associated with the AISM prevail, and local convective activity, triggered by warm sea-surface temperatures (SST), is high (Aldrian and Susanto, 2003). In contrast, from August to October, the atmospheric circulation is dominated by southeasterly flows, which transfer latent heat to the Asian mainland, decreasing regional SSTs and local convection, and thus decreasing precipitation around Lake Towuti below 150 mm/month (Aldrian and Susanto, 2003; Hendon 2003). The lake and its surroundings are heavily influenced by ENSO

events. The El Niño event 1997/1998, for instance, led to strongly reduced precipitation during the rainy season, causing a lake-level lowering of ca 3 m, and a nearly closed-basin situation (Tauhid and Arifian, 2000).

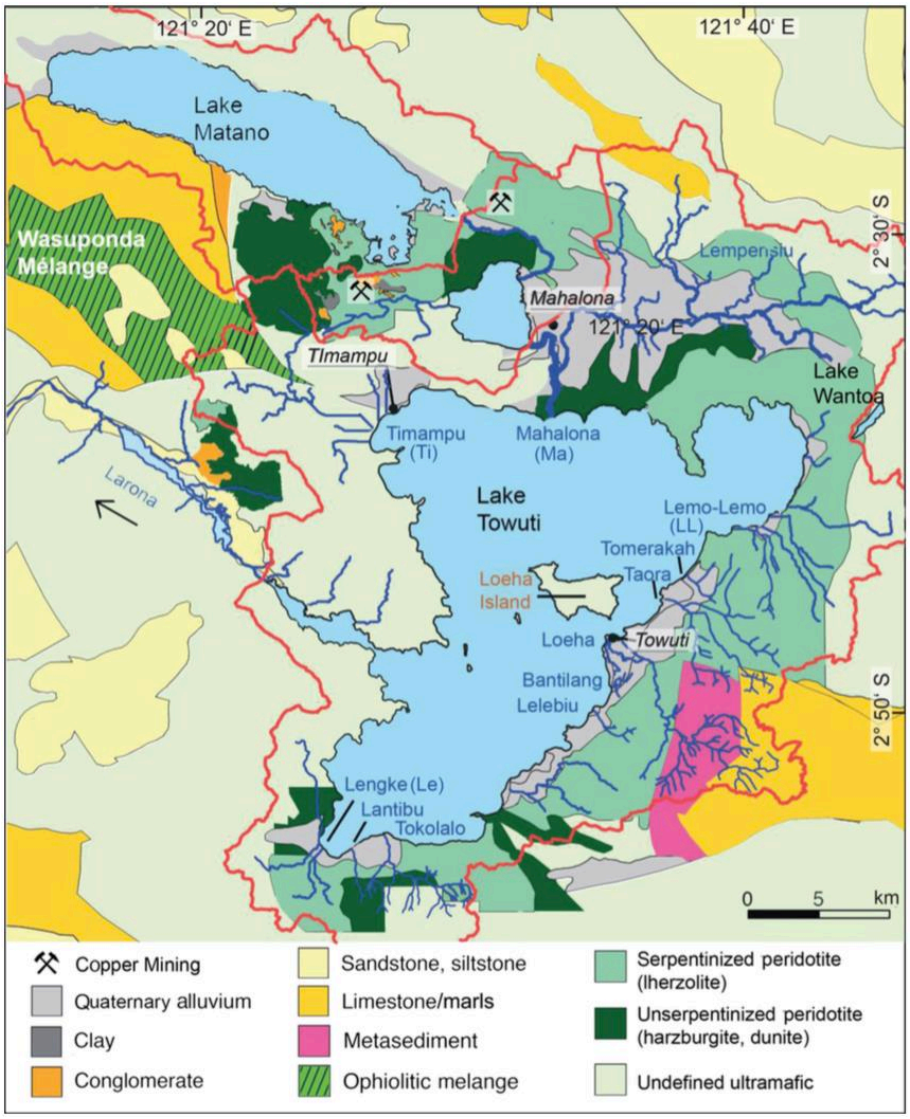

Figure I.2.2 Geological map, showing the catchment areas of the lakes Towuti, Matano, and Mahalona (red lines), along with the names of major settlements (underlined) as well as the inlets and the outlet (blue; after Costa et al., 2015, based on data from PT Vale)

Despite its importance in the global climate system, the interaction of the IPWP with climate change is still poorly constrained. To further understanding of oceanic and continental environmental conditions in the IPWP region, lake sediment cores are valuable archives as they contain highly resolved and potentially long records of climatic changes. The information presently available concerning the history of Lake Towuti is primarily based on the investigation of piston cores of up to 20 m length, which were recovered in 2010 and span the past ca 60,000 years (Russell et al., 2014; Vogel et al. 2015). Additional information is available from seismic data obtained in 2007, 2010 and 2013 (Russell et al., 2014; Vogel et al., 2015) as well as three TDP sites drilled in 2015, with sediment penetrations between 138 and 174 m below lake floor (blf; Russell et al.,

2016). These cores likely expand the existing records to at least 700,000 years (Russell and Bijaksana, 2012), providing a unique, high-resolution continental archive to investigate the influence of orbital forcing and northern hemisphere glaciations on climate variations within the IPWP region.

Organic geochemical and compositional analyses of the upper ca 10 m of the sediments indicates particularly wet conditions with closed-canopy rainforest in the catchment during MIS 3 and the Holocene (Russell et al., 2014). These conditions abruptly changed to drier conditions with more open ecosystems (seasonal forests and grasslands) during MIS 2, especially during the Last Glacial Maximum (LGM; Russell et al., 2014). The palaeoclimatic changes impacted not only the regional vegetation, but also sediment supply to the lake, water-column mixing, sediment redeposition, and lake-levels (Russell et al., 2014, 2016; Vogel et al., 2015; Costa et al., 2015; Konecky et al., 2016; Goudge et al., 2017). However, there are still many uncertainties from these studies. For instance, Russell et al. (2014) used sedimentary Ti content to infer surface runoff and erosion, whereas other studies (Costa et al., 2015; Vogel et al., 2015; Goudge et al., 2017) used sedimentary Mg content to infer sediment remobilization driven by lake-level changes. Costa et al. (2015) used Fe concentration data to infer changes in lake mixing, but lacked information about whether Fe concentrations changed across Lake Towuti's oxycline in the present day. Improved understanding of the spatial patterns of sedimentation in the modern-day lake, and the impacts of lake circulation and heterogeneous sediment source areas will significantly facilitate the interpretation of the palaeorecord lake circulation and heterogeneous sediment source areas.

I.2.4 Material and methods

I.2.4.1 Field work

Lake Towuti surface sediments were sampled during TDP drilling operations in May 2015. Eighty-four samples were collected from water depths between ca 2.8 m and ca 200 m (Table I.2.1), forming a dense, high-resolution (1 to 4 km) sampling grid that covered the entire lake (Figure I.2.1). Sampling was conducted using a grab sampler (UWITEC Corp., Mondsee, Austria) operated by a hand winch mounted to a local boat. Water depths at the sampling sites were measured by echosounder (LCX-17M; Lowrance, Tulsa, OK, USA), and the positions were determined using a hand-held global positioning system (FurunoTM GPS; Furuno Electric Co., Ltd, Mishinomiya, Japan). Material was sampled from the top 5 cm of the recovered grab sample. Based on mean Holocene sedimentation rates of 0.205 mm/year at TDP Site 1 (Russell et al., 2014), and 0.235 mm/year (excluding event layers) close to TDP Site 2 (Vogel et al., 2015), the deepwater samples integrate ca 200 to 250 years.

On site, large organic remains; such as shells, woody twigs and leaves, were removed using tweezers and the remaining sediment was divided into four homogenized aliquots. The aliquots were stored in high-density polyethylene Whirl-pak™ sample bags or 50 ml polystyrene NUNC vials and shipped to different laboratories for individual analyses.

Table I.2.1 Surface sediment samples from Lake Towuti with their locations and water depths; asterisks in front of the sample numbers indicate sediment samples that contain organic macro-remains

Sample number	Longitude	Latitude	Water depth (m)	Sample number	Longitude	Latitude	Water depth (m)
1	121·42	−2·67	6·30	43	121·56	−2·73	141·60
*2	121·44	−2·65	5·40	*44	121·58	−2·73	126·80
3	121·45	−2·67	48·40	45	121·61	−2·73	81·80
4	121·45	−2·69	97·50	46	121·61	−2·74	53·80
*5	121·48	−2·65	47·10	47	121·60	−2·75	73·90
6	121·48	−2·67	7·50	48	121·60	−2·76	92·20
7	121·45	−2·67	62·40	*49	121·59	−2·76	25·60
8	121·52	−2·67	49·00	50	121·59	−2·78	4·50
9	121·53	−2·68	96·40	*51	121·57	−2·80	4·40
10	121·52	−2·67	72·60	*52	121·57	−2·78	32·90
11	121·51	−2·68	83·40	53	121·57	−2·76	73·20
12	121·52	−2·69	124·70	54	121·56	−2·74	129·60
13	121·55	−2·68	140·00	*55	121·54	−2·76	96·00
*14	121·53	−2·69	125·40	*56	121·51	−2·75	134·90
*15	121·56	−2·67	171·20	57	121·59	−2·78	58·90
*16	121·56	−2·69	174·90	58	121·48	−2·76	127·60
*17	121·59	−2·70	195·50	59	121·48	−2·79	112·00
18	121·53	−2·67	3·50	*60	121·47	−2·82	134·30
19	121·49	−2·69	123·70	*61	121·44	−2·83	117·60
20	121·44	−2·70	75·60	*62	121·44	−2·86	117·50
21	121·48	−2·70	144·70	63	121·42	−2·87	119·60
*22	121·56	−2·70	171·40	*64	121·40	−2·89	77·50
23	121·59	−2·68	177·90	*65	121·39	−2·93	19·10
24	121·64	−2·68	133·30	66	121·41	−2·92	40·70
25	121·66	−2·70	129·20	67	121·43	−2·91	120·80
26	121·63	−2·72	137·70	68	121·45	−2·88	168·80
27	121·66	−2·73	59·30	69	121·48	−2·86	177·00
28	121·61	−2·71	194·50	70	121·48	−2·84	152·00
29	121·58	−2·71	172·10	71	121·50	−2·81	132·00
30	121·54	−2·71	147·60	72	121·51	−2·78	71·60
31	121·52	−2·71	147·40	73	121·46	−2·91	87·10
32	121·49	−2·72	153·70	*74	121·48	−2·90	93·30
33	121·47	−2·72	100·40	75	121·50	−2·88	50·60
34	121·56	−2·72	141·10	76	121·50	−2·86	160·00
35	121·54	−2·72	154·00	77	121·53	−2·85	53·40
36	121·51	−2·73	157·70	78	121·51	−2·83	119·00
37	121·48	−2·73	146·50	79	121·55	−2·83	46·80
38	121·46	−2·74	78·50	80	121·53	−2·81	99·80
*39	121·66	−2·66	101·10	81	121·46	−2·84	168·50
40	121·46	−2·75	101·20	*82	121·44	−2·93	36·10
*41	121·50	−2·74	130·10	83	121·40	−2·93	2·80
*42	121·52	−2·74	161·80	*84	121·54	−2·87	9·60

I.2.4.2 Analytical work

At the University of Cologne, Germany, a subsample was taken from one aliquot and used to produce smear slides for identification of sedimentary components using transmitted light microscopy. On selected samples, sponge spicules and diatom frustules were additionally investigated using a Zeiss Gemini Sigma 300VP scanning electron microscope (SEM; Carl Zeiss AG, Oberkochen, Germany). Furthermore, some magnetic mineral grains were identified with energy dispersive X-ray spectroscopy (EDX) of the Sigma SEM system.

Based on smear slide analyses, a set of 40 samples that contain sponge spicules, diatoms and/or tephra particles were selected for automated, non-destructive particle image analyses using a dynamic imaging system (Benchtop B3 Series VS FlowCAM®; Fluid Imaging Technologies, Inc., Scarborough, ME, USA) to quantify the

abundance of these particles. Aliquots of wet bulk samples were treated with hydrogen peroxide (H_2O_2; 30 %) for seven days at room temperature to remove organic matter (OM) and disaggregate the siliceous biogenic particles, and were subsequently sieved with 25 and 80 µm meshes. The pre-treated sample fractions were diluted with deionized water (samples <25 µm) or polyvinyl pyrrolidone (PVP, 2 %; samples 25 to 80 µm and >80 µm). Particle recording in the <25 µm and 25 to 80 µm fractions was carried out using a 100 µm flowcell, a 10x objective lens with a collimator, and a 1 ml syringe-pump (flow rate 0.3 ml/min), whereas the >80 µm fraction was recorded using a 300 µm flowcell, a 4x objective lens without collimator, and a 5 ml syringe-pump (flow rate 0.6 ml/min). Data were acquired using the software VisualSpreadsheet (Fluid Imaging Technologies, Inc., Scarborough, ME, USA) until 10.000 images were recorded or 30 ml of the sample was investigated. An automated catalogue based on training sets developed for sponge spicules, diatoms and tephra particles was compiled to differentiate and group components with comparable characteristics in the measured sample fractions.

The mass magnetic susceptibility (MS) was analyzed on wet bulk sediment aliquots using a KLY-2 Kappabridge (AGICO, Brno, Czech Republic). MS measurements were carried out on sample containers of 2 x 2 x 1.6 cm (i.e. a sample volume of 6.4 cm^3), which frequently are used for palaeo and rock magnetic measurements. The only exceptions are samples 12 and 33, which did not contain sufficient material.

For granulometric, geochemical and mineralogical analyses, approximately 25 ml of each surface sample was frozen for 24 hours and subsequently lyophilized using a Christ BETA 1-8 LDplus (Martin Christ Gefriertrocknungsanlagen GmbH, Osterode am Harz, Germany). The freeze-dried samples were homogenized and split into two aliquots. One aliquot of 1 g was used for grain-size analyses, following a three-step pre-treatment procedure adapted after Francke et al. (2013). First, OM was dissolved with 15 ml H_2O_2 (30 %) in a water bath at 50°C for 18 hours. This step was repeated once to ensure that the OM was fully dissolved. Subsequently, carbonates were dissolved by treatment with 10 ml hydrochloric acid (HCl; 10 %) at 50°C in a water bath for three hours, with regular shaking of the samples to ensure complete reaction. Finally, biogenic silica (bSi, opal) was dissolved by two treatments with 10 ml of sodium hydroxide (NaOH, 1 M) solution for one hour. Each step was followed by repeated centrifuging, decanting, and rinsing of the samples with deionized water until reaching a neutral pH. These pre-treated aliquots were subsequently diluted with 60 ml of deionized water, dispersed with sodium pyrophosphate ($Na_4P_2O_7$; 2.5 g/l), and placed on a shaker for at least 12 hours. The grain-size measurements were performed with a Beckman Coulter LS13320 laser particle analyzer (Beckman Coulter Life Sciences, Indianapolis, IN, USA) applying the Fraunhofer diffraction theory. For that purpose, each sample was pumped into the measurement tank of the analyzer and filled with deionized and degassed water until the sediment-water mixture reached the required transparency. Three measurements of each sample were used to calculate the average grain-size distribution. Results were calculated by averaging triplicate measurements of each sample and are given in volume percentages (vol. %) for 116 grain-size classes between 0.04 and 2,000 µm diameter.

The other aliquot of the freeze-dried surface samples was ground to <63 µm with a Planetary Mill Pulverisette 5 (FRITSCH GmbH, Idar-Oberstein, Germany) and used for mineralogical and geochemical analyses. The bulk mineralogy was determined on powder samples using an X-ray diffractometer (D8 Discover; Bruker, Billerica, MA, USA)

with a Cu X-ray tube (λ = 1.5418 Å, 40 kV, 30 mA) and a LYNXE XE detector (opening angle = 2.9464°). The spectrum from 3° to 100° 2-theta was measured in 0.02° steps at 1 second exposure time. Mineral identification was carried out using the software packages SEARCH (Stoe and Cie GmbH, Darmstadt, Germany) and Match! (Crystal Impact 2014, Bonn, Germany), supported by the data base pdf2 (ICDD 2003, Newton Square, PA, USA). The concentration of the minerals was evaluated using the program TOPAS Rietveld (Coelho Software, Brisbane, Australia), which yields a standard deviation of analyzed minerals varying from +/- 2 % (for quartz) to +/- 5 to 10 % (for feldspars and clay minerals; Środoń et al., 2001; Vogt et al., 2002). For the clay mineral group illite the error range can be even higher (Scott 1983). Given these uncertainties, a detection limit of 5 % is considered in the discussion of the mineralogical composition of the surface sediments.

Total organic carbon (TOC) as well as total carbon (TC), total nitrogen (TN) and total sulfur (TS) were measured with a vario MICRO cube and vario EL cube combustion elemental analyzers (Elementar Analysesysteme Corp., Langensebold, Germany), respectively. For the TOC measurements, 15 mg of sediment powder was placed into metallic silver containers, heated to 100 to 120°C, and treated three times with a few drops of HCl (32 %) to dissolve carbonates. The metallic silver containers were then wrapped and pressed into silver paper, and the resulting pellets were analyzed for their TOC concentration using the vario EL cube. All concentrations are given as mean values of duplicate measurements. For TC, TN and TS measurements with the vario MICRO cube, 10 mg of sediment powder was placed in zinc containers, with 20 mg of tungsten (VI) oxide (WO_2) added to catalyze oxidation. The total inorganic carbon (TIC) was calculated as the difference between TC and TOC. Analytical errors were determined on internal and external reference material. The C/N ratio is calculated as the weight ratio of TOC and TN.

For quantitative analyses of the inorganic element composition of the surface samples, including concentrations of selected major, minor and trace elements (Ti, K, Al, Mg, Ca, Fe, Cr and Mn), 0.5 g of dry and ground bulk sample material was digested using a near-total digestion protocol with HCl, nitric (HNO_3), perchloric ($HClO_4$) and hydrofluoric (HF) acids in heated and closed teflon vessels. Measurements were performed by means of inductively coupled plasma-mass spectroscopy (ICP-MS) at Activation Laboratories Ltd., Ancaster, ON, Canada.

Separate Si measurements were conducted by energy-dispersive X-ray fluorescence (ED-XRF) using a portable analyzer (NITON XL3t; Thermo Fisher Scientific, Waltham, MA, USA) at the University of Cologne, Germany. Triplicate measurements were performed on pellets of freeze-dried and ground sample aliquots, which were pressed into teflon rings under 12 bars, and subsequently covered with a 4 µm polypropylene film (X-ray film, TF-240-255, Premier Lab Supply, Port St. Lucie, FL, USA). Measurements were performed using a gold anode X-ray source (70 kV) and the 'mining-minerals-mode'. The secondary X-rays of element-specific photon energies were detected with a silicon drift detector and processed by a digital signal processor. Si concentrations (in ppm) were calculated from the element-specific fluorescence energies and compared with external and internal reference materials (STDS-4, BCR142R and BCR-CRM 277).

The carbon isotopic composition of bulk OM ($\delta^{13}C_{OM}$) in the sediment was measured on a set of 42 subsamples at Brown University, Providence, RI, USA. For that purpose, ca 50 mg of sediment was acidified in HCl (2 N) for one hour at 80ºC to remove

carbonate minerals. The acid-treated samples were subsequently rinsed in deionized water and centrifuged four times to remove any excess HCl. The samples were then freeze-dried and homogenized prior to isotopic analysis. The $\delta^{13}C_{OM}$ values were measured using a Carlo Erba Elemental Analyzer coupled to a Thermo DeltaV Plus isotope ratio mass spectrometer (Thermo Fisher Scientific, Waltham, MA, USA). The analytical precision determined through replicate measurements of internal sediment standards was 0.16 ‰. All results are reported relative to the Vienna PeeDee Belemnite (VPDB) standard.

I.2.4.3 Elevation model, interpolation and statistical analysis

A digital elevation model (DEM) of Lake Towuti and its surrounding was calculated using ArcGIS (Esri, Inc., Redlands, CA, USA). The model is based on open source satellite data for Sulawesi provided by the United States Geological Survey (Aster Global DEM based on the Shuttle Radar Topography Mission carried out by the National Aeronautics and Space Administration at 1 arc-second 30 m spatial resolution). Spatial interpolation of the analytical surface sediment data was carried out with the software Surfer 9 (Golden Software Inc., Golden, CO, USA) using the kriging method.

Statistical analyses employed on the surface sediment data sets comprise end-member (EM) unmixing, principal component analysis (PCA) and a redundancy analysis (RDA). EM analyses were carried out on normalized and standardized grain-size (EM_{GS}), chemical (EM_{Chem}) and mineralogical (EM_{Min}) data sets. Assuming a sedimentary mixture from different sources the mixing model in all cases can be written as:

$$X = AS + E \quad (1)$$

where X represents the n-by-m matrix of n samples (one per row) and m variables (relative abundance of individual data). Matrix A (n-by-l) denotes the mixing proportion of l end-members for the n samples, S represents the m properties of the l EMs and E is the error matrix of residuals. The uncertainties of the EM analyses are controlled by the errors of the data sets used.

The EM algorithm developed by Heslop and Dillon (2007) adopting the approach of Weltje (1997) was applied. The decision criterion of how many EMs are included in the three models is based partly on the coefficients of determination derived from the PCA. Nevertheless, the number of the respective EMs should also be reasonable in the geological context of the data set (Weltje, 1997; Weltje and Prins, 2007). Residuals of the EM models include analytical errors and non-identified additional sources of variability.

All other multivariate statistical analyses were carried out with the Excel-based software Addinsoft XLSTAT (STATCON GmbH, Witzenhausen, Germany) The PCA was conducted with the sand content and the concentrations of selected elements determined by ICP-MS and XRF analyses (Fe, Mg, Al, Si, K, Ca, Cr and Ni). In the RDA, the results derived from the PCA are expanded by the concentrations of major minerals, the MS and TOC values and the C/N ratio. The correlation matrix includes all data except $\delta^{13}C_{OM}$ and the concentrations of diatom frustules, sponge spicules and tephra particles, which all were determined on a subset of the surface samples only.

I.2.5 Results

I.2.5.1 Biological particles

The surface samples of Lake Towuti consist mostly of dark greenish-grey, structureless clastic sediments with low but varying amounts of amorphous OM, macrofossils and microfossils. Macrofossils include plant remains and wood fragments, which frequently occur in near-shore, shallow-water samples as well as a few deepwater samples in Towuti's northern basin (samples 16, 17 and 22; Table I.2.1; Figure I.2.1). In addition, mollusc macrofossils were observed in four samples (samples 18, 50, 51 and 83) that are located proximal to the shore in water depths of less than 4.5 m.

Diatom frustules and sponge spicules are the most abundant microfossils observed in the sediments (Figure I.2.3). They are, however, quite rare, and together average only 0.46 % of the total number of the detected sediment particles, with the highest concentrations reaching 2.34 % (sample 5). The concentrations of these particles relative to the total sediment mass are considerably lower, as sample pretreatment prior to particle detection enhanced their abundance. The diatom frustule content is somewhat elevated in front of the Timampu inlets at the northwestern shore and in front of the Mahalona River at the northern shore, and shows pronounced maxima in front of the Tomerakah and Taora rivers at the eastern shore and along the southeastern shore near the Lengke and Lantibu rivers (Figure I.2.1, Figure I.2.3A, Figure I.2.4A). Some of the discovered diatoms were identified as Pinnularia sp. and Surirella robust var. splendida, the latter of which is known to occur in all Malili Lakes, Lake Poso to the northwest and possibly on Java Island (Roy et al., 2007; Sabo et al., 2008; Vaillant et al., 2011; Bramburger et al., 2014).

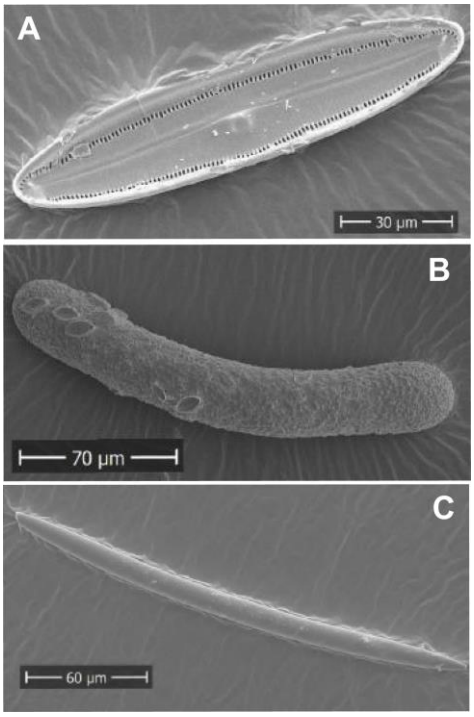

Figure I.2.3 Scanning Electron Microscope (SEM) images showing (A) a single, well-preserved benthic diatom, (B) a sponge spicule with rounded ends and smaller benthic diatoms attached, and (C) a sponge spicule with tip ends

Sponge spicules occur in two different forms, both up to 200 µm in length. One form has an ornamented surface structure with rounded ends, whereas the other is smooth with sharp tip ends (Figure I.2.3B and C). Since both types are very similarly

distributed within the lake, their abundances are shown as combined in Figure I.2.4B. The highest abundances of spicules were detected in the northern part of Lake Towuti, between the Mahalona and Timampu rivers, and in the eastern part of the lake, in particular in front of the Lemo-Lemo and Tomerakah rivers. Somewhat elevated values also occur at the southern shore, in front of the Tokolalo River.

I.2.5.2 Physical properties

The grain-size distribution (classification after Udden, 1914 and Wentworth, 1922) of surface sediments in Lake Towuti is highly variable. Sand (63 to 2000 µm) ranges from 0.0 to 82.8 % of the sediment and shows highest concentrations in the vicinity of large inlets, such as the Mahalona River, and generally higher values close to the shore (Figure I.2.5A). With increasing distance to the inlets and the shores, the sand content rapidly decreases. In the central part of the lake, sand is absent in 41 samples, but still accounts for 10.1 % and 20.5 % in samples 16 and 17 in the northernmost part of the lake, in 174.9 and 195.5 m water depths, respectively. Silt (2 to 63 µm) ranges from 11.9 to 75.9 % and also shows highest concentrations in front of major inlets, in particular the Mahalona, Timampu, and Loeha rivers (Figure I.2.5B), but reaches its highest concentrations further away from the river inlets compared to the sand fraction. The clay fraction (<2 µm) varies between 3.4 % and 71.8 % and has highest concentrations in parts of the lake most distal from the inlets (Figure I.2.5C).

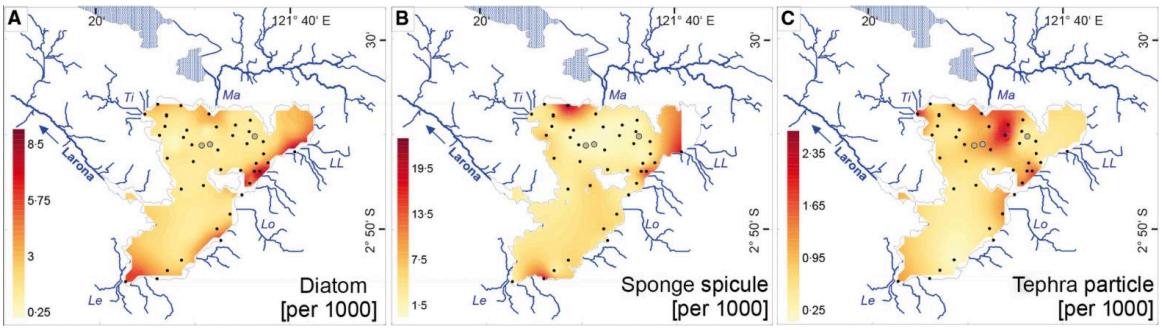

Figure I.2.4 Distribution of (A) diatoms, (B) sponge spicules, and (C) tephra particles in the surface sediments of Lake Towuti. The surface sediment samples are indicated by black dots, the ICDP drill sites by grey circles, and the names of major rivers by abbreviations (cf. Figure I.2.2)

The sand, silt, and clay distributions are reflected by two distinct non-parametric EMs, which explain 85.4 % of the variance in the grain-size data set and 93.7 % of the median variance of the samples (Figure I.2.5D). One EM_{GS} represents the fine-grained fraction, with an average of 60.6 % clay, 39.4 % silt and no sand, whereas the other EM_{GS} is characteristic for the coarse-grained fraction with 13.2 % clay, 57.9 % silt and 28.9 % sand.

The MS (0.7 to 10.4x10^{-6} kg/m^3) exhibits highest values at shallow, coastal sites along the eastern and southern shores, and in front of the Mahalona River (Figure I.2.5E). The MS values are positively correlated with the sand and silt contents (Figure I.2.5A and B).

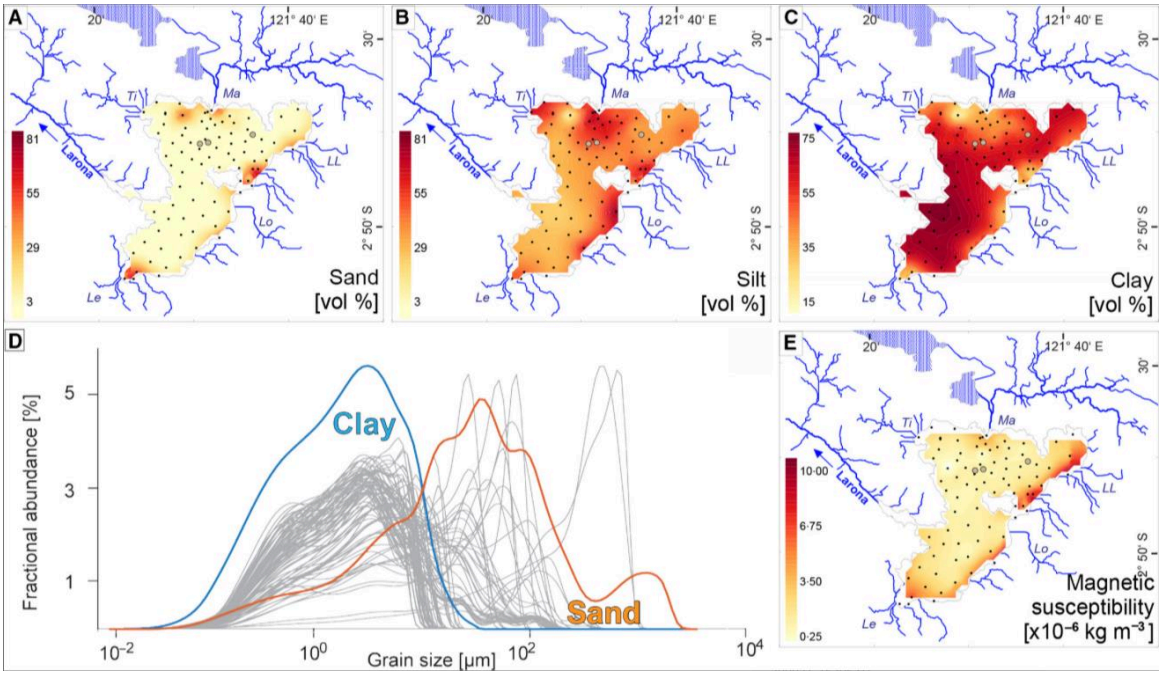

Figure I.2.5 Distribution of physical properties in the surface sediments of Lake Towuti, with (A) the sand, (B) the silt, and (C) the clay contents, (D) the grain-size variations of all 84 samples (grey curves) along with their end-members representing clay (blue) and silt and sand (red), as well as (E) the magnetic susceptibility (MS). In (A) to (C) and (E) the surface sediment samples are indicated by black dots, the ICDP drill sites by grey circles, and the names of major rivers by abbreviations (cf. Figure I.2.2)

I.2.5.3 Geochemistry

The TOC content (0.17 to 6.43 %) is highest in the northeastern and southwestern areas of the lake, close to the shores but distant from the major inlets (Figure I.2.6A). The C/N ratio (4.5 to 24.0) is elevated in some near-shore areas, in particular in the northeastern and eastern parts of the lake (Figure I.2.6B), which partly overlap with elevated TOC contents. The C/N values do not show a clear relationship with the locations of major inlets. A different pattern is shown by the $\delta^{13}C$ ratio (-37.45 to -32.18 ‰), which is characterized by distinctly heavier values in front of the Mahalona River (Figure I.2.6C).

The concentrations of Ti (0.03 to 0.41 %), K (0 to 1.56 %), Al (2.0 to 9.1 %) and Si (7.1 to 19.6 %) reach their highest values in front of the Loeha River (Figure I.2.6D to G). Ti, K and Al concentrations remain high towards the deeper central part of the southern basin, whereas Si is slightly enriched in front of the Mahalona River in the north. Mg (2.3 to 18.5 %) shows a strong maximum in front of the Mahalona River, as do Ca (0.27 to 5.31 %) and Cr (0.12 to >1 %; Figure I.2.6H to J). Ca and Cr have additional maxima in other near-shore areas, but at different location; Ca exhibits a pronounced maximum also in front of the Timampu inlets, while Cr is enriched in the southern and northeastern lake parts. The distribution of Fe (6.5 to 28.9 %) partly tracks that of Cr, with the most prominent enrichment occurring in the southern and northeastern parts of the lake (Figure I.2.6K). Nevertheless, Fe shows a distinct minimum in front of the Mahalona River, where Cr concentrations are high. The distribution of Mn (0.06 to

0.56 %) differs from all other elements, with maximum values in the northeastern lake and in the central southern part of the lake, in front of the Larona outflow (Figure I.2.6L).

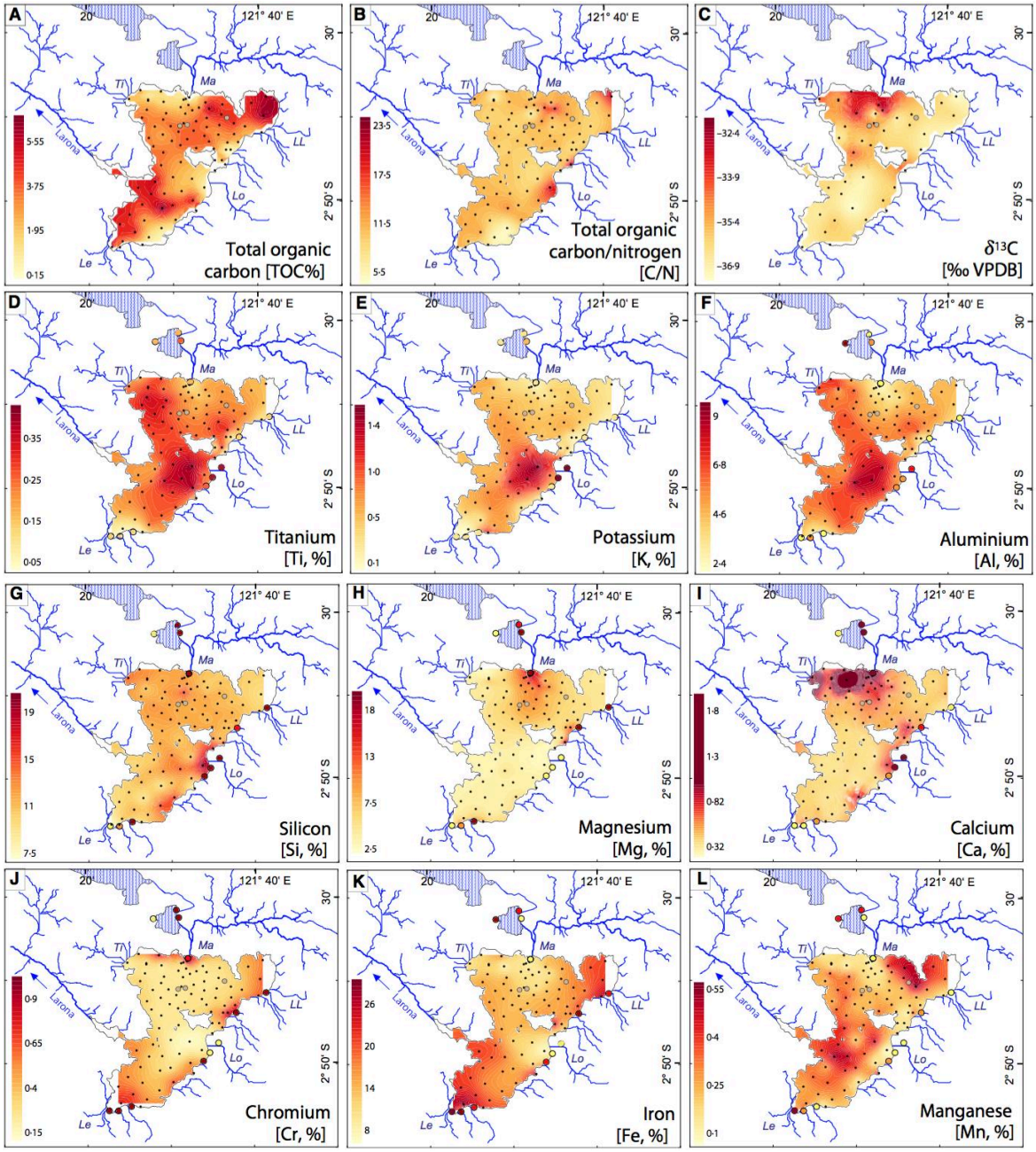

Figure I.2.6 Distribution of geochemical properties in the surface sediments of Lake Towuti, reflecting biogenic deposition (TOC, C/N, $\delta^{13}C_{OM}$) (A to C) as well as the accumulation of selected major elements (Ti, K, Al, Si, Mg, Ca, Fe) and trace elements (Cr, Mn) (D to L). For comparison, the elemental composition of river sediments (after Costa et al., 2015) is shown by open circles with the same colour scale as for the surface sediments. The surface sediment samples are indicated by black dots, the ICDP drill sites by grey circles, and the names of major rivers by abbreviations (cf. Figure I.2.2)

I.2.5.4 Mineralogy

Minerals of the serpentine group (including antigorite, nacrite, greenalite, lizardite and chrysotile) constitute 12.6 to 62.3 % of the mineral assemblage and thus are the most abundant minerals in the surface sediments of Lake Towuti (Figure I.2.7A). This group has high concentrations over a large part of the lake but particularly in front of the Mahalona, Tomerakah and Taora rivers. This is due to maxima of antigorite (Figure I.2.7B) and nacrite (not shown) in these areas, which range from 5.5 to 48.2 % and 5.7 to 17.7 % in the sediments, respectively. A clearly different pattern is shown by the serpentine mineral greenalite, which reaches up to 16.0 % in several samples from the southern basin of the lake, but is almost absent in the northern basin (Figure I.2.7C). Lizardite and chrysotile were only detected in few samples at low concentrations close to the detection limit of 5 %.

The surface sediments contain significant amounts of four clay mineral groups: smectite, illite, chlorite, and kaolinite. Smectite clays (including saponite, montmorillonite, vermiculite and other phases) constitute up to 46.4 % of the minerals present (Figure I.2.7D). They are heterogeneously distributed, but with distinct minima for instance in front of the Timampu, Mahalona and Loeha rivers. Illite has a distinct maximum (with up to 61.8 %) in front of the Timampu inlets (Figure I.2.7E). High concentrations also occur close to the Mahalona and Loeha rivers, and in southwestern parts of the lake, including the area in front of the outflowing Larona River. Chlorites are also enriched in front of the Mahalona River, reaching maximum values of 17 % (Figure I.2.7F). Except for this similarity, chlorite shows a distribution opposite to illite, with minima in front of the Timampu and Loeha rivers, and some enrichment in other near-shore areas. Compared to the other clay mineral groups, kaolinite shows a homogeneous distribution, comprising up to 22.9 % of the sediment (Figure I.2.7G). The only exception is the area in front of the Mahalona River, which has significantly reduced kaolinite concentrations.

The distribution of quartz (2.5 to 45.0 %, Figure I.2.7H) is characterized by a distinct maximum in front of the Loeha inlet and slightly enriched values in the northwestern part of the lake, particularly in front of the Timampu inlets. A generally opposite pattern is shown by goethite, which constitutes up to 16.2 % of the present minerals (Figure I.2.7I). Goethite shows highest concentrations in most of the southern lake basin and in the northeastern region of the northern basin, and minima in front of the Timampu, Mahalona and Loeha rivers. The same minima are shown by the amphibole tremolite, which ranges from 7.3 to 54.2 % (Figure I.2.7J). The amphibole hornblende was detected in only eight samples, located in front of the Timampu, Mahalona and Loeha rivers, with low concentrations of 3.6 to 5.9 % (Figure I.2.7K). Additional minerals close to the detection limit of ca 5 % are combined as ´others´ (Figure I.2.7L), which constitute 7.5 to 21.4 % of the present minerals. This group includes greenalite, magnetite, siderite, cuprite and spinel, also showing highest concentrations in front of the Timampu, Mahalona and Loeha rivers.

Tephra particles, mostly as glass shards, were found at low concentrations (<2.62 particles/1000) across the lake (Figure I.2.4C). Maxima occur southeast of the Mahalona River and, less pronounced, in other near-shore areas of the northwestern (off the Timampu inlets), eastern (off the Tomerakah, Taora, and Loeha rivers), and southern lake (off the Tokolalo, Lantibu and Lengke rivers).

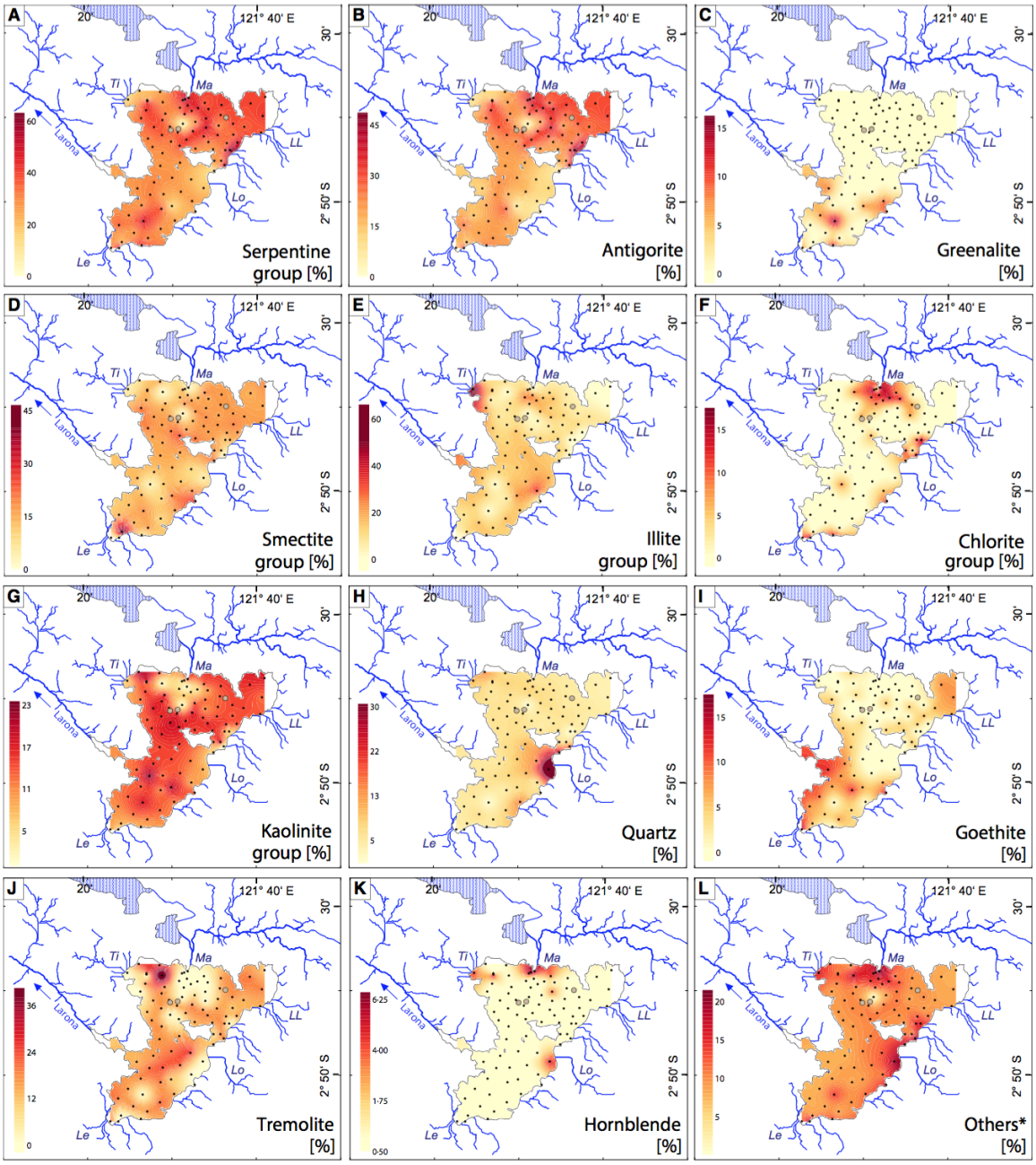

Figure I.2.7 Distribution of major minerals in the surface sediments of Lake Towuti, comprising the serpentine group with antigorite and greenalite (A-C), the clay mineral groups smectite, illite, chlorite, and kaolinite (D-G), the oxides quartz and goethite (H, I), the amphiboles tremolite and hornblende (J, K), and other minerals (L). The surface sediment samples are indicated by black dots, the ICDP drill sites by grey circles, and the names of major rivers by abbreviations (cf. Figure I.2.2)

I.2.6 Discussion

The physical, chemical, mineralogical and biological properties of the surface sediments from Lake Towuti show distinct spatial patterns (Figure I.2.4 - I.2.7) that reflect a variety of external and internal processes.

I.2.6.1 Sediment supply to the lake

Since it can be assumed that the dense vegetation in the catchment of Lake Towuti stabilizes the slopes and restricts aeolian sediment transport, the majority of allochthonous material supplied to the lake is likely of fluvial origin. This assumption is supported by strongly enriched sand and silt contents of the lake sediments in front of the major inlets, reaching values beyond those of other near-shore areas (Figure I.2.5). Furthermore, there is a generally good correspondence between the elemental compositions of these lake sediments and those of the adjacent rivers in the different geologically distinct catchments (Costa et al., 2015; Figure I.2.2 and Figure I.2.6).

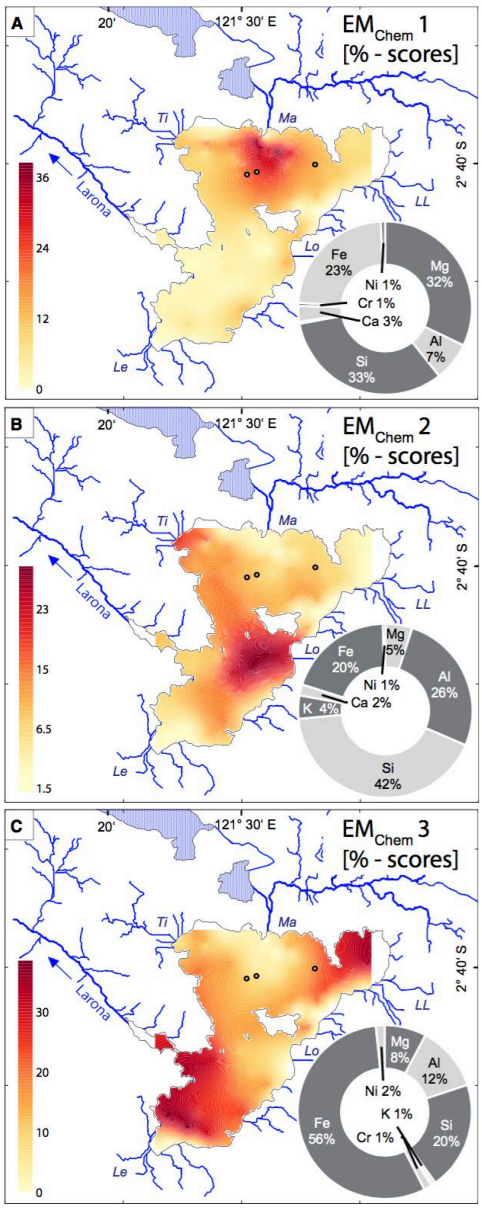

Figure I.2.8 End-member diagrams of the major and trace elements in the surface sediments of Lake Towuti, reflecting fluvial supply by the Mahalona River at the northern shore (EMChem 1; A), by the Timampu inlets at the northwestern shore and the Loeha River at the eastern shore (EMChem 2; B), and by the Lengke inlet at the southern shore and the Lemo-Lemo inlet at the northeastern shore (EMChem 3; C). The ICDP drill sites are indicated by grey circles and the names of major rivers by abbreviations (cf. Figure I.2.2)

Statistical analysis of the geochemical data from the lake sediments identifies three major chemical end-members (Figure I.2.8). $EM_{Chem\ 1}$ is characterized by the highest Mg abundance, as well as relatively high Si scores, and is clearly elevated in front of the Mahalona River. $EM_{Chem\ 2}$ is characterized by the highest Si and Al scores and shows maxima in the northern part of Towuti's southern basin and, less pronounced,

in the northwestern part of the lake. $EM_{Chem\ 3}$ is marked by a very high Fe score, and is highest in the southern and northeastern parts of the lake. Merging these with mineralogical, sedimentological and biogeochemical datasets, summarized by an RDA (Figure I.2.9), a correlation matrix of all data (Supplementary Material [SM] Figure SI.2.1), and an end-member analysis of the mineralogical data (SM Figure SI.2.2), five distinct fluvial sediment sources can be defined: (i) the Mahalona River to the north; (ii) the Timampu inlets to the northwest; (iii) the Loeha River to the east; (iv) the Lengke River to the south; and (v) the Lemo-Lemo River to the northeast of Lake Towuti (Figure I.2.2).

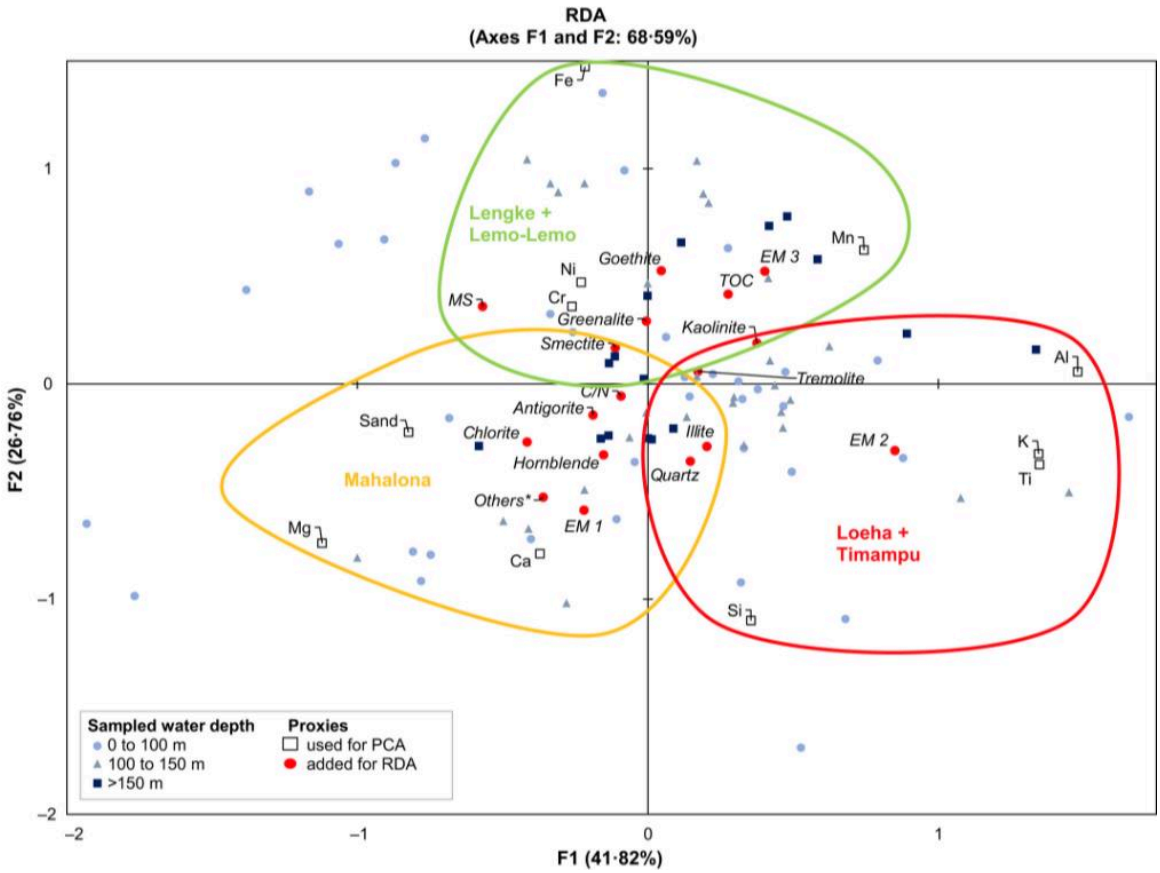

Figure I.2.9 Redundancy analysis (RDA) plot showing the surface samples from Lake Towuti, with their water depths indicated by different symbols along with most of the geochemical, physical, and mineralogical data obtained and the geochemical end-members $EM_{Chem\ 1}$ to $EM_{Chem\ 3}$ (cf. Figure I.2.8)

Mahalona River

The sediment deposited near the Mahalona River has elevated values of Mg and Si, and to a lesser extent Ca and Cr in front of the river delta ($EM_{Chem\ 1}$; Figure I.2.8A and Figure I.2.9). High Mg concentrations (Figure I.2.6H) were also found in adjacent lake surface sediment samples by Weber et al. (2015) and in the Mahalona River itself by Costa et al. (2015) and Goudge et al. (2017). The enrichment of Mg can best be explained by an elevated supply of Mg-rich serpentines (Figure I.2.7A, SM Figure SI.2.2A), for example antigorite and lizardite. Antigorite shows a maximum in front of the Mahalona River (Figure I.2.7B) and is positively correlated with Mg (r = 0.58, SM Figure SI.2.1). The Mg-end-member lizardite exclusively occurs in the same area, albeit with

low concentrations (therefore assigned to other minerals; Figure I.2.7L). Serpentines are minerals derived from the surrounding ophiolites (Figure I.2.2). They are either formed during serpentinization on the deep-sea floor through hydrothermal alteration of mafic and ultramafic rocks prior to their uplift to form the island of Sulawesi, or in the case of lizardite, occur as a secondary mineral provided by chemical weathering in the saprolite zone (Apostolidis and Distin, 1978). Another potential source of Mg could be chlorites, detected in small amounts in the serpentinized peridotites to the north of Lake Towuti. Chlorites have generally lower concentrations in Lake Towuti, but do have a distinct maximum in front of the Mahalona River (Figure I.2.7F, SM Figure SI.2.2A).

The relatively high Si concentrations in front of the Mahalona River (Figure I.2.6G) may be explained by fluvial input of silicates, including the serpentine minerals antigorite (Figure I.2.7A) and lizardite; the illite clay mineral group (Figure I.2.7E) and the chlorite clay mineral group (Figure I.2.7F), as well as hornblende (Figure I.2.7K). Additional supply may originate from quartz veins, which were observed in the saprolite and laterite horizons of soil profiles to the north of Lake Towuti (Silver et al., 1983). Furthermore, the Si distribution shows a similar pattern to that of tephra particles (Figure I.2.4C), which likely originate from volcanoes located in North Sulawesi (Wilson and Moss, 1999). The tephra particles are enriched in the surface sediments in front of the major inlets, suggesting fluvial remobilization from the catchment. The highest concentrations in front of the Mahalona River might be due to successive remobilization from the Quaternary alluvium making up most of the catchment of the Lampensiu River, a triburary of the Mahalona River (Figure I.2.1 and Figure I.2.2), where volcanic ash from several eruptions could have accumulated.

In contrast to Mg and Si, the enrichment of Ca in front and west of the Mahalona Delta (up to 5.31 %; Figure I.2.6I) cannot exclusively be traced back to supply from the Mahalona River. This is indicated by the Ca concentration in the Mahalona River sediment, which average 1.31 % (Costa et al., 2015), thereby being higher than in many of the rivers entering Lake Towuti, but lower than the concentrations observed in the lake sediment in this region (Figure I.2.7A). Hence, the Ca enrichment cannot be explained by fluvial supply from the Mahalona River alone but needs additional sources. The most likely source is in-situ production from calcareous macrofossils, such as molluscs. Molluscs are not present in the Mahalona River but were found in shallow waters of Lake Towuti (<4.5 m water depth), for instance at sample location 18 directly in front of the Mahalona Delta (Table I.2.1; Figure I.2.1).

The Cr enrichment in front of the Mahalona Delta (up to >1 %; Figure I.2.6J) also cannot solely be explained by fluvial supply, since the Cr concentrations in the Mahalona River sediments (0.93 %) are lower than the average values of the rivers entering the lake (1.35 %; Costa et al., 2015). The Cr predominantly derives from Cr-spinels, including chromite, which originate from the ultramafic and mafic catchment rocks and are included in the group of “other minerals” (Figure I.2.7L). Cr-spinels have been detected by EDX analysis on thin sections in the basal, sandy parts of turbidites occurring in a piston core (Co1230) taken in front of the Mahalona Delta (Vogel et al., 2015). Spinels observed in the smear slides of Lake Towuti´s sediments are quite large and almost euhedral mineral grains. Their presence in surface sediments in front of the Mahalona Delta is confirmed by EDX analyses. Since the observed high Cr values generally occur in coarser-grained, sandy sediments (Figure I.2.5A), the concentrations of Cr-spinels may be enriched by shallow-water winnowing leading to particle-size sorting.

Another potential source of Cr in front of the Mahalona River could be mining and smelting. Mining and smelting has taken place since 1968 to the north of Lake Towuti, in the catchments of Lake Matano and Lake Mahalona (Figure I.2.2) and thus could have significantly changed the composition of the surface sediment samples. However, since samples from this study integrate ca 200 to 250 years, any anthropogenic Cr pollution would have occurred during only 25 % of this time and thus would significantly be diluted. In any case a significant contamination of Cr from the mines and smelters is highly unlikely. First, the Cr concentrations in the lake surface and river sediments argue against a significantly increased fluvial supply via the Mahalona River; in fact, the highest Cr concentrations occur in the Lengke, Lantibu and Tokolalo inlets (1.00 to 2.38 %; Costa et al., 2015), furthest from the mine smelter. Second, an aeolian supply would have led to a Cr enrichment in particular in the lake centre via atmospheric deposition of fine particles followed by shallow-water winnowing; however, the Cr concentrations are lowest in the centre of the lake (<1200 ppm). Third, the Cr concentrations in the surface sediments close to TDP Site 1 (Figure I.2.1) are comparable to the Holocene samples of a sediment core from the same area (Costa et al., 2015), which represent the geogenic background. This also suggests that contamination by Fe from mining and smelting can be excluded, since Fe shows particularly low concentrations in front of the Mahalona River and in the central lake basin.

Loeha and Timampu Rivers

$EM_{Chem\ 2}$ is reflected by high amounts of Si, Ca, Ti, K and Al (Figure I.2.8B and Figure I.2.9) and shows the strongest maximum offshore from the Loeha and Bantilang rivers along the eastern shore in the southern part of the lake (Figure I.2.6D to G and I). A secondary maximum of $EM_{Chem\ 2}$ occurs in the northwestern corner of the lake, offshore from the Timampu inlets. Slightly higher Si concentrations in front of the Timampu and Loeha rivers than in front of the Mahalona River (see above) suggest additional Si supply from the sandstones and siltstones occurring in the Wasuponda Mélange to the northwest and from the metasediments exposed to the east of Lake Towuti, respectively (Figure I.2.2).

Elevated Ca concentrations in front of the Timampu and Loeha rivers may partially be explained by in-situ production from calcareous macrofossils, which for instance occur at sampling sites 2 and 5 close to the shore off the Timampu inlets (Table I.2.1; Figure I.2.1). Additional sources for the Loeha River may be Ca-bearing minerals in the metasediments, which are exposed in the Loeha catchment (Figure I.2.2). Even higher Ca concentrations in front of the Timampu inlets argue for additional sources in the undefined ultramafic rocks that are widespread in the Timampu catchment (Figure I.2.2). In addition, Ca supply from restricted limestone outcrops, which are known to occur in wider areas to the west of the Timampu catchment, cannot be excluded.

In contrast to Si and Ca, the enrichments of Ti, K and Al in front of the Loeha River, as well as of Ti and Al in front of the Timampu inlets, differ strongly from minimum values of these elements in the sediments in front of the Mahalona River (Figure I.2.6D to F). The enriched Ti content in front of the Loeha River is in agreement with elevated Ti concentrations in the river itself (Costa et al., 2015). Elevated Al content in the northwestern part of the lake was also observed by Weber et al. (2015). The Ti enrichment, as well as that of K and Al, in the Loeha River is likely derived from the felsic metasediments occurring in the catchment (Figure I.2.2). Elevated Ti and Al concentrations in front of the Timampu inlets, corresponding with a depletion in K, are

potentially due to significant sediment supply from the sandstones and siltstones in the Wasuponda Mélange to the northwest of Lake Towuti (Figure I.2.2). The sediment supply obviously includes illite (Figure I.2.7E) and kaolinite (Figure I.2.7G), which may result from intense weathering of silicates. Kaolinite may additionally originate from the laterite soils formed on top of serpentinized and unserpentinized bedrock in the catchment.

Lengke and Lemo-Lemo Rivers

High score percentages of $EM_{Chem\ 3}$ occur in the southern and northeastern parts of Lake Towuti, in front of the Lengke and Lemo-Lemo rivers, respectively (Figure I.2.8C and Figure I.2.9). They mainly reflect very high Fe concentrations (Figure I.2.6K), and are also characterized by elevated Cr (Figure I.2.6J) and Ni concentrations. High Fe and Cr concentrations were also reported by Costa et al. (2015) from sediment samples off of river mouths at the southern shore.

Fe enrichment can predominantly be related to supply from the saprolites and laterites that are formed on top of the peridotites in the catchment (Figure I.2.2) and are characterized by Fe concentrations of up to 49 %. The Fe oxyhydroxide goethite is the dominant mineral phase of these Fe oxides. This corresponds well with positive correlations of the $EM_{Chem\ 3}$ scores with goethite ($r = 0.72$; SM Figure SI.2.1) and Fe concentrations ($r = 0.69$; SM Figure SI.2.1). Another mineral likely contributing to the Fe enrichment in the sediments is magnetite. Magnetite has been detected with less than 5 % abundance in the surface sediments (therefore assigned to other minerals; Figure I.2.7L). It may be supplied to the lake from the catchment, where it was found to be enriched in the coarse fraction of the laterites and detected as an accessory mineral in the peridotite rocks. Magnetite is also produced in the water column of Lake Towuti (Tamuntuan et al., 2015; Vuillemin et al., 2016). In the southern lake area additional Fe supply is likely derived from greenalite, the Fe-enriched form of the serpentine group, a common mineral phase in the serpentinized ultramafic bedrock that reaches concentrations of up to 16.1 % (sample 68) in the surface sediments (Figure I.2.7C).

The elevated concentrations of Cr and Ni in the lake surface sediments can also be traced back to supply from the saprolite and laterite horizons in the catchment. There, they are enriched by secondary serpentinization at the bedrock-soil interface. In addition, weathering of Cr-spinels releases Cr and Ni, which can be incorporated into silicates such as kaolinite (Koppelman et al., 1980; Jiang et al., 2010; Figure I.2.7G). Cr may also be incorporated into goethite (Figure I.2.7I), as suggested by a distinct positive correlation ($r = 0.62$, SM Figure SI.2.1).

Steep catchment slopes

While the abundances of $EM_{Chem\ 1}$ and $EM_{Chem\ 2}$ appear to reflect distinct fluvial sediment sources, $EM_{Chem\ 3}$ may also be influenced by shoreline and catchment morphologies. Highest $EM_{Chem\ 3}$ scores occur in front of the southwestern and northeastern shores, where the slopes at the shoreline are particularly steep (Figure I.2.1). Hence, the adjacent lake sediments could be influenced not only by fluvial sediment supply but also by mass wasting and direct run-off from the slopes, (e.g. Vogel et al., 2015). These processes may have intensified recently due to increased deforestation in the catchment of Lake Towuti (Nasution, 2007), driven by manual wood factories, regional population growth as well as the expansion of the agriculture area per farmer (Dechert et al., 2004). Deforestation could have increased the vulnerability of the

slopes to mass wasting and run-off, possibly, but not exclusively in combination with high seismic activity.

When mass movement and run-off events occur, they can enter the lake, spreading fine-grained material from the laterites far into the lake, as indicated by the broad distribution of the clay fraction (Figure I.2.5C). Together with high contents of the particularly fine-grained clay mineral group smectite (Figure I.2.7D), this suggests a low-energy setting, with limited fluvial supply to the distal lake areas.

I.2.6.2 Lake-internal physical and chemical processes

The highest transport energies in Lake Towuti, as indicated by increased sand and silt content, occur in front of major inlets, in shallow waters along the lake shores, and in areas influenced by subaquatic mass movement processes (Figure I.2.5A and B).

The sediments directly in front of the inlets often show enriched sand content (Figure I.2.5A). Further offshore, the sediments are characterized by high silt content, in particular in front of the Mahalona, Timampu and Loeha rivers (Figure I.2.5B). This reflects successive deposition from suspension and hydrodynamic sorting with distance from the inlet. The extension of the silt enrichment relatively far into the lake suggests that the distribution is also influenced by hyperpycnal flows or by wave-driven sediment resuspension and focusing from the river mouths to the deeper lake areas.

High sand content also characterizes the lake areas close to shorelines in between some of the inlets (Figure I.2.5A), in particular at sampling sites with distances of less than 1 km from the shore. These areas differ from those adjacent to steep slopes, thus excluding an impact of terrestrial mass movement and rather suggesting shoreline erosion, resuspension and lateral sediment transport along the lake shores, presumably by wave action.

Recent subaquatic mass movements are indicated in the northern part of Lake Towuti, close to TDP Site 2 (Figure I.2.1). There, the surface sediments have sand contents of 10.1 %, 20.5 % and 3.2 % at sampling locations 16, 17 and 22, respectively, in water depths between 171.4 m and 195.5 m and at distances between 2.8 km and 4.5 km to the shore (Figure I.2.1). The position of this sand enrichment can neither be explained by fluvial supply nor by near-shore redeposition, so it most likely results from deposition by lateral transport via mass movement events. This suggestion is supported by the appearance of terrestrial macrofossils at all three locations, since macrofossils otherwise are enriched in near-shore samples only (Table I.2.1). Furthermore, sample 16 exhibits a characteristic bimodal grain-size distribution, which according to Vogel et al. (2015) is an indicator for increased sediment input from hyperpycnal flows in deeper, distal parts of Lake Towuti. The composition of the mass movement deposits suggests sourcing from the Mahalona Delta slopes at the northern shore. Without having detailed information on the structure of the delta, it is inferred that these mass movement deposits are turbidites. The occurrence of at least one turbidite in the surface sediments, which were deposited during the past ca 200 to 250 years, is not surprising, taking the mean turbidite recurrence rate of ca 300 years identified by Vogel et al. (2015) in a 19.8 m long sediment core covering the last ca 30,000 years close to TDP Site 2 in the same area (Figure I.2.1).

Furthermore, the composition of the surface sediments argues for at least occasional oxygenation of the entire water column. For instance, both the Fe and Mn distributions are highly heterogeneous and do not show systematically lower

concentrations in deeper water that might be expected from reductive Fe dissolution of oxides under anoxic conditions (Davison 1993; Kylander et al., 2011; Figure I.2.6K and L). Although low Mn and Fe values in the northern basin could result from the absence of oxygen, much higher values in the southern basin, reaching water depths of 160 m, clearly argue against permanently anoxic conditions. Much of this iron could reside in silicates or other minerals that are not susceptible to reductive dissolution. However, the distribution of the Fe oxyhydroxide goethite, which has a high concentration in the southern basin (Figure I.2.7I), also argues against permanent anoxia. Measurements of temperature, oxygen and dissolved iron concentration in the upper 140 m of Lake Towuti's water column, conducted between September 1995 and June 2015 (Costa et al., 2015; Vuillemin et al., 2016), suggest that Lake Towuti usually does not mix to the bottom and is oxygen depleted in water depths below ca 100 m.

I.2.6.3 Biogenic sedimentation

TOC is concentrated in the southwestern and in the northeastern parts of Lake Towuti (Figure I.2.6A), in areas close to steep catchment slopes and distant to major inflows (Figure I.2.1), and where fine-grained deposition prevails (Figure I.2.5C). The C/N ratio in the surface sediments averages 10.8, arguing for a predominance of autochthonous biogenic production. These values slightly exceed traditional end-member values for aquatic OM, but given Lake Towuti's N-poor, ultraoligotrophic status in combination with water temperatures of ca 28°C and occasional mixing of the water column, these C/N ratios at least partly result from substantial lake-internal nitrogen recycling (Talbot et al., 2006). Intermixing with allochthonous OM sources is indicated by elevated C/N ratios in front of the Mahalona and Loeha inlets, and in front of the steep slopes at the northeastern shore, suggesting fluvial and gravitational supply. This is partly supported by terrestrial macrofossil remains, such as leaves, rods and twigs, which mainly occur in near-shore samples, but also distal areas in front of the Mahalona River (Table I.2.1). Allochthonous OM supply via the Mahalona River is furthermore indicated by a distinct trend towards heavier $\delta^{13}C_{OM}$ values in the northern lake part (Figure I.2.6C). Potentially, this trend reflects stronger supply of terrestrial OM originating from tropical grasses (C4 plants; Meyers and Lallier-Vergès, 1999), which are widespread in the plain terrain of the Mahalona River. However, samples with elevated $\delta^{13}C_{OM}$ values do not have higher C/N ratios, suggesting low terrigenous OM contributions. Alternatively, autochthonous OM can obtain a terrigenous $\delta^{13}C_{OM}$ value while maintaining low C/N ratios due to algal and microbial metabolism of terrestrially-sourced dissolved inorganic and organic carbon (Webb et al., 2016). Data from this study suggests that this may occur on a catchment scale in Lake Towuti.

Additional indicators of autochthonous biological production in Lake Towuti are calcareous shells, which mainly occur in near-shore samples (3, 12, 25, 32, 73, 74 and 79; Figure I.2.1), and sponge spicules and diatoms (Figure I.2.3). The sponge spicules are enriched in near-shore areas, in front of some minor inlets (Figure I.2.4B). This suggests that the sponges prefer locations with mildly turbid waters and low sedimentation rates, which provide nutrients but do not result in burial of the filter-feeding organisms. The proximity to the inlets may be of importance for nutrient supply, including Si, given the ultraoligotrophic status of the lake. The distribution of diatoms in the surface sediments is similar to that of the sponge spicules (Figure I.2.4A). The diatoms may be partly dependent on the nutrient supply by the inlets; however, since the majority of the

diatoms in Lake Towuti are benthic, they likely derive the Si and P required for their growth from sediment reflux. If so, the distribution of the benthic diatoms is mainly supported by shallow and clear waters, with sufficient light available (modern Secci depth is 22 m, therefore light transparency is ca 40 m; Lehmuslouto et al., 1995; von Rintelen et al., 2012).

Based on the TOC contents, C/N ratios, $\delta^{13}C_{OM}$ values, and concentrations of calcareous shells, sponge spicules and diatoms in the surface sediments, the biogenic sedimentation in Lake Towuti is predominantly controlled by natural processes. Except for the potential impact of deforestation in the northeastern and southwestern lake catchments, which could lead to enhanced TOC supply via mass wasting and direct run-off, an anthropogenic impact is not discernible in data from this study. This includes the lack of evidence for increased primary production due to nutrient supply in front of major settlements (cf. Figure I.2.2).

I.2.6.4 Implications for the palaeorecord

The understanding gained from the here presented study of surface sediments concerning the modern processes operating in Lake Towuti has a number of implications for similarly structured research projects on large tropical lakes and, in this case, also for the ongoing palaeoenvironmental investigation of the TDP drill cores (Figure I.2.1). These sediment cores predominantly consist of pelagic clays, which are interrupted by turbidites, tephra layers, diatomaceous oozes, and, at the base of the core, a variety of shallow-water and fluvial deposits, such as peats, gravels and sands (Russell et al., 2016).

This study of modern lake sediments provides a detailed characterization of the chemical, sedimentological and biological signature of fluvial and other sediment sources. It will facilitate disentangling the changing influence of different sediment sources in the palaeorecord of this complex tropical setting. The pelagic sediments in Lake Towuti today are predominantly of fluvial origin, with chemical and mineralogical compositions characteristic of five distinct source areas. This finding will enable researchers to relate changes in fluvial sediment supply in the palaeorecord to environmental processes, in particular tectonic activity, lake-level fluctuations and changes in the hydrological connectivity of lakes Towuti, Mahalona and Matano (Figure I.2.1; Russell et al., 2016). As suggested by investigations in the catchment of Lake Towuti, the kaolinite content in the pelagic sediments may reflect the degree of chemical weathering. In contrast, the current study has revealed that classical proxies for lake mixing behavior, such as the concentrations of redox-sensitive elements (e.g., Fe, Mn and Cr), siderite and vivianite (Melles et al., 2012; Vuillemin et al., 2017), do not unequivocally reflect anoxia and thus have to be interpreted with caution in ancient sediments of Lake Towuti.

In short sediment records from Lake Towuti, turbidity currents have been identified as an important sedimentation process (Vogel et al., 2015). The sub-recent turbidite identified in this study in the northern basin of Lake Towuti differs from the pelagic sediments by the occurrences of coarser grains, terrestrial OM and shallow-water calcareous macrofossils. This composition indicates that the turbidites can remobilize and transport shallow-water sediments into the deep lake basin. With the multidisciplinary characterization of the various shallow-water areas in modern Lake Towuti, potentially different sources of turbidites in the palaeorecord may be attributed to

specific source areas in the lake. This in turn, could be indicative of areal changes in sediment supply and tectonic activity through time. Furthermore, variations in the frequency and thickness of turbidites may be traced back to changes in earthquake activity, lake-level, precipitation and vegetation.

Tephra occurs in the surface sediments of Lake Towuti as dispersed particles with characteristic grain shapes but not as distinct layers. This indicates that presently, tephra particles are predominantly remobilized and supplied by fluvial activity from the catchment. In the palaeorecord, tephra may thus occur both as a product of direct fallout and as a more diffuse signal of remobilized particles from the catchment. Direct fallout may be differentiated from redeposited tephra by sharper shard edges. Remobilization of the tephra deposited in the catchment can increase the supply of Si and other elements to the lake for a longer period of time. This tephra supply may have played an important role for the degree of biogenic production by diatoms and sponges, taking its high Si content and the ultraoligotrophic, Si-limited nature of the lake. Diatoms and sponge spicules are rare in the surface sediments, but occur close to areas with higher concentrations of tephra particles in the surface sediments.

The shallow-water surface sediment samples are composed of rather coarse-grained deposits with high MS values and Cr concentrations. They exclude peat and differ from all other deposits mainly by the occurrence of diatom frustules and sponge spicules. Hence, coarse-grained deposits with comparable compositions occurring in the TDP cores can be traced back to shallow-water environments at the coring site during the time of deposition, or to extensive redeposition of the sediments. The occurrence of peat layers and fluvial sediments, in contrast, represent times, when no lake existed at the drill sites.

I.2.7 Conclusion

A multi-proxy approach combining sedimentological, geochemical, mineralogical and microscopic analyses with statistical methods was performed on a set of 84 surface sediment samples from Lake Towuti, Indonesia. The results provide a detailed understanding of the major physical, chemical and biological processes controlling modern sedimentation in this tropical lake. These results will facilitate the reconstruction of the climatic and environmental history based upon the composition of Towuti Drilling Project (TDP) drill cores recovered in 2015.

The composition of the surface sediments in Lake Towuti is highly heterogeneous. Sedimentation is mainly controlled by fluvial sediment supply from five distinct source areas. The individual chemical and mineralogical signatures can be traced relatively far into the lake. Near-shore environments are additionally influenced by redeposition due to wave action. Most calm settings, with deposition of fine-grained particles and organic matter (OM), occur in the central lake, most distal to the major inlets. There, coarser grain sizes are related to aquatic mass movement events that ignite hyperpycnal flows. Biogenic silica derived from diatoms and sponges is found only in special ecological niches, which are dependent on individual water depths, light availabilities, nutrients and the degree of turbidity.

Significant anthropogenic impacts on the composition of the surface sediment samples, which average the sedimentation over the past ca 200 to 250 years, is not evident from this study’s data. However, mass wasting and direct run-off on the steep northeastern and southwestern catchment slopes may have become amplified by

deforestation. In contrast, Cr and Fe supply from mines and smelters to the north of Lake Towuti is not yet reflected in the chemistry of the surface sediments. The same holds true for human impact on the amount of biogenic accumulation, which seems unaffected by influences from nearby settlements.

In interpretation of the TDP cores, attribution of chemical and mineralogical proxies to different sediment source areas is of special importance. Based on measurements of the respective indicators on the pelagic sediments and mass movement deposits in the drill cores, the individual source areas may be reconstructed. This will help with understanding changes in palaeogeography, e.g. in the hydrological connectivity between the Malili Lakes through the Mahalona River (Figure I.2.1), which could be controlled by climatic variations within the Indo-Pacific Warm Pool (IPWP) region as well as tectonic activity. Taking the environmental limitations of diatoms and sponges today, investigations of siliceous microfossils in the TDP cores may contribute to the understanding of lake-level changes, which could be triggered by orbital-scale climate changes and/or short-term El Niño – Southern Oscillation (ENSO) events. Furthermore, they may help to reconstruct the nutrient availability in the water column, which is dependent, for instance, on the weathering conditions in the catchment, on volcanic ash supply and on lake-internal mixing.

TDP Sites 1 and 3 are located in an area (Figure I.2.1), which is dominated by pelagic sedimentation and may be influenced by all three chemically and mineralogically distinct sediment sources ($EM_{Chem\ 1\ to\ 3}$ and $EM_{Min\ 1\ to\ 3}$; Figure I.2.8 and SM Figure SI.2.2). This makes them ideal sites for reconstruction of the regional environmental and climatic history. In contrast, the upper 62 m of TDP Site 2, is mainly built up of mass movement deposits, intercalated with pelagic sediments, and in the present is primarily influenced by only two major sources, reflected by $EM_{Chem\ 1}$ and 3 (Figure I.2.8) as well as $EM_{Min\ 1}$ and 3 (SM Figure SI.2.2). This supports the use of TDP Site 2 for the reconstruction of the fluvial input and mass movement history in the northern basin of Lake Towuti, which may mainly mirror the history of the Mahalona River and the lakes further upstream, but also reflect lake-level fluctuations and seismic events.

I.2.8 Acknowledgements

The Towuti Drilling Project was partially supported by grants from the International Continental Scientific Drilling Program (ICDP), the US National Science Foundation (NSF), the German Research Foundation (DFG, grant no. ME 1169/26), the Swiss National Science Foundation (SNSF; 20FI21_153054/1 and 200021_153053/1), Brown University, Genome British Columbia, and the Ministry of Research, Technology, and Higher Education (RISTEK). PT Vale Indonesia, the US Continental Drilling Coordination Office, the GeoForschungsZentrum Potsdam, and DOSECC Exploration Services are acknowledged for the logistical assistance to the project. This research was carried out with permission from RISTEK, the Ministry of Trade of the Government of Indonesia, the Natural Resources Conservation Center (BKSDA), and the Government of Luwu Timur of Sulawesi. We like to thank Hannah Jauss, University of Cologne, for her competent help in the FlowCam analyses. Special thanks are due to Paul Hamilton for the diatom identification and information about their preferred living conditions, to Doug Haffner for providing unpublished chemical data of the water column, and to Rachel Sheppard for providing unpublished mineralogical and spectroscopically data of the surface sediment samples.

We are also grateful to two anonymous reviewers and editors Peir Pufahl and Ola Kwiecien for their comments and suggestions, which greatly helped to improve the manuscript.

I.2.9 References

Aldrian, E. and Dwi Susanto, R. (2003) Identification of three dominant rainfall regions within Indonesia and their relationship to sea surface temperature. Int. J. Climatol., 23, 1435-1452.

Apostolidis, C.I. and Distin, P.A. (1978) The kinetics of the sulphuric acid leaching of nickel and magnesium from reduction roasted serpentine. Hydrometallurgy, 3, 181-196.

Bramburger, A.J., Hamilton, P.B. and Haffner, G.D. (2014) Effects of a simulated upwelling event on the littoral epilithic diatom community of an ancient tropical lake (Lake Matano, Sulawesi Island, Indonesia). Hydrobiologia, 739, 133-143.

Chiang, J.C.H. (2009) The Tropics in Paleoclimate. Annu. Rev. Earth Planet. Sci., 37, 263-297.

Chen, D. and Cane, M.A. (2008) El Niño prediction and predictability. J Comput Physics, 227, 3625-3640.

Clement, A.C., Cane, M.A. and Seager, R. (2001) An orbitally driven tropical source for abrupt climate change. J. Climate, 14, 2369-2375.

Coelho, A.A. (2003) Indexing of powder diffraction patterns by iterative use of singular value decomposition. J. Appl. Crystallogr., 36, 86-95.

Costa, K.M., Russell, J.M., Vogel, H. and Bijaksana, S. (2015) Hydrological connectivity and mixing of Lake Towuti, Indonesia in response to paleoclimatic changes over the last 60,000 years. Palaeogeogr. Palaeoclimatol. Palaeoecol., 417, 467-475.

Davison, W. (1993) Iron and manganese in lakes. Earth-Sci. Rev., 34, 119-163.

Dechert, G., Veldkamp, E. and Anas, I. (2004) Is soil degradation unrelated to deforestation? Examining soil parameters of land use systems in upland Central Sulawesi, Indonesia. Plant and Soil, 265, 197-209.

Francke, A., Wennrich, V., Sauerbrey, M., Juschus, O., Melles, M. and Brigham-Grette, J. (2013) Multivariate statistic and time series analyses of grain-size data in Quaternary sediments of Lake El'gygytgyn, NE Russia. Clim. Past, 9, 2459-2470.

Golightly, P.J. and Arancibia, O.N. (1979) The chemical compostion and infrared spectrum of nickel-and iron-substituted serpentine from a nickeliferous laterite profile-Soroako-Indonesia. Can. Mineral., 17, 719-728.

Goudge, T.A., Russell, J.M., Mustard, J.F., Head, J.W. and Bijaksana S. (2017) A 40,000 yr record of clay mineralogy at Lake Towuti, Indonesia: Paleoclimate reconstruction from reflectance spectroscopy and perspectives on paleolakes on Mars. Geol. Soc. Am. Bull., B31569-1.

Haffner, G.D., Hehanussa, P.E. and Hartoto, D. (2001) The biology and physical processes of large lakes of Indonesia: Lakes Matano and Towuti. In: The Great Lakes of the World: Food-web, Health and Integrity (Eds M. Munawar and R.E. Hecky), pp. 183-192. Backhuys Publishers, Leiden.

Hamilton, W.B. (1979) Tectonics of the Indonesian region (Geol Surv Profess Paper 1078). US Govt. Print. Off., 308 pp.

Hecky, R.E., Campbell, P. and Hendzel, L.L. (1993) The stoichiometry of carbon, nitrogen, and phosphorus in particulate matter of lakes and oceans. Limnology and Oceanography, 38, 709-724.

Hendon, H.H. (2003) Indonesian Rainfall Variability: Impacts of ENSO and Local Air-Sea Interaction. J. Climate, 16, 1775-1790.

Heslop, D. and Dillon,M. (2007) Unmixing magnetic remanence curves without a priori knowledge. Geophys. J. Intern., 170, 556-566.

Jiang, M.Q., Jin, X.Y., Lu, X.Q. and Chen, Z.L. (2010) Adsorption of Pb (II), Cd (II), Ni (II) and Cu (II) onto natural kaolinite clay. Desalination, 252, 33-39.

Kadarusman, A., Miyashita, S., Maruyama, S., Parkinson, C.D. and Ishikawa, A. (2004) Petrology, geochemistry and paleogeographic reconstruction of the East Sulawesi Ophiolite, Indonesia. Tectonophysics, 392, 55-83.

Konecky, B., Russell, J. and Bijaksana, S. (2016) Glacial aridity in central Indonesia coeval with intensified monsoon circulation. Earth-Planet Sci. Lett., 437, 15-24.

Koppelman, M.H., Emerson, A.B. and Dillard, J.G. (1980) Adsorbed Cr (III) on chlorite, illite and kaolinite - an X-ray photoelectron spectroscopic study. Clay and Clay Minerals, 28, 119-124.

Kylander, M.E., Ampel, L, Wohlfarth, B. and Veres, D. (2011) High-resolution X-ray fluorescence core scanning analysis of Les Echets (France) sedimentary sequence: new insights from chemical proxies. J. Quatern. Sci., 26, 109-117.

Lehmusluoto, P., Machbub, B., Terangna, N., Rusmiputro, S., Achmad, F., Boer, L., Brahmana, S.S., Priadi, B., Setiadji, B., Sayuman, O. and Margana, A. (1995) National Inventory of the Major Lakes and Reservoirs in Indonesia. Expedition Indodanau Technical Report, Edita Oy, Helsinki, 71 pp.

Melles, M., Brigham-Grette, J., Minyuk, P.S., Nowaczyk, N.R., Wennrich, V., DeConto, R.M., Anderson, P.M., Andreev, A.A., Coletti, A., Cook, T.L., Haltia-Hovi, E., Kukkonen, M., Lozhkin, A.V., Rosén, P., Tarasov, P., Vogel, H. and Wagner, B. (2012) 2.8 million years of Arctic climate change from Lake El'gygytgyn, NE Russia. Science, 337, 315-320.

Meyers, P.A. and Lallier-Vergès, B.J. (1999) Lacustrine sedimentary organic matter records of Late Quaternary paleoclimates. Journal of Paleolimnology, 21, 345-372.

Monnier, C., Girardeau, J., Maury, R.C. and Cotton, J. (1995) Back-arc basin origin for the East Sulawesi ophiolite (eastern Indonesia). Geology, 23, 851-854.

Nasution, S.H., (2007) Growth and condition factor of Rainbow Selebensis (Telmatherina celebensis Boulenger) in Lake Towuti, South Sulawesi. Ind. Fish. Res. J., 13, 117-123.

Pierrehumbert, R.T. (1999) Subtropical water vapor as a mediator of rapid global climate change. In: Mechanisms of Global Climate Change at Millennial Time Scales (Eds P.U. Clark, R.S. Webb and L.D. Keigwin), American Geophys. Union, Geog. Monogr., 112, 1-35.

PT Vale (2017) vale.com/indonesia/EM/aboutvale/history/pages/default.aspx

Robinson, K.M. (1986) Stepchildren or Progress - The Political Economyof Development in an Indonesian Mining Town. SUNY Press, Albany, New York, 323 pp.

Roy, D., Paterson, G., Hamilton, P.B., Heath, D.D. and Haffner, G.D. (2007) Resource-based adaptive divergence in the freshwater fish Telmatherina from Lake Matano, Indonesia. Molecular Ecology, 16, 35-48.

Russell, J.M., Bijaksana, S., Vogel, H., Melles, M., Kallmeyer, J., Ariztegui, D., Crowe, S., Fajar, S., Hafidz, A., Haffner, D., Hasberg, A., Ivory, S., Kelly, C., King, J., Kirana, K., Morlock, M., Noren, A., Grady, R., Ordonez, L., Stevenson, J., von Rintelen, T., Vuillemin, A., Watkinson, I., Wattrus, N., Wicaksono, S., Wonik, T., Bauer, K., Deino, A., Friese, A., Henny, C., Imran, Marwoto, R., Ngkoimani, L.O., Nomosatryo, S., Safiuddin, L.O., Simister, R., Tamuntuan, G. (2016) The Towuti Drilling Project: paleoenvironments, biological evolution, and geomicrobiology of a tropical Pacific lake. Scientific Drilling, 21, 29-40.

Russell, J.M., Vogel, H., Konecky, B.L.K., Bijaksana, S., Yongsong, H., Melles, M., Wattrus, N., Costa, K. and King, J. (2014) Glacial forcing of central Indonesian hydroclimate since 60,000 y B.P. PNAS, 111, 5100-5105.

Sabo, E., Roy, D., Hamilton, P.B., Hehanussa, P.E., McNeely, R. and Haffner, G.D. (2008) The plankton community of Lake Matano: factors regulating plankton composition and relative abundance in an ancient, tropical lake of Indonesia. Hydrobiologia, 615, 225-235.

Scott, P. (1983) The Geometries of 3Manifolds. Bulletin of the London Mathematical Society, 15, 401-487.

Spakman, W. and Hall, R. (2010) Surface deformation and slab–mantle interaction during Banda arc subduction rollback. Nature Geoscience, 3, 562-566.

Silver, E.A., McCaffrey, R. and Smith, R.B. (1983) Collision, rotation, and the initiation of subduction in the evolution of Sulawesi, Indonesia. J. Geophys. Res.: Solid Earth, 88, 9407-9418.

Środoń, J., Drits, V.A., McCarty, D.K., Hsieh, J.C. and Eberl, D.D. (2001) Quantitative X-ray diffraction analysis of clay-bearing rocks from random preparations. Clay Clay Mineral., 49, 514-528.

Talbot, M.R., Jensen, N.B., Lærdal, T. and Filippi, M.L. (2006) Geochemical responses to a major transgression in giant African lakes. Journal of Paleolimnology, 35, 467-489.

Tamuntuan, P., Bijaksana, S., King, J., Russell, J., Fauzi, U., Maryunani, K. and Aufa, N. (2015) Variation of magnetic properties in sediments from Lake Towuti, Indonesia, and its paleoclimatic significance. Palaeogeography, Palaeoclimatology, Palaeoecology, 420, 163-172.

Tauhid, Y.I. and Arifian, J. (2000) Pengamatan Jangka Panjang Kondisi Air Danau Towuti. Jurnal Sains and Teknologi Modifikasi Cuaca, 1, 91-100.

Udden, J.A. (1914). Mechanical composition of clastic sediments. Geol. Soc. Am. Bull., 25, 655-744.

Vaillant, J.J., Haffner, G.D. and Cristescu, M.E. (2011) The ancient lakes of Indonesia: towards integrated research on speciation. Integrative and Comparative Biology, 51, 634-643.

Vogel, H., Wessels, M., Albrecht, C., Stich, H.B. and Wagner, B. (2010) Spatial variability of recent sedimentation in Lake Ohrid (Albania/Macedonia). Biogeosciences, 7, 3333-3342

Vogel, H., Russell, J.M., Cahyarini, S.Y., Bijaksana, S., Wattrus, N., Rethemeyer, J. and Melles, M. (2015) Depositional modes and lake-level variability at Lake Towuti, Indonesia, during the past ~29 kyr BP. J. Paleolimnol., 54, 359-377

Vogt, C., Lauterjung, J. and Fischer, R.X. (2002) Investigation of the clay fraction (<2µm) of the clay minerals society reference clays. Clay Clay Mineral., 50, 388-400.

von Rintelen, T., von Rintelen, K., Glaubrecht, M., Schubart, C.D. and Herder, F. (2012) Aquatic biodiversity hotspots in Wallacea: the species flocks in the ancient lakes of Sulawesi, Indonesia. In: Biotic Evolution and Environmental Change in Southeast Asia. (Eds D.J. Gower, K. Johnson, B. Rosen, L. Rüber and S. Williams), pp. 290-315. Cambridge University Press, Cambridge.

Vuillemin, A., Friese, A., Alawi, M., Henny, C., Nomosatryo, S., Wagner, D., Crowe, S.A. and Kallmeyer, J. (2016) Geomicrobiological features of ferruginous sediments from Lake Towuti, Indonesia. Front Microbiol., 7, 1007. doi: 10.3389/fmicb.2016.01007

Watkinson, I.M. and Hall, R. (2016) Fault systems of the eastern Indonesian triple junction: evaluation of Quaternary activity and implications for seismic hazards. In: Geohazards in Indonesia: Earth Science for Disaster Risk Reduction (Eds P.R. Cummins and I. Meilano) Geological Society, London, Special Publications, 441, SP 441-8.

Webb, M., Barker, P.A., Wynn, P.M., Heiri, O., van Hardenbroek, M., Pick, F., Russell, J.M. and Leng, M. (2016) The interpretation of carbon isotope ratios in freshwater diatom silica. J. Quatern. Sci., 31, 300-309.

Weber, A.K., Russell, J.M., Goudge, T.A., Salvatore, M.R., Mustard, J.F. and Bijaksana, S. (2015) Characterizing clay mineralogy in Lake Towuti, Indonesia, with reflectance spectroscopy. J. Paleolimnol., 54, 253-261.

Weltje, G.J. (1997) End-member modeling of compositional data: numerical-statistical algorithms for solving the explicit mixing problem. Math. Geol., 29, 503-549.

Weltje, G.J. and Prins, M.A. (2007) Genetically meaningful decomposition of grain-size distributions. Sed. Geol., 202, 409-424.

Wennrich, V., Francke, A., Dehnert, A., Juschus, O., Leipe, T., Vogt, C., Brigham-Grette, J., Minyuk, P.S. and Melles, M. (2013) Modern sedimentation patterns in Lake El'gygytgyn, NE Russia, derived from surface sediment and inlet streams samples. Climate of the Past, 9, 135-148.

Wentworth, C.K. (1922) A scale of grade and class terms for clastic sediments. J. Geology, 30, 377-392.

Wilson, M.E. and Moss, S.J. (1999) Cenozoic palaeogeographic evolution of Sulawesi and Borneo. Palaeogeogr. Palaeoclimatol. Palaeoecol., 145, 303-337.

I.2.10 Supplementary Material

Figure SI.2.1 Correlation matrix showing the dependency between the geochemical, granulometric, and mineralogical data of the surface samples from Lake Towuti. Note that this table relies on a reduced data set for only those samples, on which all proxies shown were determined; the real correlation coefficients of two proxies can be higher, when all data existing is considered.

	Fe	clay	EM_{chem} 3	TN	goethite	Ni	Mn	kaolinite	TOC	Cr	TC	Al	tremolite	K	greenalite	Ti	EM_{chem} 1
Fe	**1.00**	**0.79**	**0.96**	**0.65**	**0.69**	**0.79**	**0.59**	**0.48**	**0.46**	**0.71**	**0.46**	**0.26**	**0.29**	0.04	0.20	-0.06	-0.10
clay	**0.79**	**1.00**	**0.70**	**0.68**	**0.54**	**0.45**	**0.60**	**0.62**	**0.34**	**0.32**	**0.31**	**0.49**	0.14	**0.42**	0.23	**0.32**	**0.29**
EM_{chem} 3	**0.96**	**0.70**	**1.00**	**0.60**	**0.72**	**0.82**	**0.51**	**0.45**	**0.44**	**0.79**	**0.44**	**0.33**	**0.37**	0.07	**0.27**	-0.02	-0.06
TN	**0.65**	**0.68**	**0.60**	**1.00**	**0.53**	**0.45**	**0.54**	**0.52**	**0.63**	**0.29**	**0.68**	0.18	0.15	0.10	0.14	0.11	-0.01
goethite	**0.69**	**0.54**	**0.72**	**0.53**	**1.00**	**0.57**	**0.30**	0.24	**0.51**	**0.62**	**0.51**	0.22	0.20	0.09	0.21	-0.01	-0.07
Ni	**0.79**	**0.45**	**0.82**	**0.45**	**0.57**	**1.00**	**0.44**	0.19	**0.30**	**0.58**	**0.28**	0.19	**0.54**	-0.07	0.18	-0.10	-0.18
Mn	**0.59**	**0.60**	**0.51**	**0.54**	**0.30**	**0.44**	**1.00**	**0.43**	**0.43**	0.06	**0.41**	0.22	0.24	0.21	0.11	0.08	0.14
kaolinite	**0.48**	**0.62**	**0.45**	**0.52**	0.24	0.19	**0.43**	**1.00**	**0.27**	0.13	**0.26**	**0.40**	**0.26**	0.21	0.12	**0.28**	**0.26**
TOC	**0.46**	**0.34**	**0.44**	**0.63**	**0.51**	**0.30**	**0.43**	**0.27**	**1.00**	**0.36**	**0.89**	-0.12	-0.05	-0.10	0.15	-0.19	**-0.29**
Cr	**0.71**	**0.32**	**0.79**	**0.29**	**0.62**	**0.58**	0.06	0.13	**0.36**	**1.00**	**0.39**	0.03	0.09	-0.17	**0.34**	**-0.28**	**-0.37**
TC	**0.46**	**0.31**	**0.44**	**0.68**	**0.51**	**0.28**	**0.41**	**0.26**	**0.89**	**0.39**	**1.00**	-0.19	-0.06	-0.19	0.08	**-0.26**	**-0.36**
Al	**0.26**	**0.49**	**0.33**	0.18	0.22	0.19	0.22	**0.40**	-0.12	0.03	-0.19	**1.00**	**0.48**	**0.84**	0.22	**0.77**	**0.87**
tremolite	**0.29**	0.14	**0.37**	0.15	0.20	**0.54**	0.24	**0.26**	-0.05	0.09	-0.06	**0.48**	**1.00**	0.23	-0.18	0.24	**0.31**
K	0.04	**0.42**	0.07	0.10	0.09	-0.07	0.21	0.21	-0.10	-0.17	-0.19	**0.84**	0.23	**1.00**	0.24	**0.75**	**0.91**
greenalite	0.20	0.23	**0.27**	0.14	0.21	0.18	0.11	0.12	0.15	**0.34**	0.08	0.22	-0.18	0.24	**1.00**	0.09	0.07
Ti	-0.06	**0.32**	-0.02	0.11	-0.01	-0.10	0.08	**0.28**	-0.19	**-0.28**	**-0.26**	**0.77**	0.24	**0.75**	0.09	**1.00**	**0.81**
EM_{chem} 1	-0.10	**0.29**	-0.06	-0.01	-0.07	-0.18	0.14	**0.26**	**-0.29**	**-0.37**	**-0.36**	**0.87**	**0.31**	**0.91**	0.07	**0.81**	**1.00**
smectite	0.12	**0.31**	0.04	0.18	-0.03	-0.06	0.04	**0.33**	0.14	-0.02	0.14	-0.09	**-0.35**	0.02	0.12	0.12	-0.07
TS	0.13	0.08	0.08	0.11	0.14	0.04	0.08	-0.16	0.24	0.19	**0.31**	-0.20	-0.15	-0.09	-0.01	-0.16	-0.24
TIC	-0.07	-0.10	-0.07	0.01	-0.06	-0.09	-0.10	-0.06	**-0.36**	0.02	0.11	-0.14	-0.01	-0.17	-0.17	-0.12	-0.11
MS	0.13	**-0.25**	0.21	**-0.29**	0.16	0.05	**-0.36**	-0.23	-0.06	**0.65**	-0.02	**-0.29**	-0.13	**-0.39**	0.05	**-0.46**	**-0.48**
antigorite	-0.11	-0.17	-0.20	-0.04	**-0.25**	-0.05	-0.04	-0.05	0.08	-0.11	0.10	**-0.61**	-0.23	**-0.55**	**-0.32**	**-0.39**	**-0.59**
illite	**-0.31**	-0.20	**-0.27**	**-0.27**	-0.04	**-0.45**	**-0.26**	**-0.30**	-0.19	-0.09	-0.18	0.12	**-0.42**	0.18	0.05	0.10	**0.25**
quartz	**-0.35**	**-0.29**	**-0.28**	**-0.39**	-0.24	**-0.32**	**-0.25**	-0.16	**-0.40**	-0.23	**-0.43**	0.21	0.16	**0.40**	-0.22	0.21	**0.48**
sand	**-0.34**	**-0.61**	-0.21	**-0.34**	-0.20	**0.26**	-0.20	**-0.41**	-0.19	-0.17	-0.22	-0.09	**0.44**	-0.21	-0.08	-0.14	-0.11
hornblende	**-0.34**	**-0.37**	**-0.34**	**-0.31**	**-0.27**	**-0.34**	-0.24	-0.24	**-0.25**	-0.13	**-0.27**	**-0.33**	**-0.42**	-0.24	-0.09	-0.21	-0.19
Si	**-0.49**	**-0.29**	**-0.49**	**-0.47**	**-0.42**	**-0.48**	**-0.34**	**-0.26**	**-0.59**	**-0.42**	**-0.54**	0.12	-0.02	**0.29**	**-0.35**	**0.25**	**0.45**
Na	**-0.52**	**-0.66**	**-0.38**	**-0.51**	**-0.32**	-0.02	**-0.35**	**-0.43**	**-0.41**	**-0.32**	**-0.46**	0.11	**0.38**	-0.02	-0.10	0.06	0.19
Ca	**-0.46**	**-0.69**	**-0.33**	**-0.49**	**-0.26**	0.09	**-0.36**	**-0.49**	**-0.34**	-0.22	**-0.38**	-0.07	**0.35**	-0.22	-0.12	-0.10	-0.04
chlorite	**-0.47**	**-0.58**	**-0.48**	**-0.41**	**-0.30**	**-0.26**	-0.24	**-0.54**	-0.08	-0.22	-0.02	**-0.52**	**-0.29**	**-0.28**	-0.08	**-0.36**	**-0.34**
silt	**-0.64**	**-0.64**	**-0.66**	**-0.51**	**-0.47**	**-0.81**	**-0.55**	**-0.37**	-0.24	-0.23	-0.17	**-0.53**	**-0.61**	**-0.32**	-0.21	**-0.26**	**-0.25**
others	**-0.62**	**-0.65**	**-0.56**	**-0.66**	**-0.52**	**-0.39**	**-0.43**	**-0.40**	**-0.48**	**-0.30**	**-0.53**	-0.24	-0.14	-0.09	0.03	-0.12	-0.01
Mg	**-0.60**	**-0.60**	**-0.72**	**-0.41**	**-0.48**	**-0.47**	**-0.42**	**-0.49**	-0.14	**-0.39**	-0.10	**-0.76**	**-0.48**	**-0.55**	**-0.27**	**-0.47**	**-0.58**
EM_{chem} 2	**-0.70**	**-0.72**	**-0.79**	**-0.50**	**-0.56**	**-0.53**	**-0.50**	**-0.55**	-0.23	**-0.44**	-0.18	**-0.78**	**-0.46**	**-0.58**	**-0.32**	**-0.47**	**-0.54**

	smectite	TS	TIC	MS	antigorite	illite	quartz	sand	hornblende	Si	Na	Ca	chlorite	silt	others	Mg	$EM_{chem}2$
Fe	0.12	0.13	-0.07	0.13	-0.11	**-0.31**	**-0.35**	**-0.34**	**-0.34**	**-0.49**	**-0.52**	**-0.46**	**-0.47**	**-0.64**	**-0.62**	**-0.60**	**-0.70**
clay	**0.31**	0.08	-0.10	**-0.25**	-0.17	-0.20	**-0.29**	**-0.61**	**-0.37**	**-0.29**	**-0.66**	**-0.69**	**-0.58**	**-0.64**	**-0.65**	**-0.60**	**-0.72**
$EM_{chem}3$	0.04	0.08	-0.07	0.21	-0.20	**-0.27**	**-0.28**	-0.21	**-0.34**	**-0.49**	**-0.38**	**-0.33**	**-0.48**	**-0.66**	**-0.56**	**-0.72**	**-0.79**
TN	0.18	0.11	0.01	**-0.29**	-0.04	**-0.27**	**-0.39**	**-0.34**	**-0.31**	**-0.47**	**-0.51**	**-0.49**	**-0.41**	**-0.51**	**-0.66**	**-0.41**	**-0.50**
goethite	-0.03	0.14	-0.06	0.16	**-0.25**	-0.04	-0.24	-0.20	**-0.27**	**-0.42**	**-0.32**	**-0.26**	**-0.30**	**-0.47**	**-0.52**	**-0.48**	**-0.56**
Ni	-0.06	0.04	-0.09	0.05	-0.05	**-0.45**	**-0.32**	**0.26**	**-0.34**	**-0.48**	-0.02	0.09	**-0.26**	**-0.81**	**-0.39**	**-0.47**	**-0.53**
Mn	0.04	0.08	-0.10	**-0.36**	-0.04	**-0.26**	**-0.25**	-0.20	-0.24	**-0.34**	**-0.35**	**-0.36**	-0.24	**-0.55**	**-0.43**	**-0.42**	**-0.50**
kaolinite	**0.33**	-0.16	-0.06	-0.23	-0.05	**-0.30**	-0.16	**-0.41**	-0.24	**-0.26**	**-0.43**	**-0.49**	**-0.54**	**-0.37**	**-0.40**	**-0.49**	**-0.55**
TOC	0.14	0.24	**-0.36**	-0.06	0.08	-0.19	**-0.40**	-0.19	**-0.25**	**-0.59**	**-0.41**	**-0.34**	-0.08	-0.24	**-0.48**	-0.14	-0.23
Cr	-0.02	0.19	0.02	**0.65**	-0.11	-0.09	-0.23	-0.17	-0.13	**-0.42**	**-0.32**	-0.22	-0.22	-0.23	**-0.30**	**-0.39**	**-0.44**
TC	0.14	**0.31**	0.11	-0.02	0.10	-0.18	**-0.43**	-0.22	**-0.27**	**-0.54**	**-0.46**	**-0.38**	-0.02	-0.17	**-0.53**	-0.10	-0.18
Al	-0.09	-0.20	-0.14	**-0.29**	**-0.61**	0.12	0.21	-0.09	**-0.33**	0.12	0.11	-0.07	**-0.52**	**-0.53**	-0.24	**-0.76**	**-0.78**
tremolite	**-0.35**	-0.15	-0.01	-0.13	-0.23	**-0.42**	0.16	**0.44**	**-0.42**	-0.02	**0.38**	**0.35**	**-0.29**	**-0.61**	-0.14	**-0.48**	**-0.46**
K	0.02	-0.09	-0.17	**-0.39**	**-0.55**	0.18	**0.40**	-0.21	-0.24	**0.29**	-0.02	-0.22	**-0.28**	**-0.32**	-0.09	**-0.55**	**-0.58**
greenalite	0.12	-0.01	-0.17	0.05	**-0.32**	0.05	-0.22	-0.08	-0.09	**-0.35**	-0.10	-0.12	-0.08	-0.21	0.03	**-0.27**	**-0.32**
Ti	0.12	-0.16	-0.12	**-0.46**	**-0.39**	0.10	0.21	-0.14	-0.21	**0.25**	0.06	-0.10	**-0.36**	**-0.26**	-0.12	**-0.47**	**-0.47**
$EM_{chem}1$	-0.07	-0.24	-0.11	**-0.48**	**-0.59**	**0.25**	**0.48**	-0.11	-0.19	**0.45**	0.19	-0.04	**-0.34**	**-0.25**	-0.01	**-0.58**	**-0.54**
smectite	**1.00**	0.08	-0.01	-0.21	**0.27**	-0.03	-0.04	**-0.41**	-0.12	-0.09	**-0.48**	**-0.49**	-0.07	0.02	-0.02	0.06	0.01
TS	0.08	**1.00**	0.11	**0.28**	0.17	0.03	-0.12	-0.17	-0.13	-0.07	**-0.25**	-0.21	0.20	0.07	-0.07	0.15	0.10
TIC	-0.01	0.11	**1.00**	0.09	0.03	0.04	0.00	-0.04	-0.01	0.18	-0.05	-0.03	0.13	0.17	-0.04	0.10	0.13
MS	-0.21	**0.28**	0.09	**1.00**	0.12	0.15	-0.04	-0.04	0.17	-0.15	-0.06	0.04	0.20	**0.34**	0.18	0.11	0.11
antigorite	**0.27**	0.17	0.03	0.12	**1.00**	**-0.27**	**-0.32**	0.04	**0.27**	**-0.25**	-0.18	-0.02	**0.26**	0.17	**0.29**	**0.58**	**0.53**
illite	-0.03	0.03	0.04	0.15	**-0.27**	**1.00**	**0.28**	-0.16	**0.29**	**0.33**	0.15	0.07	0.13	**0.40**	**0.29**	0.00	0.07
quartz	-0.04	-0.12	0.00	-0.04	**-0.32**	**0.28**	**1.00**	0.08	0.05	**0.75**	**0.33**	0.18	0.17	**0.28**	**0.52**	-0.17	-0.05
sand	**-0.41**	-0.17	-0.04	-0.04	0.04	-0.16	0.08	**1.00**	0.04	0.00	**0.85**	**0.91**	**0.34**	-0.21	**0.38**	0.15	0.24
hornblende	-0.12	-0.13	-0.01	0.17	**0.27**	**0.29**	0.05	0.04	**1.00**	0.18	0.13	0.17	0.14	**0.43**	**0.41**	**0.32**	**0.38**
Si	-0.09	-0.07	0.18	-0.15	**-0.25**	**0.33**	**0.75**	0.00	0.18	**1.00**	**0.28**	0.14	0.12	**0.37**	**0.40**	0.07	0.20
Na	**-0.48**	**-0.25**	-0.05	-0.06	-0.18	0.15	**0.33**	**0.85**	0.13	**0.28**	**1.00**	**0.96**	0.24	-0.01	**0.53**	0.05	0.19
Ca	**-0.49**	-0.21	-0.03	0.04	-0.02	0.07	0.18	**0.91**	0.17	0.14	**0.96**	**1.00**	**0.30**	-0.03	**0.51**	0.17	**0.29**
chlorite	-0.07	0.20	0.13	0.20	**0.26**	0.13	0.17	**0.34**	0.14	0.12	0.24	**0.30**	**1.00**	**0.39**	**0.51**	**0.57**	**0.60**
silt	0.02	0.07	0.17	**0.34**	0.17	**0.40**	**0.28**	-0.21	**0.43**	**0.37**	-0.01	-0.03	**0.39**	**1.00**	**0.43**	**0.59**	**0.67**
others	-0.02	-0.07	-0.04	0.18	**0.29**	**0.29**	**0.52**	**0.38**	**0.41**	**0.40**	**0.53**	**0.51**	**0.51**	**0.43**	**1.00**	**0.36**	**0.46**
Mg	0.06	0.15	0.10	0.11	**0.58**	0.00	-0.17	0.15	**0.32**	0.07	0.05	0.17	**0.57**	**0.59**	**0.36**	**1.00**	**0.97**
$EM_{chem}2$	0.01	0.10	0.13	0.11	**0.53**	0.07	-0.05	0.24	**0.38**	0.20	0.19	**0.29**	**0.60**	**0.67**	**0.46**	**0.97**	**1.00**

Figure SI.2.2 End-member diagrams of the major minerals in the surface sediments of Lake Towuti, reflecting fluvial supply by the Mahalona River at the northern shore ($EM_{Min\ 1}$; A), by the Timampu inlets at the northwestern shore and the Loeha River at the eastern shore ($EM_{Min\ 2}$; B), and by the Lengke inlet at the southern shore and the Lemo-Lemo inlet at the northeastern shore ($EM_{Min\ 3}$; C). The ICDP drill sites are indicated by grey circles and the names of major rivers by abbreviations (cf. Figure I.2.2).

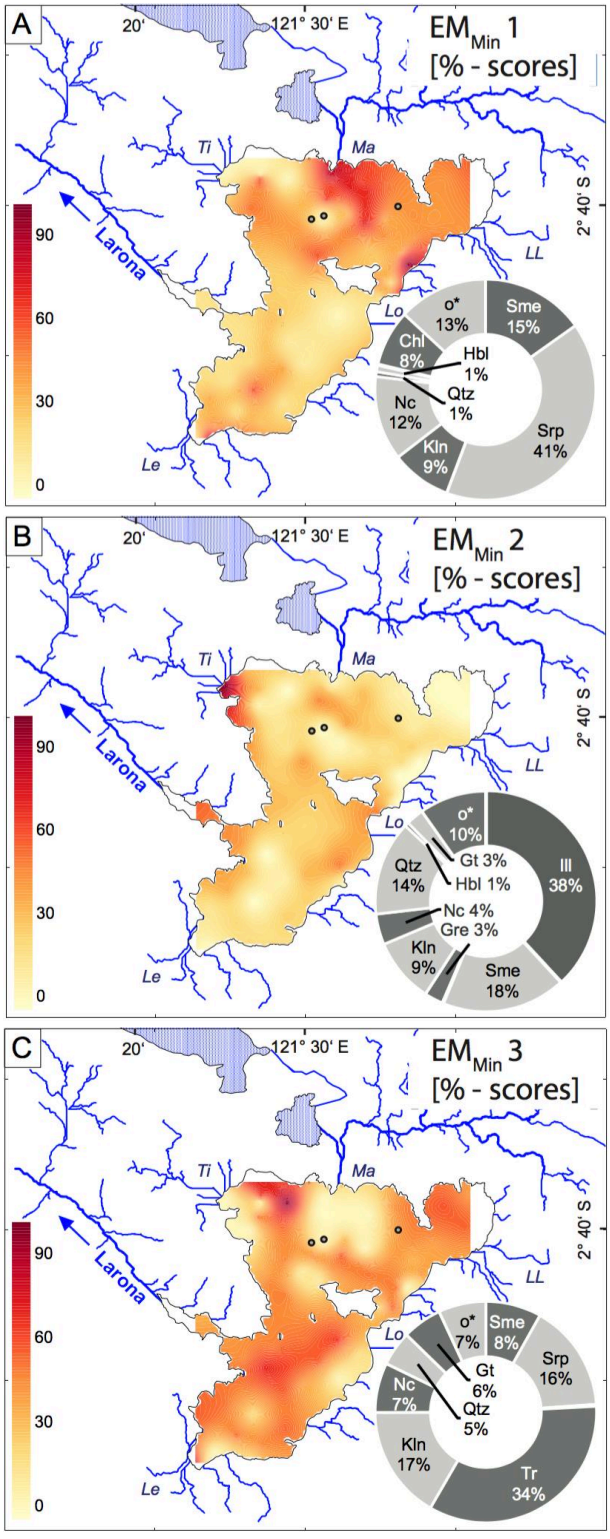

I.3. Characterization of Iron in Lake Towuti Sediment

Rachel Y. Sheppard[1], Ralph E. Milliken[1], James M. Russell[1], M. Darby Dyar[2,3], Elizabeth C. Sklute[2], Hendrik Vogel[4], Martin Melles[5], Satria Bijaksana[6], **Marina A. Morlock[4],** and Ascelina K. M. Hasberg[5]

under review in Chemical Geology

[1]*Department of Earth, Environmental, and Planetary Sciences, Brown University*

[2]*Department of Astronomy, Mt. Holyoke College*

[3]*Planetary Science Institute*

[4]*Institute of Geological Sciences & Oeschger Centre for Climate Change Research, University of Bern*

[5]*Institute of Geology and Mineralogy, University of Cologne*

[6]*Faculty of Mining and Petroleum Engineering, Institut Teknologi Bandung*

I.3.1 Abstract

Sediment collected from Lake Towuti, an ultramafic-hosted lake in Indonesia, preserve a visible alternating pattern of red and green sediments due to variations in clay mineral and Fe-oxide abundance that indicate changes in iron oxidation state through time. To better understand the starting composition of these sediments and the processes that affected them before and after deposition, we carried out spectral, mineralogical, and chemical analyses on catchment, river, and lake sediment samples from across the Malili Lakes system. Despite high Fe abundances in all samples and abundant Fe oxides in lateritic source regions, mineralogical analyses (X-ray diffraction and Mössbauer spectroscopy) of the modern lake sediment show almost no crystalline iron oxides. In addition, sequential Fe extractions suggest an increasing proportion of easily extractable poorly crystalline (X-ray amorphous) material with burial depth. XRD, bulk chemistry, and visible-near infrared (VNIR) spectral reflectance measurements demonstrate that clay mineralogy and bulk chemistry can be inferred from VNIR data. These results provide evidence for variations in Fe mineralogy and crystallinity based on location in the source to sink system. Understanding how the mineralogy and chemistry of sediments within a dilute, ferruginous lake basin are affected by transport, alteration, and deposition from source to sink on Earth, and the degree to which these trends and underlying processes can be inferred from chemical and spectral properties, may provide useful direction in assessing paleoenvironmental conditions on Mars using rover-based payloads.

I.3.2 Introduction

The oxidation state of redox-sensitive elements in lake sediment encodes information on water column conditions and potentially the relative position of the oxycline and/or shoreline through the stratigraphic section. Iron is of particular interest as it is ubiquitous in mafic systems found on Earth and Mars. Moreover, tracking oxidation state changes and mineral hosts of iron during sediment weathering, transport,

deposition, and diagenesis can elucidate varying redox conditions in modern and ancient depositional environments.

Here we examine a suite of samples from Lake Towuti, to characterize the nature of Fe in the sediment of a terrestrial redox-stratified lake. We analyze sediment sampled from soils, rivers, and the lake itself to discriminate between the roles of weathering in the source region, fluvial transport, and early diagenesis in the sediment column on the mineral hosts of Fe. We also examine if key mineralogical and chemical trends, including variations in clay mineralogy, Fe mineralogy and Fe oxidation state, can be inferred from Mössbauer and reflectance spectroscopy of the bulk sediment. Understanding current spatial variations in the mineralogy and chemistry of the uppermost surface sediment and the causes of these variations can provide a foundation for interpreting sediments in deeper lake cores, aid in reconstructing paleoenvironmental conditions on Earth, and provide insight into the chemical and mineralogical evolution of an ancient redox-stratified lake purported to exist on Mars (Hurowitz et al. 2017). In addition, assessing relationships between bulk chemical and spectral properties can lend new insight into how rapid, non-destructive techniques such as visible-near infrared reflectance spectroscopy may be used to decipher past aqueous and atmospheric conditions in mudstones.

I.3.3 Background

I.3.3.1 Malili Lakes: Physical hydrological and geological setting

Lake Towuti is the largest lake in the Malili Lakes system, a set of five tectonic lakes located near the equator on Sulawesi island, Indonesia. Lake Towuti is situated in the East Sulawesi Ophiolite, which is largely composed of unserpentinized harzburgite, dunite, and serpentinized lherzolite, which supplies large quantities of iron and other metals to the lake (Kadarusman et al. 2004). Lake Towuti is fed by several rivers that drain a catchment of approximately 1144 km^2 (Morlock et al. 2018). The main inlet, the Mahalona River, drains two smaller upstream lakes, Matano and Mahalona, and flows into Lake Towuti from the north (Figure I.3.1). Lake Towuti is an open basin, with outflow via the Larona River to the west. The Mahalona River is the largest river entering Lake Towuti, yet much of the sediment from the northern catchments is trapped in Lakes Matano and Mahalona and does not reach Lake Towuti (Costa et al. 2015). Nevertheless, the Mahalona River is also fed by the Lampenisu catchment to the northeast, and sources a large deposit of coarse-grained sediment associated with a prograding delta extending approximately 10 km into Lake Towuti from the mouth of the Mahalona river (Vogel et al. 2015; Morlock et al. 2018). Because of its significant depth, ranging up to ~200 meters, Towuti is a thermally and redox-stratified lake (Costa et al. 2015; Vuillemin et al. 2016). The entire lake system is sulfate-poor (Crowe et al. 2008; Vuillemin et al. 2016).

I.3.3.2 Lake Towuti: Studies of sediment and the water column

Lake Towuti possesses a rare continuous record of tropical sedimentation spanning several glacial cycles, and the system has been used to study sediment response to short- and long-term climate changes (Russell et al. 2014; Vogel et al. 2015; Russell et al. 2016). Because of its heavy-metal-rich mafic/ultramafic catchment (Kadarusman et al. 2004), the sediment in Lake Towuti has elevated concentrations of

redox-sensitive elements that include Cr, Fe, and Mn. Consequently, lake sediment may provide a relatively complete record of redox conditions in the lake over time. Prior studies have examined changes during the past ~60 kyrs, and demonstrate that trends in Fe and redox-sensitive trace elements document more oxidizing conditions during dry periods (Costa et al. 2015). In particular, Lake Towuti sediment exhibits a range of Fe-bearing minerals, and redox cycling is suggested by a down-core pattern of alternating red and green sediments (Costa et al. 2015; Vogel et al. 2015; Goudge et al. 2017). Previous work has inferred that red sediment is enriched in ferric oxides that form when cold, dry periods induce deep mixing and oxygenation of the lake, resulting in oxidation of the bottom waters (Costa et al. 2015). This is a useful heuristic model for changes in lake sediment geochemistry through time, but to date there has been little attempt to investigate the mineralogy of iron sources and sinks in the present-day lake, nor mineralogical changes that accompany variations in sedimentary Fe concentrations in the past.

Previous studies examined a limited number of surface sediment samples from a transect across the northern part of the lake (Weber et al. 2015) and samples from the Mahalona delta and nearby rivers (Goudge et al. 2017). Both studies concluded that the major types of clay minerals in those samples could be identified from visible-near infrared (VNIR) reflectance spectra and that the strength of absorption features within the spectra were correlated with chemical composition of the bulk sample. Recent studies used a larger suite of surface sediment samples to track changes across the lake, concluding that the Mahalona River is the main source of serpentine and its influence relative to kaolinite-rich rivers can be traced in sample X-ray diffraction (XRD) patterns, mid-infrared (MIR) spectra, and elemental abundances (Morlock et al. 2018; Hasberg et al. 2018), but these studies focused on silicate mineral sources and sinks. We conduct analyses on a set of samples used in previous studies (Goudge et al. 2017; Morlock et al. 2018; Hasberg et al. 2018) that span the Lake Towuti system from source (catchment samples) to sink (lake surface sediment samples distributed across the entire basin). We examine if previously reported chemical and clay mineral trends associated with VNIR spectral features are observed within sediments from Lake Towuti as a whole. In addition to characterizing clay mineralogy, we also evaluate differences in the mineral host(s) of Fe between these samples and determine the extent to which VNIR spectra are sensitive to changes in Fe-mineralogy, bulk mineralogy, and bulk chemistry.

I.3.4 Methods

I.3.4.1 Sampling

Samples were collected in 2013 (Costa et al. 2015; Goudge et al. 2017) and during the 2015 Towuti Drilling Project (Russell et al. 2016), and they consist of three different sample types: lateritic soils from the catchment, inflowing river bed sediment, and surficial sediment from the lake floor (Figure I.3.1).

Lateritic soils were collected from six separate, exposed weathered soil profiles. Because of limitations in accessibility, all soil beds were west or northwest of the lake. The 20 soil samples were collected at different depths within the soil profiles, spanning the top of the soil bed to bedrock. Some samples were coarse-grained with distinct pebbles and many had visible pieces of organic material (Morlock et al. 2018).

River bedload samples were collected from twelve separate rivers. The 16 total samples were primarily collected near the river mouths, with four samples collected along the largest inlet, the Mahalona River (Goudge et al. 2017; Weber et al. 2015).

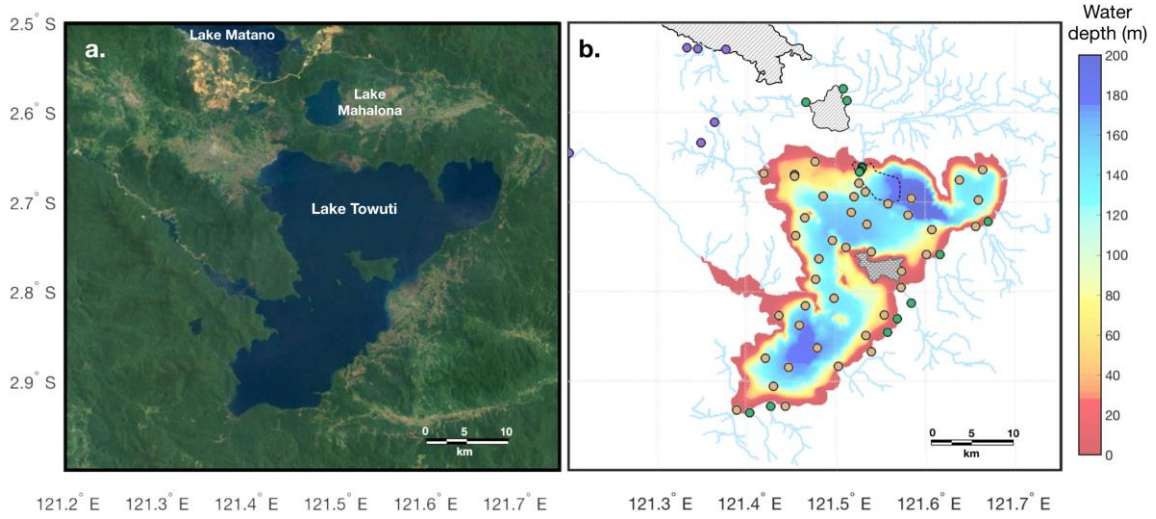

Figure I.3.1 The Malili Lakes System: Lakes Matano, Mahalona, and Towuti, with associated rivers. a. Landsat composite image of the Malili Lakes System, including southeast Lake Matano, Lake Mahalona, and Towuti. b. Bathymetry of Lake Towuti (m). Rivers are in light blue and the delta of coarse-grained material carried in by the Mahalona River is outlined by a dashed line. Brown points are surface sediment sample locations, green are river bedload samples, and purple are locations of laterite samples

Lake surface sediment samples were collected using a polnar grab sampler (UWITEC Corp., Austria). The 42 samples analyzed for this study were mostly fine-grained (most dominated by silt and clay-size material) and relatively homogeneous in appearance (Morlock et al. 2018; Hasberg et al. 2018).

Lake sediment core samples were collected in 2015 by the International Continental Scientific Drilling Program Towuti Drilling Project (ICDP-TDP) from Lake Towuti (Russell et al. 2016). These cores were subsampled at the LacCore facility at the University of Minnesota in 2016.

I.3.4.2 Reflectance spectroscopy

Mineralogy of each sample was determined by powder X-ray diffraction and reflectance spectroscopy (VNIR-IR wavelengths) at Brown University. VNIR spectral parameters, including band depths, were calculated for absorptions characteristic of certain minerals common to the Malili Lakes system (Figure I.3.2). Band depth is a measurement of the strength of an absorption feature and was calculated here based on the method of Clark and Roush (1984). A variety of factors can influence the strength of an absorption band in reflectance spectra, including particle size and strong spectral contrast between absorbing species (e.g., VNIR-transparent minerals such as quartz mixed with highly absorbing, opaque minerals such as ilmenite or magnetite). All samples studies here were ground to fine grain size, lack significant abundances of opaque phases (weak or absent peaks for magnetite and ilmenite in XRD data), and are of roughly equivalent particle size, thus band depth values may provide reasonable proxies for relative mineral abundance. Major mineral phases considered in the analysis

of spectral data were based on previous studies (Goudge et al. 2017; Weber et al. 2015), XRD patterns, and qualitative analysis of the spectra themselves.

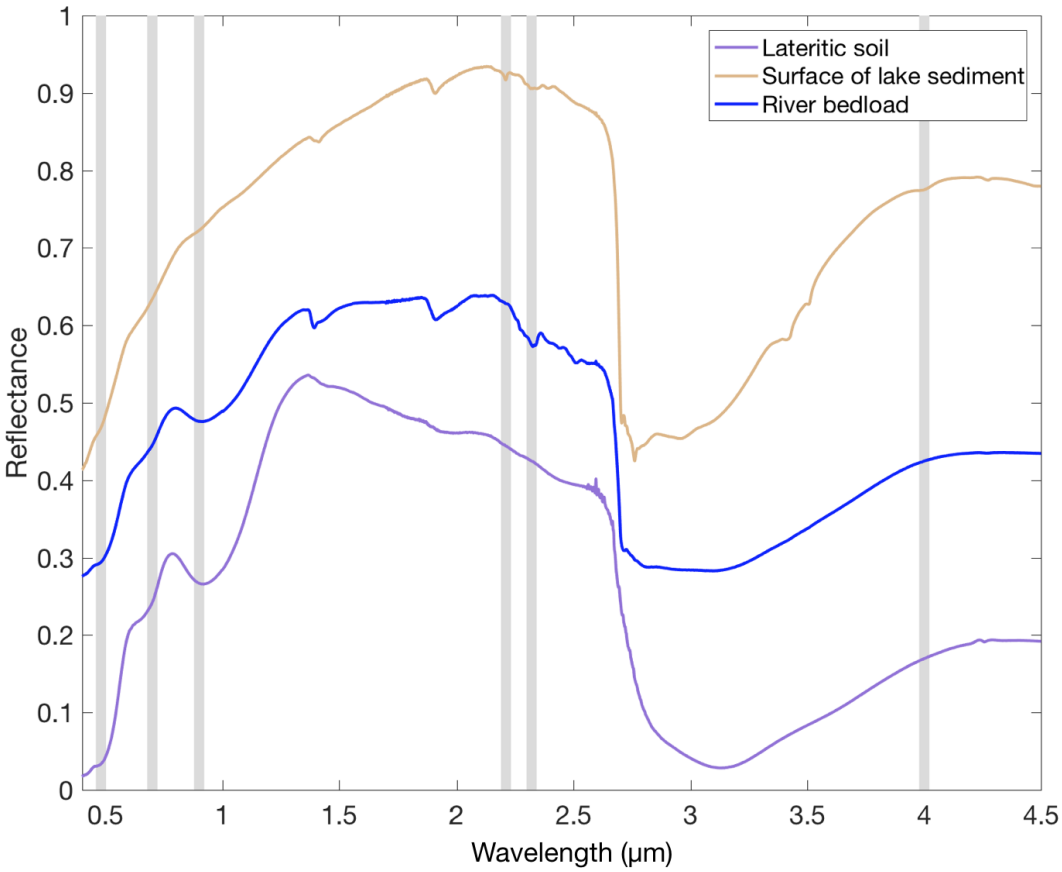

Figure I.3.2 A representative spectrum from each sample type (soil, river, and surface sediment), offset for clarity. Important absorptions are highlighted at 0.48, 0.7, and 0.9 μm (Fe) 2.21 μm (Al-OH), 2.32 μm (Mg-OH), and 4.0 μm (carbonate)

Reflectance spectra were acquired for dried, powdered samples over a wavelength range of 0.35-4.75 μm using a combination of spectrometers in the NASA Reflectance Experiment LABoratory (RELAB) facility housed at Brown University. An Analytical Spectral Devices (ASD) FieldSpec3 spectroradiometer was used for the visible-near infrared (VIS-NIR, 0.35-2.5 μm) range and a Thermo Nexus 870 FTIR spectrometer was used for the near-infrared to mid-infrared (NIR-MIR, 0.8-4.75 μm) range. ASD reflectance spectra were acquired relative to a white Spectralon standard, whereas FTIR reflectance data were acquired relative to diffuse gold (both standards from Labsphere). The two sets of spectral data were spliced together at 1.7 μm to provide a continuous spectrum.

Mg serpentine: Trioctahedral Mg phyllosilicates in the serpentine group (e.g. antigorite, chrysotile, lizardite) were identified based on a prominent asymmetric absorption centered at ~2.32 μm caused by vibrations (combination bend and stretch) of the Mg-OH bond (Weber et al. 2015).

Al clays: Absorptions near ~2.2 μm are caused by combination stretch and bend of OH and metal-OH (Weber et al. 2015). The precise location of the band at 2.21 μm and the asymmetric shoulder near 2.16 μm seen in many sample spectra from previous studies of Lake Towuti sediment are most consistent with Al-OH vibrations in kaolinite,

whereas other Al-bearing phyllosilicates (e.g. montmorillonite, illite, muscovite) exhibit a broader, more symmetric absorption in this region (Goudge et al. 2017; Weber et al. 2015; Clark et al. 1990; Bishop et al. 2008).

Fe smectite: Spectra of the dioctahedral ferric smectite nontronite exhibit a characteristic absorption at 2.28 µm caused by vibration of the Fe-OH bond (Clark et al. 1990; Bishop et al. 2008; Weber et al. 2015). Nontronite was not specifically analyzed in previous studies of more limited sample sets, but all spectra were examined for the possible presence of this mineral in this study.

Other Fe absorptions: The presence of $Fe^{2+/3+}$ in octahedral and tetrahedral coordination can give rise to a wide range of complex and sometimes overlapping absorptions in the 0.35-2.5 µm wavelength range that is measured by the ASD instrument (Burns, 1993). These features are due to electronic absorptions (intervalence charge transfer, oxygen-metal charge transfer, and crystal field splitting). Features associated with $Fe^{2+/3+}$ in oxides and poorly crystalline materials of interest to this study include absorptions at 0.48, 0.7, and 0.9µm (see Figure I.3.2). Spectra for the subset of samples processed for sequential iron extraction (described below) were also acquired for the dried samples after each extraction step. This allows for an assessment of changes in absorptions due to relative changes in $Fe^{2+/3+}$ during the extraction, which helps to link observed spectral absorptions to the presence of X-ray amorphous versus crystalline Fe phases.

Carbonate: A broad CO_3 absorption (v_1+v_3 vibration mode) is located at 3.8-4.0 µm (Gaffey et al. 1993; Sutter et al. 2007). This band is stronger than overtone absorptions observed at shorter wavelengths (<2.5 µm), does not overlap with OH absorptions assocaited with clay minerals, and is not as affected by H_2O or CO_2 absorptions (Wagner and Schade 1996).

I.3.4.3 X-ray Diffraction

Powder X-ray diffraction (XRD) measurements were made for all samples to provide qualitative information on phase identification, including measurements of d-spacing for clay minerals. Dried, powdered samples were analyzed on a Bruker D2 Phaser XRD with a Cu source. Sample cups were filled without packing to reduce preferential orientation. XRD patterns were analyzed for presence/absence of relevant peaks, in part using the patterns of nanophase iron (oxyhydr)oxides synthetsized in Sklute et al. (2017) and reference patterns from data in the American Mineralogist Crystal Structure Database (AMCSD) using the CrystalDiffract software by CrystalMaker database (Figure I.3.3).

I.3.4.4 ICP-AES

Major and minor elemental abundances were determined by inductively coupled plasma-atomic emission spectrometry (ICP-AES) at Brown University. ICP-AES was used to provide quantitative elemental abundances of sediment samples (Murray et al. 2000). Major (Al, Ca, Cr, Fe, K, Mg, Mn, Na, Ni, P, Si, Ti) and trace (Co, Cr, Cu, Mo, Ni, Sc, Sr, V, Zn, Zr) elements were analyzed in the 42 surface samples after they were dissolved using flux fusion (Murray et al. 2000). Each sample (0.04 ±0.005g) was gently mixed with lithium metaborate flux (0.16 ±0.005g) in a graphite crucible and fused at 1050°C for 10 minutes. Each fused bead was then dropped into 20 mL of 10 % nitric acid (HNO_3), shaken for 30-60 minutes, filtered with a 0.45 µm Gelman filter, and 5 mL of the

final fused solution diluted in 35 mL of 10 % HNO_3. The same process was done for standard reference materials (RGM-1, NIST1646a, BIR-1, BHVO-2, NIST2711, BCR-2, and DTS-2B).

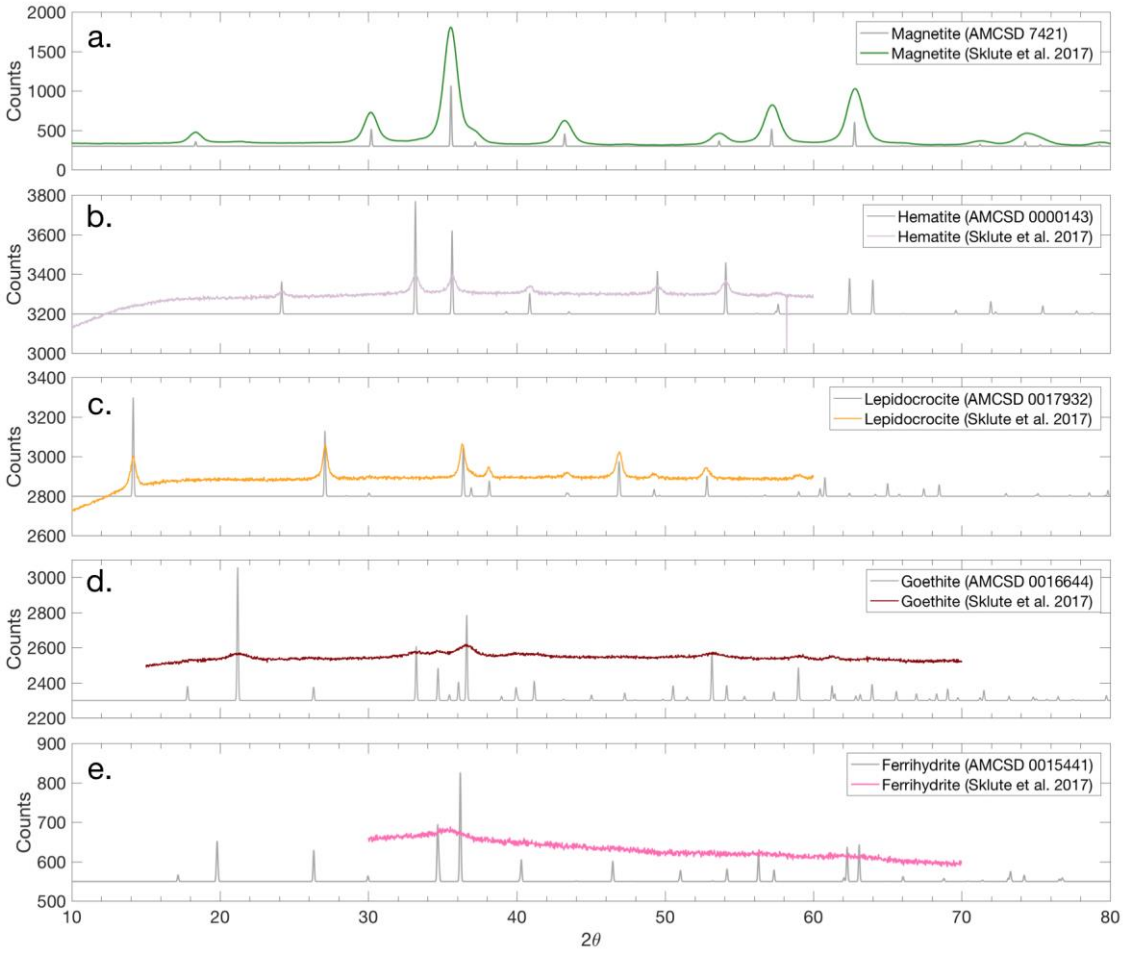

Figure I.3.3 XRD patterns of iron oxides synthesized in Sklute et al., 2017 (colored lines), with AMCSD reference patterns in gray. a. Magnetite, b. hematite, c. lepidocrocite, d. goethite, and e. ferrihydrite

Once diluted, the samples were analyzed on a Jobin Yvon JY2000 ICP-AES. Concentration data are calibrated to the fluxed standard reference materials. A drift solution comprising a small amount of each diluted sample was analyzed every 12 slots on the ICP-AES to monitor and correct for any change in signal.

I.3.4.5 Sequential Iron Extraction

To determine relative amounts of highly reactive iron (e.g. amorphous Fe phases, ferrihydrite, lepidocrocite) and crystalline iron oxy/hydroxides (e.g. hematite, goethite) in the samples, a two-stage sequential iron extraction was carried out on several laterite and surface samples using a protocol modified from Poulton and Canfied (2005), described in Table I.3.1. Fe in silicates was not removed by these extractions.

Table I.3.1 Sequential Fe Extraction Protocol

Extraction	Target Phases	Duration
Hydroxylamine HCl	Amorphous iron oxides (e.g. ferrihydrite)	48 hours
Sodium dithionite	Crystalline iron oxides (goethite and hematite)	2 hours

The hydroxylamine HCl extraction was created by mixing 69.49 g Hy-HCl into 1 L of a 25 % acetic acid solution. The extraction was performed in 50 mL plastic falcon tubes, where 100 mg of sediment and 10 mL hydroxylamine HCl were mixed and placed on a shaker table and reacted for 48 hours at room temperature.

The mixture for the sodium dithionite extraction was prepared by mixing 50 g of sodium dithionite and 51.6 g sodium citrate in 1 L DI water. Acetic acid was then added until the pH reached 4.8. Samples residues from the hydroxylamine HCl extraction were reacted with 10 mL of the sodium dithionite in falcon tubes on a shaker table for 2 hours at room temperature.

After each extraction, the falcon tubes were centrifuged and supernatant poured into a vial. The residual sediment was then washed with deionized water three times, centrifuged each time, and poured into the same vial. The residual sediment was freeze dried and spectra and XRD patterns were collected. The supernatant was dried at 60°C, rehydrated in 10 mL 2 % nitric acid, diluted 1:100 in 2 % nitric acid, and measured for total iron concentration on the ICP-AES.

I.3.4.6 Mössbauer spectroscopy

Mössbauer spectroscopy is sensitive to small energetic changes around iron atoms and so can distinguish between Fe oxides in complex, heterogeneous samples (Sklute et al. in review). Mössbauer measurements were acquired with the sample at 4 K, 130 K, and 295 K on a Web Research Co. (now See Co.) W100 spectrometer using a ~75-65 mCi ^{57}Co source in rhodium. Low temperature spectra were obtained using a Janis Research Co. Model 850 4 K closed-cycle helium compression system. The spectra were fit using the Mex_disd program. From these fits, Mössbauer parameters can be determined (Dyar et al. 2006; Sklute et al. in review). This includes isomer shift (IS), which reflects the s-electronic charge density, which is affected by bond characteristics, valence state, and coordination environment. This shift is presented in Mössbauer spectra as a velocity (mm/s) shift relative to α-Fe foil. Another relevant parameter is quadrupole splitting (QS) of nuclear energy levels which creates the distinctive doublets and sextets seen in Mössbauer spectra. Changes in Fe valence state or changes to the crystal lattice that affect the coordination or bonding environment will affect this splitting and the observed doublets and sextets. For example, grain size and composition affect the temperature at which the transition from doublet to sextet occurs, so by collecting spectra at multiple temperatures, ferric and ferrous Fe in different coordination environments can be distinguished.

I.3.5 Results

I.3.5.1 Correlation of spectral characteristics with chemical data

Sediment samples show strong spatial trends in Al and Mg (Figure I.3.4a,b) as well as associated changes in silicate mineralogy, consistent with the results of Morlock et al. (in review) and Hasberg et al. (2018). Values for Al are relatively low in the north near the Mahalona River delta and increase with distance from the delta. Values for Mg exhibit the opposite trend: Mg abundance is elevated in the Mahalona River delta and drops quickly with distance from the delta.

Surface samples have band depths of the 2.21 µm Al-OH (kaolinite) absorption correlated with Al_2O_3 abundance (positive coefficient significant at $p<0.01$); for laterites the correlation is not significant (Figure I.3.4c). Both laterite and surface samples have band depths of the 2.32 µm Mg-OH (serpentine) absorption correlated with MgO abundance (positive coefficient significant at $p<0.01$; Figure I.3.4d). See Table I.3.2 for additional information on regression statistics.

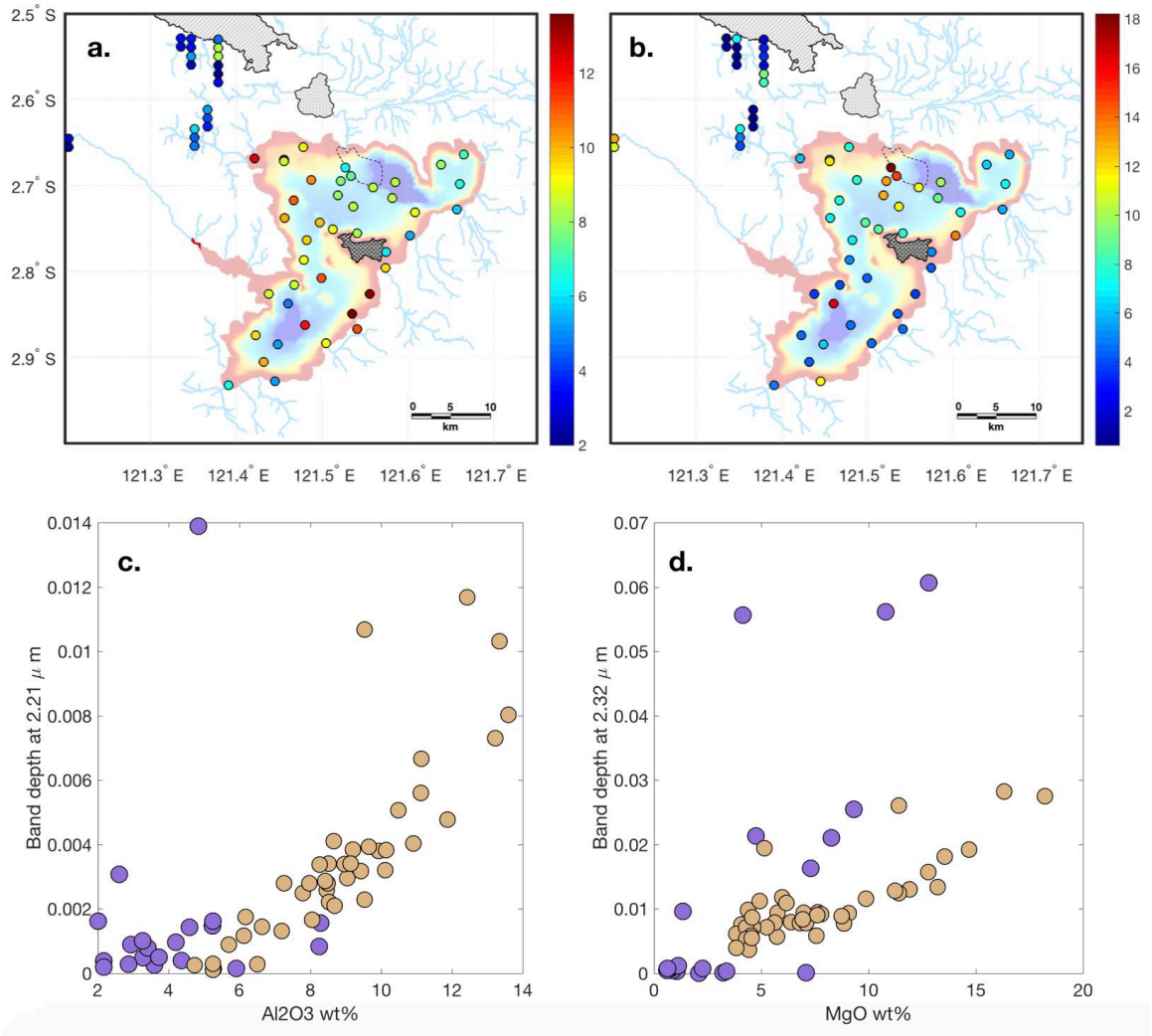

Figure I.3.4 a. Al_2O_3 (wt%) in surface and soil samples. b. MgO (wt%) in surface and soil samples. c. Band depth at 2.21 µm versus Al_2O_3 abundance in surface (brown) and soil (purple) samples. d. Band depth at 2.32 µm versus MgO abundance in surface (brown) and soil (purple) samples

Table I.3.2 Al and Mg Regression Results

	Dependent variable:			
	BD 2.21 μm, surface (1)	BD 2.21 μm, laterite (2)	BD 2.32 μm, surface (3)	BD 2.32 μm, laterite (4)
Al_2O_3, surface	0.001*** (0.0001)			
Al_2O_3, laterite		0.0002 (0.0004)		
MgO, surface			0.001*** (0.0002)	
MgO, laterite				0.004*** (0.001)
Constant	−0.005*** (0.001)	0.001 (0.002)	0.001 (0.001)	−0.003 (0.005)
Observations	42	20	42	20
R^2	0.700	0.012	0.644	0.580
Residual Std. Error	0.002 (df = 40)	0.003 (df = 18)	0.004 (df = 40)	0.014 (df = 18)
F Statistic	93.113*** (df = 1; 40)	0.210 (df = 1; 18)	72.365*** (df = 1; 40)	24.901*** (df = 1; 18)
Note:		*p<0.1; **p<0.05; ***p<0.01		

FeO abundances are very high in the lateritic catchment soils (Figure I.3.5a), with concentrations of up to 49.4 wt%, and FeO abundances are more spatially variable across the surface of the lake (Figure I.3.5b). VNIR spectra indicate the presence of Fe-oxides and Fe-bearing silicates, where the latter may include nontronite in two lake samples and several laterite samples. Because of the complex and overlapping nature of iron spectral absorptions (Figure I.3.6), two different spectral parameters are compared with ICP-determined FeO abundances (Figure I.3.5). The inverse slope of the 0.45 μm to 0.48 μm absorption band, which is observed in some Fe-oxides such as hematite and goethite and is similar to a measure of band area, is correlated with Fe abundance for both laterites and surface samples (positive coefficient significant at $p<0.01$; Figure I.3.5c). The band depth of the ~0.9-1.0 μm absorption that is commonly observed in Fe-oxides and Fe-bearing silicates (e.g. nontronite) is also correlated with Fe abundance (positive coefficient significant at $p<0.05$ for surface samples, positive coefficient significant at $p<0.01$ for laterites; Figure I.3.5d). Although both spectral parameters exhibit a correlation with ICP-derived FeO content, the correlation is strongest for the spectral slope parameter in the lake surface samples (brown points in Figure I.3.5c). The correlation between this Fe spectral slope parameter is much stronger than previous correlations of FeO abundance with spectral parameters (Weber et al. 2015). See Table I.3.3 for additional information on regression statistics.

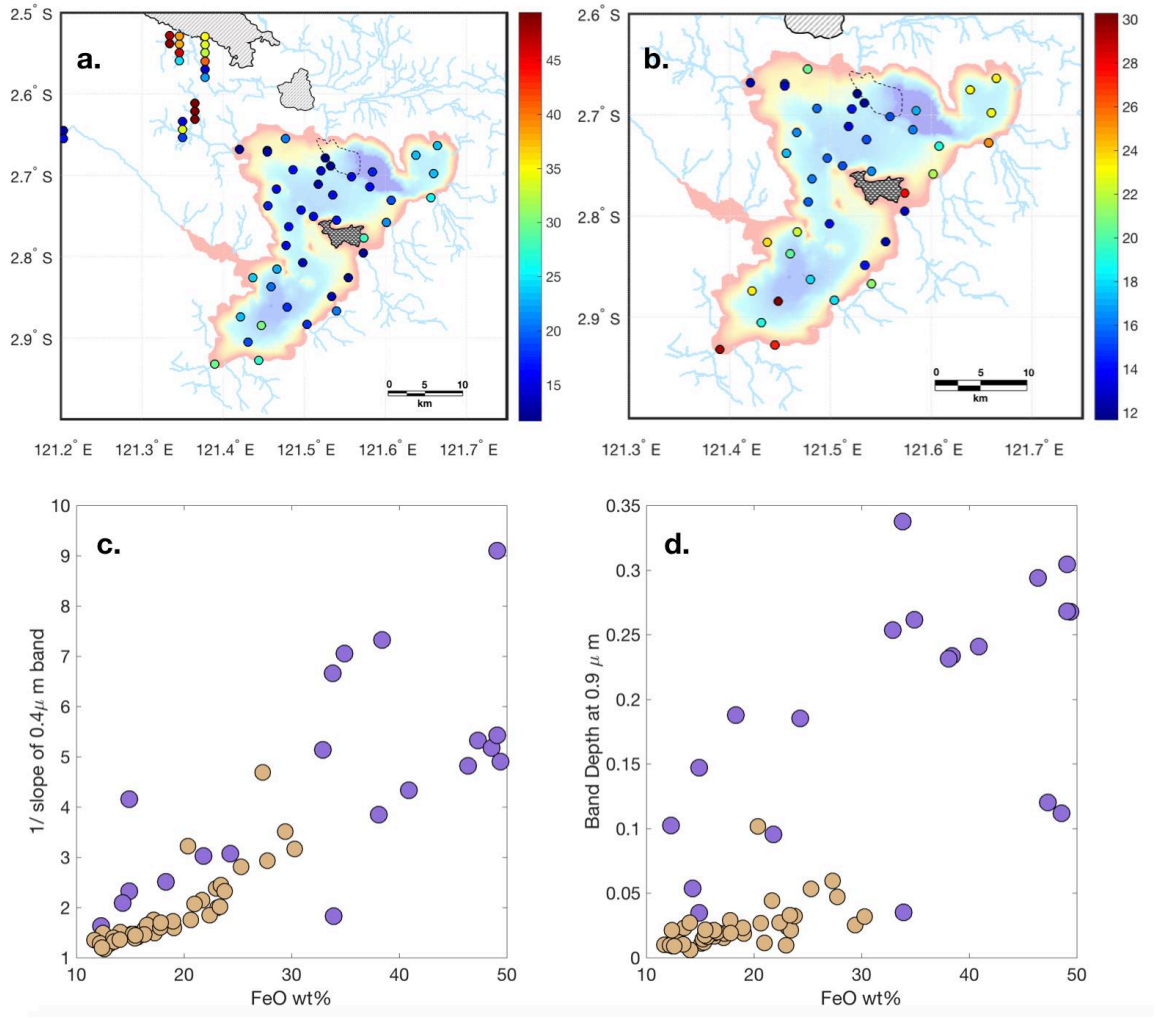

Figure I.3.5 a. ICP-determined elemental abundance of FeO (wt%) in surface and soil samples. b. ICP-determined elemental abundance of FeO (wt%) in just surface samples. c. Flatness of the 0.4 μm band versus with FeO abundance in surface sediment (brown) and soil (purple) samples. d. Band depth at 0.9 μm band versus with FeO abundance in surface (brown) and soil (purple) samples.

The lateritic soil samples are characterized by high FeO abundances (25-50 wt%) that are generally highest at the top of the soil bed and decrease with depth (Morlock et al. 2018). One laterite, located west of the others near the Larona River, the main outlet of Lake Towuti, has significantly lower FeO (~14 wt%; Figure I.3.8) and elevated MgO. All soil samples examined here have moderate-to-low Al_2O_3 values (2-8 wt%) that, like FeO, tend to be highest in the samples closest to the surface. VNIR spectra from these high-Fe samples are consistent with abundant hematite and goethite, with much lower concentrations of other Fe-bearing phases such as Fe-clay minerals or siderite.

Nontronite was identified in two shallow, coastal lake surface samples and six laterite samples based on a diagnostic (Fe-OH) absorption feature at 2.28 μm in their corresponding reflectance spectra (Figure I.3.7). In addition, spectra for a number of the laterite samples exhibit two distinct absorptions near ~2.28 μm and ~2.31 μm (purple spectrum, Figure I.3.7a). The strength of these features varies independently within the sample group as a whole, suggesting the doublet absorption is the result of two distinct mineral phases that vary in their relative abundance between samples (i.e., the doublet

is not the result of a single mineral phase). The position of the 2.28 μm feature is similar to that of Fe-OH in nontronite, and the position of the 2.31 μm feature is similar to that of Mg-OH in saponite; neither is consistent with absorptions typical of serpentine. However, the absorptions in these laterite samples are narrower than what is commonly observed in reflectance spectra of pure nontronite or saponite, thus the origin of these spectral features is somewhat ambiguous. It is possible that the observed doublet is a result of a mixture of nontronite and saponite, perhaps poorly crystalline forms of these clay minerals.

Table I.3.3 Fe Regression Results

	Dependent variable:			
	1/slope 0.4 μm band, surface (1)	1/slope 0.4 μm band, laterite (2)	BD 0.9 μm, surface (3)	BD 0.9 μm, laterite (4)
FeO, surface	0.126***		0.005**	
	(0.012)		(0.002)	
FeO, laterite		0.102***		0.008***
		(0.026)		(0.002)
Constant	−0.437*	1.107	0.118***	0.349***
	(0.229)	(0.940)	(0.034)	(0.066)
Observations	42	20	42	20
R^2	0.733	0.453	0.142	0.501
Residual Std. Error	0.384 (df = 40)	1.536 (df = 18)	0.058 (df = 40)	0.108 (df = 18)
F Statistic	109.810*** (df = 1; 40)	14.889*** (df = 1; 18)	6.626** (df = 1; 40)	18.067*** (df = 1; 18)
Note:		*p<0.1; **p<0.05; ***p<0.01		

I.3.5.2 Complex iron mineralogy

Consistent with the ICP data (Figure I.3.5) and VNIR spectra (Figure I.3.6, Figure I.3.7), XRD patterns indicate that crystalline Fe-oxides are more abundant in laterite samples than in lake surface sediment samples (Figure I.3.8). Detailed examination of the laterite XRD patterns (Figure I.3.9) show sharp, relatively high goethite peaks in almost every laterite sample, sharp magnetite peaks in several samples, and hematite in few samples. In the surface sediment samples (Figure I.3.10), the peaks are broadened and decreased in height. There is still evidence of Fe oxides (goethite, magnetite, hematite), but they are less abundant compared to other iron phases including serpentine, siderite, Cr spinel, olivine, amphibole, pyroxene, and feldspar. There is also a notable paucity of crystalline Fe-oxides in lake sediment samples corresponding to the coarse-grained Mahalona delta deposits as well as samples located close to other river inlets (Figure I.3.11).

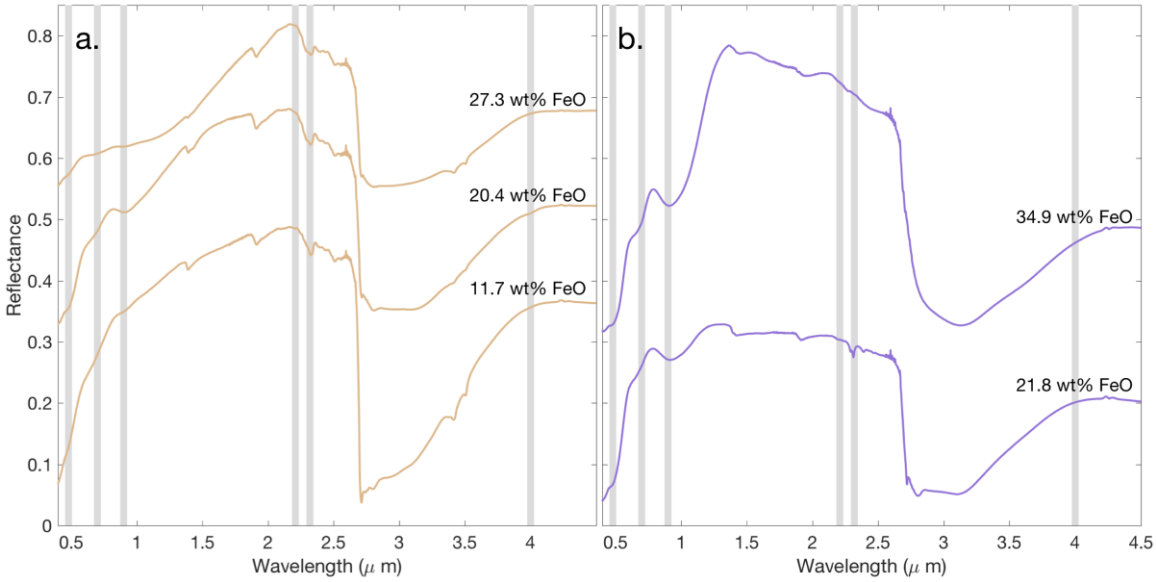

Figure I.3.6 Example spectra, with relevant band locations highlighted, labeled with their ICP-determined FeO abundances (wt%). a. Three example surface sediment spectra, offset for clarity. The top two are from the southern end of the lake and the bottom spectrum is from the coarse-grained, serpentine-rich Mahalona river delta. b. Two example laterite spectra, offset for clarity. Top spectrum is from the top of one laterite bed (10 cm from the surface) and bottom spectrum is from the bottom of the same bed (3.5 m from surface). Note the increase in Fe absorption band strengths (0.4-1.5 μm) and decrease in Mg-serpentine band strength (~2.32 μm) in the spectrum for the upper soil sample compared with that of the lower soil sample, consistent with increased abundance of Fe oxides at the expense of serpentine during progressive weathering of the serpentinized bedrock

To further investigate these observed differences in the mineral host of Fe as sediment moves through the system, we performed sequential extractions to quantify the abundance of Fe in crystalline vs. amorphous phases in laterites, surface samples, and samples from sediment cores (*Figure I.3.12*). Total Fe abundances are similar in the lake surface and core samples, but the manner in which this Fe is partitioned between mineral phases is quite different between the two sample groups. The proportion of Fe in amorphous or highly reactive phases (i.e. the extraction 1 supernatant) versus crystalline phases (i.e. extraction 2 supernatant) is roughly equivalent in surface sediment samples, whereas samples from deeper within the sediment column (core samples) contain more iron in what appear to be X-ray amorphous phases. The laterites, which are a dominant sediment source in this system, all exhibit significantly higher total Fe concentrations and are dominated by crystalline Fe-oxides (e.g., goethite, hematite). Not all of the iron is necessarily being extracted by this process, with summed supernatant Fe abundances of some samples up to 9 wt% Fe below the original sample.

The fact that the extractions are not removing all the iron can also be seen in the XRD patterns of one surface sample after each step in the process (Figure I.3.13). The intensity of the goethite peak is reduced but a portion of the goethite appears to be resistant to the extractions. Processing the sample with extraction 2 a second time removed additional goethite, resulting in near-complete removal of goethite peaks in the XRD patterns.

Mössbauer results show that the Fe mineralogy of the surface sediment is extremely complex, with a large nanocrystalline component, both ferrous and ferric phases, and interparticle effects causing broadening of the doublets and sextets during magnetic ordering (Figure I.3.14).

Surface sediment sample 270 (Figure I.3.14a-c) is in the northeastern lake. At 295 K, the Mössbauer fits suggest two unremarkable pairs of ferrous and ferric doublets. One ferrous doublet has a very low IS value and moderate QS value, likely attributable to a clay. There is no evidence for ilmenite, which should be easy to see at room temperature. At 130 K, the ferrous phase QS only slightly increases, consistent with being a clay. A broad sextet appears at this temperature (Figure I.3.14b., orange curve) that is consistent with magnetite. At 4 K, the ferrous Fe is undergoing strong magnetic orientation because of the higher symmetry of the electrons around ferrous Fe. The spectral fits are very complex at this temperature, and suggest highly disordered, nanocrystalline phases with both ferrous and ferric components.

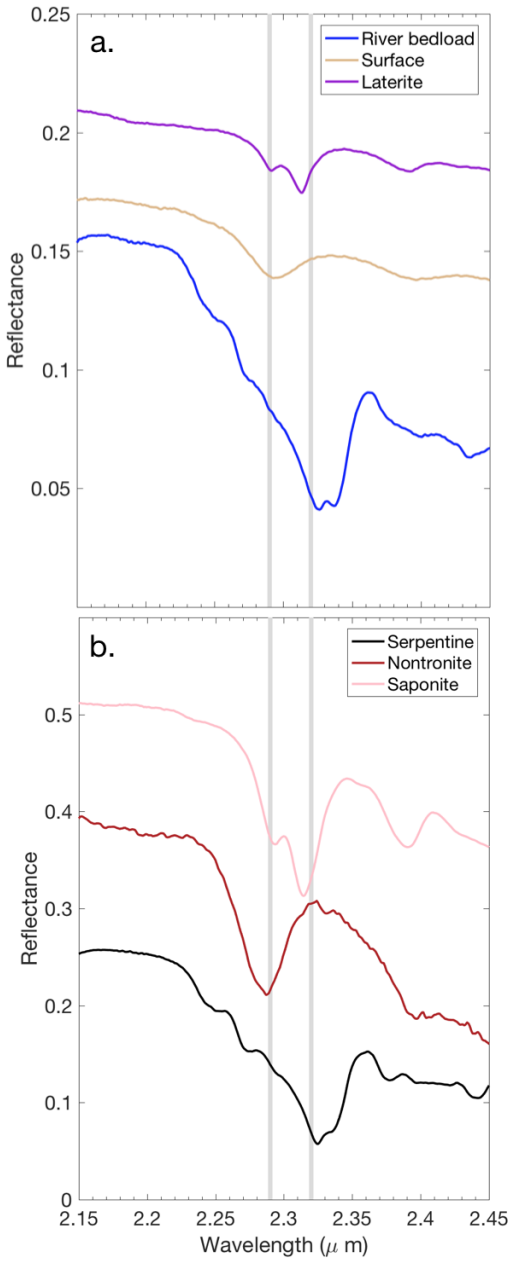

Figure I.3.7 a. Four example reflectance spectra (offset for clarity): a laterite sample, surface sample with 2.28 μm absorptions attributed to nontronite, and Mahalona River bedload sample with no nontronite but a strong 2.32 μm feature attributed to serpentine. b. Laboratory spectra (offset for clarity) of serpentine (lizardite, NMNHR 4687), nontronite (NG-1), and saponite (SapCa-1)

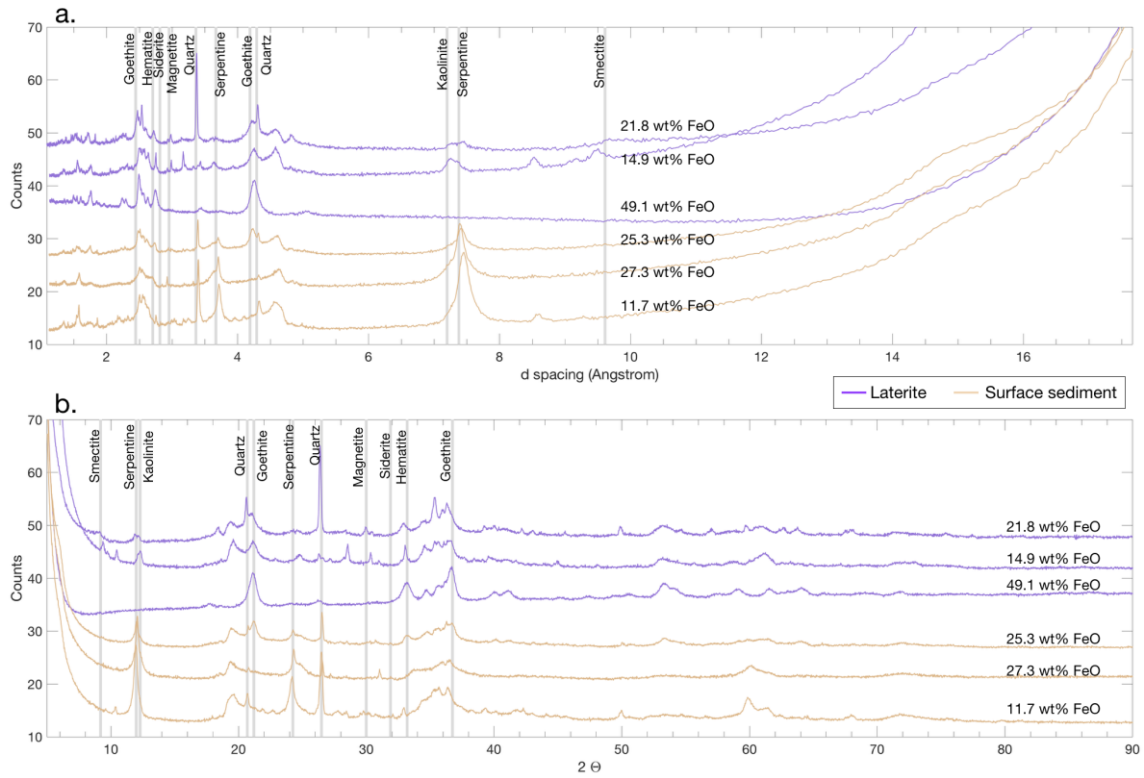

Figure I.3.8 XRD patterns (offset for clarity) of three laterites (purple) and three surface samples (tan) presented in terms of a. d-spacing and b. 2τ. Patterns are offset for clarity and labeled with the samples' ICP-determined FeO abundance (wt%). Vertical gray bars highlight the peak location of relevant phases.

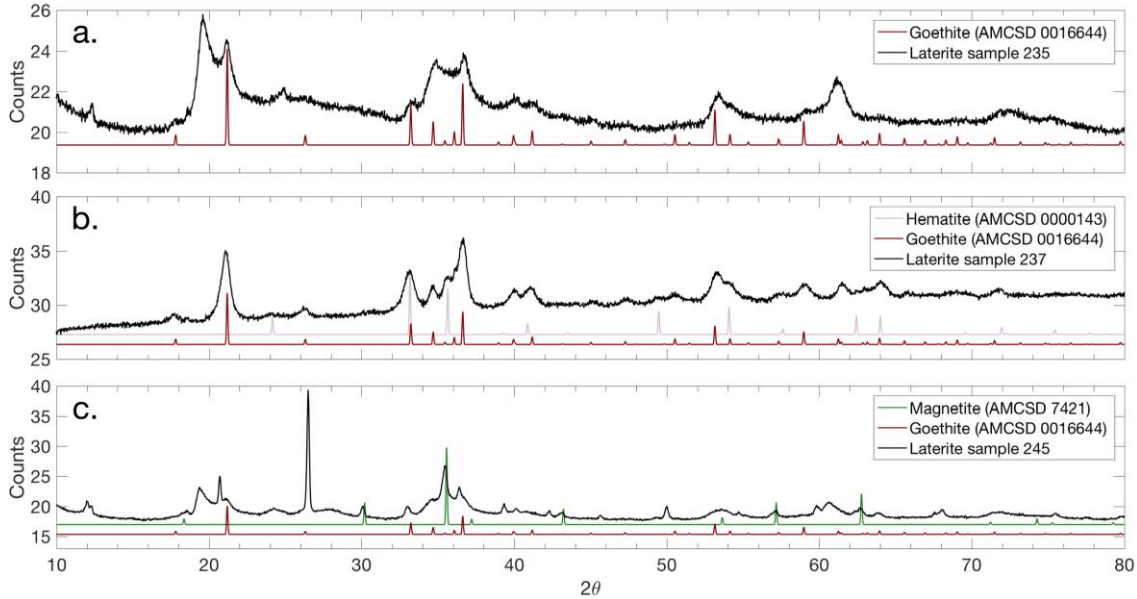

Figure I.3.9 XRD patterns (offset for clarity) of three lateritic soil samples (black lines), with ideal peak locations of the Fe phases identified in that sample below (colored lines). a. A laterite with abundant goethite. b. A laterite with abundant goethite and hematite. c. A laterite with magnetite and a small amount of goethite

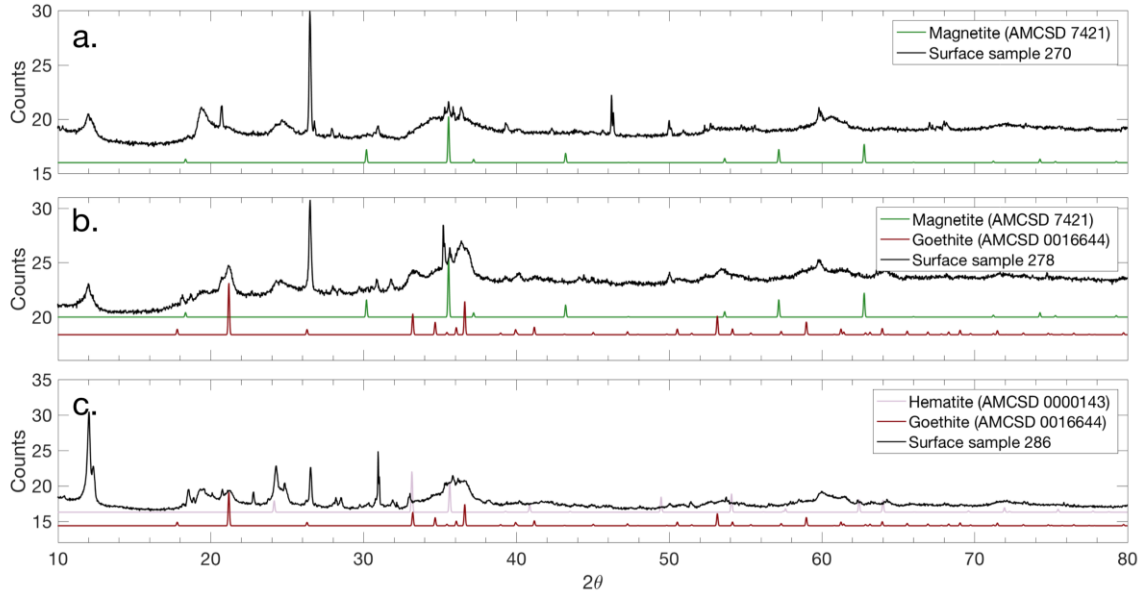

Figure I.3.10 XRD patterns (offset for clarity) of three surface soil samples (black lines), with ideal peak locations of the Fe phases identified in that sample below (colored lines). a. A surface sample with magnetite. b. A surface sample with magnetite and goethite. c. A surface sample with goethite and hematite

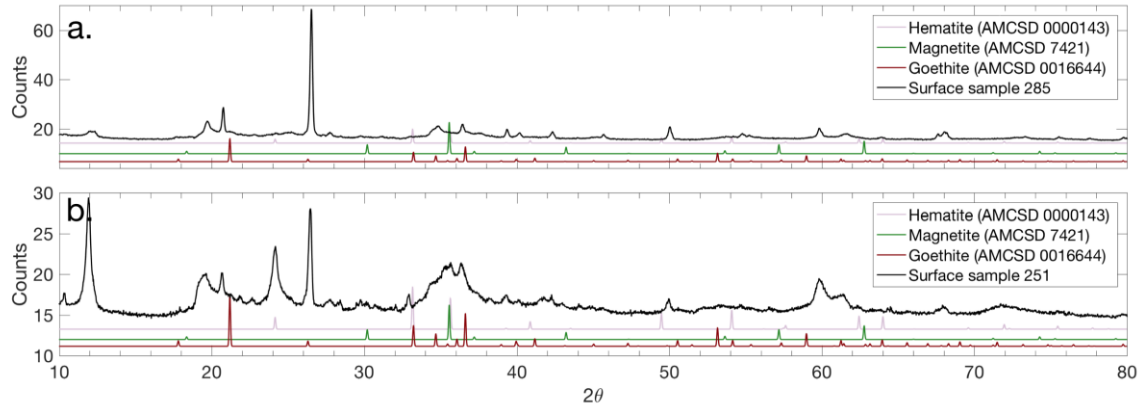

Figure I.3.11 XRD patterns (offset for clarity) of two surface samples (black lines) that are near riverine inputs and have low/no Fe phases in them. Ideal peak locations of Fe phases are shown below (colored lines). a. A southeastern lake sample and b. a Mahalona river delta sample

Surface sediment sample 286 (Figure I.3.14d-f) is in the southern lake. At 295 K, the parameters are closest to those of ferrous clays or possibly pyroxene (and are inconsistent with olivine, feldspar, sulfate, or phosphate). There is evidence for two ferrous doublets and two ferric doublets at this temperature. At 130 K, the ferric phases move to broad, disordered sextets, consistent with nanophase hematite, goethite, or possibly akaganeite. At 4 K, these sextets are even more prominent and the fits are indicative of great disorder in the samples. Trace siderite could explain the broad, unsplit blue curve (Figure I.3.14f.), which disappears at higher temperatures. Siderite doesn't appear in these samples in the spectra or XRD patterns, so may be ~5 % abundance, below the detection limit for those methods but possibly still detectable in the Mössbauer data.

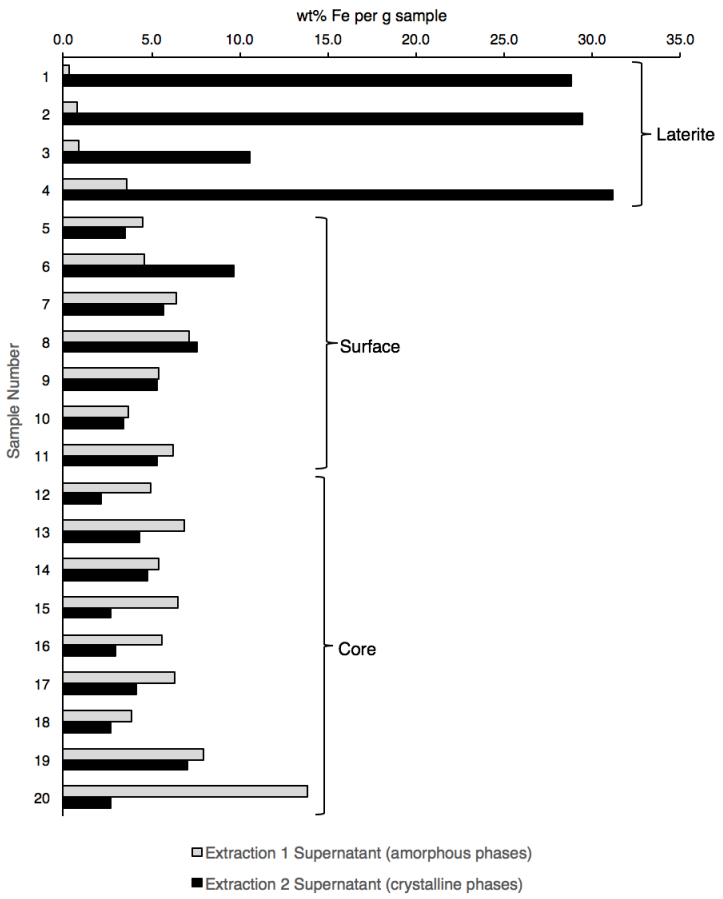

Figure I.3.12 Comparison of the wt% Fe per g sample in each supernatant produced via extraction 1 (gray, amorphous phases) and extraction 2 (black, crystalline phases). Laterite samples are from depths of 10 cm to 2 m from the surface; core samples are from 2-77 m depth, with one tephra (sample 20); surface samples represent sediment depths of <5 cm and are from varying locations, including one from the Mahalona delta (sample 5)

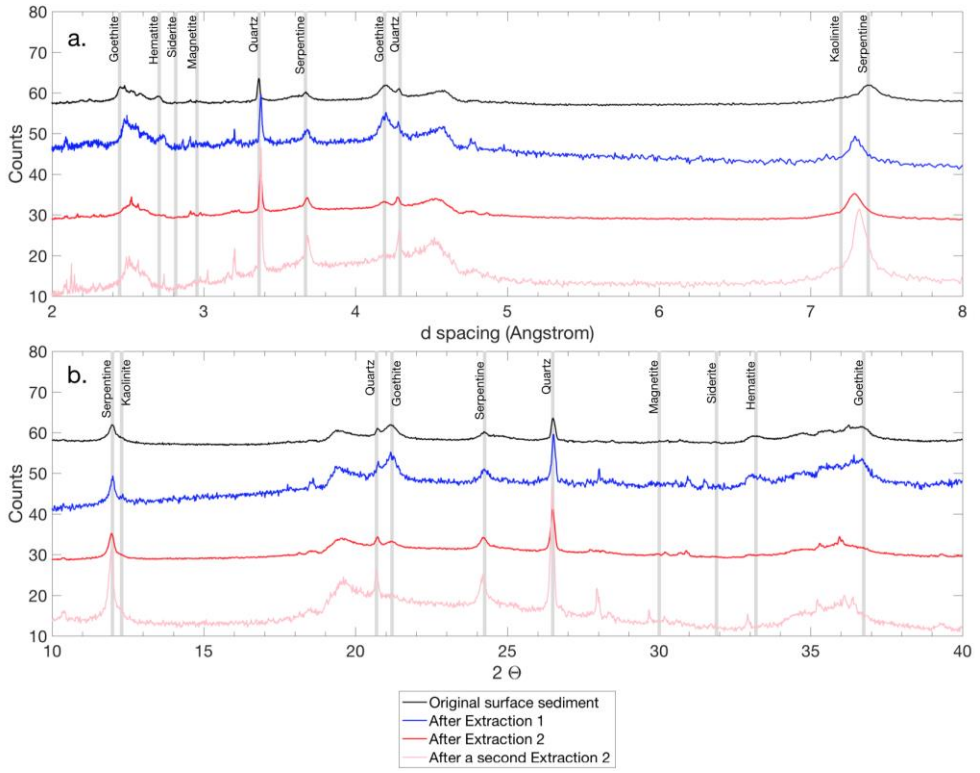

Figure I.3.13 Zoomed-in XRD patterns (offset for clarity) of one surface sample throughout the sequential extraction process in terms of a. d-spacing and b. 2τ. Patterns are offset for clarity and diagnostic peaks of relevant phases are highlighted in gray

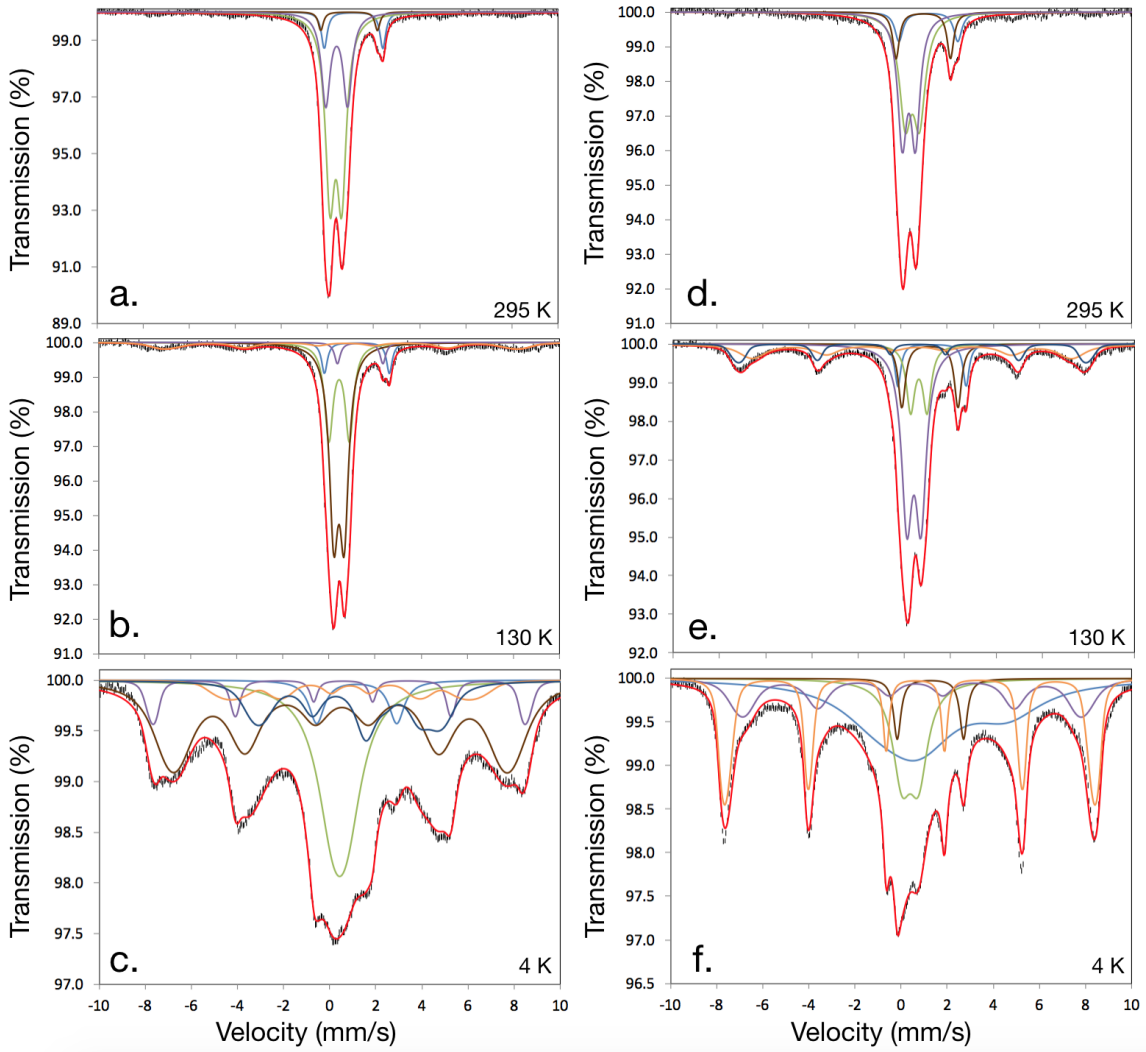

Figure I.3.14 Mössbauer patterns for surface sample 270 at a. 295 K, b. 130 K, and c. 4 K. Mössbauer patterns for surface sample 286 at d. 295 K, e. 130 K, and e. 4 K

I.3.6 Discussion

The dominant chemical variations observed in Lake Towuti laterites and surface sediments are in Mg, Al, and Fe contents. In the lake, Mg and Al abundances are strongly linked to mineralogy, particularly the relative abundance of detrital Mg-serpentine vs. kaolinite from the catchment. The coarser-grained samples acquired closer to the Mahalona river are mainly composed of serpentine, which is inherently coarser-grained in this system because the river is transporting relatively unweathered fragments of serpentinized bedrock from the sediment source region (Hasberg et al. 2018). The abundance of Mg is thus a proxy for serpentine content which is in turn the dominant phase in the coarser-grained sediment. This can be seen in the spatial distribution of high-Mg lake surface samples which conforms to the boundaries of the Mahalona delta in Figure I.3.4b. In contrast, kaolinite (and thus Al) abundance increases in the finer-grained detrital component because it is forming in the soil weathering horizons. To the extent that these relationships hold true through geologic time, lateral and vertical variations in the relative abundance of serpentine and kaolinite may thus

record important information about sediment flux, water depth/distance to shoreline, and surface weathering conditions through time (Goudge et al. 2017; Morlock et al. 2018). The ability of VNIR reflectance spectroscopy to accurately identify and distinguish kaolinite from serpentine, both of which are 7Å clay minerals, highlights the usefulness of this technique for rapid, non-destructive analysis of sediments and sediment cores to help infer paleoenvironmental conditions in the Malili Lakes system.

The variation of the Fe mineralogy from source to sink reflects a complex and dynamic system that is actively cycling Fe between a range of mineral hosts and affecting crystallinity and grain size. XRD and spectral analyses of the catchment soils show that they are characterized by a range of crystalline Fe oxides, with goethite dominating. Elemental FeO abundances are also very high in the catchment soils, consistent with heavy weathering in tropical laterites. Magnetite is present in several samples and appears to be more abundant at greater soil depths, consistent with at least some of the magnetite originating from unweathered bedrock (Morlock et al. 2018). Magnetite is also removed by weathering, consistent with its almost complete absence in river samples and deep-water surface samples. Hematite is also present in laterite samples and is likely derived from weathering of primary Fe-bearing minerals (e.g., olivine and pyroxene).

Within the lake itself, dissolved oxygen declines below 100 m depth and reaches anoxic conditions around 130 m depth, consistent with evidence that the water-sediment interface is oxic at shallow sites and anoxic and enriched in ferrous Fe at intermediate and deep sites (Vuillemin et al. 2016). XRD analyses show that hematite and magnetite are only present in a few of the shallow coastal samples, and are largely absent from the Mahalona River delta. This is consistent with a detrital origin for magnetite and early settling due to its higher density (Tamuntuan et al. 2015). Despite the decline (and in some cases absence) of XRD peaks associated with crystalline Fe-oxides, ICP results show that lake surface samples contain high concentrations of Fe. This suggests that much of the Fe within the lake may be in the form of poorly crystalline, X-ray amorphous phases originating from transformation of soil iron minerals by iron cycling and reduction within the lake. The broadening and decrease in peak height seen in the surface sample XRD patterns (Figure I.3.8, Figure I.3.10) can be due to a combination of reduction of Fe oxide abundance, decreased grain size, and disorder in the crystal lattice. The majority of VNIR spectra for the lake surface samples do exhibit absorptions consistent with the presence of $Fe^{2+/3+}$, but the shapes and positions of these features are not consistent with the presence of only goethite and/or hematite.

Goethite is present across the lake surface, although greatly reduced in abundance compared with the catchment soils. The loss of goethite is presumably due to its reduction in the anoxic water column and in shallow sediments. However, goethite persists in the lake sediment samples, even those obtained from deep, anoxic waters. This, together with the persistence of goethite after sequential Fe extractions, suggests that some portion of the goethite may be resistant to alteration/diagenesis. The cause of this is unknown but may result from goethite acting as a cementing agent in detritus from the lateritic soils, thus forming more slightly resistant particulates. The total Fe content in surface sediment and down-core samples are similar, but surface samples are roughly equal in their distribution of crystalline and amorphous Fe (based on Fe in the supernatant after each extraction step), whereas all core samples have more Fe in amorphous phases with a lesser amount in well-crystalline Fe-oxides such as goethite.

Mössbauer results support the observations of reflectance spectra, XRD patterns, and sequential extractions, suggesting that the Fe mineralogy is extremely complex within the surface sediment. Pattern fits suggest a large nanocrystalline component with both ferrous and ferric phases. The low-temperature data (Figure I.3.14e) in particular suggest highly disordered, fine-grained material. Only the finest-grained nanophase iron (oxyhydr)oxides would still be unsplit at 4 K, so at least 40 % spectral area seems to be attributable to iron (oxyhydr)oxide.

These changes in Fe mineralogy within the lake during settling and subsequent burial must account for the increase in amorphous Fe material observed from catchment to lake surface to subsurface. If laterites accurately represent the sediment input into the lake, some process or suite of processes liberating iron from the ferric crystalline phases in the water column or shortly after deposition and promoting the formation of new Fe-bearing X-ray amorphous phases. Interestingly, there is no clear correlation between the relative abundance of crystalline Fe oxides in the surface sediments and water depth: most surface sediments that were sampled at water depths above the modern oxycline also exhibit less goethite and hematite than observed in soils, even though total Fe content remains high. This, together with the presence of goethite in sediments below the oxycline indicates there is less of a gradient in Fe mineralogy across the modern oxycline than might be expected. However, the substantial increase in amorphous Fe phases in lake sediment samples indicate lake iron cycling exerts strong controls on Fe burial throughout the lake. Possible explanations include: (i) conditions in shallow water settings allowing for some reductive dissolution of Fe in oxidizing water, (ii) frequent enough mixing to precipitate more oxidized species in deep water, (iii) a portion of detrital goethite is slow to react even when transported beneath the oxycline. However, it remains that a significant fraction of Fe in the lake surface sediment cannot be accounted for by crystalline Fe-oxides as observed in XRD patterns, despite the fact that the majority of Fe likely enters the lake in this form.

Iron cycling has been studied in the water column Lake Matano, another of the Malili lakes that is non-sulfidic, permanently redox-stratified, and more than twice as deep as Lake Towuti (Crowe et al. 2011). Studies of its water column chemistry have shown that the surface mixed layer of Lake Matano is in a pH/pE range in which iron (hydr)oxides are stable, whereas the hypolimnion favors $Fe(OH)^{2+}$ and Fe^{2+} (Crowe et al. 2008). Fe cycles between different species/oxidation states as (i) Fe^{3+} species sink through the metalimnion, where they are reduced; (ii) high concentrations of dissolved ferrous iron accumulate in the hypolimnion, (iii) some ferrous iron diffuses upward in the metalimnion, and (iv) ferrous iron that reaches the oxycline is oxidized and precipitated again (Crowe et al. 2008). It is possible that similar cycling is encouraging Fe to move from the crystalline Fe oxide form to more nanophase components. Ferric oxides may be settling below the oxycline, where they are then rapidly reduced and/or altered to amorphous phases. Though we cannot exclude authigenic goethite, it seems more likely that some of the incoming goethite is relatively resistant and escapes reductive dissolution. The lake is very S-poor, thus appreciable quantities of pyrite do not form even below the oxycline. Fe that is reduced and dissolved at depth, either in the water column or in the sediment, can migrate upward to form new amorphous Fe minerals in the water column or in very shallow sediment. Occasional lake mixing events may form substantial quantities of new Fe^{3+}-bearing minerals that are spread throughout the lake. This would be consistent with the conclusions of Tamuntuan et al. (2015) that the main factor driving diagenesis within short sediment cores is iron oxide dissolution.

I.3.6.1 Lake Towuti as an analogue for martian paleolakes?

The mafic/ultramafic East Sulawesi Ophiolite shares some compositional similarities with the mafic martian crust (Bibring et al. 2005; McSween et al. 2009; Kadarusman et al. 2004). Examining chemical and mineralogical relationships in Mg/Fe-rich sediment in the Lake Towuti system, located on the island of Sulawesi, Indonesia, may have implications for interpreting geochemical data of ancient lake sediments on Mars (Goudge et al. 2017; Weber et al. 2015). Examining relationships between elements such as Mn, Zn, and Ti in Mg/Fe-rich sediment from Lake Towuti, which is redox-stratified but not influenced by acid-sulfate alteration, thus provides a means to test if the chemical correlations observed on Mars are truly diagnostic indicators of temperature and pH conditions.

The NASA Mars Curiosity rover is currently characterizing the chemistry and mineralogy of a ~5 km thick sequence of strata deposited within Gale Crater (Grotzinger et al. 2014). This sequence includes a ≥200 m thick section of mudstones interpreted to have been deposited in a lacustrine-fluvial/alluvial environment (Grotzinger et al. 2015; Hurowitz et al. 2017). These mudstones contain a range of hydrous and Fe-bearing minerals, including primary igneous phases (olivine, pyroxene), sulfides/sulfates, Fe-bearing clay minerals, hematite, and magnetite (Grotzinger et al. 2014; Vaniman et al. 2014; Rampe et al. 2017). Trends in the chemistry and mineralogy of these rocks are still being examined, but variations in Fe mineralogy and oxidation state have been observed as a function of stratigraphic position by the rover (Hurowitz et al. 2017) as well as from orbit (Milliken et al. 2010). Variations in iron mineralogy, and correlations between elements such as Zn, Ni, and Si, have been interpreted as evidence for changing martian environmental conditions during the evolution of the Gale crater lake. Hurowitz et al. (2017) suggest the data are consistent with the presence of a redox-stratified lake in which oxidizable cations become enriched through seepage of more reduced (ferrous) groundwaters. In this model, mineral assemblages vary as a function of lake water depth, wherein magnetite and silica phases precipitate in the reducing deep water below the oxycline and hematite-phyllosilicate assemblages reflect more oxidizing, shallow water influenced by the surface environment. However, others have suggested that concurrent trends in redox-sensitive elements in Gale Crater indicate acid sulfate alteration of mafic materials (Yen et al. 2017; Rampe et al. 2017). Positive correlations between Si and Ti have been observed in Gale Crater and elsewhere on Mars, and this relationship has been interpreted as evidence for acid-sulfate leaching such as occurs in volcanic fumarole environments on Earth (Yen et al. 2008; Squyres et al. 2008), and/or as an indication of non-acidic hot spring environments (Ruff et al. 2011; Ruff and Farmer 2016).

Studying a terrestrial redox stratified lake in a mafic/ultramafic catchment can provide useful information on transport and alteration processes as well as evidence of what environmental factors may be recorded in the resulting sediment deposits. In the Malili Lakes system, VNIR spectral characteristics are a useful proxy for both chemistry and mineralogy (Weber et al. 2015; Goudge et al. 2017). This has relevant applications for the study of martian paleolake basins. Gale Crater has orbital spectral evidence of clay minerals (Milliken et al. 2010), in situ XRD measurements that confirm the presence of clays in this crater, and evidence for significant fractions of X-ray amorphous components (Grotzinger et al. 2014; Vaniman et al. 2014; Rampe et al. 2017). Understanding source regions and hydrologic history through clay mineralogy in martian

paleolakes requires distinguishing chemical and mineralogical trends using remote techniques such as VNIR spectroscopy (Ehlmann et al. 2008; Milliken et al. 2010). Lake Towuti is a useful analogue in that it provides proof of the link between chemistry, mineralogy, and spectroscopy in lacustrine sediments (Weber et al. 2015).

One intriguing observation in Lake Towuti sediments that may be useful for understanding martian counterparts is the relationship between the abundance of Si and Ti. A positive correlation between these elements has been observed at several sites on Mars, including lacustrine mudstones in Gale Crater and non-lacustrine rocks and soils in Gusev Crater. This trend has been cited as evidence for acid sulfate leaching in both locations (Squyres et al. 2008; Morris et al. 2008; Yen et al. 2017; Rampe et al. 2017). A similar correlation is seen in Lake Towuti samples (positive coefficient significant at $p<0.01$; Figure I.3.15, Table I.3.4), where it is likely driven by trends in physical weathering and transport (Russell et al. 2014; Morlock et al. 2018). Variations in Ti in Towuti have been used as a proxy for increased weathering in the source region because this leads to an increase in the detrital influx of ilmenite (Russell et al. 2014). The similarity of the strong positive correlation between Si and Ti in the circum-neutral Lake Towuti system (Costa et al. 2015) suggests that sediments in Gale Crater that exhibit this elemental relationship need not have been formed in or affected by low-pH fluids, particularly if Ti-bearing phases are available and variable in the sediment source region.

Of greater interest is the potential for systems like Towuti to provide insight into Fe cycling and mineralogy in a redox-stratitifed lake dominated by mafic compositions. Strata examined by the Curiosity rover as it has ascended Mt. Sharp in Gale Crater have been interpreted as being deposited in a lacustrine-fluvial/alluvial environment (Grotzinger et al. 2014, 2015). The transition from the Bradbury group to the Mt. Sharp group at the base of Mt. Sharp represents interfingered coarse-grained alluvial and delta deposits prograding over fine-grained lake deposits (Grotzinger et al. 2015). A thick section of lacustrine mudstones within the Murray formation of the Mt. Sharp group contains a range of Fe-bearing minerals with variable oxidation state (Rampe et al. 2017). Some mudstones contain both reduced and oxidized forms of Fe whereas others are dominated by oxidized forms, with a potential increase in oxidation state upsection (Grotzinger et al. 2014, 2015; Vaniman et al. 2014; Rampe et al. 2017; Hurowitz et al. 2017). This transition from magnetite and clay-bearing facies to strata dominated by hematite and sulfate, in addition to recent identification of potential desiccation cracks in the mudstones, may be evidence of fluctuations in lake level.

Several models have been proposed to explain these mineralogical changes. One is redox stratification in the Gale Crater lake (Hurowitz et al. 2017), wherein redox sensitive mineral assemblages vary as a function of lake water depth. Magnetite and Si phases were precipitated in the reducing environment of deep water below the oxycline, and hematite and phyllosilicate phases precipitated in oxidizing shallow water influenced by the surface environment. This could provide further constraints on the depth and duration of the lake in Gale Crater. Whether the basin hosted water for one continuous period of time or several transient lakes occupied the crater would help to constrain how long the climate of Mars was amenable to the presence of liquid water at the surface.

The occurrence of magnetite in Lake Towuti, some of which is authigenic (Tamuntuan et al. 2015), in relatively shallow surface samples well above the oxycline may be evidence that this mixed-valence phase is not necessarily indicative of deposition in a reducing bottom water environment, as suggested in the redox-stratified

Gale Crater lake model. However, as with any terrestrial analogue, the influence of organic matter and biology on the rate of redox processes in Towuti must be considered, though Lake Towuti is notable for being one of the least productive tropical lakes on the planet (Haffner et al. 2001). Nontronite is also a useful mineral for addressing the water oxidation state on Earth and Mars. There is evidence that this ferric smectite may form from ferrous precursors precipitated under initially reducing conditions (Muller and Forstner 1973; Harder 1976; Pedro et al. 1978; Decarreau and Bonnin 1986), and thus its presence would indicate a change in oxidation state. Nontronite has been identified in several places on Mars, including Gale Crater (Poulet et al. 2005; Bishop et al. 2008; Milliken et al. 2010; Ehlmann et al. 2009), and it may form more commonly on Mars than on Earth because of the abundance of Fe in pyroxene and olivine in Mars's basaltic crust. It is rare in terrestrial lakes (Bristow and Milliken 2011), and if the nontronite in the Lake Towuti surface sediments is authigenic then it could provide valuable information on changes in the redox interface in the lake at those locations, and future study of this phase in these samples is warranted. Similarly, in situ identification of nontronite by Curiosity could be used to constrain redox conditions and evolution in the Gale crater lake, particularly if it over or underlies beds with greater proportions of ferric oxides.

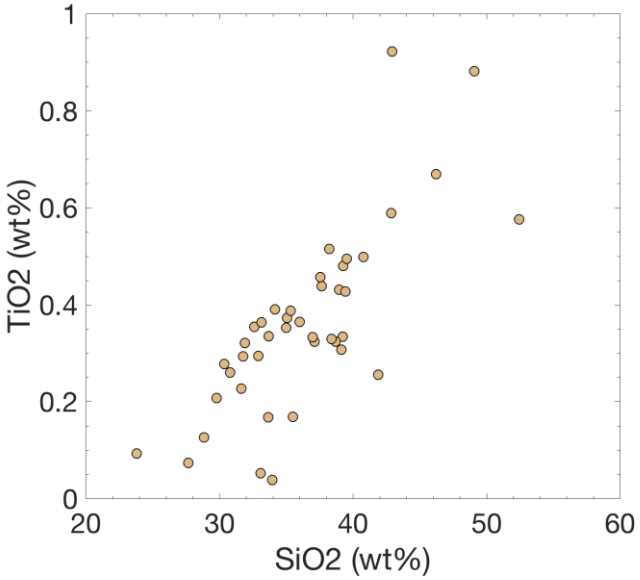

Figure I.3.15 ICP-determined Si and Ti abundances for Lake Towuti surface samples

Finally, as Curiosity has ascended Mt. Sharp, the overall abundance of FeO has remained relatively constant. However, the mineral hosts of Fe have changed tremendously, leading to various theories on the structure of the lake. In Lake Towuti, there is a similar overall steadiness in elemental FeO (Figure I.3.5, *Figure I.3.12*) with great diversity in Fe mineralogy (Figure I.3.8). While redox transformations of iron do support many types of microbial life, especially in warm tropical environments, this will catalyze reactions that are otherwise thermodynamically feasible without them, increasing the rate but not necessarily fundamentally altering the way iron may be cycled in the environment (Davison 1993). Though the tropical setting of the Towuti system is clearly not a perfect analogue for Mars, it nevertheless provides a modern setting for understanding how to infer sediment-water interactions in a redox stratified lake via chemical and mineralogical information. Understanding how chemical, grain size, and crystallinity trends might be able to inform our understanding of Fe cycling and Fe

mineralogy is necessary to fully utilize the vast amounts of chemical data that have been acquired by the rover, as sediment mineralogy is clearly being affected by many processes in the catchment and lake. In the case of Lake Towuti, VNIR reflectance spectra are clearly linked to chemical and mineralogical trends in bulk sediment samples. Similarly, certain elements (Al, Mg) provide useful proxies for mineralogy. Combined with bulk chemical measurements, VNIR spectra thus provide a rapid and non-destructive means to gain a first order understanding of sediment deposition and diagenesis across modern Lake Towuti and presumably through time, and the same may be true for lacustrine sequences on Mars.

Table I.3.4 Si Ti Regression Results

	Dependent variable:
	TiO_2, surface
SiO_2, surface	0.026***
	(0.003)
Constant	−0.594***
	(0.125)
Observations	42
R^2	0.597
Residual Std. Error	0.121 (df = 40)
F Statistic	59.187*** (df = 1; 40)
Note:	*p<0.1; **p<0.05; ***p<0.01

I.3.7 Conclusions

We find the sediment throughout the Malili Lakes system to be highly variable in terms of mineralogy and bulk chemistry, particularly with respect to the type and abundance of secondary Fe-bearing phases. The role and distribution of Fe is complex, and abundant crystalline Fe phases in the iron-rich, lateritic soils are rapidly altered after deposition on the lake surface. Hematite and magnetite are rare but present in some shallow coastal samples and absent in more distal, deeper settings. Goethite is reduced in abundance but persists to some degree in samples across the modern surface of the lake, even below the current oxycline. Although we do not know the exact processes acting in this system, it is a redox-stratified lake with low primary productivity, so the observed changes could be facilitated by Fe cycling across the oxycline.

VNIR spectroscopy and chemical analyses provide a rapid and easy way to track changes caused by weathering and transport throughout a complex ultramafic catchment and lake basin. VNIR spectral parameters are well correlated with the relevant ICP elemental abundances, demonstrating that reflectance spectra, which require little to no sample preparation, can provide useful proxies for bulk chemistry of these sediments.

Fe mineralogy is easily characterizable in the catchment but very complex in the lake, as seen in XRD patterns, and VNIR and Mössbauer spectra. Fe abundance remains high in surface samples, as seen in ICP results, but mineralogy is changing quickly to complex, highly amorphous phases. Sequential Fe extractions show a decrease in the ratio of crystalline to amorphous Fe phases from laterites to surface sediment to cores. The spatial variability in Fe hosts across the modern lake sediment surface is likely affected by variations in source composition as well as Fe cycling in the water column and early diagenetic processes.

Understanding the effects of transport, deposition, and diagenesis on sediment composition, particularly changes in Fe mineralogy, in terrestrial mafic/ultramafic lakes will continue to aid interpretation and climatic implications of Fe mineral assemblages observed in lacustrine sediments in Gale Crater and other martian paleolakes.

I.3.8 Acknowledgments

Funding for laboratory experiments was provided by Brown University Presidential Fellowship and NASA Astrobiology Institute (MIT team, award NNA13AA90A). Sample collection during the Towuti Drilling Project was supported by grants from the International Continental Scientific Drilling Program (ICDP), the US National Science Foundation (NSF-EAR #1401448), the German Research Foundation (DFG; ME 1169/26), the Swiss National Science Foundation (SNSF; 20FI21_153054/1 & 200021_153053/1&2), Brown University, Genome British Columbia, and the Ministry of Research, Technology, and Higher Education (RISTEK). PT Vale Indonesia and the US Continental Drilling Coordination Office are acknowledged for the logistical assistance to the project. This research was carried out with permission from RISTEK, the Ministry of Trade of the Government of Indonesia, the Natural Resources Conservation Center (BKSDA), and the Government of Luwu Timur of Sulawesi. We are very grateful to Dave Murray and Joe Orchardo for assistance with the ICP-AES and to Luis Gabriel Ordonez Rendon for advice on the sequential extraction protocol. Christopher Yen and Grant Rutherford assisted in laboratory work and data collection. Sample material was provided in part by the National Lacustrine Core Facility (LacCore).

I.3.9 References

Bibring J-P, Langevin Y, Gendrin A, Gondet B, Poulet F, Berthe M, Soufflot A, Arvidson R, Mangold N, Mustard J, Drossart P, the OMEGA team. Mars surface diversity as revealed by the OMEGA/Mars Express observations. Science, 2005.

Bishop JL, Lane MD, Dyar MD, Brown AJ. Reflectance and emission spectroscopy study of four groups of phyllosilicates: smectites, kaolinite-serpentines, chlorites and micas. Clay Minerals, 43 (1): 35–54, 2008

Bristow TF, Milliken, RE. Terrestrial perspective on authigenic clay mineral production in ancient martian lakes. Clays and Clay Minerals, 59 (4): 339–358, 2011.

Clark RN, Roush TL. Reflectance spectroscopy: quantitative analysis techniques for remote sensing applications. JGR, 89 (7): 6329–6340, 1984.

Clark RN, King TVV, Klejwa M, Swayze GA, Vergo N. High spectral resolution reflectance spectroscopy of minerals. Journal of Geophysical Research: Solid Earth, 95 (B8): 12653–12680, 1990.

Costa KM, Russell JM, Vogel H, Bijaksana S. Hydrological connectivity and mixing of lake towuti, Indonesia in response to paleoclimatic changes over the last 60,000 years. Palaeogeography, Palaeoclimatology, Palaeoecology, 417: 467–475, 2015.

Crowe SA, O'Neill AH, Katsev S, Hehanussa P, Haffner GD, Sundby B, Mucci A, Fowle DA. The biogeochemistry of tropical lakes: A case study from Lake Matano, Indonesia. Limnology and Oceanography, 2008.

Crowe SA Katsev S, Leslie K, Sturm A, Magen C, Nomosatryo S, Pack MA, Kessler JD, Reeburgh WS, Roberts JA, Gonzalez L, Haffner GD, Mucci A, Sundby B, Fowle DA. The methane cycle in ferruginous Lake Matano. Geobiology, 2011. 10.1111/j.1472-4669.2010.00257.x.

Davison W. Iron and manganese in lakes. Earth-Science Reviews, 34 (2): 119 – 163, 1993. ISSN 0012-8252. https://doi.org/10.1016/0012-8252(93)90029-7.

Decarreau A, Bonnin D. Synthesis and crystallogenesis at low temperature of Fe(III)-smectites by evolution of coprecipitated gels: experiments in partially reducing conditions. Clay Minerals, 1986.

Dyar MD, Agresti DG, Schaefer MW, Grant CA, Sklute EC. Mössbauer spectroscopy of earth and planetary materials. Annu. Rev. Earth Planet. Sci., 2006.

Ehlmann BL, Mustard JF, Fassett CI, Schon SC, Head III JW, Des Marais DJ, Grant JA, Murchie SL. Clay minerals in delta deposits and organic preservation potential on Mars. Nature Geoscience, 1: 355–358, 2008.

Ehlmann BL, Mustard JF, Swayze GA, Clark RN, Bishop JL, Poulet F, Des Marais DJ, Roach LH, Milliken RE, Wray JJ, Barnouin-Jha O, Murchie SL. Identification of hydrated silicate minerals on Mars using MRO-CRISM: Geologic context near Nili Fossae and implications for aqueous alteration. Journal of Geophysical Research-Planets, 114, 2009.

Gaffey SJ, McFadden LA, Nash D, Pieters CM. Remote geochemical analysis: elemental and mineralogical composition, chapter Ultraviolet, Visible, and Near-Infrared Reflectance Spectroscopy: Laboratory Spectra of Geologic Materials, pages 43–78. Cambridge University Press, 1993.

Goudge TA, Russell JM, Mustard JF, Head JW, Bijaksana S. A 40,000 yr record of clay mineralogy at Lake Towuti, Indonesia: Paleoclimate reconstruction from re ectance spectroscopy and perspectives on paleolakes on Mars. GSA Bulletin, 2017.

Grotzinger JP, Sumner DY, Kah LC, Stack K, Gupta S, Edgar L, Rubin D, Lewis K, Schieber J, Mangold N, Milliken R, Conrad PG, DesMarais D, Farmer J, Siebach K, Calef III F, Hurowitz J, McLennan SM, Ming D, Vaniman D, Crisp J, Vasavada A, Edgett KS, Malin M, Blake D, Gellert R, Mahaffy P, Wiens RC, Maurice S, Grant JA, Wilson S, Anderson RC, Beegle L, Arvidson R, Hallet B, Sletten RS, Rice M, Bell III J, Griffes J, Ehlmann B, Anderson RB, Bristow TF, Dietrich WE, Dromart G, Eigenbrode J, Fraeman A, Hardgrove C, Herkenhoff K, Jandura L, Kocurek G, Lee S, Leshin LA, Leveille R, Limonadi D, Maki J, McCloskey S, Meyer M, Minitti M, Newsom H, Oehler D, Okon A, Palucis M, Parker T, Rowland S, Schmidt M, Squyres S, Steele A, Stolper E, Summons R, Treiman A, Williams R, Yingst A. A habitable fluvio-lacustrine environment at Yellowknife Bay, Gale Crater, Mars. Science, 343, 2014.

Grotzinger JP, Gupta S, Malin MC, Rubin DM, Schieber J, Siebach K, Sumner DY, Stack KM, Vasavada AR, Arvidson RE, Calef III F, Edgar L, Fischer, WF Grant JA, Griffes J, Kah LC, Lamb MP, Lewis KW, Mangold N, Minitti ME, Palucis M, Rice M, Williams RM, Yingst RA, Blake D, Blaney D, Conrad P, Crisp J, Dietrich WE, Dromart G, Edgett KS, Ewing RC, Gellert R, Hurowitz JA, Kocurek G, Mahaffy P, McBride MJ, McLennan SM, Mischna M, Ming D, Milliken RE, Newsom H, Oehler D, Parker TJ, Vaniman D, Wiens RC, Wilson SA. Deposition, exhumation, and paleoclimate of an ancient lake deposit, Gale crater, Mars. Science, 350. doi: 10.1126/science.aac7575, 2015.

Haffner GD, Hehanussa P E, Hartoto D. The biology and physical processes of large lakes of Indonesia: Lakes Matano and Towuti. In Munawar M, Hecky RE, editors, The Great Lakes of the World (GLOW): Food-web, Health and Integrity, page 129–155. Blackhuys Publishers, 2001.

Harder H. Nontronite synthesis at low temperatures. Chemical Geology, 1976.

Hasberg AKM, Melles M, Wennrich V, Just J, Held P, Morlock MA, Vogel H, Russell JM, Bijaksana S, Opitz S. Modern sedimentation processes in Lake Towuti, Indonesia, revealed by the composition of surface sediments. Sedimentology, 2018.

Hurowitz JA, Grotzinger JP, Fischer WW, McLennan SM, Milliken RE, Stein N, Vasavada AR, Blake DF, Dehouck E, Eigenbrode JL, Fairen AG, Frydenvang J, Gellert R, Grant JA, Gupta S, Herkenhoff KE, Ming DW, Rampe EB, Schmidt ME, Siebach K, Stack-Morgan K, Sumner DY, and Wiens RC. Redox stratification of an ancient lake in Gale Crater, Mars. Science, 2017.

Kadarusman A, Miyashita S, Maruyama S, Parkinson CD, Ishikawa A. Petrology, geochemistry and paleogeographic reconstruction of the East Sulawesi Ophiolite, Indonesia. Tectonophysics, 392 (1): 55 – 83, 2004.

McSween HY, Taylor GJ, Wyatt MB. Elemental composition of the martian crust. Science, 2009.

Milliken RE, Grotzinger JP, Thompson BJ. Paleoclimate of Mars as captured by the stratigraphic record in Gale Crater. Geophysical Research Letters, 37, 2010. 10.1029/2009GL041870.

Morlock MA, Vogel H, Nigg V, Ordonez L, Hasberg AKM, Melles M, Russell JM, Bijaksana S. Climatic and tectonic controls on source-to-sink processes through space and time in a tropical ultramafic lake catchment: Lake Towuti, Indonesia. J. Paleolimnol. online first,2018.

Morris RV, Klingelhofer G, Schroder C, Fleischer I, Ming DW, Yen AS, Gellert R, Arvidson RE, Rodionov DS, Crumpler LS, Clark BC, Cohen BA, McCoy TJ, Mittlefehldt DW, Schmidt ME, de Souza Jr PA, Squyres SW. Iron mineralogy and aqueous alteration from Husband Hill through Home Plate at Gusev Crater, Mars: Results from the Mossbauer instrument on the Spirit Mars Exploration Rover. JGR, 2008.

Muller G, Forstner U. Recent iron ore formation in Lake Malawi, Africa. Mineral. Deposita, 1973.

Murray RW, Miller DJ, Kryc KA. Analysis of major and trace elements in rocks, sediments, and interstitial waters by inductively coupled plasma-atomic emission spectrometry (ICP-AES). ODP Technical Note, (1): 1–27, 2000.

Pedro G, Carmouze JP, Velde B. Peloidal nontronite formation in recent sediments of Lake Chad. Chemical Geology, 23: 139–149, 1978.

Poulet F, Bibring JP, Mustard JF, Gendrin A, Mangold N, Langevin Y, Arvidson RE, Gondet , Gomez , Berthe M, Erard S, Forni O, Manaud N, Poulleau G, Soufflot A, Combes M, Drossart P, Encrenaz T, Fouchet T, Melchiorri R, Bellucci G, Altieri F, Formisano V, Fonti S, Capaccioni F, Cerroni P, Coradini A, Korablev O, Kottsov V, Ignatiev N, Titov D, Zasova L, Pinet P, Schmitt B, Sotin C, Hauber E, Hoffmann H, Jaumann R, Keller U, Forget F, the Omega Team. Phyllosilicates on Mars and implications for early martian climate. Nature, 2005.

Poulton SW, Canfied DE. Development of a sequential extraction procedure for iron: implications for iron partitioning in continentally derived particulates. Chemical Geology, 2005.

Rampe EB, Ming DW, Blake DF, Bristow TF, Chipera SJ, Grotzinger JP, Morris RV, Morrison SM, Vaniman DT, Yen AS, Achilles CN, Craig PI, Des Marais DJ, Downs RT, Farmer JD, Fendrich KV, Gellert R, Hazen RM, Kah LC, Morookian JM, Peretyazhko TS, Sarrazin P, Treiman AH, Berger JA, Eigenbrode J, Fairen AG, Forni O, Gupta S, Hurowitz JA, Lanza NL, Schmidt ME, Siebach K, Sutter B, Thompson LM. Mineralogy of an ancient lacustrine mudstone succession from the Murray formation, Gale crater, Mars. EPSL, 471: 172–185, 2017.

Ruff SW, Farmer JD, Calvin WM, Herkenhoff KE, Johnson JR, Morris RV, Rice MS, Arvidson RE, Bell JF, Christensen PR, Squyres SW. Characteristics, distribution, origin, and significance of opaline silica observed by the Spirit rover in Gusev crater, Mars. Journal of Geophysical Research, 2011.

Ruff SW, Farmer JD. Silica deposits on Mars with features resembling hot spring biosignatures at El Tatio in Chile. Nature Communications, 2016.

Russell JM, Vogel H, Konecky BL, Bijaksana S, Huang Y, Melles M, Wattrus N, Costa K, King JW. Glacial forcing of central Indonesian hydroclimate since 60,000 y B.P. 111 (14): 5100–5105, 2014.

Russell JM, Bijaksana S, Vogel H, Melles M, Kallmeyer J, Ariztegui D, Crowe S, Fajar S, Hafidz A, Haffner D, Hasberg A, Ivory S, Kelly C, King J, Kirana K, Morlock M, Noren A, O'Grady R, Ordonez L, Stevenson J, von Rintelen T, Vuillemin A, Watkinson I, Wattrus N, Wicaksono S, Wonik T, Bauer K, Deino A, Friese A, Henny C, Imran, Marwoto R, Ngkoimani LO, Nomosatryo S, Safiuddin LO, Simister R, Tamuntuan G. (2016). The Towuti Drilling Project: paleoenvironments, biological evolution, and geomicrobiology of a tropical Pacific lake. Scientific Drilling, 21, 29-40. doi: 10.5194/sd-21-29-2016

Sklute EC, Kashyap S, Dyar MD, Holden JF, Tague T, Wang P, Jaret SJ. Spectral and morphological characteristics of synthetic nanophase iron (oxyhydr)oxides. Physics and Chemistry of Minerals, 2017. 10.1007/s00269-017-0897-y.

Sklute EC, Dyar MD, Kashyap S, Holden JF, Brady JB. Multi-temperature mossbauer spectra of nanophase iron (oxyhydr)oxides. Physics and Chemistry of Minerals, in review.

Squyres SW, Arvidson RE, Ruff S, Gellert R, Morris RV, Ming DW, Crumpler L, Farmer JD, Des Marais DJ, Yen A, McLennan SM, Calvin W, Bell III JF, Clark BC, Wang A, McCoy TJ, Schmidt ME, de Souza Jr PA. Detection of silica-rich deposits on Mars. Science, 320: 1063–1067, 2008.

Sutter B, Dalton JB, Ewing SA, Amundson R, McKay CP. Terrestrial analogs for interpretation of infrared spectra from the martian surface and subsurface: Sulfate, nitrate, carbonate, andphyllosilicate-bearing Atacama Desert soils. Journal of Geophysical Research, 2007.

Tamuntuan G, Bijaksana S, King J, Russell J, Fauzi U, Maryunani K, Aufa N, Safiuddin LO. Variation of magnetic properties in sediments from Lake Towuti, Indonesia, and its paleoclimatic significance. Palaeogeography, Palaeoclimatology, Palaeoecology, 2015.

Vaniman DT, Bish DL, Ming DW, Bristow TF, Morris RV, Blake DF, Chipera SJ, Morrison SM, Treiman AH, Rampe EB, Rice M, Achilles CN, Grotzinger JP, McLennan SM, Williams J, Bell III JF, Newsom HE, Downs RT, Maurice S, Sarrazin P, Yen AS, Morookian JM, Farmer JD, Stack K, Milliken RE, Ehlmann BL, Sumner DY, Berger G, Crisp JA, Hurowitz JA, Anderson R, Des Marais DJ, Stolper EM, Edgett KS, Gupta S, Spanovich N. Mineralogy of a Mudstone at Yellowknife Bay, Gale Crater, Mars. Science, 343, 2014.

Vogel H, Russell JM, Cahyarini SY, Bijaksana S, Wattrus N, Rethemeyer J, Melles M. Depositional modes and lake-level variability at Lake Towuti, Indonesia, during the past 29 kyr BP. Journal of Paleolimnology, 2015.

Vuillemin A, Friese A, Alawi M, Henny C, Nomosatryo S, Wagner D, Crowe SA, Kallmeyer J. Geomicrobiological features of ferruginous sediments from Lake Towuti, Indonesia. Frontiers in Microbiology, 2016. 10.3389/fmicb.2016.01007.

Wagner C, Schade U. Measurements and calculations for estimating the spectrometric detection limit for carbonates in martian soil. Icarus, 1996.

Weber AK, Russell JM, Goudge TA, Salvatore MR, Mustard JF, Bijaksana S. Characterizing clay mineralogy in Lake Towuti, Indonesia, with reflectance spectroscopy. Journal of Paleolimnology, 54 (2): 253–261, 2015.

Yen AS, Morris RV, Clark BC, Gellert R, Knudson AT, Squyres S, Mittlefehldt DW, Ming DW, Arvidson R, McCoy T, Schmidt M, Hurowitz J, Li R, and Johnson JR. Hydrothermal processes at Gusev Crater: An evaluation of Paso Robles class soils. Journal of Geophysial Research, 2008.

Yen AS, Ming DW, Vaniman DT, Gellert R, Blake DF, Morris RV, Morrison SM, Bristow TF, Chipera SJ, Edgett KS, Treiman AH, Clark BC, Downs RT, Farmer JD, Grotzinger JP, Rampe EB, Schmidt ME, Sutter B, and Thompson LM. Multiple stages of aqueous alteration along fractures in mudstone and sandstone strata in Gale Crater, Mars. Earth and Planetary Science Letters, 2017.

Appendix II

XRF correction workflow

II.1 Element-wise correction of quasi-continuous XRF core scanner data

In total, 106 split cores of the upper ~100 m composite core succession from TDP Site 1 were scanned on an XRF core scanner (ITRAX, Cox Ltd., Sweden) equipped with a chromium anode X-ray tube (Cr-tube; first run) and a molybdenum anode X-ray tube (Mo-tube; second run) set to 30 kV, 50 mA, and 50 s integration time at 5 mm resolution at the University of Bern, Switzerland. Cores were scanned consecutively in order of the sediment splice. Prior to each measured core section, a site-specific standard (10 x 10 x 0.5 cm), prepared from dried and homogenised sediment recovered from Lake Towuti in 2010, was measured to assess changes in X-ray source intensity. Cores were kept at room temperature ~1-2 h prior to measuring and the core surface was let to dry before the core was covered by an ultrathin plastic foil to avoid desiccation during the measurement. Beginning and end points of the XRF measurement were marked in the sediment during the Cr-tube sequence. With little effort, this procedure helps to assure a synchronous start and end point between both measurement setups.

Raw XRF spectra were processed in the software Q-spec (version 8.6.0). For Cr-tube measurements, two settings files were used. For each core, the settings file, which resulted in the lowest mean-square error in spectra evaluation, was chosen. This depended mostly on the amount of siderite in the sediments. The settings files are therefore termed ‘sideritic’ and ‘not_sideritic’. Sections of uneven core surface, gaps, and event layers were manually identified based on high Ar-counts and low total counts, and were removed from the data set. All further adjustments to the measurement sequence were done in R (R Development Core Team, 2017).

Both XRF data sets (Cr-tube and Mo-tube measurements) were corrected for tube aging by evaluating the site-specific standard measurement series. As suggested by Ohlendorf et al. (2015), tube aging does not affect all elements in the same way but is dependent on the atomic number of the element. Measurements show a linear trend in tube aging, with opposing signs for light and heavy elements, respectively (Figure S5.2). Based on these measurements, a linear regression correction was applied to the sediment core sequence. For most major elements, this correction is visible, but comparatively small (Figure S5.2).

To correct for changes in interstitial water, a potential water film between core surface and covering foil, and grain size variations, a linear regression model was calculated between core surface scans and sample measurements performed on dried and homogenized samples. For this, 188 discrete samples (48-cm spacing, ~8 cm^3) of TDP Site 1 were freeze-dried, homogenised, and an aliquot pressed into sample holders (2.2 x 2.2 x 0.2 cm), which were built from small plastic container lids (Licefa GmbH, Germany). The small volume (~1 cm^3) allows the analysis of discrete samples even if material is precious and only small quantities are available. Filled sample holders were aligned on a flat piece of cardboard to fit the core scanning assembly (Figure S5.1). With this simple setup, a total of ~65 samples can be sequentially analysed. Discrete samples were scanned at 2 mm resolution at the same tube settings (30 kV, 50 mA, 50 s) as the sediment cores, yielding ~10 2 mm-integral XRF measurements per sample. All 188 samples were scanned with the Mo-tube, 87 samples (1.5 m spacing down-core) were scanned with the Cr-tube. The average of 8 core measurements equivalent to 4 cm of sample was correlated to the average of the corresponding dried homogenised discrete

sample (10 measurements). Correlations were evaluated for each element individually and a linear regression was calculated to convert wet XRF counts to dry XRF counts. In several cases, the relationships were dependent on lithology, water content, or other parameters. If such systematic effects were detected, the data set was split and sections were corrected separately. Details for each element are given below in individual data sheets. XRF measurements are reported in XRF counts, ICP-AES data in wt-%.

To combine Cr- and Mo-tube measurement series into one consistent data set of maximum data quality, the distinction between tubes was made based on the correlation coefficients between corrected XRF core measurements and absolute concentrations from ICP-AES. Sediment core measurements of both X-ray tubes are highly correlated for K, Ca, Ti, and Fe ($r > 0.9$), as well as for Mn, Ni, Zn, Zr ($r > 0.8$). Minor differences in depth scales (<1 cm) were adjusted manually during post-processing.

The final selection of elements used for end-member analysis was made based on comparison of the corrected XRF data set with ICP-AES measurements (Spearman's rank correlation), XRF spectrum evaluation, and geologic context. In total, 19 elements were selected for the end-member analysis.

II.1.1 Comparison to other proposed correction methods

The need to correct XRF measurements for systematic biases in the data set has received increasing attention in recent years (Croudace & Rothwell, 2015; Löwemark et al., 2011; Tjallingii et al., 2007) and several methods to approach this issue have been suggested (Chen et al., 2016; Kido et al., 2006; Lyle et al., 2012; Weltje & Tjallingii, 2008). Particularly, Weltje and Tjallingii (2008) argue for a correction based on centred-log-ratio calculations rather than corrections based on linear relationships. However, in the complex setting of Lake Towuti, where numerous processes influence sedimentation at the coring site, correction techniques that require the calculation of ratios are difficult to apply. In contrast to simple lake systems (i.e. two compositional endmembers), the chemical composition of the clastic sediments varies strongly. Hence, selecting a common denominator for ratio calculations is challenging, because frequently used elements such as Al or Ti do not capture the variation in all lithologies. Secondly, elements with similar atomic number are favoured for ratio calculation, because matrix effects have opposing signals in light and heavy elements. Towuti sediments cover a wide range of elements (Mg to Zr), i.e. at least two elements would be necessary as denominators to ensure that the atomic number is not too different from the numerator. The correction of XRF sediment core-scanning results by XRF scans of dried, homogenised samples allows eliminating effects of water content, grain size, and core surface roughness. Matrix effects may not be fully accounted for by this technique, but this bias can be estimated by comparison to ICP measurements and elements with high divergence from ICP measurements can be discarded. XRF measurement corrections based on dry samples have the advantage of a direct empirical correction, where elements with a good fit can be clearly identified in the correction process.

II.1.2 References

Chen Q, Kissel C, Govin A, Liu Z, Xie X. (2016). Correction of interstitial water changes in calibration methods applied to XRF core-scanning major elements in long sediment cores: Case study from the South China Sea. Geochemistry, Geophysics, Geosystems, 17(5), 1925-1934. doi: 10.1002/2016gc006320

Croudace IW, Rothwell RG. (2015). Micro-XRF Studies of Sediment Cores. Application of a non-destructive tool for the environmental sciences. Dordrecht: Springer.

Kido Y, Koshikawa T, Tada R. (2006). Rapid and quantitative major element analysis method for wet fine-grained sediments using an XRF microscanner. Marine Geology, 229(3-4), 209-225. doi: 10.1016/j.margeo.2006.03.002

Löwemark L, Chen HF, Yang TN, Kylander M, Yu EF, Hsu YW, Lee TQ, Song SR, Jarvis S. (2011). Normalizing XRF-scanner data: A cautionary note on the interpretation of high-resolution records from organic-rich lakes. Journal of Asian Earth Sciences, 40(6), 1250-1256. doi: 10.1016/j.jseaes.2010.06.002

Lyle M, Oliarez Lyle A, Gorgas T, Holbourn A, Westerhold T, Hathorne E, Kimoto K, Yamamoto S. (2012). Data report: raw and normalized elemental data along the Site U1338 splice from X-ray fluorescence scanning. doi: 10.2204/iodp.proc.320321.203.2012

Morlock MA, Vogel H, Hadi J, Foubert A, Ariztegui D, Melles M, Russell JM, Bijaksana S. (in review). Temporal and spatial Variability of Siderite formation in ferruginous Sediments. submitted to Geology.

R Development Core Team (2017) R: A language and environment for statistical computing. R Foundation for Statistical Computing. Available at: www.r-project.org

Tjallingii R, Röhl U, Kölling M, Bickert T. (2007). Influence of the water content on X-ray fluorescence core-scanning measurements in soft marine sediments. Geochemistry, Geophysics, Geosystems, 8(2), doi: 10.1029/2006gc001393

Vuillemin A, Horn F, Friese A, Winkel M, Alawi M, Wagner D, Henny C, Orsi WD, Crowe SA, Kallmeyer J. (in press). Metabolic potential of microbial communities from ferruginous sediments. Environmental Microbiology. doi: 10.1111/1462-2920.14343

Weltje GJ, Tjallingii R. (2008). Calibration of XRF core scanners for quantitative geochemical logging of sediment cores: Theory and application. Earth and Planetary Science Letters, 274(3-4), 423-438. doi: 10.1016/j.epsl.2008.07.054

Elements

II.2 Cr-tube

Magnesium (Mg)

Average for Mg in original wet XRF core measurements was 300 counts.

Mg	adj. R^2	Regression intercept	Regression slope	n
XRF cores - dry XRF	0.83	112.6	0.36	81
dry XRF - ICP-AES	0.92	50.2	119	78
XRF cores - ICP-AES	0.73	133.4	42.4	78
final XRF - ICP-AES	r = 0.86*	p-value: 0.00		76

* Spearman's rank correlation (for all elements)

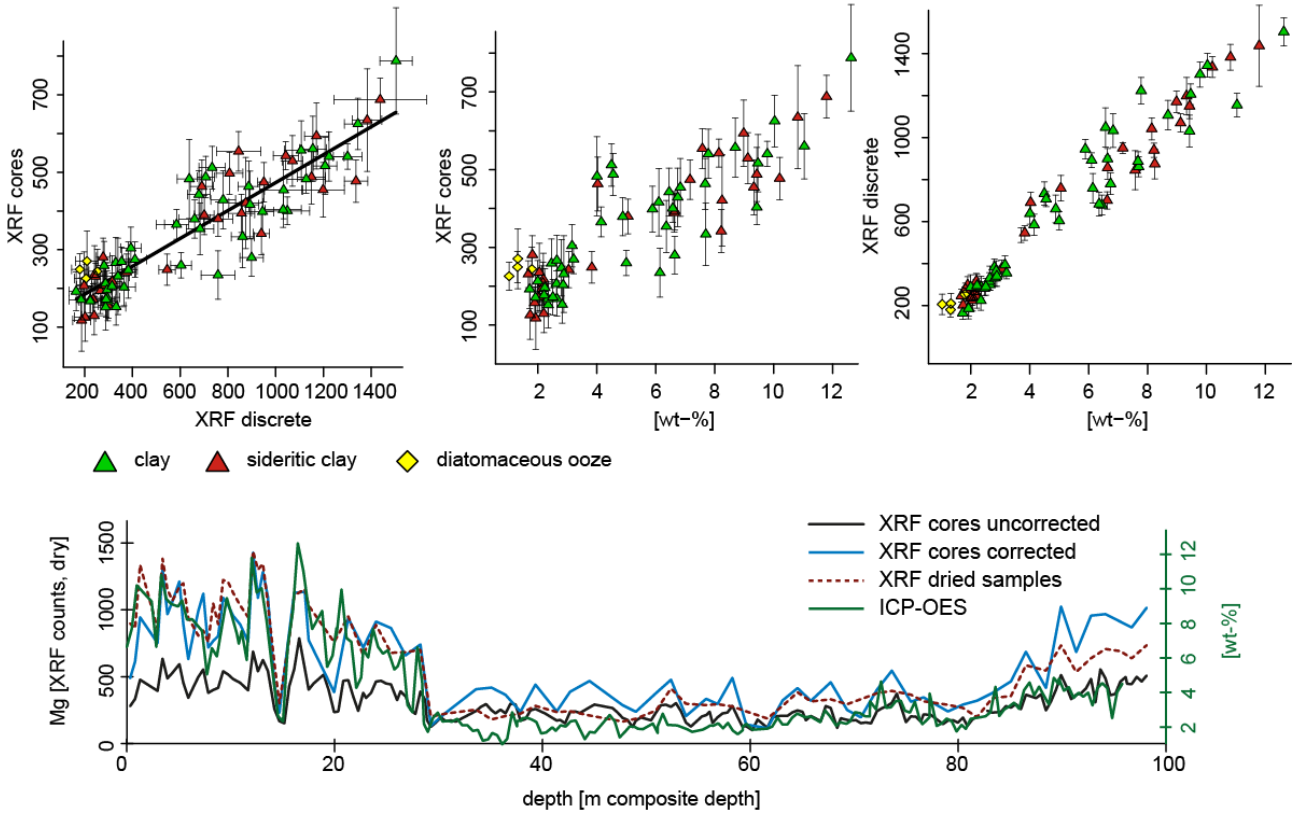

Aluminium (Al)

Average for Al in original wet XRF core measurements was 3,030 counts. Two outliers were removed in the ICP-AES data set.

Al	adj. R^2	Regression intercept	Regression slope	n
XRF cores - dry XRF	0.51	181.3	0.55	81
dry XRF - ICP-AES	0.78	206.8	863.7	78
XRF cores - ICP-AES	0.30	604.9	414.2	78
final XRF - ICP-AES	r = 0.60*	p-value: 0.00		76

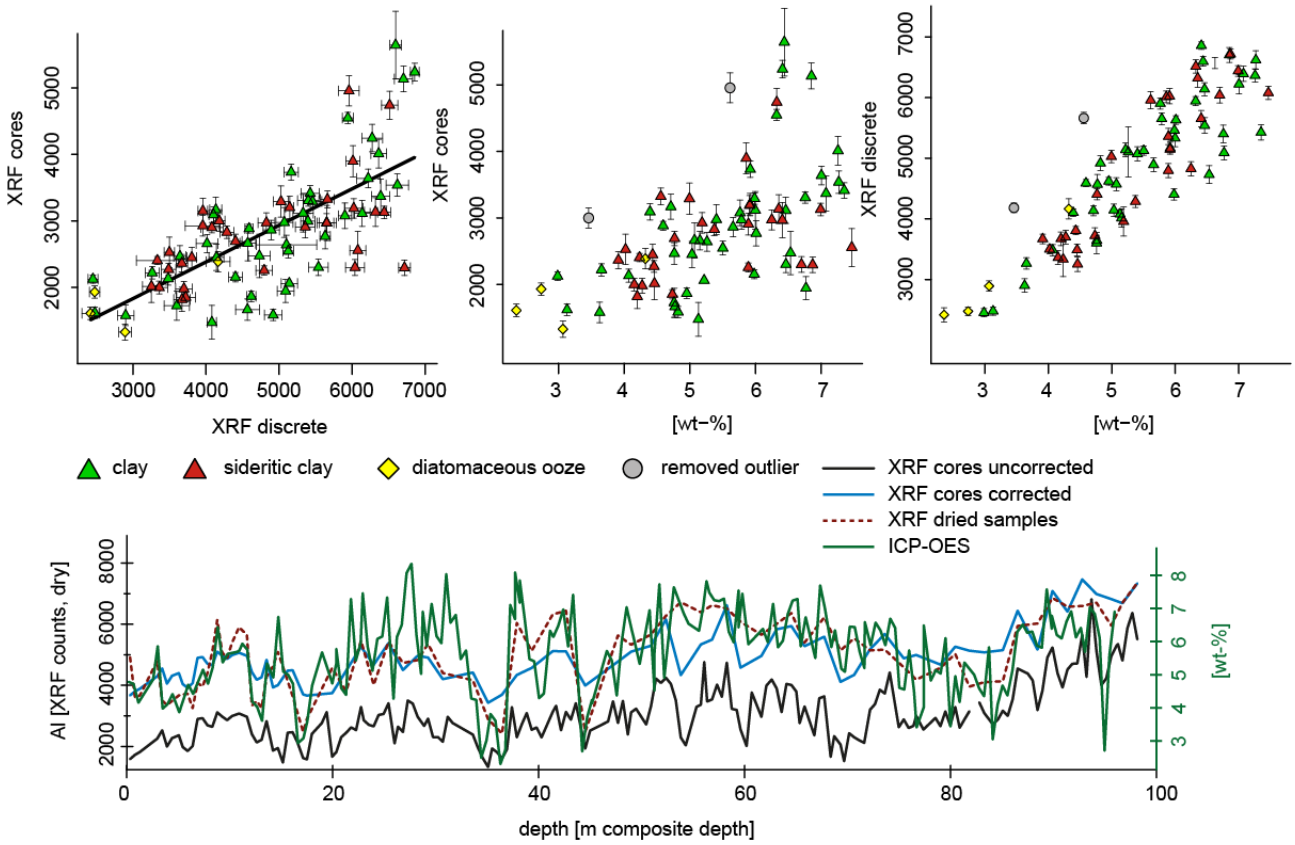

Silicon (Si)

Average for Si in original wet XRF core measurements was 37,000 counts. The data set was split for linear regression correction. Splitting was based on lithology, separating the diatomaceous ooze from all other lithologies and on the settings file used, which largely depends on the amount of siderite in the sample.

Si	adj. R^2	Regression intercept	Regression slope	n
XRF cores - dry XRF (joint)	0.45	10100	0.44	81
XRF cores - dry XRF (diatom ooze)	0.65	73560	0.83	4
XRF cores - dry XRF *(sideritic)*	0.28	30300	0.6	31
XRF cores - dry XRF *(not_sideritic)*	0.43	42000	0.47	46
dry XRF - ICP-AES	0.29	26800	1470	78
XRF cores - ICP-AES	0.16	19700	740	78
final XRF - ICP-AES	r = 0.65*	p-value: 0.00		76

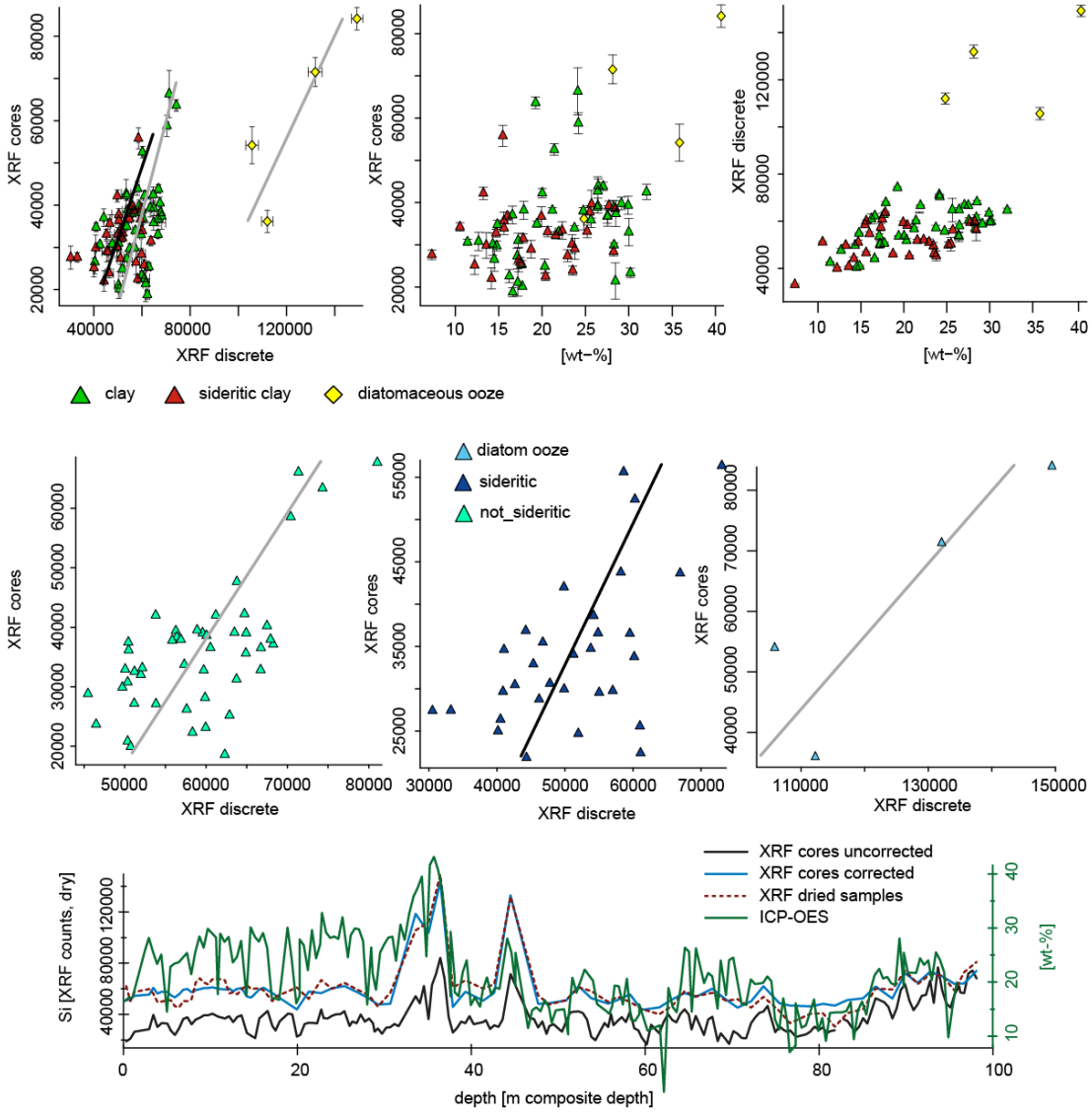

Phosphorus (P)

Average for P in original wet XRF core measurements was 1,020 counts. The data set was split for linear regression correction. Splitting was based on the settings file used, which largely depends on the amount of siderite in the sample. A satisfying relationship could be established for the samples based on the settings file *sideritic*, whereas the correlation for the settings file not_*sideritic* is poor.

P	adj. R^2	Regression intercept	Regression slope	n
XRF cores - dry XRF (joint)	0.06	458	0.63	81
XRF cores - dry XRF *(sideritic)*	0.62	694	0.42	31
XRF cores - dry XRF *(not_sideritic)*	0.08	830	0.54	50
dry XRF - ICP-AES	0.48	731	4507	78
XRF cores - ICP-AES	0.16	707	6317	78
final XRF - ICP-AES	r = 0.74*	p-value: 0.00		75

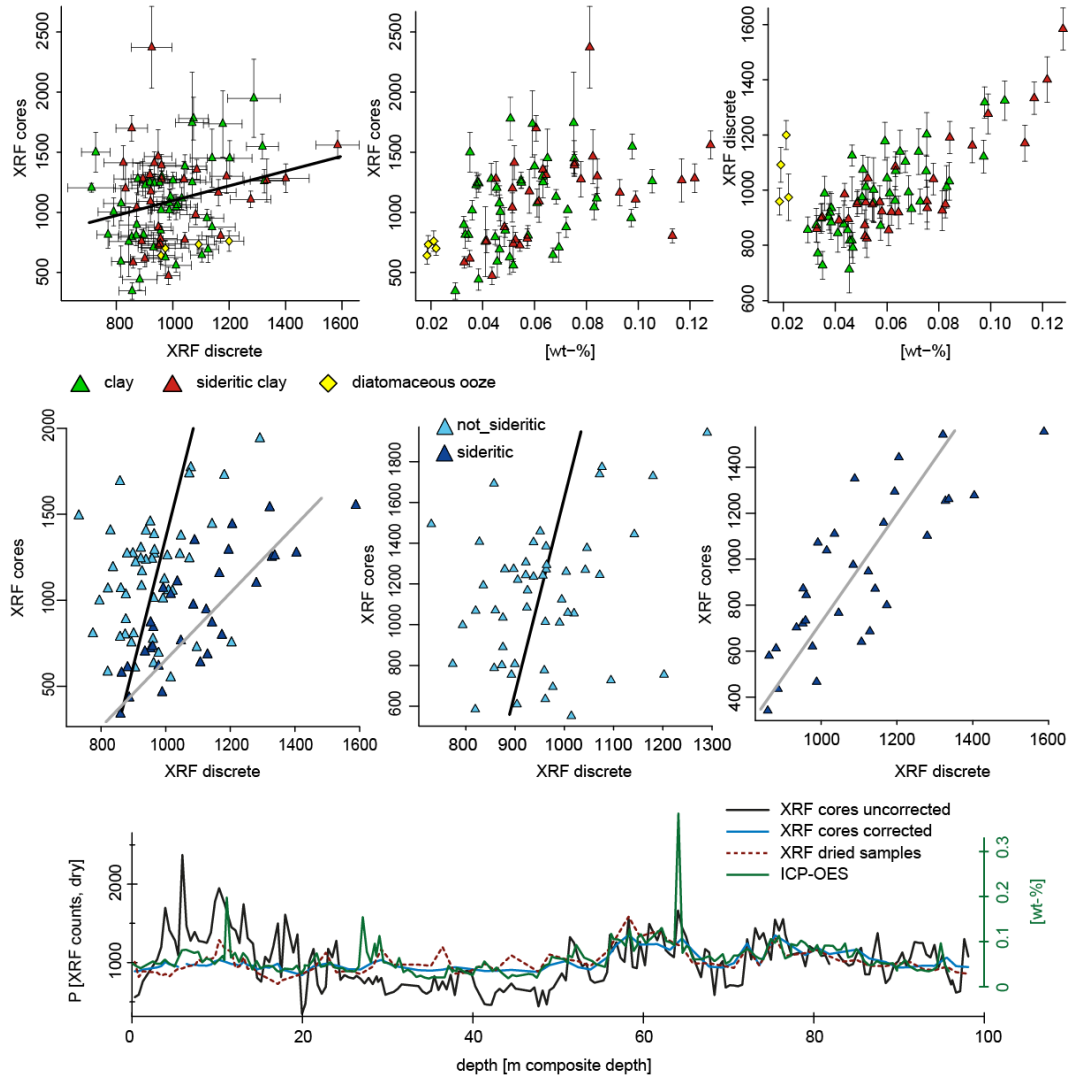

Sulphur (S)

Average for S in original wet XRF core measurements was 1,640 counts.

S	adj. R^2	Regression intercept	Regression slope	n
XRF cores - dry XRF	0.67	347	0.6	81

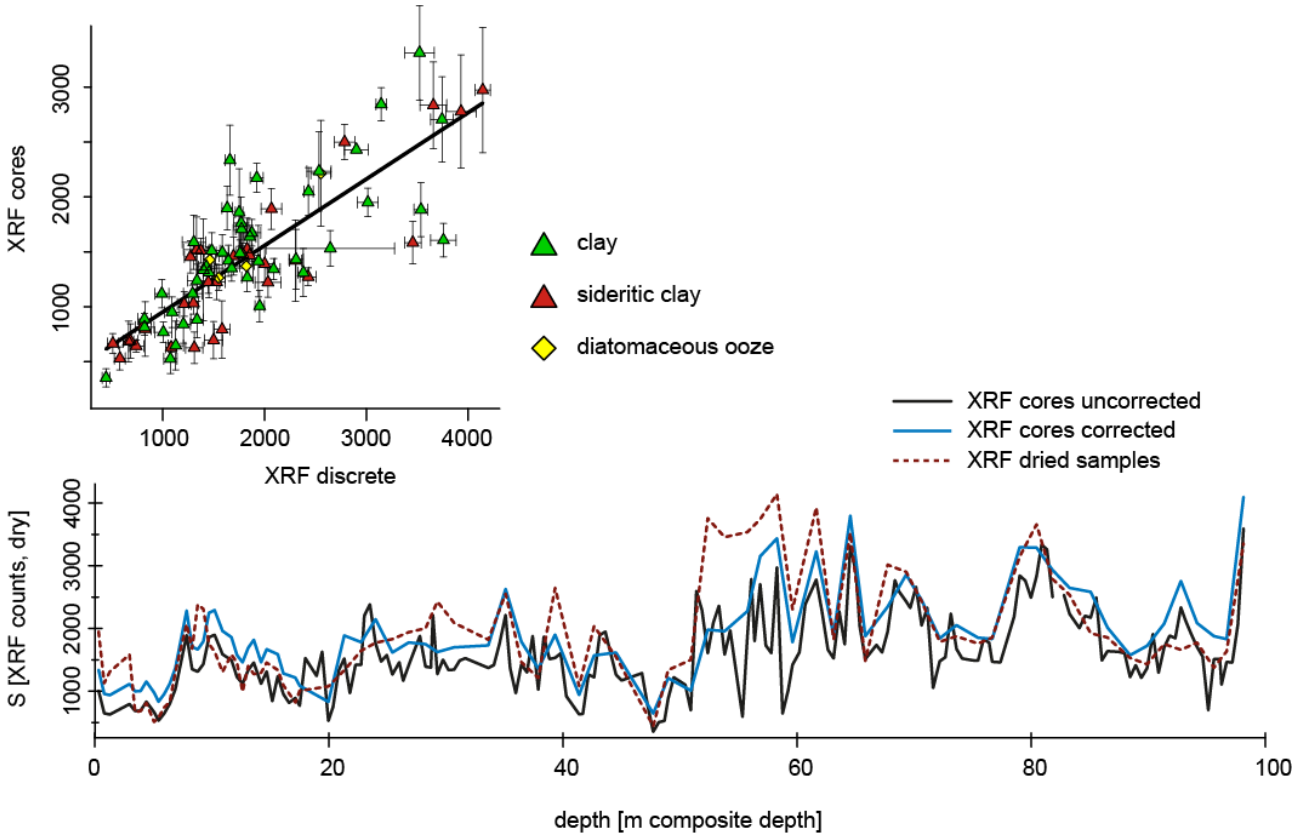

Scandium (Sc)

Average for Sc in original wet XRF core measurements was 2,680 counts. The data set was split for linear regression correction. Splitting was based on lithology, separating the diatomaceous ooze from all other lithologies.

Sc	adj. R^2	Regression intercept	Regression slope	n
XRF cores - dry XRF	0.71	269	1.28	81
XRF cores - dry XRF (diatom ooze)	0.70	-878	1.44	4
XRF cores - dry XRF (all other lithologies)	0.66	396	0.54	77

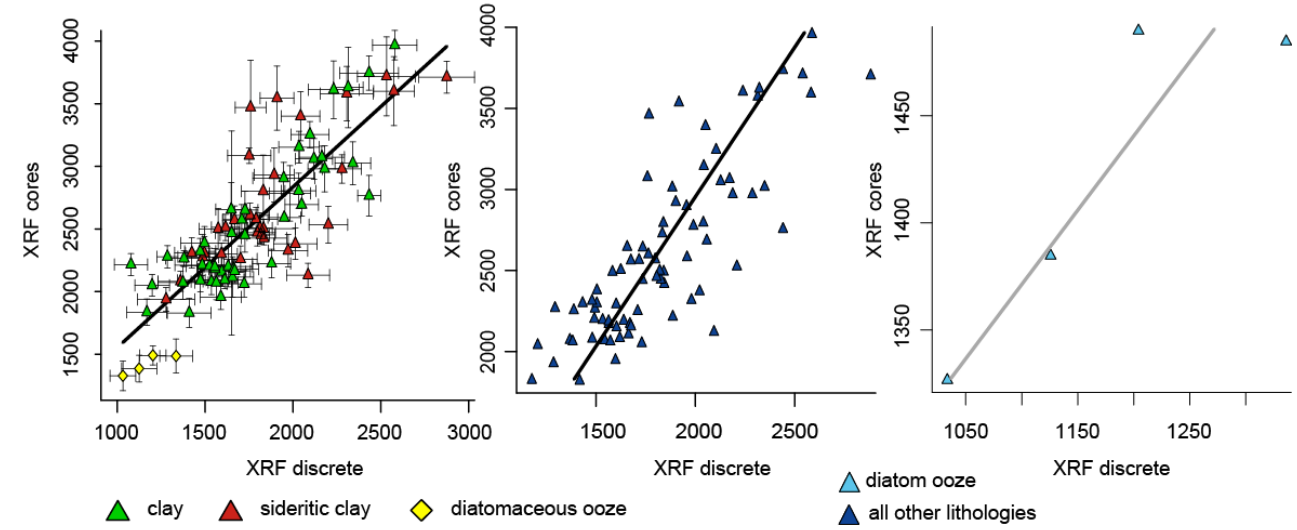

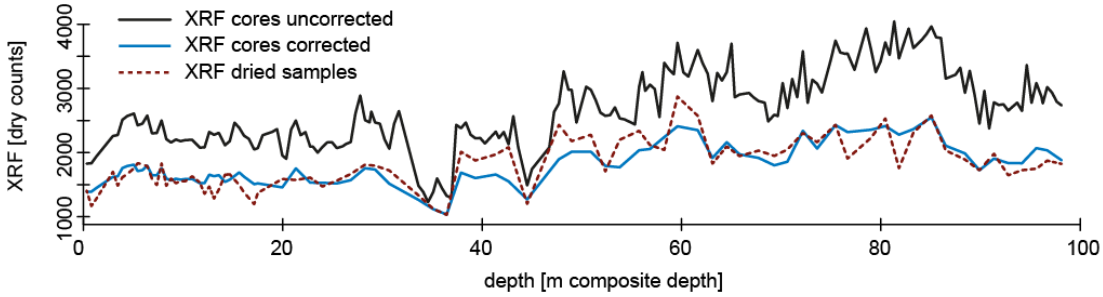

Nickel (Ni)

Average for Ni in original wet XRF core measurements was 75,000 counts. Ni measurements have high standard deviations for the wet XRF core measurements because nickel in Lake Towuti sediments occurs in the authigenic mineral millerite, which forms concretions in the sediment (Morlock et al., in review).

Ni	adj. R^2	Regression intercept	Regression slope	n
XRF cores - dry XRF	0.60	4648	0.65	81
dry XRF - ICP-AES	0.67	48800	105400	78
XRF cores - ICP-AES	0.71	26200	91600	78
final XRF - ICP-AES	r = 0.75*	p-value: 0.00		76

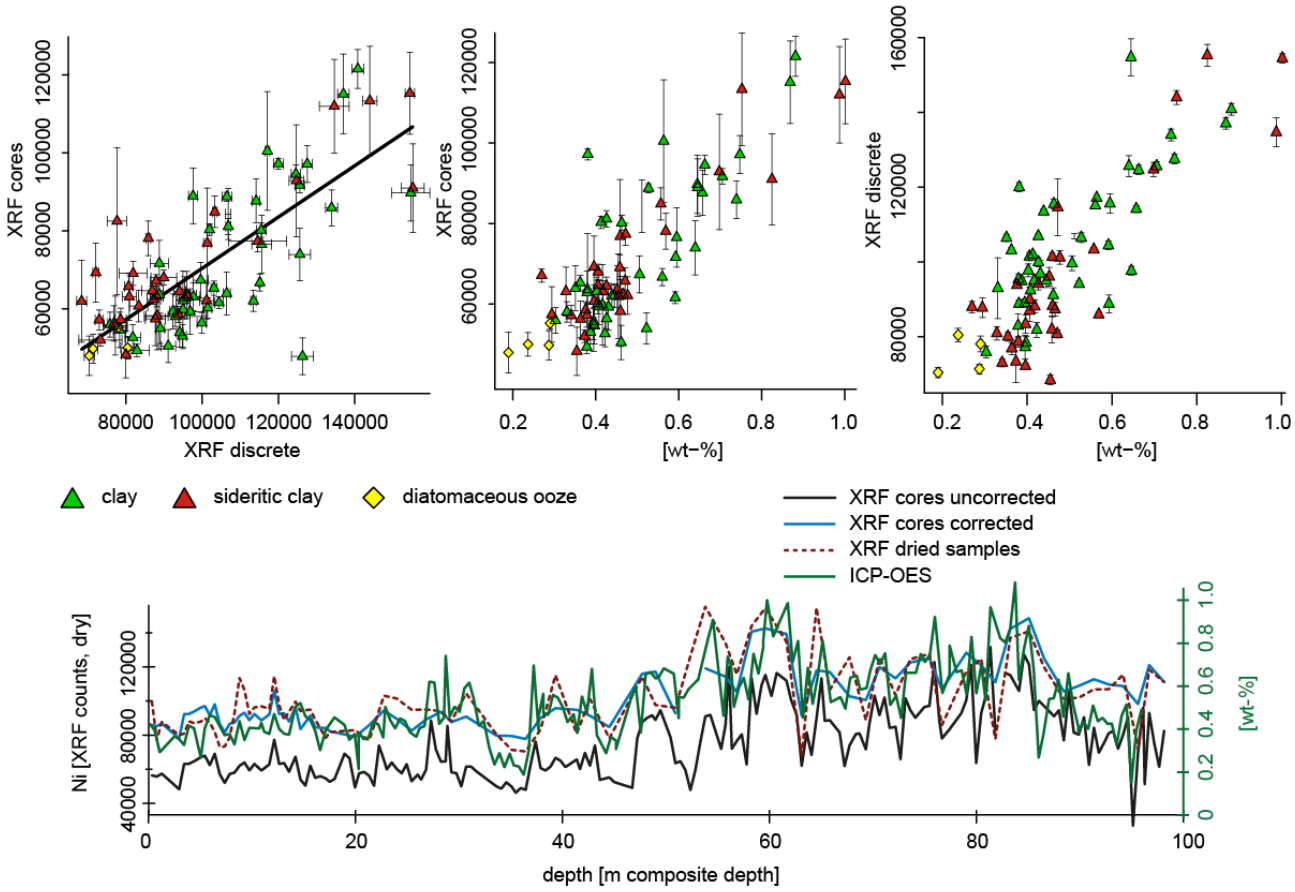

Strontium (Sr)

Average for Sr in original wet XRF core measurements was 830 counts. The data set was split for linear regression correction. Splitting was based on lithology, separating the diatomaceous ooze from all other lithologies. For diatom ooze sediments, no clear linear regression model could be established, but samples clearly differed from all other lithologies. Hence, a different correction was applied: Diatom ooze sediments were corrected based on the linear regression model for all other elements. This leads to a strong overestimation of corrected dry counts. Therefore, the mean offset between all corrected wet samples from the oozes and all dried homogenised samples from the oozes (1058 counts) was subtracted from the initially calculated values. This provides a good fit between dried sample values and corrected XRF cores (see time series plot below).

Sr	adj. R^2	Regression intercept	Regression slope	n
XRF cores - dry XRF	0.40	318	0.36	81
XRF cores - dry XRF (all other lithologies)	0.60	416	1.04	76

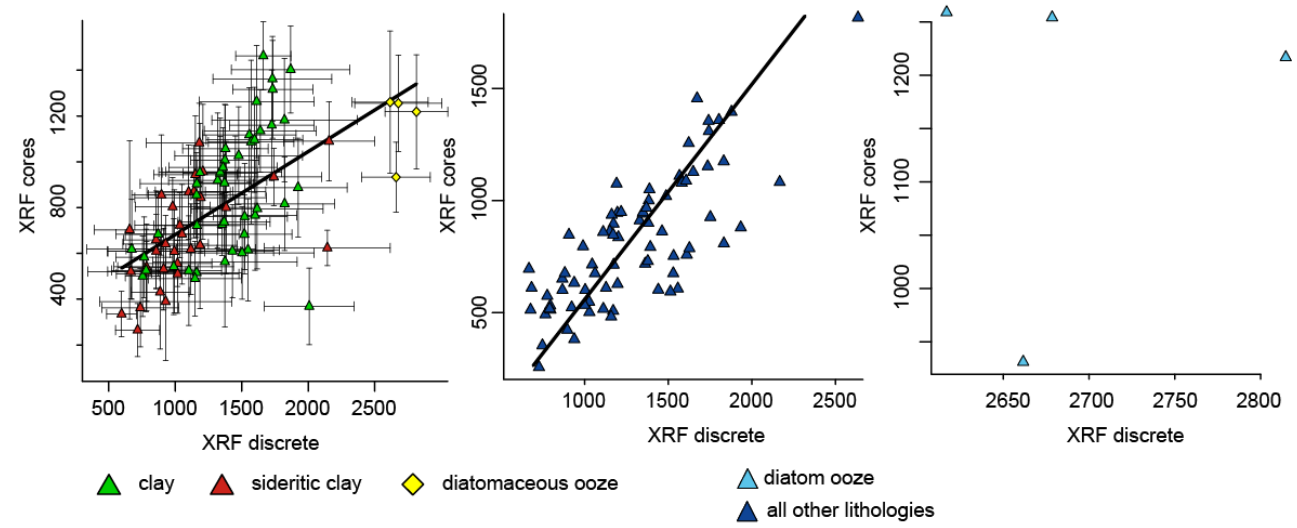

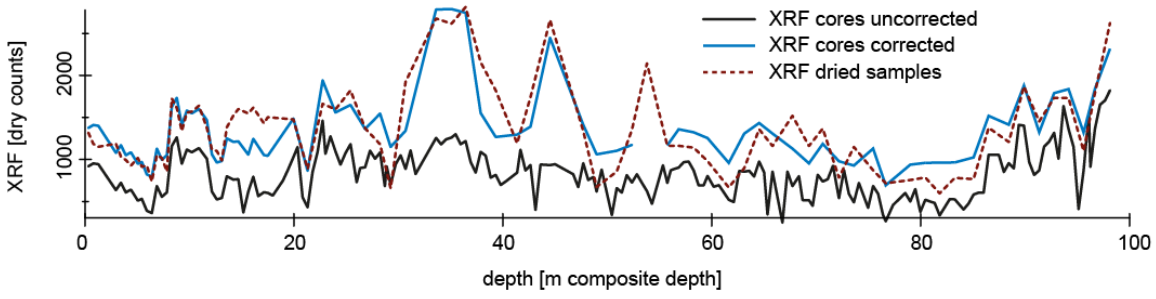

Zirconium (Zr)

Average for Zr in original wet XRF core measurements was 1,200 counts.

Zr	adj. R^2	Regression intercept	Regression slope	n
XRF cores - dry XRF	0.87	-124	0.93	81

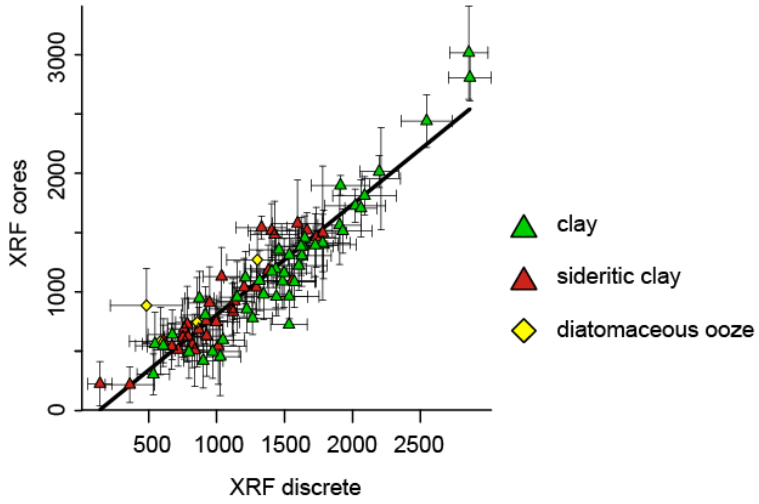

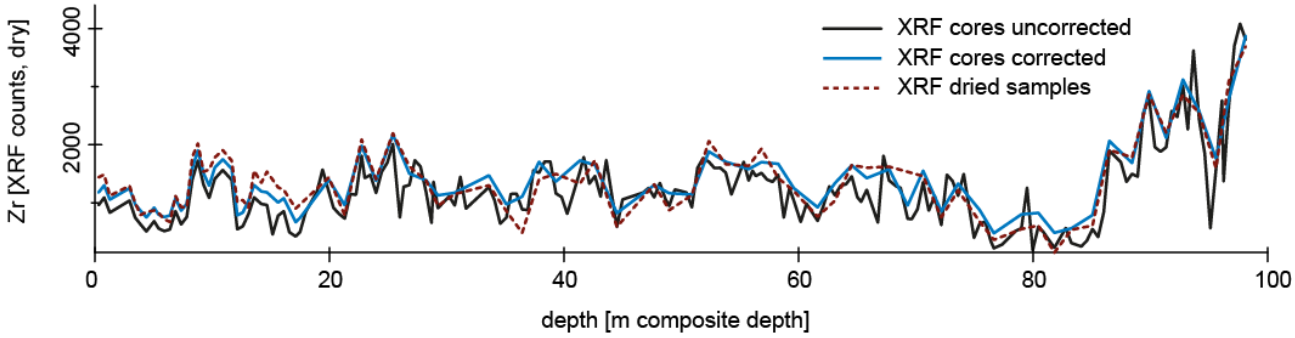

II.3 Mo-tube

Potassium (K)

Average for K in original wet XRF core measurements was 8,800 counts. The data set was split for linear regression correction. Splitting was based on sediment composition, which changes below 70 m composite depth. One outlier was removed in the ICP-AES data set.

K	adj. R^2	Regression intercept	Regression slope	n
XRF cores - dry XRF (joint)	0.82	-1,610	0.72	186
XRF cores - dry XRF (0-70 m depth)	0.81	2,900	1.4	132
XRF cores - dry XRF (70-100 m depth)	0.96	1,181	1.2	54
dry XRF - ICP-AES	0.92	0.01	0.00004	173
XRF cores - ICP-AES	0.69	300	14,079	177
final XRF - ICP-AES	r = 0.92*	p-value: 0.00		174

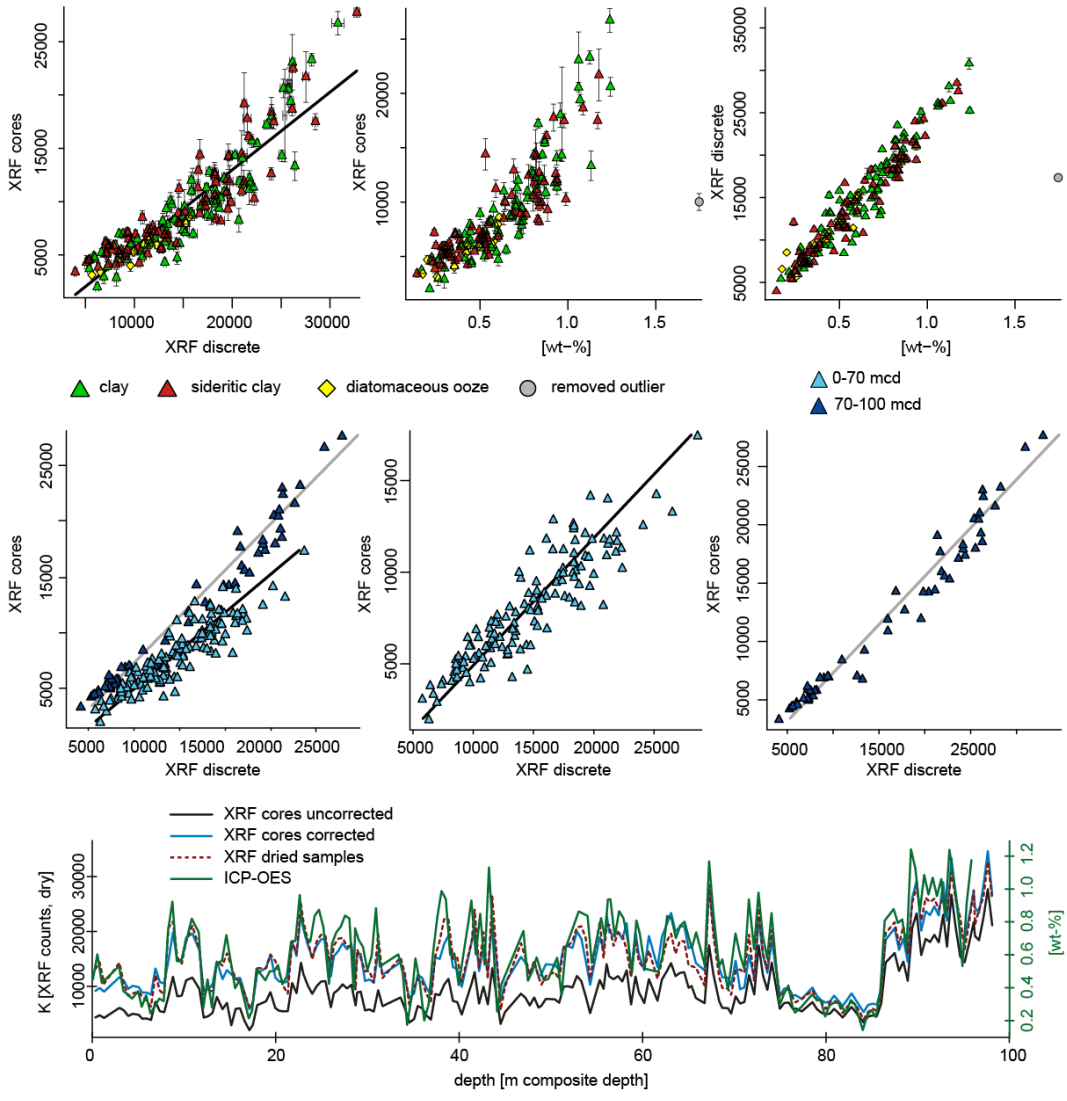

Calcium (Ca)

Average for Ca in original wet XRF core measurements was 10,000 counts. The data set was split for linear regression correction, because water content and compaction strongly influenced Ca counts in the upper 20 m of the sequence. Three outliers were removed in the ICP-AES data set.

Ca	adj. R^2	Regression intercept	Regression slope	n
XRF cores - dry XRF (joint)	0.82	-480	0.83	186
XRF cores - dry XRF (0-20 m depth)	0.30	1840	1.18	38
XRF cores - dry XRF (20-100 m depth)	0.91	2,320	0.99	148
dry XRF - ICP-AES	0.75	0.007	0.00002	171
XRF cores - ICP-AES	0.68	1,480	31,500	177
final XRF - ICP-AES	r = 0.76*	p-value: 0.00		174

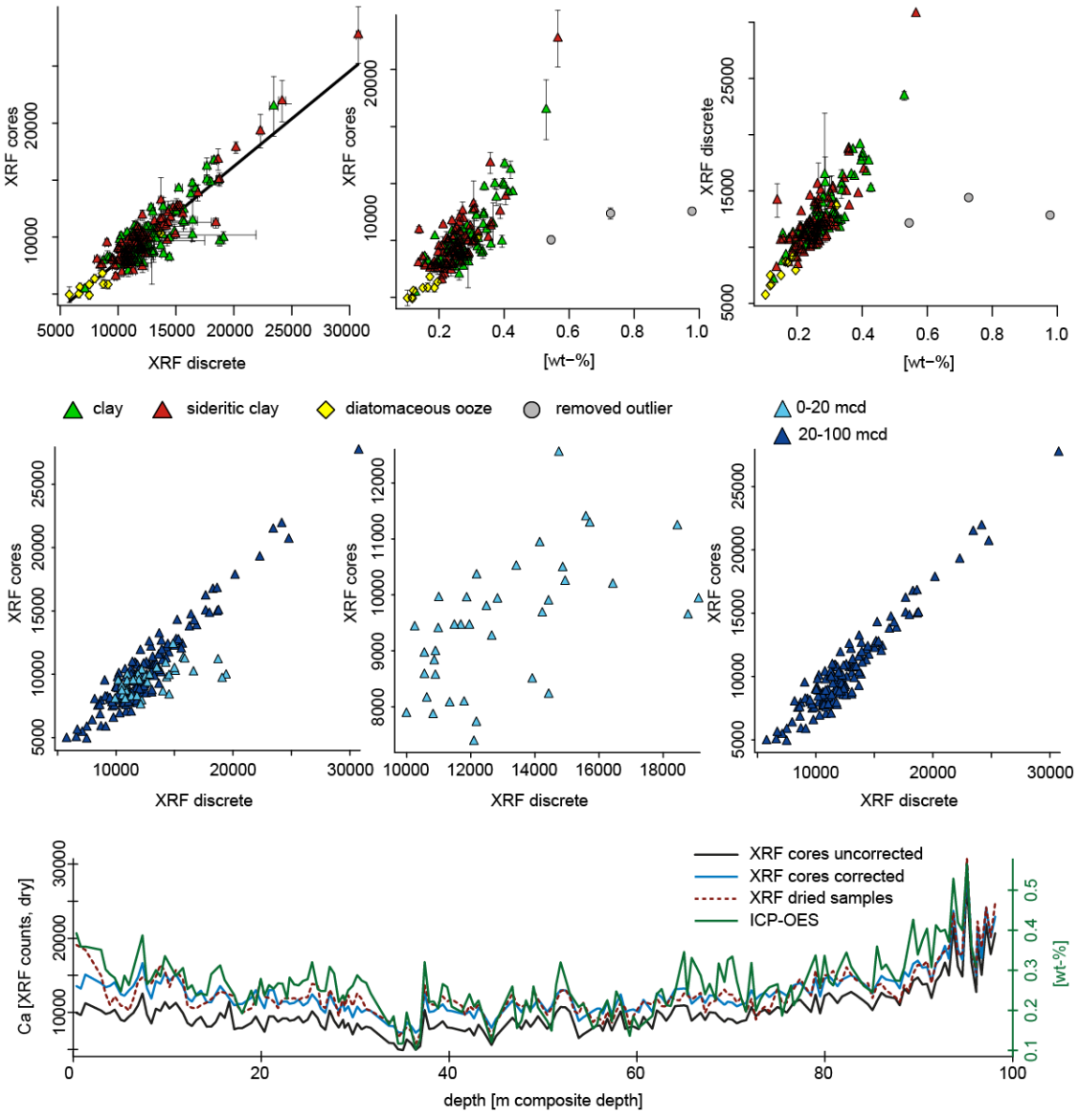

Titanium (Ti)

Average for Ti in original wet XRF core measurements was 22,400 counts. The data set was split for linear regression correction. Splitting was based on sediment composition, which changes below 70 m composite depth. One outlier was removed in the ICP-AES data set.

Ti	adj. R^2	Regression intercept	Regression slope	n
XRF cores - dry XRF (joint)	0.75	-2,690	0.82	186
XRF cores - dry XRF - 0-70 m depth	0.80	7,321	1.24	132
XRF cores - dry XRF (70-100 m depth)	0.93	5,200	1.06	54
dry XRF - ICP-AES	0.94	-0.025	0.00001	169
XRF cores - ICP-AES	0.72	1,250	80,000	177
final XRF - ICP-AES	r = 0.91*	p-value: 0.00		169

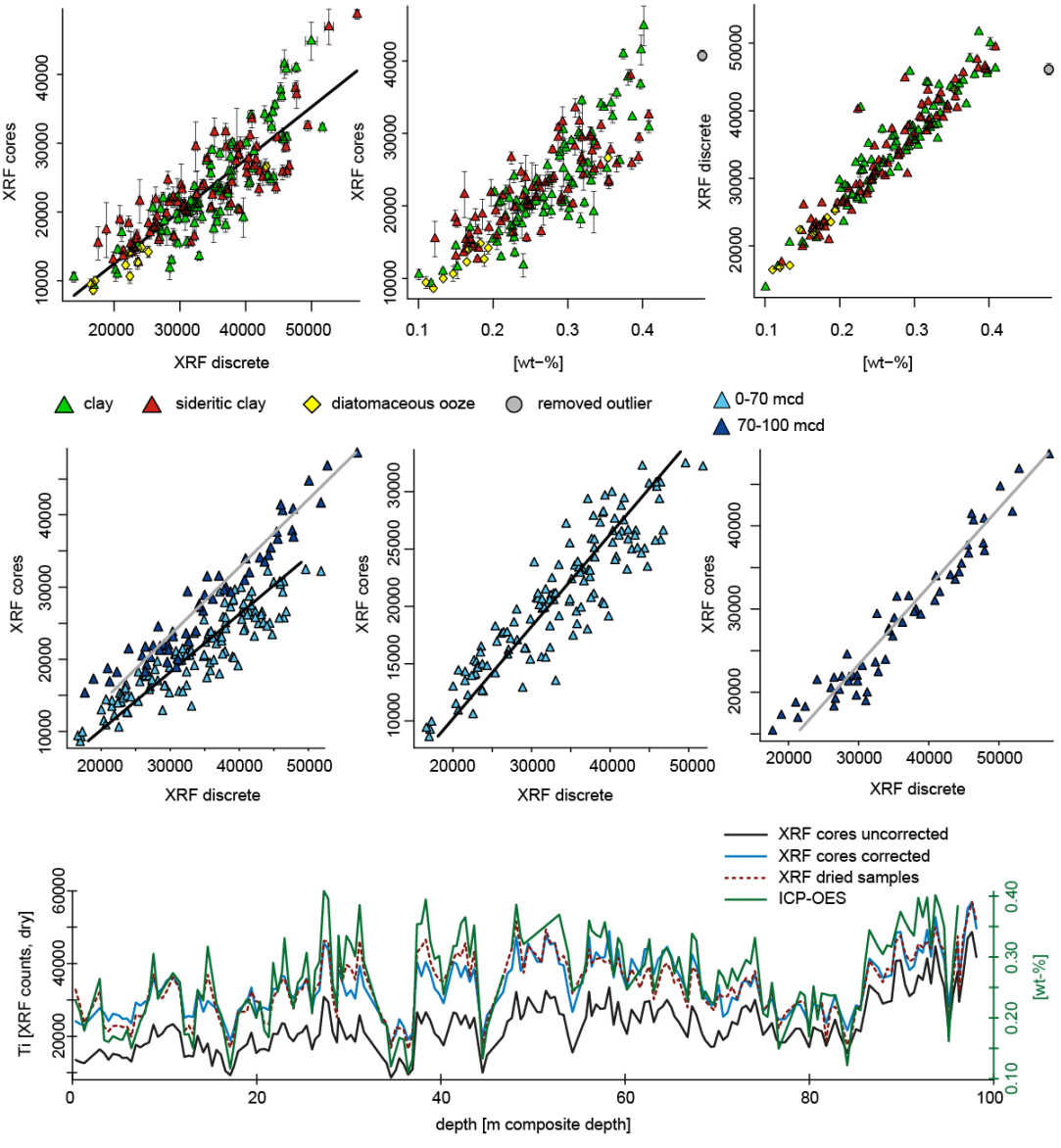

Vanadium (V)

Average for V in original wet XRF core measurements was 2,400 counts. The data set was split for linear regression correction. Splitting was based on sediment composition, which changes below 70 m composite depth.

V	adj. R^2	Regression intercept	Regression slope	n
XRF cores - dry XRF (joint)	0.78	-181	0.82	186
XRF cores - dry XRF (0-70 m depth)	0.87	650	1.1	132
XRF cores - dry XRF (70-100 m depth)	0.76	-390	1.28	54

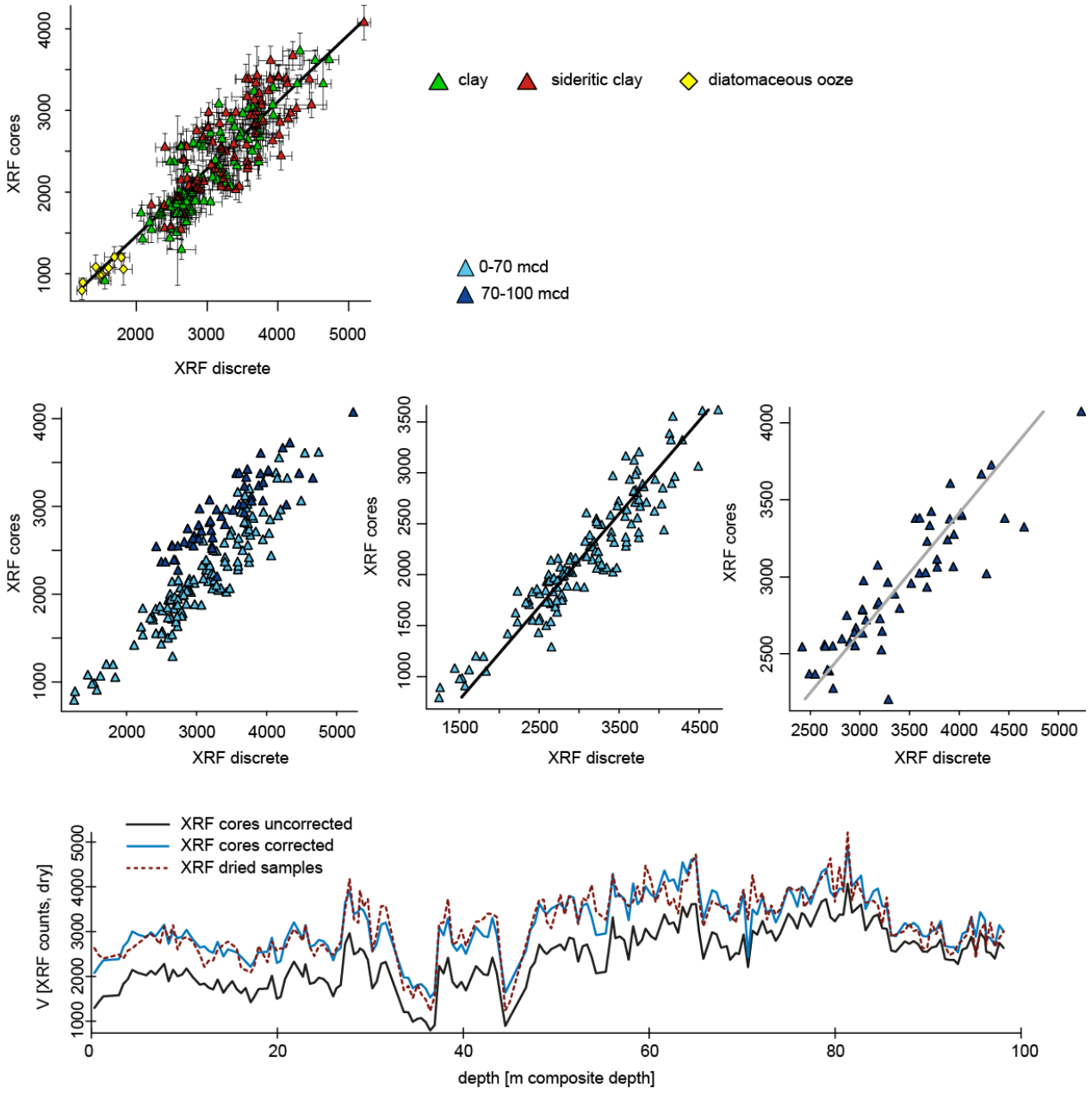

Chromium (Cr)

Average for Cr in original wet XRF core measurements was 69,400 counts. The data set was not split for linear regression correction.

Cr	adj. R^2	Regression intercept	Regression slope	n
XRF cores - dry XRF	0.86	-8,600	0.79	186
dry XRF - ICP-AES	0.91	-0.01	0.000004	174
XRF cores - ICP-AES	0.77	40	191,500	177
final XRF - ICP-AES	r = 0.91*	p-value: 0.00		174

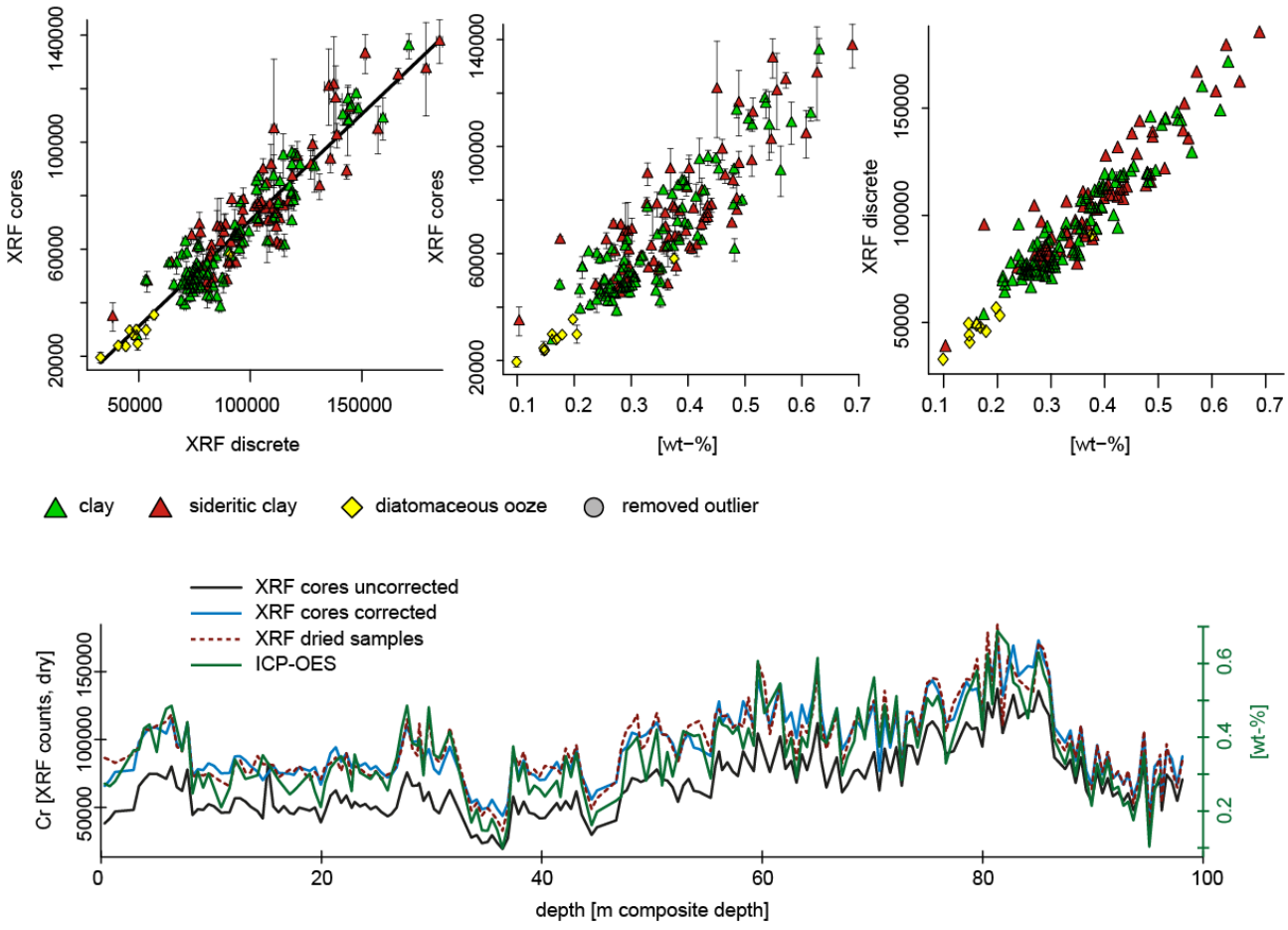

Manganese (Mn)

Average for Mn in original wet XRF core measurements was 70,000 counts. The data set was not split for linear regression correction. Mn measurements have high standard deviations for the wet XRF core measurements because manganese in Lake Towuti sediments is enriched in the authigenic mineral siderite, which forms concretions in the sediment (Morlock et al., in review; Vuillemin et al., in press).

Mn	adj. R^2	Regression intercept	Regression slope	n
XRF cores - dry XRF	0.78	6,700	0.58	186
dry XRF - ICP-AES	0.83	-0.03	0.000004	174
XRF cores - ICP-AES	0.73	18,000	136,000	177
final XRF - ICP-AES	r = 0.91*	p-value: 0.00		174

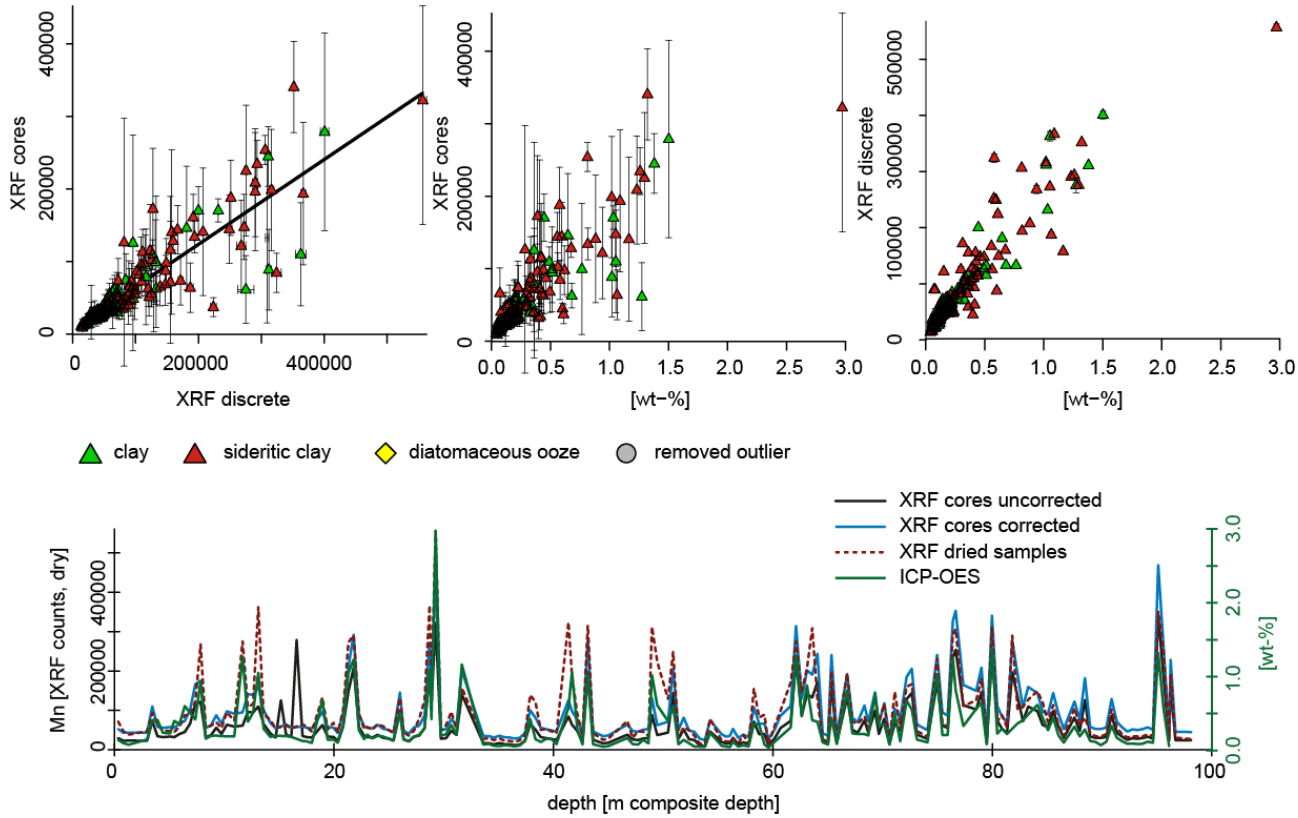

Iron (Fe)

Average for Fe in original wet XRF core measurements was 5,100,000 counts. The data set was not split for linear regression correction. One outlier was removed from the ICP-AES data set.

Fe	adj. R^2	Regression intercept	Regression slope	n
XRF cores - dry XRF	0.91	-620,000	0.91	186
dry XRF - ICP-AES	0.93	1.09	0.0000003	174
XRF cores - ICP-AES	0.80	1,420,000	230,000	177
final XRF - ICP-AES	r = 0.87*	p-value: 0.00		174

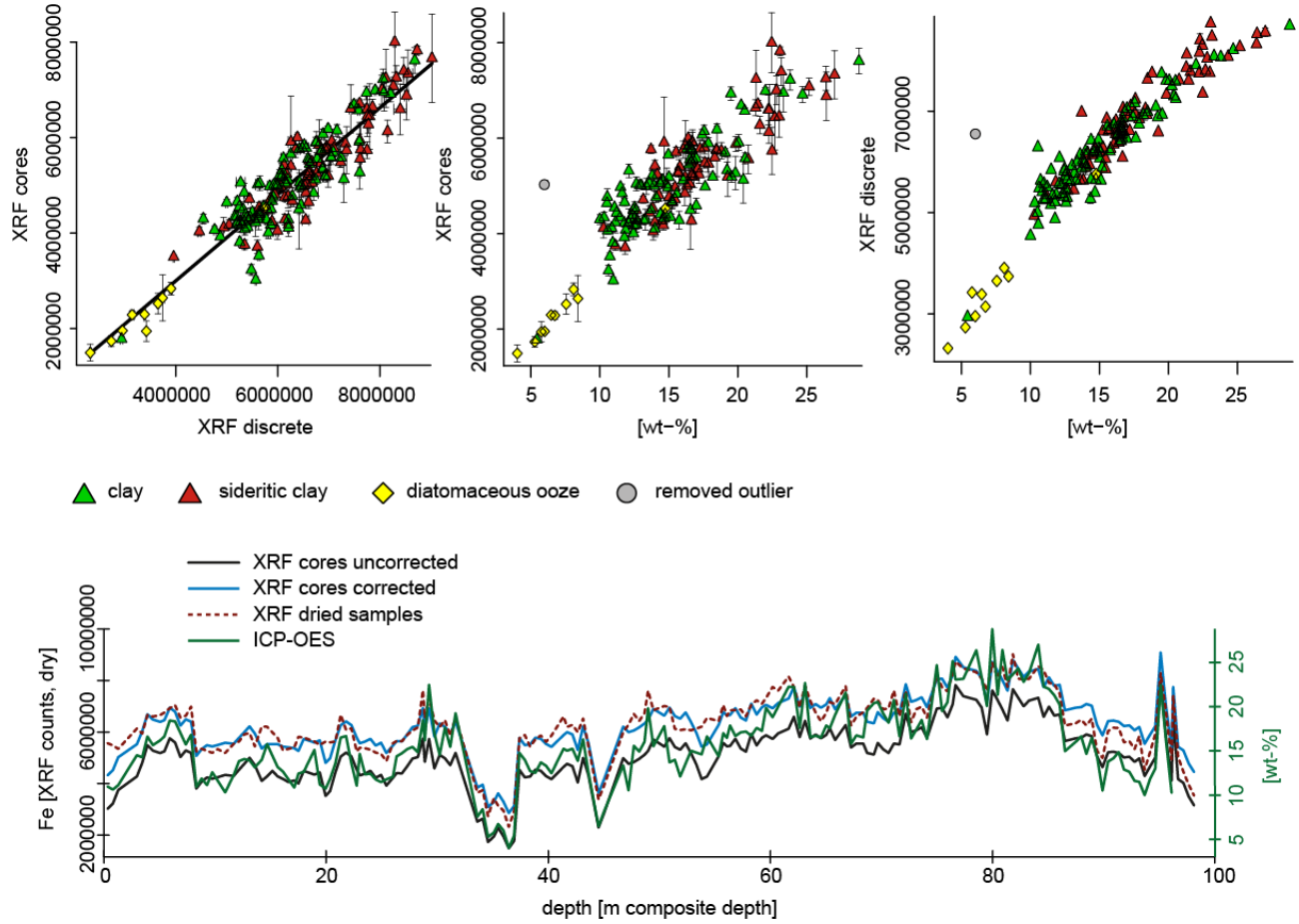

Cobalt (Co)

Average for Co in original wet XRF core measurements was 8,100 counts. The data set was split for linear regression correction. Splitting was based on sediment composition, which changes below 70 m composite depth. Co measurements have high standard deviations for the wet XRF core measurements because cobalt in Lake Towuti sediments occurs in the authigenic mineral siderite, which forms concretions in the sediment (Morlock et al., in review).

Co	adj. R^2	Regression intercept	Regression slope	n
XRF cores - dry XRF (joint)	0.71	-1,760	0.72	186
XRF cores - dry XRF (0-70 m depth)	0.70	4,900	1.25	132
XRF cores - dry XRF (70-100 m depth)	0.91	2,900	0.95	54

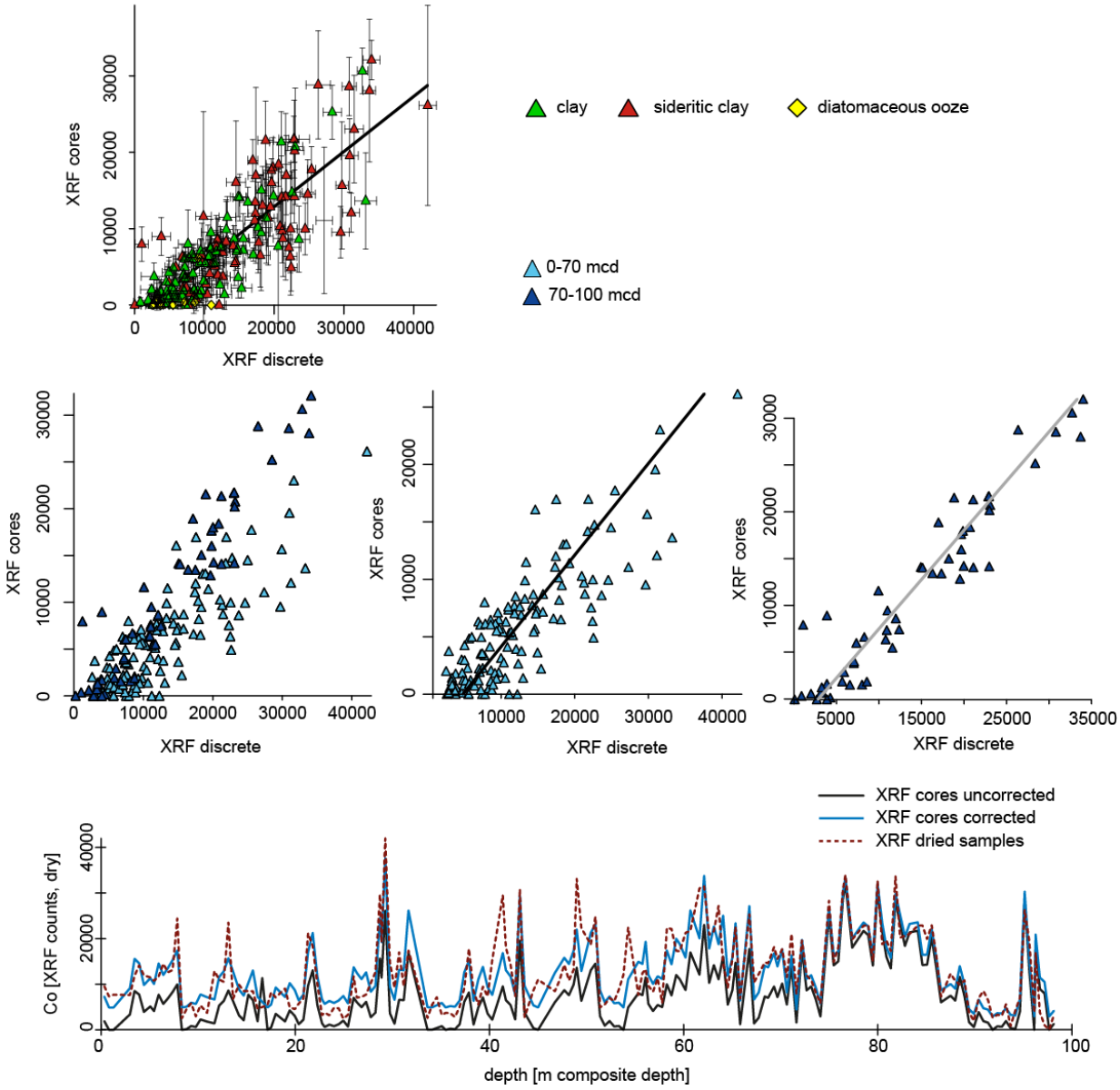

Copper (Cu)

Average for Cu in original wet XRF core measurements was 1,800 counts. The data set was split for linear regression correction. Splitting was based on sediment composition, which changes below 70 m composite depth.

Cu	adj. R^2	Regression intercept	Regression slope	n
XRF cores - dry XRF (joint)	0.45	-740	0.64	186
XRF cores - dry XRF (0-70 m depth)	0.47	2,900	0.62	132
XRF cores - dry XRF (70-100 m depth)	0.33	2,300	0.79	54

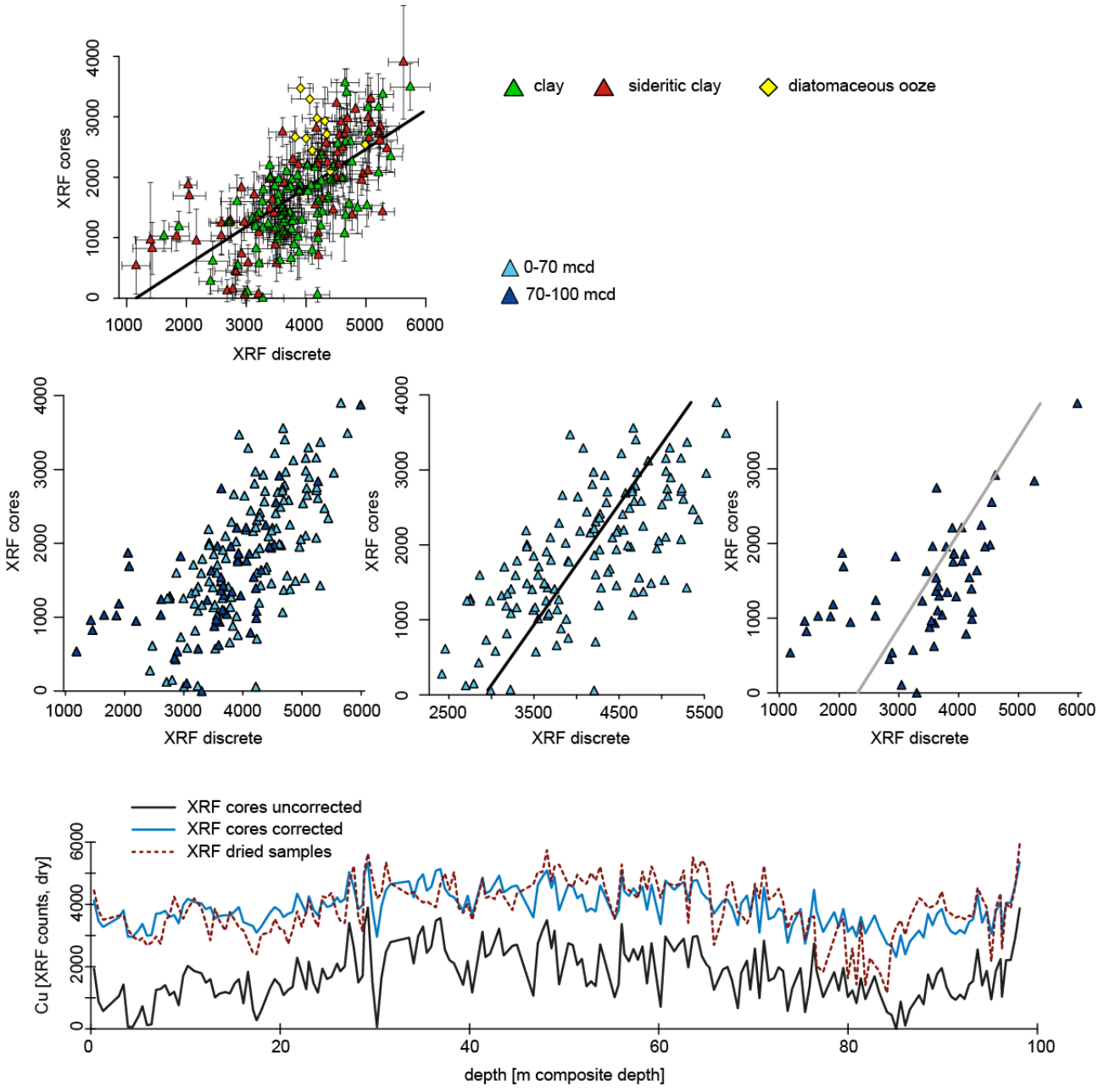

Zinc (Zn)

Average for Zn in original wet XRF core measurements was 5,000 counts. The data set was split for linear regression correction. Splitting was based on sediment composition, which changes below 70 m composite depth.

Zn	adj. R^2	Regression intercept	Regression slope	n
XRF cores - dry XRF (joint)	0.52	-420	0.76	186
XRF cores - dry XRF (0-70 m depth)	0.64	3,500	0.78	132
XRF cores - dry XRF (70-100 m depth)	0.82	421	1.12	54

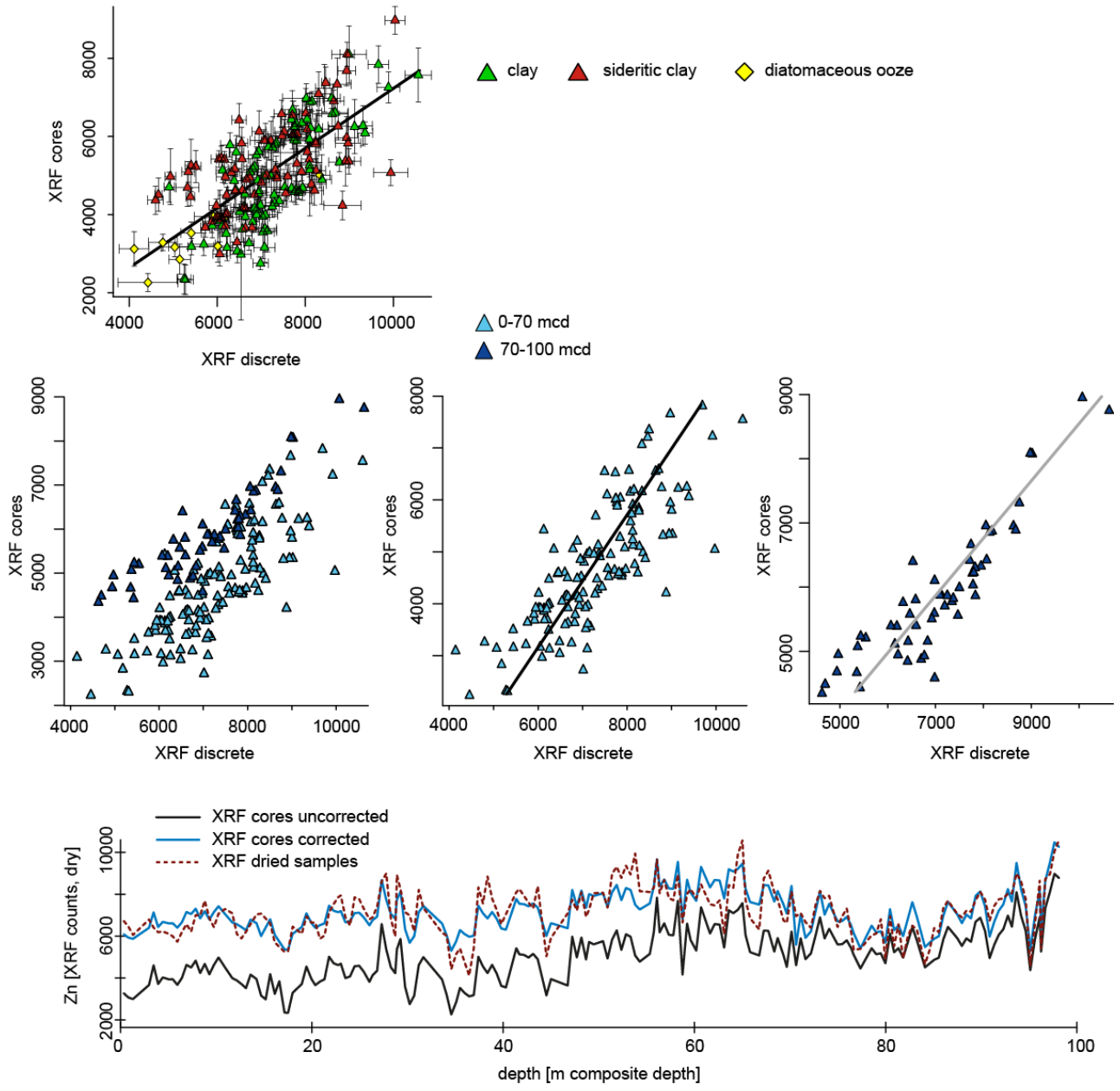

Appendix III

Summary of all measured samples

III.1 Summary of all measured samples

Method / Analysis	Full name	Measured parameter	Sample type	Number of samples (or data points)	Device	Device location
clay XRD	Clay mineralogy X-ray diffraction	clay mineralogy	soil, lake sediments	130 (+120)	PANalytical Cubix^3 goniometer	University of Bern, CH
XRD	X-ray diffraction	bulk mineralogy	soil, rock, lake sediments	20	PANalytical X'Pert Pro	University of Bern, CH
FTIRS	Fourier-Transform-Infrared Spectroscopy	clay mineralogy, siderite	soil, rock, lake sediments	450	Bruker Vertex 70	University of Bern, CH
Grain size analysis	-	grain size	lake sediments	300	Beckman Coulter LS13320 laser diffractometer	University of Cologne, GER
Coulomat / EA	Coulomat / Elemental Analyser	TIC, TOC, TC	lake sediments	18	Bruker G4 Icarus / Elemental Analyser 1108 (Carlo Erba Instruments)	University of Bern, CH
EA	Elemental Analyser	C, N, S concentrations	lake sediments	18	Elemental Analyser 1108 (Carlo Erba Instruments)	University of Bern, CH
MSCL	Multi-Sensor Core Logger	*p* wave velocity, mag. susc.	lake sediments	ca. 25,000	Geotek	Field lab, Indonesia
XRF core scanning	X-ray fluorescence core scanner	geochemical composition	lake sediments	18,000 (2x106 cores)	ITRAX, Cox	University of Bern, CH
XRF dried samples		geochemical composition	lake sediments	350	ITRAX, Cox	University of Bern, CH
***μ*XRF mapping**	high-resolution X-ray fluorescence scanner	geochemical composition	lake sediments	16	Eagle III μ-XRF spectrometer	University of Geneva, CH

Method / Analysis	Full name	Measured parameter	Sample type	Number of samples (or data points)	Device	Device location
μCT	X-ray computed micro-tomography	density differences	lake sediments	16	multi-scaled Bruker-Skyscan 2211	University of Fribourg, CH
Direct shearing test	-	shear strength, cohesion	soil	2	Normed direct shear device	University of Applied Sciences, Burgdorf, CH
Geotechnical parameters	-	plasticity index, sieving lines	soil	5	Dry / wet sieving	University of Applied Sciences, Burgdorf, CH
Thin section analysis	-	visual description	rock, lake sediments	34	Light microscope	University of Bern, CH
GIS-based analysis	-	hydrologic catchment characteristics	-	-	ArcGIS	University of Bern, CH
Smear slide analysis	-	visual sediment characterisation	lake sediments	50	Light microscope	University of Bern, CH
ICP-MS*	Inductively-Coupled Plasma Mass-Spectrometer	geochemical composition	soil, rock, lake sediments	140	-	ActLabs, Canada
ICP-AES*	Inductively-Coupled Plasma Atomic Emission Spectrometer	geochemical composition	lake sediments	210	Jobin Yvon JY2000	Brown University, USA
WD-XRF*	Wavelength-dispersive X-ray fluorescence scanner	geochemical composition	soil, rock	45	Philips PW2400 WD-XRF spectrometer	University of Lausanne, CH

* not measured by myself, but measurements contribute significantly to this thesis

Declaration

under Art. 28 Para. 2 RSL 05

Last, first name: Morlock, Marina Alexandra

Matriculation number: 12-102-281

Programme: Climate Sciences

Bachelor ☐ Master ☐ Dissertation ☑

Thesis title: Depositional modes and post-depositional mineral formation in a Pleistocene sediment record from Lake Towuti, Indonesia

Thesis supervisor: PD Dr. Hendrik Vogel

Prof. Dr. Flavio S. Anselmetti

I hereby declare that this submission is my own work and that, to the best of my knowledge and belief, it contains no material previously published or written by another person, except where due acknowledgement has been made in the text. In accordance with academic rules and ethical conduct, I have fully cited and referenced all material and results that are not original to this work. I am well aware of the fact that, on the basis of Article 36 Paragraph 1 Letter o of the University Law of 5 September 1996, the Senate is entitled to deny the title awarded on the basis of this work if proven otherwise.

Bern, 27 November 2018

.....

Signature